Fritz Laboratory Reports

Civil and Environmental Engineering

1975

Load distribution in skewed beam-slab highway bridges, Dec. 1975

E. S. deCastro

C. N. Kostem

Recommended Citation

deCastro, E. S. and Kostem, C. N., "Load distribution in skewed beam-slab highway bridges, Dec. 1975" (1975). *Fritz Laboratory Reports.* Paper 441.
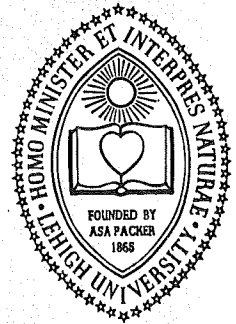http://preserve.lehigh.edu/engr-civil-environmental-fritz-lab-reports/441

LEHIGH UNIVERSITY

OFFICE

OF

RESEARCH

LOAD DISTRIBUTION IN SKEWED

BEAM-SLAB HIGHWAY BRIDGES

BY

ERNESTO S. DECASTRO

CELAL N. KOSTEM

FRITZ ENGINEERING LABORATORY REPORT No. 378A.7

LOAD DISTRIBUTION IN SKEWED

BEAM-SLAB HIGHWAY BRIDGES

by

Ernesto S. deCastro

Celal N. Kostem

Fritz Engineering Laboratory

Department of Civil Engineering

Lehigh University

Bethlehem, Pennsylvania

December 1975

TABLE OF CONTENTS

TABLE OF CONTENTS (continued)

ABSTRACT

This dissertation presents the load distribution behavior of skewed, beam-slab highway bridge superstructures. Bridges with pre-stressed concrete I-beams and prestressed concrete spread box-beams are investigated. The finite element method is employed to analyze beam-slab bridges under statically applied design vehicular loads.

A study is made of the effects of skew on the design moments and on the lateral distribution of the loads. The effects of skew on bridges of different widths, span length, number of beams and number of design lanes are correlated and an empirical relationship between skew and distribution factor is presented. The applicability of the method of analysis to bridges with curbs and parapets, and with interior-span diaphragms is demonstrated. The suitability of the method of analysis to related composite steel-girder bridge superstructures, and to continuous bridge structures is also shown.

The effect of the skew is to reduce the distribution factor in the interior beams and increase the distribution factor for the exterior beams. This effect is largely a function of the skew angle and of the bridge span and beam spacing.

The effect of curbs, parapets and diaphragms is to distribute the load more uniformly to the beams of the bridge. However, these effects becomes insignificant for longer bridges or when the bridge is fully loaded.

-1-

1. INTRODUCTION

1.1 Object and Scope of the Investigation

Skewed beam-slab bridges are common structures in modern highway bridge construction. The live load distribution provisions for these bridges however, are not covered in the current specifications (Refs. 2, 3).

Field tests of in-service beam-slab type, prestressed concrete bridges in Pennsylvania indicated the need to refine the specification provisions on live load distribution for right bridges (Refs. 7, 8,16,21,22,31,57), and to include provisions for skew bridges (Ref. 51). The investigation on simply-supported right bridges with prestressed concrete spread box-beams has resulted in the new live load distribution provision for this type of bridge (Refs. 2,38). A similar study is underway to develop the load distribution formulae for the right bridges with prestressed concrete I-beams (Ref. 62). However, very little work has been done on skew bridges, and virtually no work has been done on skewed beam-slab bridges with prestressed concrete I-beams or with prestressed concrete box-beams (Ref. 63).

This investigation will extend the live load distribution studies in prestressed concrete bridges to include the effects of skew. Design recommendations are proposed for the I-beam bridges based on the analyses of numerous bridges with varying width, spacing, span, number of beams and angle of skew. These design recommendations cover the

interior and exterior beams. Due to the limited scope of the box-beam studies, only preliminary recommendations are presented for the box-beam bridges.

This study will also demonstrate: (1) the effects of curbs and parapets in the load distribution behavior of right I-beam bridges, (2) the effects of midspan diaphragms, or multiple diaphragms along the span, and (3) the extension of the study to continuous bridges.

The two basic beam-slab bridge sections utilized in this study are shown in Fig. 1. Fig. 1a shows a typical cross-section of the bridge with prestressed concrete I-beams. Fig. 1b shows a typical section with prestressed concrete box-beams. The beams are equally spaced, and are parallel to the direction of traffic (Fig. 2). The design loading on the bridge is the HS20-44 standard truck shown in Fig. 3 and described in Ref. 2. The vehicle used in the field testing of bridges is also shown in Fig. 3. The test vehicle simulates the HS20-44 design vehicle. This vehicular loading is employed in the correlation studies between the field test and the results of the analytical formulation.

The skew angle in this study is defined as the acute angle between the support line and the longitudinal axis of the beams (Fig. 2b). When the angle is 90 degrees, the bridge structure becomes a right bridge (Fig. 2a). A distinction, however, should be made between the skewness and the angle of skew of a bridge. For example, a 60 degree skew bridge has a small skew but a large skew angle. On the other hand, a 30 degree skew bridge has a large skew but a small skew angle.

1.2 Previous Studies

The problem of lateral load distribution in bridges has been investigated by many researchers in the past. A summary of the completed research and a bibliography is reported in Ref. 63. A detailed description of the studies in beam-slab bridges including the different methods of analysis is given by Sanders and Elleby in Ref. 49, by Motarjemi and VanHorn in Ref. 38, and also by Wegmuller and Kostem in Ref. 58.

Sanders and Elleby indicated the methods of analysis applicable to load distribution by investigators and discussed their results (Ref. 49). Sanders and Elleby then used the theoretical methods and test results of these investigators on the different types of highway bridges to arrive at a proposed load distribution criteria for highway bridges. The resulting proposals for distribution of live load in highway bridges were complicated and not quite practical as a design aide. The study did not include the skew bridges.

Motarjemi and VanHorn developed a method of analysis suitable for spread box-beam slab type bridges (Ref. 38). In this method, the bridge superstructure is reduced to an articulated structure by introducing a series of beam and plate elements. Using the flexibility approach, the bridge superstructure is solved for stresses and displacement. This method of analysis had been used to arrive at the newly accepted provision on load distribution for spread box-beam bridges (Ref. 2).

Wegmuller and Kostem used the finite element method in the analysis of prestressed concrete I-beam bridges (Ref. 58). In the method, the bridge superstructure is discretized into plate and eccentrically attached stiffener elements. The method was applied to field tested beam-slab type highway bridges constructed with prestressed concrete I-beam bridges. A study of several variables that affect load distribution was made. The authors showed that a stiffened plate superstructure can be adequately idealized by the given model and finite element approach. The analytical modeling technique for the above approach is given by Kostem in Ref. 29.

The finite element approach with the use of plate and eccentrically attached stiffener elements as applied to highway bridges was reported by deCastro and Kostem (Ref. 13). Zellin, Kostem and VanHorn used the method of analysis to determine live load distribution factors for prestressed concrete I-beam bridges (Ref. 62). Distribution factors were determined for several bridge configurations with varying width, spacing, number of beams and span length under the critical HS20-44 vehicular loadings. Based on the results, simplified distribution factor equations were obtained for the interior beams and exterior beams of right bridges.

Very little experimental data is available on skewed beam-slab bridges (Ref. 63). A field test comparison of an actual 45° skew spread box-beam bridge with that of a right bridge of nearly identical dimensions is reported by Schaffer and VanHorn in Ref. 51. A

laboratory test on a 60° skew composite bridge with steel I-beams is reported by Hondros and Marsh in Ref. 25.

The field test results for the 45° skew spread box-beam bridge indicated that the experimental distribution factor for interior girders was considerably less than the design distribution factor (Refs. 42,51). However, for exterior girders, the experimental values were greater than the design values. The authors in the same study indicated the desirability of including the curbs and parapets in future design procedures. The observation from the 60° skew composite bridge with steel I-beams was that the skew caused a general reduction in the beam strains of about 17 percent (Ref. 25).

Among the analytical studies in skewed beam-slab structures, two major works are noted: the work by Chen, Newmark and Siess (Ref. 9); and the work by Gustafson and Wright (Ref. 23).

Chen, Newmark and Siess used the finite difference method in the analysis of skew bridges. Finite difference operators in skewed coordinates were generated and the system of difference equations was solved by computer. The major assumptions employed in addition to those usually made for plates are (Ref. 9);

1. There is no composite action between the beam and the slab;

2. Diaphragms and their effects are neglected;

3. The beam acts on the slab along a line and not distributed over a finite width;

4. There is no overhang at the edge of the bridge; the edge beams are located at the sides of the bridge; and

5. The value of Poisson's ratio is assumed to be zero.

Influence values for moments and deflections are computed for various ratios of spacing and lengths, relative stiffness of the beam to the slab, and for different angles of skew. Influence surface for moments and deflections are then derived for some of the structures studied. Moment coefficients for skew bridges subjected to standard truck loadings were determined and some general relationships pertaining to design had been derived.

Because of the assumptions, the analysis procedure and results are applicable to noncomposite steel I-beam bridges. For composite bridges, the procedure could still be made applicable by using the composite section in the beam stiffness computation. However, the accuracy of the results with this approach cannot be assessed. Moreover, because of the third assumption, the width of the beam which affects the load distribution in prestressed concrete I-beam bridges as reported in Ref. 62, cannot be taken into account. Finally the analysis procedure was carried out only for five-beam bridges.

Gustafson and Wright (Ref. 23) presented a finite element method of analysis employing parallelogram plate elements and eccentric beam elements. Two typical composite skew bridges with steel I-beams were analyzed and the behavior due to the skew, and the effects of adding midspan diaphragms were illustrated. The parallelogram plate

elements used did not satisfy slope compatibility requirements at element boundaries and therefore, accuracy could not be ascertained. The work was not carried out to cover load distribution analysis of general skewed beam-slab structures.

The other works on skew bridges are summarized in Ref. 63. Most of these reports on skew are on skew slab bridges, skew cellular bridges, and skew bridges with only edge beams. Thus, their contributions are not directly applicable to the present study.

1.3 Method of Analysis

The finite element method is chosen as the analytical basis for this research. Among the many methods of analysis as listed in Ref. 63, and the drawbacks of some of the methods as mentioned in Section 1.2, the finite element method of analysis can model the skew bridge structure realistically. The method can take directly into account the loading procedures and information necessary for a lateral load distribution analysis. The loading procedure involves the application of the design vehicular load anywhere on the bridge structure; and the information necessary is the beam and slab moments at the critical sections.

There are two basic approaches to the finite element method of analysis: (1) the stiffness approach, and (2) the flexibility approach. It has been found that for complex structures of arbitrary form, the displacement method over the flexibility method provides a more systematic formulation (Ref. 65). Consequently the computer

programming is simplified and an efficient solution of large and complex structural systems is obtained. The displacement approach is therefore adopted in this study.

The basic concepts and steps necessary in the development of the analysis procedure for a finite element analysis are given in this Section. A general formulation is presented. Its extension to the elements used in beam-slab superstructure is shown in subsequent chapters.

1.3.1 Introduction to the Finite Element Method of Analysis

The basic concept of the finite element method is that the structure may be idealized into an assemblage of individual structural components, or elements. The structure consists of a finite number of such elements interconnected at a finite number of joints, or nodal points (Ref. 65).

The finite element method of analysis may be divided into the following basic steps: (1) structural idealization, (2) evaluation of element properties, (3) assembly of the force displacement equations, and (4) structural analysis.

Structural idealization is the subdivision of the original structure into an assemblage of discrete elements. These elements are generally simple structural components of sizes and shape that retain the material and physical properties of the original structure. The proper structure idealization is obtained by using element shapes that follow the shape and boundaries of the original structure.

The structural idealizations for the beam-slab bridge structures considered in this research are shown in Figs. 4 and 5. Fig. 4 illustrates the idealization of a beam-slab bridge with prestressed concrete I-beams into plate elements and eccentric beam elements. The plates are general in shape and follow the beam delineation and structural boundaries. The beams are eccentrically attached to the plate elements along the element boundaries.

Figure 5 illustrates the structural idealization of a spread box-beam bridge. Plate finite elements model the deck and the top and bottom plate of the box-beams. Web elements model the web of the box-beams and interconnect the top and bottom plate elements.

The finite element idealization requires that each element deform similarly to the deformations developed in the corresponding region of the original continuum. This is accomplished by prescribing deformation patterns which provide internal compatibility within the elements and at the same time achieve full compatibility of displacements along the boundary (Ref. 65).

Since the elements are interconnected only at the nodes, the elastic characteristics of the element must be adequately represented by the relationship between forces applied to a limited number of nodal points and deflections resulting therefrom. The force deflection relationship is expressed conveniently by the stiffness properties of the finite element.

Once the element properties have been defined, the analysis
of stresses and deflections become a standard structural problem. As
in any structural analysis, the requirements of equilibrium, compati-
bility and force displacement relationship must be satisfied by the
solution. In the finite element model, internal element forces must
equilibrate externally applied forces at the nodes and element deforma-
tions must be such that they are compatible at the nodes and boundaries
before and after the loads are applied. It should be noted that this
analysis procedure does not insure equilibrium of stresses along ele-
ment boundaries. In general stresses in adjacent elements are not
similar. Intuitively, finite elements that satisfy compatibility
along the boundaries would give better results.

1.3.2 Basic Equations of the Finite Element Theory

The displacement method of analysis consists basically of the
following operations (Ref. 65). First, the stiffness properties of the
individual structural elements are evaluated, usually in a convenient
local coordinate system. Second, the element stiffness matrix is
transformed from its local coordinate system to the global coordinate
system of the complete structural assemblage. Third, the structural
stiffness matrix at each node is assembled by the superposition of the
individual element stiffnesses contributing to the nodal point.
Fourth, equilibrium equations are formulated by expressing the rela-
tionship between the applied forces {R} at the nodes and the resulting
nodal displacements {r}:

$$\{R\} = [K]\,\{r\} \tag{1.1}$$

The system of equations is solved for the unknown displacements $\{r\}$ with the cognizance that the stiffness matrix $[K]$ is generally sparsely populated, banded and well conditioned. Finally element deformations are evaluated from the computed nodal displacements by kinematic relationships. Element forces are then determined from the element deformation by means of the element stiffness matrix.

From the assumed finite element deformation pattern, the stiffness properties of any element can be evaluated in the following procedure (Ref. 65):

1. Express the element displacement field $\{v\}$ in terms of displacement functions $[M]$ and generalized coordinates $\{\alpha\}$:

$$\{v\} = [M]\,\{\alpha\} \tag{1.2}$$

   The number of independent functions in M should equal the number of nodal point displacement components.

2. Evaluate the nodal displacements in terms of the generalized coordinates:

$$\{v_i\} = [A]\,\{\alpha\} \tag{1.3}$$

   The matrix $[A]$ is obtained by evaluating the displacement functions at the nodes.

3. Express the generalized coordinates in terms of the nodal displacements by solving for $\{\alpha\}$ in Eq. 1.3:

$$\{\alpha\} = [A]^{-1}\,\{v_i\} \tag{1.4}$$

4. Express internal displacement field in terms of the nodal displacements by substituting Eq. 1.4 to Eq. 1.2:

$$\{v\} = [M] \ [A]^{-1} \ \{v_i\} \qquad\qquad (1.5)$$

5. Evaluate the strain $\{\varepsilon\}$

$$\{\varepsilon\} = [B] \ \{\alpha\} \qquad\qquad (1.6)$$

where [B] is obtained from Eq. 1.2 by the appropriate differentiation of the displacement function.

6. Evaluate the stress field $\{\sigma\}$ in terms of the nodal point displacements:

$$\{\sigma\} = [D] \ \{\varepsilon\} = [D] \ [B] \ [A]^{-1} \ \{v_i\} \qquad\qquad (1.7)$$

The specific characteristics of the finite element material are represented in the stress–strain matrix [D].

7. With the use of the principle of virtual displacement, evaluate the element stiffness matrix [k]:

$$[k] = [A^{-1}] \ \int [B]^T \ [D] \ [B] \ dV \ [A]^{-1} \qquad\qquad (1.8)$$

Equation 1.5 expresses the displacement field in terms of the nodal displacements. With the use of special coordinates, the displacement function can be expressed directly using the concept of interpolation polynomial (Refs. 5,33). Steps 2 to 4 and the inversion of matrix [A] can be bypassed with the proper choice of interpolation function. Thus,

$$\{v\} = [\Phi]\ \{v_i\} \qquad\qquad (1.9)$$

where the matrix $[\Phi]$ contains the necessary interpolation functions which are based on shape functions assumed for the element (Refs. 17,33).

The nodal strains can then be obtained by differentiation of Eq. 1.9 and evaluating the strains at the node points. Hence,

$$\{\varepsilon_c\} = [\Phi_c]\ \{v_i\} \qquad\qquad (1.10)$$

where the column vector $\{\varepsilon_c\}$ contains the components of the strain at the nodes and the matrix $[\Phi_c]$ is the matrix $[\Phi]$ differentiated and evaluated with corresponding nodal point coordinates.

Given the nodal strains, the strain field can be expressed by a strain interpolation function $[\Phi_\varepsilon]$

$$\{\varepsilon\} = [\Phi_\varepsilon]\ \{\varepsilon_c\} \qquad\qquad (1.11)$$

The strain interpolation functions in general are of an order lower than $[\Phi]$ and describes the strain variation within the element.

By using Eq. 1.10 and Eq. 1.11, it can be seen that,

$$\{\varepsilon\} = [\Phi_\varepsilon]\ [\Phi_c]\ \{v_i\} \qquad\qquad (1.12)$$

wherein the strains are expressed directly in terms of the nodal point displacements.

Application of the principle of virtual displacement leads to the following form of stiffness matrix expression (Ref. 33).

$$[k] = [\Phi_c]^T \int [\Phi_\epsilon]^T [D] [\Phi_\epsilon] \, dV \, [\Phi_c] \qquad (1.13)$$

The resulting relationship therefore between element forces $\{F_i\}$ and displacements $\{v_i\}$ at the nodes can be written as

$$\{F_i\} = [k] \, \{v_i\} \qquad (1.14)$$

where $[k]$ is given by Eq. 1.8 or Eq. 1.13. The stiffness matrix is of the form

$$[k] = \begin{bmatrix} [k_{ii}] & \cdots \cdots & [k_{ij}] \\ \cdot & & \cdot \\ \cdot & & \cdot \\ \cdot & & \cdot \\ [k_{ji}] & \cdots \cdots & [k_{jj}] \end{bmatrix} \qquad (1.15)$$

in which $[k_{ii}]$, $[k_{ij}]$, etc., are submatrices of size $\ell \times \ell$ where ℓ is the number of force components or degrees of freedom considered at a node.

1.3.3 Static Condensation Procedure

The additional nodes necessary in order to make use of all the terms of the assumed displacement functions can be conveniently located inside the element (Ref. 17). These interior nodes can be eliminated from the stiffness expression given in Eq. 1.15 by a static condensation procedure (Refs. 17,18). This procedure is particularly useful in complex-shaped structures where the interior nodes would be practically unmanageable in terms of input preparation (Ref. 18). In terms of computational effort, a decrease in the size of the problem can be obtained.

-15-

The element stiffness equation expressed by Eq. 1.15 can be written in the following form:

$$\left\{ \begin{array}{c} F_E \\ \hline F_I \end{array} \right\} = \left[\begin{array}{c|c} k_{EE} & k_{EI} \\ \hline k_{IE} & k_{II} \end{array} \right] \left\{ \begin{array}{c} v_E \\ \hline v_I \end{array} \right\} \qquad (1.16)$$

where $\{F_E\}$ = Applied nodal forces at external nodes

$\{F_I\}$ = Applied nodal forces at interior nodes

$\{v_E\}$ = Nodal displacements at exterior nodes

$\{v_I\}$ = Nodal displacements at interior nodes

k_{EE}, k_{EI}, k_{IE}, k_{II} = the partitioned element stiffness matrices corresponding to $\{F_E\}$ and $\{F_I\}$ with $\{v_E\}$ and $\{v_I\}$ respectively.

Solving for $\{v_I\}$ in the second part of Eq. 1.16 and substituting the result to the first part of Eq. 1.16 results in the following expression:

$$\{F_E\} - [k_{EI} \ k_{II}^{-1}] \ \{F_I\} = [k_{EE} - k_{EI} \ k_{II}^{-1} \ k_{IE}] \ \{v_E\} \qquad (1.17)$$

Defining the modified force vector as:

$$\{F'\} = \{F_E\} - [k_{EI} \ k_{II}^{-1}] \ \{F_I\} \qquad (1.18)$$

The element stiffness matrix for the element with the reduced number of nodes is:

$$[k'] = [k_{EE} - k_{EI} \ k_{II}^{-1} \ k_{IE}] \qquad (1.19)$$

-16-

1.3.4 Assembly and Solution

The condition of overall equilibrium for the element is satis-
fied by Eq. 1.14. It is then necessary to establish equilibrium condi-
tions at the nodes of the complete structure.

The system of nodal displacement for the element may be
listed in the order of the nodal displacement of the structure $\{r\}$.
Corresponding to these nodal displacements are the external forces on
the structures applied at the nodes: $\{R\}$.

At a typical node i, the sum of component forces contributed
by the elements meeting at node i is equated to applied nodal force at
R_i. Thus,

$$\{R_i\} = \Sigma \{F_i\} \tag{1.20}$$

The summation is for all the elements at node i.

Using the sub-matrices of Eq. 1.15, the above equation can
be rewritten for all the nodes n (Ref. 64)

$$\{R_i\} = \sum_{m=i}^{M} [k_{im}] \{r_m\} \tag{1.21}$$

The summation in Eq. 1.21 is taken over all the elements M of the struc-
ture. If the element contains no sub-matrices corresponding to node i,
its contribution to the summation is zero.

The system of equations resulting from Eq. 1.21 can be solved
once prescribed support and boundary conditions have been imposed.
Where components of the displacement at a node are zero, the number of

-17-

equilibrium equation can be reduced by deleting the corresponding equation corresponding to that particular component.

The time consuming procedure of eliminating terms in Eq. 1.21 and reorganizing computer storage to account for boundary conditions can be avoided by using a numerical technique. Instead of eliminating the equilibrium equation at which displacement is specified, the diagonal term of the assembled matrix [k] at the node of the associated displacement component is multiplied by a large number (Refs. 58,64). The resulting system of equations is then solved for all displacement components.

Once the solution of unknown displacements has been obtained, it is a matter of substitution to compute internal stress and forces by Eq. 1.7.

1.4 Development of Bridge Design Criteria

The 1971 AASHO Bridge Specifications (Ref. 1) provides the live load distribution factor equation for which the interior and exterior beams of beam-slab bridges must be designed. The expressions are different for different types of bridges, and are functions of the center-to-center spacing of the beams only. In 1973, AASHTO adopted the new specification provision including the width, length, number of lanes, and number of beams among the parameters governing the load distribution in spread box-beam bridges (Ref. 2). A similar refinement to the specification provisions for prestressed concrete I-beams is given in Ref. 62.

This research is aimed at developing the specification provisions that will include the skew among the load distribution criteria. Three major steps are involved: (1) the theoretical development of an analysis procedure suitable for general skew beam-slab structures subjected to vehicular loadings, (2) the application of the method of analysis to highway bridges that represent general beam-slab bridge configurations; and from the results, (3) development of a simple expression for the determination of design load of interior and exterior beams.

The analytical developments are presented in Chapters 2 and 3. The application to highway bridges with prestressed concrete I-beam bridges is presented is Chapter 4 where the development of a simplified equation is also shown. The additional theoretical development for the analysis of box-beam bridges is presented in Chapter 5. The application to highway bridges with spread box-beams and the development of a simplified design equation are also presented in that chapter.

2. ANALYSIS OF SKEWED ELASTIC PLATES

2.1 Introduction

Plate problems with arbitrary geometrical boundaries are invariably complex and difficult to analyze. Their solution however, is of considerable importance in enabling the construction of safe and efficient structures like skew slabs, skew bridges, swept wings and skew-shaped floor systems. The classical solutions, e.g. theory of elasticity, for these problems are limited; and, in general restricted to the very simple cases. However, the finite element method is powerful enough to handle arbitrary geometry, boundary conditions and loading configurations. The finite element approach to these types of problems has already been demonstrated (Refs. 10,11,18,35,56,64).

This chapter presents a finite element analysis technique for skew plates. The formulation has been kept general enough to permit its extension to skew, eccentrically stiffened structures (see Chapter 3). Because of the eccentricity of the beams to the plate in these structures, the plate develops in-plane and plate bending response. Thus, both the in-plane and plate bending analyses are included.

The elements representing the in-plane and out-of-plane behavior of the plate will make up the basic plate finite element that is used in the analysis of general stiffened plates in Chapter 3, skew bridges with prestressed concrete I-beams in Chapter 4, and skew bridges with prestressed concrete spread box-beams in Chapter 5.

2.2 Skew Plate In-Plane Analysis

The skew plate also known as a parallelogram is a special
case of a quadrilateral plate when opposite sides are parallel
(Fig. 6). The acute angle between two adjacent sides is called the
skew angle as shown in the figure. The rectangular plate is a special
case of the skew plate when the skew angle is $90°$.

2.2.1 Methods of Solutions

The solutions to skew in-plane problems have been arrived at
by using the theory of elasticity in rectangular, oblique and polar co-
ordinate systems (Ref. 37). As reported by Morley in Ref. 37, solu-
tions in rectangular and oblique coordinates have been obtained by
Hemp, Favre, Lardy and Theodorescu; and solutions in the polar coordi-
nate system have been obtained by Coker and Filon, Williams, and
Mansfield. Solutions in terms of the Airy stress function expressed
in complex variables, trigonometric series, and infinite series have
been obtained by Green and Zerna (Ref. 20) and Pickett (Ref. 44).

2.2.2 Assumptions and Basic Equations

The skew plate under any in-plane forces is assumed to be a
plane stress problem. Stresses σ_x, σ_y and τ_{xy} and the generalized
forces N_x, N_y and N_{xy} in an infinitesimal element are shown in Fig. 7.
The components of stress and generalized forces shown in the figure
indicate the assumed positive direction. The generalized forces are
the stresses integrated over the thickness of the element.

The displacement at any point of the plate is defined by the components of the vector field {v}:

$$\{v\} = \begin{Bmatrix} u \\ v \end{Bmatrix} \qquad (2.1)$$

where u and v are in the x and y directions respectively. The strain field at any point is defined from the displacement field by the relationship:

$$\{\varepsilon\} = \begin{Bmatrix} \varepsilon_{xx} \\ \varepsilon_{yy} \\ \gamma_{xy} \end{Bmatrix} = \begin{Bmatrix} \dfrac{\partial u}{\partial x} \\ \dfrac{\partial v}{\partial y} \\ \dfrac{\partial u}{\partial y} + \dfrac{\partial v}{\partial x} \end{Bmatrix} \qquad (2.2)$$

where ε_{xx}, ε_{yy}, γ_{xy} are the well known components of strain.

The usual stress-strain relationship as defined by Eq. 1.6 for the general orthotropic case is given by Ref. 64:

$$\begin{Bmatrix} \sigma_x \\ \sigma_y \\ \tau_{xy} \end{Bmatrix} = \frac{E_2}{(1 - n\nu_2^2)} \begin{bmatrix} n & n\nu_2 & 0 \\ n\nu_2 & 1 & 0 \\ 0 & 0 & m(1 - n\nu_2^2) \end{bmatrix} \cdot \begin{Bmatrix} \varepsilon_x \\ \varepsilon_y \\ \gamma_{xy} \end{Bmatrix} \qquad (2.3)$$

where

$$n = \frac{E_1}{E_2}$$

$$m = \frac{G_2}{E_2}$$

in which E_1 and E_2 are the principal elastic moduli in the x and y direction, ν_2 is the Poisson's ratio, and G_2 is the shear modulus. For the isotropic case, $E_1 = E_2$, $\nu_2 = \nu$, and $m = \dfrac{1}{2(1 + \nu)}$.

2.3 In-Plane Finite Element Analysis of Skew Plates

2.3.1 Geometry and Displacement Field

Consider a quadrilateral in-lane finite element as shown in Fig. 8. The local coordinate system with the origin at the centroid of the element is indicated by ζ and η. The nodes are numbered counter-clockwise with the node at the centroid being the fifth node. The edges 1-2 and 3-4 of the quadrilateral are represented by $\zeta = -1$ and $\zeta = 1$. The edges 2-3 and 4-1 are represented by $\eta = -1$ and $\eta = 1$.

The in-plane element has eight external and three internal degrees of freedom (Fig. 8). The external degrees of freedom are the displacements u_i and v_i specified at the external nodes i, i = 1 to 4. The three internal degrees of freedom are the displacements u_5 and v_5 and the strain γ_{xy}. The displacement u_5 and v_5 are specified at the fifth node while the strain γ_{xy} is assumed to be constant throughout the element. This element was originated by Doherty who designed the element based on physical concepts and was derived by Williams using concise variational formulation (Ref. 59).

The geometrical relationships between the global coordinates and the local coordinates can be expressed in matrix form by the following expressions:

$$\left\{\begin{array}{c} x \\ y \end{array}\right\} = \left[\begin{array}{cc} \Phi_x & 0 \\ 0 & \Phi_y \end{array}\right] \left\{\begin{array}{c} x_i \\ y_i \end{array}\right\} \qquad (2.4)$$

where

$$\Phi_x = \frac{1}{4} (1 + \zeta\zeta_i) (1 + \eta\eta_i)$$

$$\Phi_y = \frac{1}{4} (1 + \zeta\zeta_i) (1 + \eta\eta_i)$$

in which x_i and y_i are the global coordinates of node i, and η_i and ζ_i are the local coordinates of node i.

The displacement function for the element is assumed to be a linear shape function for the corner points and a quadratic interpolation function for the interior point. The internal shape function selected is the quadratic interpolation scheme with vanishing values at the boundaries (Ref. 59). Thus, Eq. 1.9 in Section 1.3 for this element can be written as follows:

$$\left\{\begin{array}{c} u \\ v \end{array}\right\} = \left[\begin{array}{cccccccccc} f_1 & 0 & f_2 & 0 & f_3 & 0 & f_4 & 0 & f_5 & 0 \\ 0 & f_1 & 0 & f_2 & 0 & f_3 & 0 & f_4 & 0 & f_5 \end{array}\right] \left\{\begin{array}{c} u_i \\ v_i \end{array}\right\} \qquad (2.5)$$

where,

$$\left\{\begin{array}{c} u_i \\ v_i \end{array}\right\}^T = \left\{\begin{array}{cccccccccc} u_1 & v_1 & u_2 & v_2 & u_3 & v_3 & u_4 & v_4 & u_5 & v_5 \end{array}\right\} \qquad (2.5a)$$

and,

$$f_1 = \frac{1}{4} (1 - \zeta) (1 - \eta) \tag{2.5b}$$

$$f_2 = \frac{1}{4} (1 + \zeta) (1 - \eta) \tag{2.5c}$$

$$f_3 = \frac{1}{4} (1 + \zeta) (1 + \eta) \tag{2.5d}$$

$$f_4 = \frac{1}{4} (1 - \zeta) (1 + \eta) \tag{2.5e}$$

$$f_5 = (1 - \zeta^2) (1 - \eta^2) \tag{2.5f}$$

2.3.2 Derivation of Element Stiffness Matrix

The strain field can be derived from the standard strain displacement relationship. With the assumption of constant shear strain and with the additional strain degree of freedom, the strain components can be written (Ref. 59)

$$\begin{Bmatrix} \varepsilon_{xx} \\ \varepsilon_{yy} \\ \gamma_{xy} \end{Bmatrix} = \begin{bmatrix} U & 0 & 0 \\ 0 & V & 0 \\ 0 & 0 & 1 \end{bmatrix} \begin{Bmatrix} u_i \\ v_i \\ \alpha \end{Bmatrix} \tag{2.6}$$

where

$$U = \frac{\partial f_i}{\partial x} \tag{2.6a}$$

$$V = \frac{\partial f_i}{\partial y} \tag{2.6b}$$

and α is the generalized coordinate associated with the constant shear strain degree of freedom. The derivatives of the functions in Eqs. 2.6a and 2.6b can be written with the help of the chain rule (Ref. 45):

$$\frac{\partial f_i}{\partial x} = \frac{\dfrac{\partial f_i}{\partial \zeta} \cdot \dfrac{\partial y}{\partial \eta} - \dfrac{\partial f_i}{\partial \eta} \cdot \dfrac{\partial y}{\partial \zeta}}{\dfrac{\partial x}{\partial \zeta} \cdot \dfrac{\partial y}{\partial \eta} - \dfrac{\partial x}{\partial \eta} \cdot \dfrac{\partial y}{\partial \zeta}} \qquad (2.7)$$

$$\frac{\partial f_i}{\partial y} = \frac{\dfrac{\partial f_i}{\partial \eta} \cdot \dfrac{\partial x}{\partial \eta} - \dfrac{\partial f_i}{\partial \eta} \cdot \dfrac{\partial x}{\partial \zeta}}{\dfrac{\partial x}{\partial \zeta} \cdot \dfrac{\partial y}{\partial \eta} - \dfrac{\partial x}{\partial \eta} \cdot \dfrac{\partial y}{\partial \zeta}} \qquad (2.8)$$

The evaluation of the element stiffness for the resulting finite element model is given in Appendix A. The final stiffness matrix is obtained by the application of the static condensation procedure on the interior node as described in Section 1.3.3. The element is known as Q8D11.

The explicit integration of the stiffness matrix integral is a lengthy process and difficult. The usual procedure in this case is to use the numerical integration procedure (Refs. 45,59,64).

In the procedure, the terms of the matrices are evaluated at several points call integration points. The Gaussian quadrature formulation is found to be most useful for the present problem. In the formulation, the polynomial function is integrated as the sum of the weighted values at specified points.

Thus, a function $\int_{-1}^{1} f(\zeta)\,d\zeta$ can be replaced by a summation

$$\int_{-1}^{1} f(\zeta)\,d\zeta = \sum_{j=1}^{n} W_j \, f(a_j) \qquad (2.9)$$

where W_j are the weight coefficients and a_j are the values of the function at the n specified points.

The double integral of the form

$$I = \int_{-1}^{1} \int_{-1}^{1} f(\zeta, \eta) \, d\zeta \, dn \qquad (2.10)$$

can be replaced by the following summation (Ref. 64):

$$I = \sum_{i=1}^{n} \sum_{j=1}^{n} W_j W_i f(a_j, b_i) \qquad (2.11)$$

The numerical values of the coordinates at the integration points and the weight coefficients for different values of n are given by Zienkiewicz (Ref. 64). For this element, William has shown that the 2 x 2 Gaussian quadrature formula provides better results in stiffness than the improved 3 x 3 Gaussian integration scheme (Ref. 59). The coordinates of the integration points are shown in Fig. 9 and the weight coefficients are equal to 1 (Ref. 64).

The following should be noted in connection with this element. First, since a different shape function is used to describe individual displacement and strain components, the variation of displacement is not homogeneous. The stiffness property of the element is therefore directional. Secondly, monotonic convergence and boundedness is lost according to the Melosh criterion (Ref. 34). This criterion requires that interpolation function of internal nodes must be lower than the external node. However, this element has been shown to give more flexible and better results among the 8 degree of freedom family displacement models (Ref. 59).

The Q8D11 element has been tested and compared with other finite elements by William (Ref. 59). The same study showed the efficiency and accuracy of the element among the other finite elements. This element will be combined with the plate bending element in Section 2.5 to make up the basic plate element used in this study. Numerical examples are provided to illustrate the accuracy of the element.

2.3.3 Numerical Examples and Comparisons

The accuracy of the finite element solution for rectangular plate problems as compared with theoretically exact answers has been reported and shown by Zienkiewicz, and Tottenham and Brebbia (Refs. 56,64). Unfortunately, very little data is available for skew plate problems except for the very simple cases.

The method of analysis must be applicable for all angles of skew. Therefore, the first test example is a rectangular plate under uniform edge loading and under pure shear loading. The plate properties and dimensions are shown in Fig. 10. The skew angle is 90° and the exact solution can be found from the theory of elasticity. The results are tabulated in Tables 1 and 2. It can be noted that uniform strain for these loadings is accurately predicted by the element. The CST, that is, constant strain triangle (Ref. 52), finite element

solution is also shown in Tables 1 and 2 for comparison. The CST discretization in this example was with the use of 8 triangular elements formed by connecting two opposite corner nodes of the complete plate and connecting the midpoints of opposite sides.

The second example is a skew plate under uniform edge loading as shown in Fig. 11. The state of stress for this problem is uniform throughout the element and can be found directly from equilibrium. The example illustrates the applicability of the element to plate problems with a parallelogram shape. The discretization into four rhombic elements is shown in Fig. 11a. The discretization into eight triangular elements for the CST analysis follows the same procedure as the first example. The numerical results are tabulated in Table 3. Since the exact solution is that of constant strain, the analytical results verified the analytical model.

The third example is a skew plate under in-plane concentrated loads. The plate shown in Fig. 12 is fixed at the supports and subjected to two concentrated loads near midspan. This problem is chosen to illustrate the accuracy of the element under this type of loading. There is no exact solution for this problem. The solutions are provided by using linear strain equilateral -LSE (Ref. 60), constant strain triangle -CST (Ref. 52), and the reported values from Ref. 59. The results are tabulated in Table 4.

Q8D8 refers to the quadrilateral element with only four nodes and two degrees of freedom at each node. Q8D11(3) refers to the derived finite element using the 3 x 3 integration rule. The Q8D11(2)

-29-

refers to the element formulation using the 2 x 2 integration rule.
The accuracy of the element using the relaxed integration rule
can be seen from the table.

The final example is the problem of the beam with inclined
faces under a concentrated load at midspan. The structure is shown on
Fig. 13a and the two selected discretizations are shown in Figs. 13b
and 13c. The analytical solution is compared to the solution by
Sisodiya and Cheung (Ref. 53) who used a higher order element that
gives good results for the given type of structure and loading. The
results are tabulated in Table 4. The advantage of the element over
the standard Q8D8 is made obvious in this example.

It should be emphasized that this example is the most severe
case the element will be subjected to. In the application of this
element to the beam slab problem, the element will represent the
in-plane behavior of the deck slab. As such, the typical type of load-
ing would be in-plane loads in the direction of span thus producing
column behavior rather than beam behavior. The results of this example
are the reasons for the choice of another element to represent the
in-plane behavior of webs for box-beam bridges in Chapter 5.

2.4 Skew Plate Bending Analysis

2.4.1 Methods of Solutions

The exact solution to the differential equation of skew
plates in bending is difficult to obtain if at all possible. For the

simple cases, the problem is solved by direct integration of the differential equation under associated boundary conditions, or by the application of conformal mapping (Ref. 27). Subsequently, a number of studies have been concerned with investigations of the methods of solution, the most common being the series solutions and the method of finite difference (Ref. 26). Solutions in oblique coordinates, trigonometric series, and finite difference solutions by several authors are listed and referenced by Morley in Ref. 37. Solutions by polynomials and trigonometric functions have been obtained by Jumppanem (Ref. 27) and Kennedy and Simon (Ref. 28).

Based on model tests Rusch (Ref. 48) produced design data in the form of influence surfaces for bending and torsional moments of simply-supported slabs with various angles of skew. A series of thirteen skew slab models of different side to length ratio were investigated. The slab models tested were all simple span structures and made of gypsum plaster. As in any model study, it was not possible to investigate all parameters.

One of the earliest solutions using the finite difference methods was made by Jensen (Ref. 26). This was followed by Chen et al. in 1957 and by Robinson in 1959 (Refs. 9, 47).

Within the past decade, the finite element technique has been employed successfully to analyze plates of arbitrary shape (Refs. 5,10, 18). Zienkiewicz and Cheung, and Melosh used the technique to analyze plates in bending (Refs. 34,64) using rectangular elements. Based on the same deformation pattern used in the rectangular plate element

-31-

Dawe (Ref. 11) developed the stiffness matrices for parallelogram elements. Subsequently triangular elements were introduced, the most common being those by Zienkiewicz and Cheung (Ref. 64) and by Clough and Tocher (Ref. 10). Further improvements in accuracy were subsequently obtained by Felippa and Clough (Ref. 18), and Bogner et al. (Ref. 5) with the use of refined and higher order elements.

2.4.2 Assumptions and Basic Equations

A typical element from a skew plate structure is shown in Fig. 14. The element is of differential dimensions whose sides are parallel to the orthogonal x-y system of coordinates. The reference plane is assumed to lie on the mid-plane of the plate. Forces, displacements and the adopted sign conventions are shown in the positive directions in Fig. 14. The plate is assumed to be elastic, homogeneous, orthotropic and of uniform thickness, t. The standard assumptions in small deflection theory of plates are employed:

1. Stresses normal to the plate are negligible

2. Deflections are small relative to the plate thickness

3. Deflection in the z direction is a function of x and y only

4. Shear strains γxz, γyz in the x and y faces of the element and in the direction of z are equal to zero.

The consequence of the above assumptions is that normals to the plate remain normal after deformation.

-32-

From the above assumptions, the displacement equations may be written as:

$$U(z) = u - z \frac{\partial w}{\partial x} \qquad (2.12a)$$

$$V(z) = v - z \frac{\partial w}{\partial y} \qquad (2.12b)$$

where $U(z)$ and $V(z)$ are the displacement components of the point at distance z from the reference plane; and u, v, and w are the displacement components of the point on the reference plane.

Equations 2.12a and 2.12b can be differentiated to obtain the relationship of the strains to displacements:

$$\left\{ \begin{array}{c} \varepsilon_x \\ \\ \varepsilon_y \\ \\ \gamma_{xy} \end{array} \right\} = \left\{ \begin{array}{c} \dfrac{\partial u}{\partial x} - z \dfrac{\partial^2 w}{\partial x^2} \\ \\ \dfrac{\partial v}{\partial y} - z \dfrac{\partial^2 w}{\partial z^2} \\ \\ \dfrac{\partial u}{\partial y} + \dfrac{\partial v}{\partial x} - 2z \dfrac{\partial^2 w}{\partial x \partial y} \end{array} \right\} \qquad (2.13)$$

The stress-strain relationship given by Eq. 2.3 in Section 2.2.1 can then be rewritten explicitly by substituting the above expressions for ε_x, ε_y and γ_{xy}:

$$\sigma_x = C_{11} \left(\frac{\partial u}{\partial x} - z \frac{\partial^2 w}{\partial x^2} \right) + C_{12} \left(\frac{\partial v}{\partial y} - z \frac{\partial^2 w}{\partial y^2} \right) \qquad (2.14a)$$

$$\sigma_y = C_{21} \left(\frac{\partial u}{\partial x} - z \frac{\partial^2 w}{\partial x^2} \right) + C_{22} \left(\frac{\partial v}{\partial y} - z \frac{\partial^2 w}{\partial y^2} \right) \qquad (2.14b)$$

$$\gamma_{xy} = C_{33} \left(\frac{\partial u}{\partial y} + \frac{\partial v}{\partial x} - 2z \frac{\partial^2 w}{\partial x \partial y} \right) \tag{2.14c}$$

where C_{11}, C_{12}, C_{21}, C_{33} are the material constants evaluated from Eq. 2.3.

The stress resultants per unit of the plate shown in Fig. 14b are found by integrating over the thickness.

Thus,
$$M_x = \int_{-t/2}^{t/2} \sigma_x \, z \, dz \tag{2.15a}$$

$$M_y = \int_{-t/2}^{t/2} \sigma_y \, z \, dz \tag{2.15b}$$

$$M_{xy} = \int_{-t/2}^{t/2} \sigma_{xy} \, z \, dz \tag{2.15c}$$

Using Eq. 2.14 and the assumption of plane sections, the above equations can be integrated easily resulting to the following equations in matrix form:

$$\begin{Bmatrix} M_x \\ M_y \\ M_{xy} \end{Bmatrix} = \begin{bmatrix} D_{11} & D_{12} & 0 \\ D_{21} & D_{22} & 0 \\ 0 & 0 & D_{33} \end{bmatrix} \begin{Bmatrix} \dfrac{\partial^2 w}{\partial x^2} \\ \dfrac{\partial^2 w}{\partial y^2} \\ -2\dfrac{\partial^2 w}{\partial x \partial y} \end{Bmatrix} \tag{2.16}$$

where

$$D_{11} = \frac{C_{11} t^3}{12}$$

$$D_{12} = D_{21} = \frac{C_{12} t^3}{12}$$

$$D_{33} = \frac{C_{33} t^3}{12}$$

Equation 2.16 is the explicit form of Eq. 1.7 applied to plate bending.

2.5   A Finite Element Analysis of Skew Plates in Bending

In this section, the general quadrilateral element is presented. The element is developed by Felippa and reported in Ref. 18. This element is employed in the reported investigation. The element has been tested under a variety of boundary conditions and the results compare favorably with the theory of elasticity solutions (Ref. 18).

The quadrilateral element is a conforming element formed from four triangular elements which satisfy deflection and slope continuity along the boundaries. Each one of the triangular elements is known as the LCCT-11 or the linear curvature compatible triangle with eleven fundamental degrees of freedom. The LCCT-11 is a simplified form of the triangular element LCCT-12 which has twelve degrees of freedom. The LCCT-11 is obtained from LCCT-12 by imposing the linear variation of the slope normal to one side of the triangle.

The element formulation is outlined in the following sections. Detailed derivations can be found in Refs. 17, 46 and 50.

2.5.1 Element Coordinate Systems

The geometry of a triangular element can be expressed by the projected dimensions in cartesian coordinate system (Fig. 15), by intrinsic dimensions (Fig. 16), or by dimensions in the natural coordinate system (Fig. 17).

In Fig. 17, A_1, A_2, A_3 are the three subtriangles subtended by point P such that

$$\zeta_i = \frac{A_i}{A} \tag{2.17}$$

where the index $i = 1$, 2, or 3 designates the number of the corner opposite to A_i and A is the total area of the complete triangle.

From Fig. 16, Eq. 2.17 can also be written as

$$\zeta_i = \frac{n_i}{h_i} \tag{2.18}$$

where n_i is the normal distance of point P and h_i is the height of node i from side i. These relationships are used to simplify the expressions in the element stiffness formulations.

The relationship between cartesian and natural coordinates is expressed as follows (Ref. 33):

$$\left\{ \begin{array}{c} 1 \\ x \\ y \end{array} \right\} = \left[\begin{array}{ccc} 1 & 1 & 1 \\ x_1 & x_2 & x_3 \\ y_1 & y_2 & y_3 \end{array} \right] \left\{ \begin{array}{c} \zeta_1 \\ \zeta_2 \\ \zeta_3 \end{array} \right\} \tag{2.19}$$

where x_i and y_i are the coordinates of the nodes i, i=1, 2, 3.

The inverse relationship can be obtained by solving for ζ_1, ζ_2, and ζ_3 from Eq. 2.19:

$$\left\{ \begin{array}{c} \zeta_1 \\ \zeta_2 \\ \zeta_3 \end{array} \right\} = \frac{1}{2A} \left[\begin{array}{ccc} 2A_1 & b_1 & a_1 \\ 2A_2 & b_2 & a_2 \\ 2A_3 & b_3 & a_3 \end{array} \right] \left\{ \begin{array}{c} 1 \\ x \\ y \end{array} \right\} \tag{2.20}$$

where a_i and b_i are the projected dimensions shown in Fig. 15.

The derivatives of a function $f(\zeta_1, \zeta_2, \zeta_3)$ with respect to the x, and y axes and a normal n_i can be obtained by the chain rule (Ref. 33):

$$\frac{\partial f}{\partial n_i} = \frac{1}{2A} \left(\frac{\partial f}{\partial \zeta_i} \ell_i + \frac{\partial f}{\partial \zeta_j} (d_i - \ell_i) - \frac{\partial f}{\partial \zeta_k} d_i \right) \tag{2.21}$$

$$\frac{\partial f}{\partial x} = \frac{1}{2A} \left(\frac{\partial f}{\partial \zeta_1} b_1 + \frac{\partial f}{\partial \zeta_2} b_2 + \frac{\partial f}{\partial \zeta_3} b_3 \right) \tag{2.22}$$

$$\frac{\partial f}{\partial y} = \frac{1}{2A} \left(\frac{\partial f}{\partial \zeta_1} a_1 + \frac{\partial f}{\partial \zeta_2} a_2 + \frac{\partial f}{\partial \zeta_3} a_3 \right) \tag{2.23}$$

where coordinates d_i and ℓ_i are shown in Fig. 16.

The above relationships are used in the formulation of the element displacement field and stiffness properties in Sections 2.5.2 and 2.5.3.

2.5.2 Construction of the Element Displacement Field

The twelve fundamental degrees of freedom for the LCCT-12 element at the external nodes of the triangular element are shown in Fig. 18. These can be expressed as components of the nodal displacement vector $\{r\}$:

$$\{r\}^T = \{w_1 \; \theta_{x1} \; \theta_{y1} \; w_2 \; \theta_{x2} \; \theta_{y2} \; w_3 \; \theta_{x3} \; \theta_{y3} \; \theta_4 \; \theta_5 \; \theta_6\} \qquad (2.24)$$

where w_i, θ_{xi} and θ_{yi} are the transverse displacement, rotation about the x-axis, and rotation about the y-axis respectively of node i. θ_4, θ_5 and θ_6 are normal slopes at the midside nodes of the element boundaries.

As proposed by Felippa (Ref. 17) the element is subdivided into three subtriangles or subelements as shown in Fig. 18. Each subelement has three displacement components at each node and one rotation component at the midpoint of the outer side (Fig. 18). Point 0 is located at the centroid of the complete triangular element. Independent cubic displacement functions are then assumed for each subelement.

The nodal displacements for each triangle can be listed as follows:

$$\{r^{(1)}\}^T = \{w_2 \; \theta_{x2} \; \theta_{y2} \; w_3 \; \theta_{x3} \; \theta_{y3} \; w_0 \; \theta_{x0} \; \theta_{y0} \; \theta_5\} \tag{2.25a}$$

$$\{r^{(2)}\}^T = \{w_3 \; \theta_{x3} \; \theta_{y3} \; w_1 \; \theta_{x1} \; \theta_{y1} \; w_0 \; \theta_{x0} \; \theta_{y0} \; \theta_6\} \tag{2.25b}$$

$$\{r^{(3)}\}^T = \{w_1 \; \theta_{x1} \; \theta_{y1} \; w_2 \; \theta_{x2} \; \theta_{y2} \; w_0 \; \theta_{x0} \; \theta_{y0} \; \theta_7\} \tag{2.25c}$$

Since each subelement has ten degrees of freedom a complete cubic polynomial expression can be used (Ref. 18). Thus for subelement i:

$$w^{(i)} = [\Phi^{(i)}] \{r^{(i)}\} \tag{2.26}$$

where $[\Phi^{(i)}]$ is the interpolating polynomial that relates displacements within the element to the nodal displacements as defined in Eq. 1.9. The explicit expression for $\Phi^{(i)}$ for i=1 has been derived and presented by Felippa in Ref. 18:

$$\Phi^{(1)^T} = \begin{bmatrix} \zeta_1^2 \, (3 - 2\zeta_1) + 6\mu_3^{(1)} \, \zeta_1 \zeta_2 \zeta_3 \\[6pt] \zeta_1^2 \, (b_3^{(1)}\zeta_2 - b_2^{(1)}\zeta_3) + (b_3^{(1)}\mu_3^{(1)} - b_1^{(1)}) \, \zeta_1 \zeta_2 \zeta_3 \\[6pt] \zeta_1^2 \, (a_3^{(1)}\zeta_2 - a_2^{(1)}\zeta_3) + (a_3^{(1)}\mu_3^{(1)} - a_1^{(1)}) \, \zeta_1 \zeta_2 \zeta_3 \\[6pt] \zeta_2^2 \, (3 - 2\zeta_2) + 6\lambda_3^{(1)} \, \zeta_1 \zeta_2 \zeta_3 \\[6pt] \zeta_2^2 \, (b_1^{(1)}\zeta_3 - b_3^{(1)}\zeta_1) + (b_2^{(1)} - b_3^{(1)}\lambda_3^{(1)}) \, \zeta_1 \zeta_2 \zeta_3 \\[6pt] \zeta_2^2 \, (a_1^{(1)}\zeta_3 - a_3^{(1)}\zeta_1) + (a_2^{(1)} - a_3^{(1)}\lambda_3^{(1)}) \, \zeta_1 \zeta_2 \zeta_3 \\[6pt] \zeta_3^2 \, (3 - 2\zeta_3) \\[6pt] \zeta_3^2 \, (b_2^{(1)}\zeta_1 - b_1^{(1)}\zeta_2) \\[6pt] \zeta_3^2 \, (a_1^{(1)}\zeta_1 - a_1^{(1)}\zeta_2) \\[6pt] 4h_3^{(1)} \, \zeta_1 \zeta_2 \zeta_3 \end{bmatrix} \tag{2.27}$$

where, $\quad \lambda_i = \dfrac{d_i}{\ell_i}$

and, $\quad \mu_i = 1 - \lambda_i$

The above interpolation function is a complete polynomial based on the choice of nodal system for n=3, i.e. cubic polynomial (Refs. 17,33).

The subscripts used in the above correspond to the renumbered node in Fig. 19; and therefore the function is the same for the other elements except for the superscript.

The vector of all the nodal displacements is expressed in the order given by Eq. 2.25. The displacement w of the complete triangular element can then be expressed by:

$$\left\{ \begin{array}{c} w^{(1)} \\ w^{(2)} \\ w^{(3)} \end{array} \right\} = \left[\begin{array}{cc} \Phi_e & \Phi_o \\ \Phi_e & \Phi_o \\ \Phi_e & \Phi_o \end{array} \right] \left\{ \begin{array}{c} r_e \\ r_o \end{array} \right\} \qquad (2.28)$$

where the superscripts refer to the subelement number and

$\quad \Phi_e$ refers to the interpolation polynomial associated with the displacements $\{r_e\}$ at the external nodes, and

$\quad \Phi_o$ refers to the interpolation polynomial associated with the displacements $\{r_o\}$ at the internal node

Transverse displacement of two adjacent subelements are identical along the juncture line. However, along this line their normal slopes differ. To impose slope compatibility along the internal edges, additional nodes 7, 8 and 9 are located at midpoint of these edges (Fig. 20). The normal slopes are computed from Eq. 2.21 and evaluated at nodes 7, 8 and 9. The resulting compatibility equations are then used to evaluate the displacements at the internal node $\{r_o\}$ in terms of the displacements at the external nodes $\{r_e\}$.

The final displacement field is then written only in terms of the external degrees of freedom:

$$\left\{ \begin{array}{c} w^{(1)} \\ w^{(2)} \\ w^{(3)} \end{array} \right\} = \left[\begin{array}{c} \hat{\phi}^{(1)} \\ \hat{\phi}^{(2)} \\ \hat{\phi}^{(3)} \end{array} \right] \{r\} \tag{2.29}$$

The explicit expression for $\hat{\phi}^{(i)}$ is given in Appendix B for ready reference.

2.5.3 Derivation of the Element Stiffness Matrix

The stiffness matrix for each subelement can be derived following the procedure outlined in Section 1.3.2 together with the displacement function given in Eq. 2.28.

From Eq. 2.16, $\{\epsilon\}$ is defined to be:

$$\{\varepsilon\} = \left\{ \begin{array}{c} \dfrac{\partial^2 w}{\partial y^2} \\[3ex] \dfrac{\partial^2 w}{\partial y^2} \\[3ex] -2\,\dfrac{\partial^2 w}{\partial x \partial y} \end{array} \right\} \tag{2.30}$$

and is known as the curvature field.

For subelement i, the curvature field can be obtained by proper differentiation of the displacement function given by Eq. 2.28, and the use of Eqs. 2.22 and 2.23

$$\{\varepsilon^{(i)}\} = \left[\begin{array}{c} \dfrac{\partial^2 \hat{\phi}^{(i)}}{\partial x^2} \\[3ex] \dfrac{\partial^2 \hat{\phi}^{(i)}}{\partial y^2} \\[3ex] -2\,\dfrac{\partial^2 \hat{\phi}^{(i)}}{\partial x \partial y} \end{array} \right] \{r\} = [T^{(i)}]\,\{r\} \tag{2.31}$$

The nodal values of the curvature can be obtained by evaluating Eq. 2.30 at the nodes. Thus

$$\{\dot{\varepsilon}_c^{(i)}\} = [\phi_B^{(i)}]\,\{r\} \tag{2.32}$$

where $\{\varepsilon_c^{(i)}\}$ is the vector of nodal curvatures and $[\phi_B^{(i)}]$ is the matrix $[T^{(i)}]$ evaluated at the node points of element i.

The linear curvature variation within the subelement can now be expressed in terms of the nodal curvatures by a linear interpolating function $[\Phi_\varepsilon]$ such that

$$\{\varepsilon^{(i)}\} = [\Phi_\varepsilon^{(i)}] \{\varepsilon_c^{(i)}\} \tag{2.33}$$

where

$$[\Phi_\varepsilon^{(i)}] = \begin{bmatrix} \zeta_1 & \zeta_2 & \zeta_3 & 0 & 0 & 0 & 0 & 0 & 0 \\ 0 & 0 & 0 & \zeta_1 & \zeta_2 & \zeta_3 & 0 & 0 & 0 \\ 0 & 0 & 0 & 0 & 0 & 0 & \zeta_1 & \zeta_2 & \zeta_3 \end{bmatrix}$$

With Eqs. 1.13, 2.16 and 2.32, the stiffness matrix can be evaluated:

$$[k^{(i)}] = [\Phi_B^{(i)}]^T \int [\Phi_\varepsilon^{(i)}]^T [D] [\Phi_\varepsilon^{(i)}] \, dA \, [\Phi_B^{(i)}] \tag{2.34}$$

Since the stiffness matrix of a subelement is expressed in terms of the same set of nodal coordinates, the stiffness matrix of the complete triangular element is obtained by adding the contributions of the three subelements, thus,

$$[k] = [k^{(1)}] + [k^{(2)}] + [k^{(3)}] \tag{2.35}$$

Four of these triangular elements are assembled to form the quadrilateral. The midpoint nodes at the outermost side of the quadrilateral are however undesireable. These nodes require special programming procedures for identification in input and in the calculation of the global stiffness matrix. Moreover, these nodes increase the band

-43-

width of the assembled equations. In order to avoid this difficulty, without violating compatibility requirements, the midside node can be eliminated by imposing the normal slope to vary linearly along the side (Ref. 18). For example θ_4 in Fig. 18 can be expressed as the average of the corresponding slope at nodes 1 and 2. Since θ_4 is expressed now in terms of θ_x and θ_y at nodes 1 and 2, Eq. 2.28 is reduced to eleven components. The resulting element is the LCCT-11.

The partially constrained elements are assembled to a quadrilateral element such that there are no midside nodes at the exterior edges (Fig. 20). The resulting general quadrilateral has nineteen degrees of freedom and more commonly known as Q-19. The seven internal degrees of freedom are eliminated by a static condensation procedure as discussed in Section 1.3.3. Thus the final quadrilateral is fully compatible, with linear variation of normal slopes at the edges. The element has twelve degrees of freedom: one translation and two rotations at each of the corner nodes.

2.5.4 Numerical Examples and Comparisons

Several example problems are presented to illustrate the application of the quadrilateral element to plate bending problems. Different discretization schemes are used in some of the problems to compare the accuracy and convergence of the solution with tests and other reported solutions. The different cases studied for each problem are depicted in Fig. 21.

The first example is the square plate shown in Fig. 22. The dimensions of the plate are shown in Fig. 22a. Due to symmetry only a quarter of the plate is analyzed. The discretization schemes used for this problem are illustrated in Figs. 22b to 22f. The three cases considered for this problem are: (1) concentrated load at the center of the plate with completely fixed supports, (2) concentrated load at the center of the plate with simple supports, and (3) uniform load throughout the plate with simple supports. For all these cases Poisson's ratio is assumed to be equal to 0.3.

The error in percent of deflection at the center of the plate resulting from the analyses and those reported in literature are shown in Figs. 23 and 24 and Tables 6 and 7 for the first two cases. In these figures, the lines corresponding to elements developed by Wegmuller-Kostem (WK), Adini, Clough and Melosh (ACM), Melosh (M), and Pappenfuss (P) are taken from Ref. 58. The bending moments M_x and M_y for the third case are shown in Fig. 25. Shown also in this figure are the theoretical moments from Ref. 55. The above example shows the good convergence of the displacements and moments.

The second problem is a skew plate with uniform load and simply supported on all sides. The plate is ideally a rhombic plate, all sides of which are equal, and whose skew angle is varied (Fig. 26, inset). The plate is discretized into 64 equal skew elements. Rotation about the skew supports is allowed except at the corners which are completely fixed. The reduction in the deflection at the center of a skew plate due to the increase of skew is depicted in Fig. 26. The change

in the principal moments M_1 as the skew angle is varied is shown in Fig. 27. For comparison, the finite difference and series solutions from Ref. 37 are also shown. The large decrease in deflection and in moment especially at skew angles beyond 60° can be observed.

The third example is a 45° skew plate which is simply supported on two sides. The plate is subjected to a concentrated load P at the center. Plate dimensions, material properties and the discretization for this problem are illustrated in Fig. 28. The theoretical results for the deflection and principal moments using finite difference, finite element and experimental values are listed in Table 8. The finite element results are comparable with the numerical values of the experiment. In most cases, the finite element results are between the experimental and the finite difference solution employing the finer mesh.

The fourth example is a skew slab model made of gypsum plaster. Two cases are studied: one with uniform load throughout the slab model and another with a concentrated load at the center. The test results are reported by Rusch in Ref. 48. The slab model is shown in Fig. 29 with the properties and dimensions indicated. Points A, B, and E are specifically selected for comparison of moments. Point A is at midspan and near the edge, point B is at the center of the slab and point E near the obtuse corner of the support (Fig. 29). Three discretizations have been tried as shown in Figs. 29 and 30. Different discretizations are used so that finer discretization could be employed near the points of interest. Table 9 shows the comparison of moments at points A, B, and E between the model test and the finite element

solutions for a uniform load of 100 psi. Table 10 lists the results for a concentrated unit load at the center of the plate. The values of the moments at points A and B are quite comparable with the experimental values. However, at point E, large discrepancies are observed. The third discretization gave only slightly improved results for point E. It is important to note here that computed values near the obtuse angle corners are questionable since they are near a region of high moment gradient.

The final example is a skew plate supported on two sides with varying angle of skew but with constant width to span ratio. The deflections and moments at the center of the plate using the finite difference solution and the finite element procedure are shown in Figs. 31 and 32. Good correlation is observed between finite difference and finite element except at the 60° skew where the available value of the width to span ratio is 0.52 instead of 0.50. A sharp decrease in the principal moment is observed for the skews beyond 60° and a much sharper decrease in deflection is obtained beyond 75°.

2.6 Summary

The analysis of skew plates under in-plane and lateral forces have been presented in this chapter. The development of the analysis technique with the use of the finite element method of analysis was illustrated for the in-plane and the plate bending elements. Numerical examples were shown to demonstrate the application of the method of analysis to skew in-plane and plate bending problems subjected to uniform and concentrated in-plane and lateral forces.

-47-

3. ELASTIC ANALYSIS OF SKEW STIFFENED PLATES AND BRIDGES

3.1 Introduction

In this chapter, the analysis of a general stiffened structure using the finite element procedures is presented. As was done for rectangular stiffened plate problems by Wegmuller and Kostem (Ref. 58), the structure is discretized into deck plates and stiffener elements (Fig. 4). The stiffness matrices of the finite elements for in-plane and out-of-plane plate behavior in Chapter 2 are used for the deck slab. An eccentric beam finite element with shear deformation properties is introduced to represent the beam and the spacers or diaphragms.

The method is used to analyze skew and right bridges. Comparisons are made with available solutions and field tests. The applicability of the method of analysis to beam-slab highway bridge superstructures is demonstrated. The behavior of highway bridges with and without curbs and parapets, and diaphragms are also shown and discussed.

3.2 Methods of Analysis of Stiffened Structures

A brief survey of the methods of analyzing plates with stiffeners is given by Wegmuller and Kostem in Ref. 58. In general, the methods of analysis may be classified according to the following structural idealizations: (1) orthtropic plate model, (2) equivalent grid model, (3) plate and stiffeners model, and (4) folded plate model. Each method has limitations imposed on it because of the associated modeling scheme (Refs. 58,59).

The equivalent plate model idealizes the behavior of stiffened plates by plate bending action. In this method the properties of the stiffeners are "smeared" to the plate, and the resulting structure is analyzed as a plate problem.

In the equivalent grid model the structure is idealized as a grillage of beam elements. Where only the slab connects the longitudinal stiffeners, the slab is modeled by transverse beam elements at sufficient intervals. The analysis follows the standard structural analysis procedure.

The difficulty with the equivalent plate or equivalent grid model is twofold. First is the determination of the adequate plate and beam properties that will truly represent the actual structure. Second is the computation of the actual stresses in the beams and the slab from the analyzed equivalent structure.

The plate with stiffeners model and the folded plate model have gained full acceptance in the analysis of stiffened plates (Refs. 23,58,60). The actual properties of the plate and the stiffeners are used, and the actual stresses are derived directly from the analysis. In the reported investigation, the plate and stiffeners model is used for the I-beam bridges and the folded plate model is used for the box-beam bridges.

The analysis of structures with plate and stiffeners can be formulated by combining the classical plate and beam theories (Ref. 58). The standard assumptions for the plate are listed in Section 2.4.2.

For the beam, the assumption is that all deformations can be described in terms of the vertical displacement of the longitudinal axis and rotation of the beam section. This assumption neglects the deformation of the cross-section of the beam, and hence strains normal to the longitudinal axis of the beam are not conisdered. The classical approach results to a system of equation which is not easily solved except for the very simple loads and boundary conditions. The problem becomes even more involved for skew structures.

From the objectives of the overall study as mentioned in Section 1.1, and the requirements set forth in Section 1.5, the method of analysis must be sufficiently general so that design details may be considered separately without "smearing". The method should also be applicable to a variety of structural configurations and loading considerations without difficulty. Since the finite element method of analysis meet these requirements, this method is used in this investigation.

3.3 A Finite Element Analysis of Skewed Stiffened Plates

The type of structure considered in this section is shown in Fig. 4. The plate or deck in this case can have arbitrarily shaped boundaries. The stiffeners or the beams can be eccentrically or concentrically attached to the deck.

When the stiffeners are eccentrically attached to the plate, the bending of the stiffeners causes in-plane deformations in the plate in addition to the plate bending deformations. These in-plane

-50-

deformations are normally not considered in classical plate theory. In the finite element method of analysis, the in-plane and out-of-plane behavior can easily be represented with the use of in-plane and plate bending elements.

The in-plane and out-of-plane plate elements have been described in Chapter 2. In this section, the stiffener element is described. Since the plane of reference for the plate elements has been defined at the midplane of the plate, the behavior of the stiffener or beam element is also defined about this plane.

Five displacement components are selected at each node in the present finite element approach. These are the displacement u, v, and w in the x, y and z directions respectively, and two slopes θ_x and θ_y about the x and y axis respectively (Fig. 33).

3.3.1 Derivation of the Beam Element Stiffness Matrix

The stiffener element with the plane of reference as the middle plane of the plate is shown in Fig. 33. It is assumed that the stiffener is attached to the plate along the boundary of a plate element. It is further assumed that external loads are applied only to the plate elements or directly at the nodes. Bending about the z-axis is neglected.

In order to satisfy compatibility of displacement along the juncture of the plate and the stiffener elements, the displacement functions of the plate along the juncture must be the same as for the

stiffener element. Since the assumed in-plane behavior of the plate is linear and the out-of-plane behavior is cubic, a linear displacement functions is assumed for the in-plane behavior of the beam, and a cubic displacement function is assumed for the out-of-plane behavior of the beam. Furthermore, since the normal slope of the plate is assumed to vary linearly along the boundary, the twist of the beam along this boundary is assumed to be linear.

The geometry of the beam element can be described in terms of non-dimensional coordinates:

$$\zeta_1 = \frac{L - x}{L} \tag{3.1a}$$

$$\zeta_2 = \frac{x}{L} \tag{3.1b}$$

where L is in the direction of the x-axis.

The linear displacement function for u and the cubic displacement function for w can then be written as

$$u = \alpha_1 \zeta_1 + \zeta_2 \zeta_2 \tag{3.2}$$

$$w = \alpha_3 \zeta_1^3 + \alpha_4 \zeta_2^3 + \alpha_5 \zeta_1^2 \zeta_2 + \alpha_6 \zeta_1 \zeta_2^2 \tag{3.3}$$

In matrix notation:

$$
\left\{ \begin{array}{c} u \\ w \end{array} \right\} = \left[\begin{array}{cccccc} \zeta_1 & \zeta_2 & 0 & 0 & 0 & 0 \\ 0 & 0 & \zeta_1^3 & \zeta_2^3 & \zeta_1^2 \zeta_2 & \zeta_1 \zeta_2^2 \end{array} \right] \left\{ \alpha \right\} \tag{3.4}
$$

-52-

where $\{\alpha\}^T = \{\alpha_1 \quad \alpha_2 \quad \alpha_3 \quad \alpha_4 \quad \alpha_5 \quad \alpha_6\}$ are unknown coefficients.

The coefficients α_1 and α_2 can be determined from the two in-plane model displacements at the two nodes, and α_3, α_4, α_5, and α_6 can be determined from the two out-of-plane displacements and two rotations at the two nodes.

The nodal displacements can be written as,

$$\{r_s\}^T = \{u_i \quad w_i \quad \theta_{yi} \quad u_k \quad w_k \quad \theta_{yk}\} \tag{3.5}$$

where u_i and u_k are the in-plane displacements, and w_i, w_k, θ_{yi}, and θ_{yk} are the out-of-plane displacements and rotations, at nodes i and k respectively. θ_y can be expressed by definition and the use of the chain rule,

$$\theta_y = \frac{\partial w}{\partial x} = \frac{\partial w}{\partial \zeta_1} \cdot \frac{\partial \zeta_1}{\partial x} + \frac{\partial w}{\partial \zeta_2} \cdot \frac{\partial \zeta_2}{\partial x} \tag{3.6}$$

The nodal displacements can now be expressed in terms of the unknown coefficients from Eqs. 3.4 and 3.6

$$
\begin{Bmatrix} u_i \\ w_i \\ \theta_{YI} \\ u_k \\ w_k \\ \theta_{yk} \end{Bmatrix}
=
\begin{bmatrix}
1 & 0 & 0 & 0 & 0 & 0 \\
0 & 0 & 1 & 0 & 0 & 0 \\
0 & 0 & -3/L & 0 & 1/L & 0 \\
0 & 1 & 0 & 0 & 0 & 0 \\
0 & 0 & 0 & 1 & 0 & 0 \\
0 & 0 & 0 & 3/L & 0 & -1/L
\end{bmatrix}
\begin{Bmatrix} \alpha_1 \\ \alpha_2 \\ \alpha_3 \\ \alpha_4 \\ \alpha_5 \\ \alpha_6 \end{Bmatrix}
\tag{3.7}
$$

The vector of unknown coefficients can be expressed in terms of the nodal displacements by solving for $\{\alpha\}$ in Eq. 3.7. Hence,

$$\begin{Bmatrix} \alpha_1 \\ \alpha_2 \\ \alpha_3 \\ \alpha_4 \\ \alpha_5 \\ \alpha_6 \end{Bmatrix} = \begin{bmatrix} 1 & 0 & 0 & 0 & 0 & 0 \\ 0 & 0 & 0 & 1 & 0 & 0 \\ 0 & 1 & 0 & 0 & 0 & 0 \\ 0 & 0 & 0 & 0 & 1 & 0 \\ 0 & 3 & L & 0 & 0 & 0 \\ 0 & 0 & 0 & 0 & 3 & -L \end{bmatrix} \begin{Bmatrix} u_i \\ w_i \\ \theta_{yi} \\ u_k \\ w_k \\ \theta_{yk} \end{Bmatrix} \tag{3.8}$$

Substitution of Eq. 3.8 into Eq. 3.4 leads to the displacement function expression in the form of Eq. 1.9:

$$\begin{Bmatrix} u \\ w \end{Bmatrix} = \begin{bmatrix} f_{s1} & 0 & 0 & f_{s2} & 0 & 0 \\ 0 & f_{s3} & f_{s4} & 0 & f_{s5} & f_{s6} \end{bmatrix} \begin{Bmatrix} r_s \end{Bmatrix} \tag{3.9}$$

where

$$f_{s1} = \zeta_1 \tag{3.9a}$$

$$f_{s2} = \zeta_2 \tag{3.9b}$$

$$f_{s3} = \zeta_1^3 + 3\,\zeta_1^2\zeta_2 \tag{3.9c}$$

$$f_{s4} = \zeta_1^2\zeta_2\,L \tag{3.9d}$$

$$f_{s5} = \zeta_2^3 + 3\,\zeta_1\zeta_2^2 \tag{3.9e}$$

$$f_{s6} = -\,\zeta_1\zeta_2^2\,L \tag{3.9f}$$

It should be noted that the resulting interpolation functions are the same functions as the in-plane and plate bending elements along the boundary.

Defining $\varepsilon_x = \dfrac{\partial u}{\partial x}$, and $C = -\dfrac{\partial^2 w}{\partial x^2}$ to be the strain and the curvature respectively, at any point along the reference axis of the stiffener element, then from Eq. 1.10:

$$
\left\{ \begin{array}{c} \varepsilon_x \\ \\ C \end{array} \right\} =
\begin{bmatrix}
\dfrac{\partial f_{s1}}{\partial x} & 0 & 0 & \dfrac{\partial f_{s2}}{\partial x} & 0 & 0 \\[3ex]
0 & \dfrac{\partial^2 f_3}{\partial x^2} & \dfrac{\partial^2 f_4}{\partial x^2} & 0 & \dfrac{\partial^2 f_5}{\partial x^2} & \dfrac{\partial^2 f_6}{\partial x^2}
\end{bmatrix}
\left\{ r_s \right\}
\tag{3.11}
$$

The components of C can be determined with the use of the chain rule,

$$
\frac{\partial}{\partial x^2} = \frac{\partial^2}{\partial \zeta_1^2} \left(\frac{\partial \zeta_1}{\partial x} \right)^2 + \frac{2\partial^2}{\partial \zeta_1 \zeta_2} \left(\frac{\partial \zeta_1}{\partial x} \cdot \frac{\partial \zeta_2}{\partial x} \right) + \frac{\partial^2}{\partial \zeta_2^2} \left(\frac{\partial \zeta_2}{\partial x} \right)^2
\tag{3.12}
$$

The normal strain and curvature at the nodes can be evaluated by applying Eq. 3.12 to Eq. 3.11 and substituting coordinate values of the node under consideration:

$$
\left\{ \begin{array}{c} \varepsilon_x \\ \\ C_i \\ \\ C_k \end{array} \right\} = \begin{bmatrix} -1/L & 0 & 0 & 1/L & 0 & 0 \\ \\ 0 & -6/L^2 & -4/L & 0 & 6/L^2 & 2/L \\ \\ 0 & 6/L^2 & 2/L & 0 & -6/L^2 & 4/L \end{bmatrix} \left\{ \begin{array}{c} u_i \\ w_i \\ \theta_{yi} \\ u_k \\ w_k \\ \theta_{yk} \end{array} \right\} \quad (3.13)
$$

or $\{\varepsilon_c\}_s = [\Phi_c]_s \{r_s\}$ (3.13a)

where $\{\varepsilon_c\} = \varepsilon_x$, C_i, C_k are the normal strain and curvatures at node i and k

$[\Phi_c]$ = Normal strain and curvature interpolating functions evaluated at the nodes.

With the assumption that plane sections remain plane before and after deformation, the displacement equation for any point on the beam at a distance of z from the reference plane can be written as:

$$
U(z) = u - z \frac{\partial w}{\partial x} \quad (3.14)
$$

The normal strain ε_x can be defined by differentiating Eq. 3.14, from which the stress-strain relation for the beam becomes

$$
\sigma_s = E_s \left(\frac{\partial u}{\partial x} - z \frac{\partial^2 w}{\partial x^2} \right) \quad (3.15)
$$

-56-

where σ_s = stress on a stiffener element at distance z from the reference axis

E_s = is the modulus of elasticity of the beam

assuming only a uniaxial state of stress for the beam.

The generalized forces acting on the beam section can be evaluated by integrating Eq. 3.15,

$$N_s = \int_{-t/2}^{t/2} \sigma_s \, dA \qquad (3.16)$$

$$M_s = \int_{-t/2}^{t/2} \sigma_s \, z \, dA \qquad (3.17)$$

These generalized forces can then be expressed in matrix form as,

$$\left\{ \begin{array}{c} N_s \\ \\ M_s \end{array} \right\} = E_s \left[\begin{array}{cc} A_s & S_s \\ \\ S_s & I_s \end{array} \right] \left\{ \begin{array}{c} \dfrac{\partial u}{\partial x} \\ \\ -\dfrac{\partial^2 w}{\partial x^2} \end{array} \right\} \qquad (3.18)$$

where A_s = Cross-sectional area of the stiffener

S_s = First moment of the stiffener area with respect to the plane of reference

I_s = Moment of inertia of the stiffener area with respect to the plane of reference

-57-

Given the normal strain and curvatures at the nodes as expressed by Eq. 3.13, the strain and curvature expressions can be written in terms of strain interpolation functions. Thus

$$\left\{ \begin{array}{c} \dfrac{\partial u}{\partial x} \\[3mm] -\dfrac{\partial^2 w}{\partial x^2} \end{array} \right\} = \left[\begin{array}{ccc} 1 & 0 & 0 \\[3mm] 0 & \zeta_1 & \zeta_2 \end{array} \right] \left\{ \begin{array}{c} \varepsilon_x \\[1mm] C_i \\[1mm] C_k \end{array} \right\} \tag{3.19}$$

or
$$\{\varepsilon\}_s = [\Phi_\varepsilon]_s \, \{\varepsilon_c\}_s \tag{3.20}$$

where $\{\varepsilon\}_s$ = Normal strain and curvature $\dfrac{\partial u}{\partial x}$ and $-\dfrac{\partial^2 w}{\partial x^2}$ along the axis of the beam element about the reference plane

$[\Phi_\varepsilon]_s$ = Strain interpolation functions which express a con-stant variation of normal strain and a linear vari-ation of curvature

$\{\varepsilon_c\}_s$ = Normal strain ε_x and curvature C at the nodes

The specific characteristics for the beam element can be expressed from Eq. 3.18 to be,

$$[D]_s \qquad \left[\begin{array}{cc} A_s & S_s \\[2mm] S_s & I_s \end{array} \right] \tag{3.21}$$

which are already integrated for the complete beam section.

The integral of the triple product in the expression for Eq. 1.13 can be evaluated from $[\Phi_\varepsilon]_s$ from Eq. 3.20, and $[D]_s$ from Eq. 3.21. Thus after integration,

-58-

$$\int [\Phi_\epsilon]_s^T [D]_s [\Phi_\epsilon]\, dx = E_s L \begin{bmatrix} A_s & \dfrac{S_s}{2} & \dfrac{S_s}{2} \\[2mm] \dfrac{S_s}{2} & \dfrac{I_s}{3} & \dfrac{I_s}{6} \\[2mm] \dfrac{S_s}{2} & \dfrac{I_s}{6} & \dfrac{I_s}{3} \end{bmatrix} \qquad (3.22)$$

The integration in Eq. 3.22 is carried out only through the length because [D] is already expressed for the cross-section in Eq. 3.18.

The stiffness matrix expression for the beam element can now be evaluated with Eqs. 3.13 and 3.22:

$$[k]_s = [\Phi_c]_s^T \int [\Phi_\epsilon]_s^T [D]_s [\Phi_\epsilon]_s\, dx\, [\Phi_c]_s$$

$$\begin{bmatrix}
\dfrac{A_s}{L} & 0 & \dfrac{S_s}{L} & -\dfrac{A_s}{L} & 0 & -\dfrac{S_s}{L} \\[3mm]
 & \dfrac{12 I_s}{L^3} & -\dfrac{6 I_s}{L^2} & 0 & -\dfrac{12 I_s}{L^3} & -\dfrac{6 I_s}{L^2} \\[3mm]
 & & \dfrac{4 I_s}{L} & -\dfrac{S_s}{L} & \dfrac{6 I_s}{L^2} & \dfrac{2 I_s}{L} \\[3mm]
 & & & \dfrac{A_s}{L} & 0 & \dfrac{S_s}{L} \\[3mm]
 & \text{Symmetric} & & & \dfrac{12 I_s}{L^3} & \dfrac{6 I_s}{L^2} \\[3mm]
 & & & & & \dfrac{4 I_s}{L}
\end{bmatrix} \qquad (3.23)$$

It should be noted that the above expression is only for the bending stiffness of the beam. The torsional stiffness is derived separately in the following paragraphs.

For the present analysis, only St. Venant torsion is considered. It has been shown that for rectangular and stocky beam cross-sections, most of the applied twisting moment is resisted by St. Venant torsion (Ref. 58).

The twisting moment $T_{s.v.}$ in the beam element is related to the angle of twist ϕ by the relation:

$$T_{s.v.} = GK_t \, \phi'$$

(3.24)

where $\phi' = \dfrac{\partial}{\partial x} \left(\dfrac{\partial w}{\partial y} \right)$ or the rate of change of angle of twist

G = shear modulus

K_t = St. Venant torsional constant

With the assumption that the angle of twist varies linearly along the length of the element, and recognizing that the angle of twist at the nodes corresponds to the rotation about the longitudinal axis of the beam, the torsional rotation function can be written in terms of linear interpolation functions and the nodal rotations. Thus

$$\{\phi\} = [\zeta_1 \quad \zeta_2] \left\{ \begin{array}{c} \theta_{xi} \\ \\ \theta_{yi} \end{array} \right\}$$

(3.25)

$$\{\phi'\} = \begin{bmatrix} -\dfrac{1}{L} & \dfrac{1}{L} \end{bmatrix} \left\{ \begin{array}{c} \theta_{xi} \\ \\ \theta_{yi} \end{array} \right\} \tag{3.26}$$

Following the procedure for the beam bending element and using the given rotation function, the following matrices can be defined:

$$[D]_t = Gk_t \tag{3.27}$$

$$[\Phi_\epsilon]_t = [1] \tag{3.28}$$

$$[\Phi_c]_t = \begin{bmatrix} -\dfrac{1}{L} & \dfrac{1}{L} \end{bmatrix} \tag{3.29}$$

From the expression for the stiffness matrix, given by Eq. 1.13, integration along the length leads to

$$[k]_t = [\Phi_c]_t^T \int_t [\Phi_\epsilon]_t^T [D] [\Phi_\epsilon]_t \, dx \, [\Phi_c]_t$$

$$= \frac{Gk_t}{L} \begin{bmatrix} -1 & -1 \\ \\ -1 & 1 \end{bmatrix} \tag{3.30}$$

3.3.2 Assembly of the System Stiffness Matrix

The stiffness matrices of the individual elements are assembled to form the structural stiffness matrix of the complete system. The procedure follows the requirement of Eq. 1.21. In the following, the assembly of the elements is illustrated in matrix form to show the

-61-

interaction of individual elements as defined by the global force and displacement vectors.

The in-plane and bending plate elements are assembled first to form a combined element with five degrees of freedom at each node. Since the in-plane plate element and out-of-plane plate element both lie on the same reference plane, there is no interaction between them. Hence, for example

$$[k_{ii}] = \begin{bmatrix} k_I & 0 \\ & \\ 0 & k_{II} \end{bmatrix} \qquad (3.31)$$

where k_I is a 2 x 2 matrix associated with u and v displacement components and k_{II} is a 3 x 3 matrix associated with the w, θ_x, θ_x displacement and rotation components.

For the whole plate element with nodes 1, 2, 3 and 4,

$$\begin{Bmatrix} F_1 \\ F_2 \\ F_3 \\ F_4 \end{Bmatrix} = [k_{ij}] \begin{Bmatrix} r_1 \\ r_2 \\ r_3 \\ r_4 \end{Bmatrix} \qquad (3.32)$$

where the submatrices of $[k_{ij}]$ are in the form of Eq. 3.31, and

$$\{F_i\}^T = \{F_{xi} \quad F_{yi} \quad F_{zi} \quad M_{xi} \quad M_{yi}\} \qquad (3.33)$$

$$\{r_i\}^T = \{u_i \quad v_i \quad w_i \quad \theta_{xi} \quad \theta_{yi}\} \qquad (3.34)$$

for i = 1, 2, 3, or 4.

-62-

The bending and torsional stiffness matrices of the beam element are assembled in a similar manner. The stiffness terms associated with the neglected displacement component are taken as zero in forming the complete five degrees of freedom system at the node. Hence, from Eq. 3.23 and Eq. 3.30 at beam nodes i and k,

$$
\begin{Bmatrix} F_{xi} \\ F_{yi} \\ F_{zi} \\ M_{xi} \\ M_{yi} \\ F_{xk} \\ F_{yk} \\ F_{zk} \\ M_{xk} \\ M_{yk} \end{Bmatrix}
=
\begin{bmatrix}
A_sL^2 & 0 & 0 & 0 & S_sL^2 & -A_sL^2 & 0 & 0 & 0 & -S_sL^2 \\
 & 0 & 0 & 0 & 0 & 0 & 0 & 0 & 0 & 0 \\
 & & 12I_s & 0 & -6I_sL & 0 & 0 & -12I_s & 0 & -6I_sL \\
 & & & \frac{Gk_t}{E_s}L^2 & 0 & 0 & 0 & 0 & -\frac{Gk_t}{E_s}L^2 & 0 \\
 & & & & 4I_sL^2 & -S_sL^2 & 0 & 6I_sL & 0 & 2I_sL^2 \\
 & & & & & A_sL^2 & 0 & 0 & 0 & S_sL^2 \\
 & & & & & & 0 & 0 & 0 & 0 \\
 & \text{Symmetric} & & & & & & 12I_s & 0 & 6I_sL \\
 & & & & & & & & \frac{Gk_t}{E_s}L^2 & 0 \\
 & & & & & & & & & 4I_sL^2
\end{bmatrix}
\begin{Bmatrix} u_i \\ v_i \\ w_i \\ \theta_{xi} \\ \theta_{yi} \\ u_k \\ u_k \\ w_k \\ \theta_{xk} \\ \theta_{yk} \end{Bmatrix}
$$

(3.35)

The stiffness matrix expression for the beam element in Eq. 3.35 can be modified to include the additional deflection due to shear (Ref. 45). Defining

$$\Gamma = \frac{12\,E_s I_s}{G_s A_s L^2} \tag{3.36}$$

The beam stiffness matrix can be rewritten to include the shear deformation (Ref. 45).

$$[k]_s = \frac{E_s}{L^3}
\begin{bmatrix}
A_s L^2 & 0 & 0 & 0 & S_s L^2 & -A_s L^2 & 0 & 0 & 0 & -S_s L^2 \\
 & 0 & 0 & 0 & 0 & 0 & 0 & 0 & 0 & 0 \\
 & & \frac{12 I_s}{(1+\Gamma)} & 0 & \frac{-6 I_s L}{(1+\Gamma)} & 0 & 0 & \frac{-12 I_s}{(1+\Gamma)} & 0 & \frac{-6 I_s L}{(1+\Gamma)} \\
 & & & \frac{Gk_t}{E_s}L^2 & 0 & 0 & 0 & 0 & -\frac{Gk_t}{E_s}L^2 & 0 \\
 & & & & \frac{(4+\Gamma) I_s L^2}{(1+\Gamma)} & -S_s L^2 & 0 & \frac{6 I_s L}{(1+\Gamma)} & 0 & \frac{(2-7) I_s L^2}{(1+\Gamma)} \\
 & & & & & A_s L^2 & 0 & 0 & 0 & S_s L^2 \\
 & & & & & & 0 & 0 & 0 & 0 \\
 & & \text{Symmetric} & & & & & \frac{12 I_s}{(1+\Gamma)} & 0 & \frac{6 I_s L}{(1+\Gamma)} \\
 & & & & & & & & \frac{Gk_t}{E_s}L^2 & 0 \\
 & & & & & & & & & \frac{(4+\Gamma) I_s L^2}{(1+\Gamma)}
\end{bmatrix} \tag{3.37}$$

The beam stiffness matrix is given for the beam element whose longitudinal axis is parallel to the x-axis. When the beam elements are not parallel to the x-axis, standard tensor transformation must be applied to the beam stiffness matrix before assembly into the structural system (Ref. 64).

The displacements of the plate and beam elements at common nodes are expressed by Eq. 3.32 and Eq. 3.35 in terms of the global degrees of freedom. The elements have equal number of degrees of freedom at the nodes and therefore can be assembled directly to the system stiffness matrix following the procedure specified in Section 1.3.4.

3.3.3 Application of Boundary Conditions

One of the advantages of the finite element method of analysis is its adaptability to solutions of problems with various boundary conditions. If a degree of freedom at the boundary is fixed, the corresponding row and column of the stiffness matrix is easily eliminated from the solution procedure. If the support at the boundary is flexible, the stiffness of the support is simply added to the stiffness of the element at that boundary (Ref. 65).

In certain cases, the nodes are constrained to displace in a specified direction, and to rotate at a specified angle. For example, the u displacement of a node may be specified to displace in the direction of a line at an angle ω from the x-axis and the θ_x rotation may be specified to rotate about a line at an angle β from the x-axis. For

these cases, the stiffness matrix must be transformed accordingly. It
is shown in Ref. 64 that the required transformation is of the form

$$[k'] = [T]^T [k] [T] \tag{3.38}$$

where $[k']$ = the transformed stiffness matrix

$[k]$ = the original stiffness matrix

$[T]$ = the transformation matrix

It should be noted that the transformation can be carried out in the
element stiffness level $[k]$ or at the assembled system stiffness matrix
$[K]$. It should be noted further that the applied nodal forces and the
resulting deformations are in the direction specified by the constraint.

For the five degree of freedom system in this study, the
transformation matrix for a given node is

$$[T] = \begin{bmatrix} \cos\omega & \sin\omega & 0 & 0 & 0 \\ -\sin\omega & \cos\omega & 0 & 0 & 0 \\ 0 & 0 & 1 & 0 & 0 \\ 0 & 0 & 0 & \cos\beta & \sin\beta \\ 0 & 0 & 0 & -\sin\beta & \cos\beta \end{bmatrix} \tag{3.39}$$

where ω = the angle from the global x-axis along which u displaces,
measured clockwise; and

β = the angle from the global x-axis about which θ_x rotates,
measured clockwise.

3.3.4 Application of Loads

The components of the force vector as defined by Eq. 3.33 are applied at the nodes in the direction of the associated displacements. For uniformly distributed loads, the force vector can be computed from (Ref. 17).

$$\{F_e\} = - \int [\Phi]^T \, p \, (x,y) \, dV \qquad (3.40)$$

The uniform load is conveniently equated to a set of concentrated forces and moments applied at the nodes. For concentrated loads, the discretization can be made such that the load will be directly on a node; and hence the loads can be applied directly to the global force vector. However, the procedure of changing the discretization to accommodate concentrated loads is obviously inefficient especially for the analysis of one structure under different types of loading. For this reason, the concept of a statically equivalent force vector for a concentrated load is introduced. In this concept, the element with a concentrated load is analyzed as a substructure, and the reaction forces at the nodes are computed. The negative of these reaction forces at the nodes become the applied nodal forces for the assembled structure. In this study only the concentrated load normal to the plate element is considered.

The stiffness equation for the Q-19 element gives the force displacement relationships of a quadrilateral element with the fifth node at the center of the element. If the fifth node is located at the point where the concentrated load is applied, the resulting structure

is a quadrilateral plate of four triangles with a concentrated load at the interior node (Fig. 34). The stiffness of the four triangles can be recomputed and reassembled in the form:

$$\left\{ \begin{array}{c} F_E \\ \\ F_I \end{array} \right\} = \left[\begin{array}{cc} k_{EE} & k_{EI} \\ \\ k_{IE} & k_{II} \end{array} \right] \left\{ \begin{array}{c} 0 \\ \\ r_I \end{array} \right\} \tag{3.41}$$

where 0 refers to the supported nodes and, where the subscripts E and I refer to the external nodes and the internal node respectively. The external nodes in this case are completely fixed in displacements and rotations. $\{F_E\}$ can therefore be easily found to be

$$\{F_E\} = [k_{EI}] \ [k_{II}]^{-1} \ \{F_I\} \tag{3.42}$$

Since Eq. 3.41 is an equilibrium equation, $\{F_E\}$ is a statically equivalent force vector. In cases however when the concentrated load is very near to a corner node of the quadrilateral, the stiffness formulation may get into numerical difficulty because of the resulting shape of one or more of the triangular elements. In such cases, the concentrated load is applied directly to the nearest node. When the concentrated load is on the boundary of the element but not on the node, the load is proportioned to the two nodes of that boundary. The components of the equivalent force vector due to a concentrated load normal to a quadrilateral element is illustrated in Fig. 34.

3.4 Numerical Examples and Comparisons

The purpose of this section is to show numerical examples with the use of the combined plate and beam elements. Comparisons with available solutions and field test data are made to assess the accuracy of the results. The behavior of these types of structures are investigated in order to provide a better insight into the subsequent load distribution studies. The analysis procedure in this section is the analytical basis for the lateral load distribution analysis of pre-stressed concrete I-beam bridges in Chapter 4.

3.4.1 Beam Moments in Skewed Non-Composite Bridges

One of the beam-slab bridge configurations analyzed in Ref. 9 is investigated here by the finite element method of analysis for purposes of comparison. The bridge, in view of the assumptions for the reported solution (Section 1.2), is non-composite. The structure is a five-beam bridge with spacing to span ratio of 0.1. The plate to beam stiffness ratio H, defined as the ratio of beam rigidity to the plate rigidity, is equal to 5. Poisson's ratio and the beam eccentricity are taken as zero.

The beam slab structure, as a right bridge or 90° skew, and as a skew bridge with 30° skew, is shown in Fig. 35. The same bridge with 60° and 45° skew is shown in Fig. 36. The right bridge and the 30° skew bridge are shown in the same figure to show the change in geometry due to the skew. The loading is a single concentrated load P at midspan on Beam C. The discretization, as shown in Figs. 35 and 36,

is with two elements between the beams and eight elements along the span. The figures also show the location of maximum moment determined from the finite element analysis.

The moment coefficients for each beam as determined by the analysis, the reported results from Ref. 9, and another finite element solution from Ref. 23 are shown in Fig. 37.

The finite difference analysis underestimates the two finite element results. The following observation can be made from the finite element results.

1. There is a decrease in the moment coefficients of the interior beams as the skew angle changes from 90° to 30°. A slight increase in the exterior beam moment can be noted.

2. The rate of decrease is gradual from 90° to 45° skew but abrupt beyond 45°. The rate of change is relatively constant for the exterior beam.

3. The location of maximum moment response is towards the obtuse angle corner of the structure. The section of maximum response is not the skew centerline but varies for different angles of skew.

The decrease in the total beam moments in a bridge superstructure as the skew angle is changed is reflected in the above results. For the same width and span, the skew bridge transfers the load more efficiently to the supports. The interior beam moment is further reduced by the increase in the participation of the exterior beams.

-70-

3.4.2 Beam Moments in Composite Skew Bridges

The beams in composite bridge structures are eccentrically attached to the slab. It is necessary to include the eccentricity in order to arrive at a more realistic analysis. In the following example, the effect of considering the eccentricity is demonstrated by comparing the analysis with the previous example.

The five-beam structure in the previous comparison is analyzed as a composite bridge. An eccentricity of 28 inches corresponding to a beam moment of inertia of 126584.0 in.^{4} and area of 576.0 in.^{2} is introduced. A torsional ratio $GK_T/EI = 0.035$ is also included for a more representative bridge analysis. The principal ratios and the beam slab dimensions are comparable to those for the Bartonsville Bridge in Ref. 7.

The difference between composite and non-composite analysis is shown in Fig. 38. The following observations can be deduced from the figure:

1. The beam directly under the load carries a major portion of the total load as a composite structure. The increase in moment coefficients of beams B and C is balanced by the decrease in the moment coefficient of beam A. The remaining difference is carried by the slab.

2. The reduction and the rate of reduction in moment coefficients for the interior beam seems to be almost the same for both composite and non-composite analyses.

The above example shows the necessity of including the eccentricity of the beam when the beams are integrally and eccentrically connected to the slab.

The effect of constraining the supports to rotate about the line of support can be seen in Table 11 for the 45° case. For this problem, it can be seen that the effect is quite negligible.

3.4.3 Load Distribution in a Reinforced Concrete Skew Bridge

An actual reinforced concrete skew bridge has been tested under static loads (Ref. 6). The bridge has a 60° skew, simple span, and with four reinforced concrete beams which are monolithic with the deck slab. The field tests were done by the team of Burdette and Goodpasture of the University of Tennessee (Ref. 6). The bridge is located on U.S. 41A over Elk River, with a span of 50 ft. and beam spacing of 6 ft. 10 in. center-to-center.

The loads are applied as shown in Fig. 39. The distribution of load is shown in Table 12. Good agreement between field test and analytic results can be observed.

3.5 Applications to Highway Bridge Constructions

The method of analysis has several applications to highway bridges. In this section a study is made of the effect of the variables that affect the behavior of beam-slab bridges in general. Field test results where available are also shown. Four cases are investigated:

(1) composite versus non-composite behavior, (2) effect of curbs, parapets and diaphragms, (3) effect of multiple diaphragms, and (4) effect of continuity.

3.5.1 Composite Versus Non-Composite Behavior

For this part of the study, the bridges tested by AASHO in the AASHO road test series (Ref. 24) are used for comparison. The composite bridges, designated 2B and 3B in the report, are shown in Fig. 40. The bridges have three beams, 15 ft. width, and 50 ft. span length. The difference between Bridge 2B with 3B is in the beam section properties as indicated in Fig. 40. The steel I-beams are connected to the slab by shear connectors designed for full composite action. The structure is loaded by a test vehicle with front axle load of 6.8 kips and rear axle load of 14.3 kips. First, the vehicle is positioned with the drive wheel at midspan in the longitudinal direction and at the center of the width in the transverse direction. The structure is then analyzed as a composite bridge and as a non-composite bridge. The percent of the total moment carried by the beams from the field test values and the finite element analyses are listed in the second column of Table 13. The following observation can be made.

1. The finite element results predicted higher percentage of load carried by the beams as a composite structure. The values are comparable with field test results.

2. As expected a higher percentage of the total moment is carried by the beams when acting compositely with the slab.

3. The load carried by the beams is higher for the stiffer beam
    sections.

4. For this type of loading, there is very little difference in
    the percent of load carried by each beam as shown in Table 13.

As a second comparison, the design moments are computed for
each beam and compared to the 1953 provisions of the AASHO. The drive
wheels are placed at midspan and the truck is positioned across the
width that would produce the critical loading condition. The structure
is then analyzed as a composite and non-composite bridge. The com-
parison of distribution factors computed for each case and also from
the field test can be seen in Fig. 41. The comparison shows that the
distribution factor for the center beams is overestimated by the AASHO
specification provision. However, the distribution factor for the
exterior beams is substantially underestimated.

3.5.2 Effect of Curbs, Parapets and Diaphragms

Two field tested bridges, the Lehighton Bridge (Ref. 8) and
the Bartonsville Bridge (Ref. 7) are selected for this study. The
Lehighton Bridge is a six-beam bridge superstructure and 36 ft. wide.
This bridge has a curb and parapet only on one side of the structure.
The bridge was tested first with the midspan diaphragms in place. Sub-
sequent tests were conducted with the midspan diaphragms removed. The
Bartonsville Bridge is a five-beam bridge superstructure and 32 ft.
wide. This bridge has curbs and parapets on both sides of the structure

-74-

and midspan diaphragms. The two bridges were tested by using the test vehicle shown in Fig. 3. The vehicle transversed the bridge over several lanes. These lanes are located directly over the beams and in between the beams (Figs. 42 and 43).

In the actual structure, the diaphragms are monolithic with the slab but are not fully continuous over the beams. The curbs, by construction practice, are not made fully integral with the deck slab; and the parapets are with a number of gaps along the span. Therefore, only a portion of the diaphragm section and the curb and parapet sections can be considered effective.

An analytical study was made on the effect of a partially and fully effective curb and parapets. In the study, the thickness of the slab elements under the curbs and parapets is increased to a thickness that would correspond to the predetermined area of the curb and parapet section. It is found that a partially effective curb and parapet whose cross-sectional area is 50% of the actual area closely approximates the bridge behavior. The good agreement between the field test results and the analytical results using partially effective curb and parapet section can be seen from the uppermost curves of Fig. 42.

In determining the effective section of the diaphragms, the bridge superstructure is first analyzed with truck loads on different lanes of the bridge using the full diaphragm cross-section. The resulting maximum moment is then used in computing the effective moment of inertia as defined by Section 9.5.2.2 of the ACI Code (Ref. 4). For the Lehighton bridge, the effective moment of inertia is computed to be 40%

of the gross moment of inertia. The agreement between field tests and analytical values using 40% effective moment of inertia for the diaphragms can be seen from the lower curves in Fig. 42. However, for the Bartonsville Bridge, a better agreement is obtained using only 20% effective moment of inertia for the diaphragms (Fig. 43). The Bartonsville Bridge and the Lehighton Bridge have diaphragm dimensions of 9" x 34" and 10" x 28" respectively. From the given diaphragm dimensions, approximately 20 ins. of the diaphragm depth are effective for the two cases.

The distribution factors for the Lehighton Bridge are given in Tables 14 for the cases without diaphragms, with diaphragms, partially effective, diaphragms effective only in shear, and diaphragms fully effective. The distribution factors are given for a design lane of 12 ft. with the leftmost lane 2 ft. from the edge of the bridge. Table 15 gives the distribution factors with the leftmost lane starting at the edge of the bridge. It can be seen that the distribution factors depend considerably on the lane locations. Further, it can be seen that the diaphragms with only shear stiffness are practically equivalent to having no diaphragms at all. The distribution factors for the Bartonsville Bridge is given in Table 16.

The effect of curbs, parapets and diaphragms on bridges with three specific widths can be seen in Figs. 44 through 49. The bridges have beam spacing of 8 ft. 0 in. and span of approximately 64 ft. The number of beams are 4, 5 and 7 corresponding to bridge widths of 24, 32, and 48 ft. Influence lines for moment are shown for the exterior

and the interior beams for the following cases: (1) without curb and parapets, (2) with curbs and parapets only, (3) with diaphragms only, and (4) with curbs, parapets and diaphragms. The computed distribution factors are shown in Figs. 50 and 51. The following observations can be made:

1. The curb and parapets and diaphragms provide a more uniform distribution of the load. Consequently, the participation of the exterior beams is increased.

2. The effect of the curb and parapet is negligible for very wide bridges, for example 72 ft. wide.

3. The diaphragms distribute the load efficiently to all the beams of the bridge. However, when the structure is fully loaded, the effect of the diaphragm becomes negligible regardless of the bridge width.

The above observations are for a specific spacing of 8 ft. and a span of 64 ft. For closer spacing which provides a greater lateral distribution effectiveness of the slab, the effect of the diaphragms in distributing the load may be expected to decrease. The effect of the curb and parapet in increasing the participation of the exterior beams may be expected to be more significant.

3.5.3 Effect of Multiple Diaphragms

Very little is known about the effect of several lines of diaphragms across the span of a prestressed concrete I-beam bridge. To

investigate this, a 71 ft. long, 36 ft. wide bridge is analyzed under standard HS20 vehicular load with one, two, three and four lines of diaphragms. The diaphragms are placed equidistant from each other at distances of 1/2, 1/3, 1/4 and 1/5 of the span respectively as shown in Fig. 52. For comparison, the same bridge is also analyzed without diaphragms.

The influence lines for moment for the five different cases are shown in Fig. 53. The computed distribution factors are shown in Fig. 54 and Table 17. The following observations can be made:

1. For the interior beam, the midspan diaphragm is the most effective in distributing the load. The least effective is with diaphragm at L/4.

2. For the exterior beam, a larger participation is induced by the diaphragms at L/4.

3. When the structure is fully loaded, the difference between the multiple diaphragm cases is not very significant.

3.5.4 Effect of Continuity

The purpose of this section is to show the effect of continuity on the lateral distribution of load. First, a comparison of the moment coefficients for a four-span continuous bridge is made between field test results and analysis. Second, a three-span prestressed concrete continuous bridge is analyzed under standard HS20 vehicular loading. In the latter the load distribution behavior at midspan and at the support are shown and discussed.

-78-

The four-span continuous bridge which had been field tested is reported in Ref. 6. The bridge is a 70'-90'-90'-70' composite structure with 36 in. steel I-beams, continuous over the two interior supports and simply supported at the ends. The structure is illustrated in Fig. 55. Computations are made for the beams of the second span. In the first loading condition, the structure is subjected to a University of Tennessee test vehicle traveling over the bridge at crawl speed. The truck has a front wheel load of 7.2 kips, drive wheels of 54.3 kips and rear wheels of 71.0 kips (Fig. 56). Computations for moments are made when the truck is over the second span. In the second loading condition, static loads are placed in the structure as shown in Fig. 55b.

The comparison of moment percentages obtained by field test and analysis is shown in Table 18. Close agreement between test and analysis confirms the applicability of the method of analysis to continuous structure. It should be noted that since the loads are symmetric, the moment coefficients must also be symmetric.

The second span is studied with completely fixed supports and with simple supports. The object of this procedure is to see the effect on the lateral distribution of the load due to different boundary conditions. The results are tabulated in Table 19 for the two load cases. It can be observed that the greatest distribution of load occurs with the simple span, then the continuous span construction and finally the single span with completely fixed supports.

The structure idealization for the three-span continuous prestressed concrete I-beam bridge is shown in Fig. 57. The structure is

a three-lane, six-beam bridge, 36 ft. wide and loaded by standard HS20 vehicles. In determining the moment coefficients at midspan the centroid of the truck is placed at midpoint of the center span. In determining the moment coefficients at the support, a truck is placed on each of the first two spans. The truck is placed on the individual span such that the centroid of the truck load falls at the center of the span. The analyses are then carried out with the truck at different locations across the width of the bridge.

The influence lines for moment at midspan and support for the exterior and interior beams are illustrated in Figs. 58, 59 and 60. For the interior beams, the moment coefficients at the supports are slightly higher than at midspan. However for the exterior beams, the moment coefficients are higher at midspan. In terms of distribution factors as shown in Fig. 61 and Table 20 the difference is very small especially when all the lanes of the structure are loaded.

It is of interest to note that the influence line for moment at midspan is nearly identical to the influence line for moment of a 71 ft. bridge of equal beam spacing. The above can be seen by comparing Fig. 53 and Fig. 60.

3.6 Summary

The analysis of stiffened plates has been presented in this chapter. The method of analysis has been applied to highway beam slab bridges and compared favorably with field test results. The effects of curbs, parapets, diaphragms and continuity have been investigated and evaluated.

-80-

4. LATERAL LOAD DISTRIBUTION IN SKEWED I-BEAM BRIDGES

4.1 Introduction

In the design of beam-slab highway bridges, the live load bending moments are determined with the use of load distribution factors. The distribution factor determines the fraction of the wheel loads that is applied to a longitudinal beam. The applicable distribution factor is given by AASHTO in the Standard Specifications for highway bridges for right bridges (Section 1.5 and Ref. 3). However, as indicated in the scope of the work in Section 1.1, load distribution factors are not given for skew bridges.

This chapter presents the lateral load distribution analysis of skewed beam-slab bridges with prestressed concrete I-beams. Skew bridges of various widths, spacing, span length and number of beams are analyzed using the finite element method of analysis presented in Chapter 3. Live load distribution factors are computed for the interior and exterior beams of the bridges for design vehicle loading. Distribution factors resulting from the critical combination of vehicular loadings are selected and correlated with bridge parameters to arrive at a simplified equation for the distribution factor.

4.2 Beam Moments in Skewed I-Beam Bridges

The HS 20-44 design vehicle as defined in Section 1.1 is used in the following lateral load distribution study (Ref. 2). The moment in a beam produced by one design vehicle placed anywhere on the bridge

is expressed in terms of the moment coefficient. This coefficient is the ratio of the composite beam moment to the total right bridge moment which is numerically equal to the moment produced by the given load on a simple beam of equal span. For convenience, the coefficient is expressed in percent. The plot of the moment coefficients against the lateral position of the load results in the influence line for moment of the beam under consideration.

4.2.1 Computation of Load Distribution Factors

The load distribution factor is applied to the wheel loads in the design of the beams in beam-slab bridges (Ref. 3). This factor can be determined from the plot of the moment coefficients, i.e., influence lines, following the requirements of the AASHTO Specifications (Ref. 3). According to the specification provisions on live load distribution, the design traffic lane must be 12 ft. wide (Fig. 62). The design truck, which occupies 6 ft. of the lane, should be positioned in the lane, and the lane should be positioned on the bridge, such that the loading will produce the maximum moment response for the beam being considered. The same definition of loading applies to bridges with two or more lanes, except that the lanes should not overlap (Ref. 3 and Fig. 62). A minimum distance of 2 ft. is specified between the edges of the lane and the wheel of the design vehicle. The sum of the moment coefficients for the beam at the specified portions of the trucks gives the distribution factor for the particular beam. Thus,

$$D.F. = \frac{\Sigma \text{ moment coefficients } (\%)}{100\%} \qquad (4.1)$$

for axle loading, and

$$D.F. = \frac{2 \Sigma \text{ moment coefficients } (\%)}{100\%} \qquad (4.2)$$

for wheel loading.

The positioning of the truck loads in order to arrive at the maximum distribution factor for a particular beam proceeds as follows. First, a 12 ft. lane is placed on the structure at $x = 0$, where x is the distance of the leftmost boundary of the lane from the leftmost curb (Fig. 62a). Second, a truck load is positioned within the lane such that the highest moment coefficient from the influence line for moment of the beam is obtained. The position of the truck in the lane is determined by the distance x_1 which is greater than or equal to 2 ft. but is less than or equal to 4 ft. to maintain the 2 ft. clearance between the line of wheels and the boundaries of the lane. Third, the lane is moved to a new value of x, e.g. $x = 1$, and the truck is repositioned again within the lane such that the highest moment coefficient value is obtained for this new lane position. The procedure is repeated until the lane has covered the entire width of the birdge. The maximum moment coefficient value obtained in the above process is used in the distribution factor calculation in Eq. 4.2. For two or more design lanes, the corresponding number of lanes is placed on the bridge (Fig. 62b). The second step is repeated for all lanes until all trucks are positioned in each lane that the sum of the moment coefficients is maximum. The lanes are then moved to a new position on the bridge and

the procedure of positioning the trucks in each lane is repeated. The largest sum of the moment coefficients obtained in the above process is used in the distribution factor calculation in Eq. 4.2.

4.2.2 Maximum Beam Moments

The maximum moment caused by the HS 20-44 truck on a simple span right bridge occurs under the drive wheels, when the center of gravity of the wheel loads and the drive wheels are equidistant from the center of the span (Ref. 19). Consequently, in the lateral load distribution analysis of right bridges, the design truck load is placed on the bridge so that the drive wheels are at d/2 distance from midspan where d is the distance from the centroid of the wheel loads to the drive wheels (Ref. 62). The beam moments in the distribution factor calculations are also computed at the section under the drive wheels.

For skew bridges, however, the position of the load that produces the maximum response in a beam, and the location of the beam section where the maximum moment occurs are not known. Moreover, for the same beam, the location of the maximum moment section differs for different lane positions of the truck. The position of the load to produce the maximum moment response, and the location of the maximum moment section in a beam of a skew bridge, are different from those of a right bridge. This feature can be illustrated in the following example.

The structure is a five-beam bridge, 24 ft. wide and 60 ft. long, with a relative beam-to-slab stiffness ratio of 5. The beams are

equally spaced at 6 ft., and the slab is 7-1/2 ins. throughout. The HS 20-44 truck loads are placed one at a time at five positions across the width of the bridge, so that the distance of the centroid of each truck from its consecutive position is 4.5 ft. In each of the lane positions, the longitudinal position of the truck is varied until the maximum moment is obtained for each beam. The distance of the centroid of the truck between longitudinal positions is $d/2 = 2.33$ ft. This distance is selected primarily for convenience, and because the change in the computed moments near the midspan between two consecutive longitudinal positions is less than 1%. The above loading procedure is carried out for each beam of the bridge at skew angle of 90° (right bridge), 45°, and 30° (Figs. 63 through 67). The direction of the truck is always with the front wheels towards the right (Fig. 3). The computed moments are based on the averaged nodal moments.

The positions of the truck centroid and the location of maximum moment in beam A are shown in Fig. 63 for the bridge with skews of 90°, 45° and 30°. While the maximum moment section occurs at $d/2$ from midspan for all angles of skew, the positions of the truck differ for each case. Similar observations can be made for beams B and C (Figs. 64 and 65). For beams D and E, the positions of the truck centroid and the location of the maximum beam moment section are shown in Figs. 66 and 67. In these cases the maximum moment section and the positions of the load are different for different angles of skew. Based on these results, one would expect the critical load position and the location of the maximum beam moment section, to be different for

-85-

another skew bridge with a different number of beams, spacing or span length.

Obviously, there is great difficulty in carrying out the above procedure for all the beams of the bridges that must be investigated in a lateral load distribution analysis. This, however, can be greatly simplified if the maximum moment can be approximated by the moment produced in the beam with the load centroids at midspan.

4.2.3 Beam Moments with Load Centroid at Midspan

In this section, the beam moments in the skew bridge of Section 4.2.2 caused by the HS 20-44 truck loads, but with the load centroids at midspan, are determined. These moments are computed at the beam section d/2 from midspan and in the direction of the obtuse angle corner at the supports. The object of this procedure is to determine if there is a significant difference between these moments and the maximum moments as determined in the previous section.

The moments for beam C with the load centroid at midspan, and the moments from the procedure in Section 4.2.2, are shown in Fig. 68. Moments are shown for the five lane positions across the width at skew angles of 45° and 30°. The figure shows that there is a small difference in the moments between the two load positions. The larger difference occurs at larger skews and at lane loads away from beam C. It is also of interest to compare the moments in beam C with the loads at lane 1 and 5. It can be seen that the larger moment is produced with the truck going in the direction of the acute angle corner of the support, i.e., lane 5 (Figs. 65 and 68).

-86-

The above investigation indicates that the load centroid at midspan can approximate the true load position in producing the maximum moment response in a beam without great loss in accuracy. Also, the beam section at d/2 from midspan and towards the obtuse angle corner at the supports indicates the ideal section to compute the desired moment for the lateral load distribution study.

It should be noted here, however, that in general the distance from the midspan of the beam to the section of maximum moment will not be d/2 for the other bridges. A study of the beam moments in the skew bridges analyzed in Section 4.4, shows that the moment at d/2, if different from the maximum moment, can be in error by 2% for the shorter bridges and less than 1% for the longer ones. However, for practical purposes, the estimated error is within practical design limits.

4.3 Effect of Skew on Load Distribution

In order to gain an initial insight into the behavior of skew bridges and to determine the important parameters that must be considered in load distribution studies, an analytical investigation was carried out for two basic bridge widths. This section presents the findings based on the analyses of thirty bridges with curb-to-curb widths of 24 ft. and 42 ft.

4.3.1 Effect of Skew on Beam Moments

The effect of skew on the individual beam moments is shown in Fig. 69. The bridge analyzed was a five-beam bridge, 60 ft. long and 24 ft. wide with beam spacing of 6 ft. The truck was placed on the skew bridge as it would be placed on a right bridge to produce the maximum moment. The skew angle was then varied and the moment percentages were computed for each case.

The two load positions indicated in Fig. 69 show the shift in distribution of the load for the skew angle changes. The results showed a more uniform distribution of load with decreasing angle of skew. The angle of skew did not have a significant effect on the exterior beam directly under the load. The load distribution in a 60° skew bridge was also not significantly different from the right bridge.

4.3.2 Effect of Skew and Number of Beams

A 24 ft. wide bridge with a span of 60 ft. was analyzed with two design lanes. The truck loads were placed near the center of the bridge section as close as possible to each other as allowed by the 1973 AASHTO Specification (Ref. 3). Beginning with four beams, the number of beams was increased to five and then to six to make up two new sets of bridges keeping the span length constant. Consequently the beam spacing changed from 8 ft. to 6 ft. and 4.75 ft. respectively. For each set, the skew angles investigated were 90° (right bridge), 60°, 45° and 30°. Thus, a total of twelve bridges were analyzed.

Figure 70 shows the distribution factors resulting from the analysis. Also shown for comparison is the current AASHTO specification of S/5.5 (Ref. 3). The distribution factor decreased as the angle of skew decreased. The decrease in the distribution factor was gradual from 90° to 45°. The number of beams and spacing did not seem to affect the rate of reduction.

4.3.3 Effect of Skew with Span Length

The five-beam bridge, 24 ft. wide with 6 ft. beam spacing, was further investigated with different span lengths. In addition to the 60 ft. bridge in Section 4.3.2, the five-beam bridge was analyzed with a span of 30 ft. and 120 ft. The appropriate beam sizes in accordance with the standards for Bridge Design BD-201 (Ref. 43) were used. For each length, the skew angles considered were 90°, 45° and 30°. Distribution factors for the beams were computed based on the critical location of one or two HS 20-44 design vehicle(s) positioned across the width of the bridge. For this initial study, the vehicle was positioned in the longitudinal direction, as it would be placed on the right bridge to produce the maximum moment.

The distribution factors for the beams are seen in Fig. 71. Beams B and C of the 30 ft. series with skews are not shown. For these configurations, one rear wheel and one front wheel were off the bridge so that load distribution comparison with longer bridges was not practical.

-89-

In beam C, the amount of reduction in the distribution factor is marginal from 90° to 45° skew for the lengths considered. However, a considerable change in the rate of reduction was observed for skew angles less than 45°. Also, for the long span bridges, the rate or reduction decreases as the skew angle decreases.

Exterior beam A had practically no reduction in the distribution factor as the angle of skew decreased, except for the 30 ft. case. It should be noted that for the 30 ft. span and small skew angles some of the wheels of the vehicle were off the bridge.

4.3.4 Effect of Skew on Distribution Factor versus S/L

The plots of the distribution factors versus S/L for the 24 ft. wide bridges with five beams and at skew angles of 90°, 45°, and 30° are shown in Fig. 72. Similar plots for the 42 ft. wide bridges with six beams are shown in Fig. 73. The span lengths investigated were 30 ft., 60 ft., and 120 ft. for the 24 ft. wide bridges; and 42 ft., 59 ft., and 101 ft. for the 42 ft. wide bridges. These dimensions correspond to W_c/L ratio of 0.80, 0.40, and 0.20 for the 24 ft. wide bridges and 1.0, 0.70 and 0.42 for the 42 ft. wide bridges.

The two figures indicate that at a high S/L ratio there is a larger decrease in the distribution factor as the skew angle decreases. Furthermore, the decrease in the distribution factor is larger at smaller skew angles for the wider bridge. The above results imply that the aspect ratio of the bridge is an important parameter which governs the amount of reduction with the skew.

-90-

4.4 Load Distribution in Skewed Beam-Slab Bridges

with Prestressed Concrete I-Beams

In the development of the distribution factor formula for right bridges, about 300 bridges were investigated (Ref. 62). These bridges varied in width, number of beams, and span length to cover the bridge configurations encountered in practice. In this section, thirty of these representative right bridges were selected and each one was analyzed for skew angles of 90° (right bridge), 60°, 45°, and 30°. Thus, in effect a total of 120 bridges were analyzed.

4.4.1 Design of the Experiment

The bridges analyzed with different skew angles are listed in Table 21. The basic widths considered were 24, 48 and 72 ft., curb-to-curb. The number of beams were varied from 4 to 16, and consequently, the beam spacings varied from 4'-10" to 9'-6". Different lengths ranging from 36'-0" to 120' inclusive were used. The details in the design of a particular bridge are discussed in Ref. 62. Reference 43 was used in the determination of beam properties.

4.4.2 Distribution Factors in Skew Bridges

With the use of the procedure outlined in Section 4.2.1, distribution factors were computed for all the interior and exterior beams. Distribution factors were computed based on one up to the maximum number of design lanes that can be placed on a given bridge width. The maximum interior and exterior beam distribution factors for each

bridge were selected and are listed in Tables 22 and 23 respectively.
The full list of distribution factors for different design lanes can be
found in Ref. 12.

The interior beam distribution factors for the 24 ft. wide
bridges with four, five and six beams are plotted against S/L in
Fig. 74. Similar plots are presented for the 48 ft. wide bridges with
six, nine and eleven beams in Fig. 75, and for the 72 ft. wide bridges
with nine, twelve, and sixteen beams in Fig. 76. In addition to the
observations made in Section 4.3, the following can be seen from the
figures:

1. The rate of reduction is usually larger for larger spacing,
   for wider bridges and at smaller angles of skew.

2. There is, however, a limit to the increase in the rate of
   reduction.

The second observation may be interpreted as follows. At
large spacing and short spans the lateral distribution of the load is
small and hence the distribution factor is small. At narrow beam spac-
ing, the distribution factor is also small. Consequently, the amount
of reduction because of the skew is found to be relatively smaller for
these cases. The influence line plots for moments in the individual
beams in this study are given in Ref. 12.

The plots of the maximum distribution factors for the exter-
ior beams against the S/L ratio are shown in Figs. 77, 78, and 79 for
the three bridge widths. Compared to the interior beams, a similar but

but smaller reduction in the distribution factor was observed for the shorter bridges. However, an increase in the distribution factor was observed at longer bridge spans. The increase in the distribution factor may be attributed to the greater participation of the exterior beams when the bridge has a skew.

4.4.3 Development of the Distribution Factor Equation

The distribution factors for prestressed concrete I-beam bridges with no skew is the subject of a comprehensive study in Ref. 62. It is therefore the aim of this section to provide only the reduction factor for these bridges given the angle of skew.

The reduction factor in the interior beams in a given bridge is computed from the amount of reduction in the beam distribution factor using the right bridge (90° skew) with the same width, number of beams and span length as the base. These reduction factors are expressed as percent reductions, and are always zero for right bridges. With the use of the Lehigh University Amalgamated Package for Statistics, LEAPS (Ref. 30), the correlation of the percent reduction with variables such as skew angle, span length, number of beams, number of loaded lanes, bridge width and their combinations was investigated. The variables found to have good correlation with the percent reduction were the spacing-to-length ratio S/L and the bridge width-to-span ratio W_c/L in combination with the square of the cotangent of the skew angle. A regression analysis of the percent reduction against these variables resulted in the following equation:

$$PCTR = \left(45 \frac{S}{L} + 2 \frac{W_c}{L} \right) \cot^2 \phi \qquad (4.3)$$

where   PCTR = Applicable reduction factor in percent to the distribution factor of the interior beam of a right bridge with the given S, W_c, and L

     S   = Beam spacing

     L   = Span length

     ϕ = Skew angle

For the exterior beams, a simplified equation was determined by trial and error and proposed as follows:

$$PCTR_{(EXT)} = 50 \left(\frac{S}{L} - 0.12 \right) \cot \phi \qquad (4.4)$$

where $PCTR_{(EXT)}$ = Applicable reduction (positive) or amplification (negative) to the distribution factor of the exterior beams of a right bridge with the given S, W_c and L.

The above equations are limited to the following bridge dimensions:

$$4'-6'' \leq S \leq 9'-0''$$

$$48'-0'' \leq L \leq 120'-0''$$

$$30° \leq \phi \leq 90°$$

The computed distribution factors and the percent reductions based on the above equations and the analytical results for the bridges investigated are listed in Ref. 12. The equation is found to be conservative in most cases except the case of the large spacing, 30° skew and very short span. The plots of the proposed equation for the interior beams are shown in Figs. 80, 81 and 82 for the bridges investigated.

4.5 Design Recommendations

From the results of this study, the following simplified procedures are recommended for the determination of the live load distribution factors in prestressed concrete I-beam bridges with skew:

1. The load distribution factors in the interior beams may be determined by applying to the distribution factor in the interior beams of the bridge without the skew a reduction specified by the following formula:

$$DF_\phi = DF_{90} \left(1.0 - \frac{PCTR}{100} \right) \tag{4.5}$$

where DF_ϕ = Distribution factor for the interior beam of the bridge with skew angle ϕ

DF_{90} = Distribution factor for the interior beam of the bridge without skew, and

PCTR = Reduction in percent as specified by Eq. 4.3.

2. The load distribution factors in the exterior beams shall be determined by applying to the distribution factor in the

exterior beams of the bridge without the skew a factor speci-
fied by the following formula:

$$DF_{\phi(EXT)} = DF_{90(EXT)} \left(1.0 - \frac{PCTR_{(EXT)}}{100} \right) \qquad (4.6)$$

where $DF_{\phi(EXT)}$ = Distribution factor in the exterior beam of
the bridge with skew angle ϕ

$DF_{90(EXT)}$ = Distribution factor in the exterior beam of
the bridge without skew, and

PCTR = Amplification or reduction factor as speci-
fied by Eq. 4.4

A plot of the smallest and the largest percent reduction in
the distribution factors for interior beams using the proposed equation
and the bridge dimensions investigated in this study is shown in
Fig. 83. A similar plot for the exterior beams is shown in Fig. 84.

4.6 Summary

The load distribution behavior of skewed I-beam bridges under
design vehicular loads have been presented. Load distribution factors
were computed for the interior and exterior beams of bridges with pre-
stressed concrete I-beams. The skew angles investigated were 90°, 60°,
45° and 30°. In the analyzed bridges, the following were observed:

1. The load distribution factor decreases with decreasing angle
of skew.

2. The rate of reduction in the distribution factor is gruadual from 90° to 45° but is abrupt from 45° to 30°.

3. The rate of reduction in the distribution factor decreases with increasing span length.

4. The bridge width-to-span ratio, and beam spacing-to-span ratio largely affects the amout of reduction.

Based on the statistical correlation of the bridge parameters with the numberical results, simplified distribution factor formulae were obtained for the interior and exterior beams.

5. LATERAL LOAD DISTRIBUTION IN SKEWED SPREAD BOX-BEAM BRIDGES

5.1 Introduction

The spread box-beam bridge (Fig. 1b) is one of the more recent developments in bridge design practice. The load distribution characteristics for this type of bridge have been the subject of several investigations (Section 1.1.2 of Ref. 63). Extensive field investigations of spread box-beam bridges have been carried out by Lehigh University (Refs. 16, 21, 22, 31, 51, 57). Except for Ref. 51, all of the above investigations have been for right bridges.

The investigations confirmed the need for a realistic live load distribution procedure for spread box-beam bridges with and without skew. The theoretical analysis developed by Motarjemi and VanHorn (Ref. 38) provided a new specification provision for lateral load distribution for right bridges with prestressed concrete spread box-beams (Ref. 2). This chapter presents an analysis procedure for right and skew box-beam bridges. Through the application of the method, formulae have been determined for the lateral load distribution for skewed spread box-beam bridges.

The developed analysis scheme employs finite element concept and method of solution discussed in Chapter 1. The bridge superstructure is treated as an assemblage of plate and web finite elements (Fig. 5). Plate finite elements in Chapter 2 model the deck slab and the bottom plate of the box-beam. Web finite elements

which are introduced in this chapter, model the sides of the box-beams. Following the procedures outlined in Chapter 3 for the assembly of the elements and the solution of the resulting equations, the validity of the modeling is checked through comparisons of analytical results with field test values. The method is then applied to the analysis of 72 spread box-beam bridges with skew angles of 90°, 60°, 45° or 30°.

Using the results, the load distribution behavior of spread box-beam bridges is presented and a load distribution procedure is developed. Because of the limited number of bridges in the analysis scheme, and the limited scope of the loading investigated, the presented load distribution formulae can be considered as tentative.

5.2 Theoretical Development

The analytical procedure in the analysis of box-beam bridges is similar to the analysis of stiffened plates described in Chapter 3. Instead of eccentric beam elements, web plate elements which can model the sides of the box-beams are used (Fig. 5). The element has top and bottom nodes to interconnect with the deck slab and the bottom plate of a box-beam. The in-plane and out-of-plane behavior of the webs are considered.

In this analysis, the top plate of the box-beam segment is incorporated into the deck slab by adding its thickness to the corresponding deck element (for example see Fig. 94). The bottom

-99-

plate is represented by the plate element which is also used for the deck slab. The formulation, description, and accuracy of the deck and bottom plate elements are described in Chapter 2 and are not repeated here. The in-plane and out-of-plane behavior of the web element are formulated separately and are combined in a procedure analogous to the deck elements as described in Section 3.3.2.

The analysis of spread box-beam bridges presents a problem in the computer storage requirements. Because of the large difference in the node numbers of the assembled elements, the size of the bandwidth, which determines the amount of computer storage needed, becomes excessively large. The number of elements and the resulting system of equations are also larger than a corresponding I-beam bridge with equal number of beams. Consequently, the computational effort for any given analysis is substantial. In an analysis procedure investigated, the solution of a very large system of equations requires very extensive computational effort. The necessity, therefore, of using the minimum number of elements and at the same time obtaining a reasonable amount of accuracy is apparent. In this part of the investigation, emphasis was given to the selection of the web element that can represent the webs of the box-beams with one element through the depth. As in any structural analysis problem, care was taken in the numbering scheme to minimize the bandwidth.

5.2.1 In-Plane Stiffness Formulation

The in-plane behavior of the web element is approximated by a quadrilateral with four nodes and twelve degrees of freedom (Fig.

85). The degrees of freedom are represented by the components of the vector $\{r_w\}$ where

$$\{r_w\}^T = \{u_1 \quad w_1 \quad \theta_{y1} \quad u_2 \quad w_2 \quad \theta_{y2} \quad u_3 \quad w_3 \quad \theta_{y3} \quad u_4 \quad w_4 \quad \theta_{y4}\} \qquad (5.1)$$

The element displacement field, proposed by William in Ref. 59 for the web of cellular structures, is used. The element describes a u displacement which is linear in the ζ direction, and a w displacement which is cubic in the ζ direction and linear in the η direction. The displacement field associated with the local derivatives at the nodes is defined also by a cubic function (Ref. 60). The element is known as the Q8SP12 element. The derivation of the element stiffness matrix is given by William in Ref. 59 and is outlined in Appendix C.

5.2.2 Bending Stiffness Formulation

The out-of-plane behavior of the web is represented by a rectangular element with out-of-plane bending about the x-axis only. Bending about the z-axis is ignored. The assumption for the element is that one-way bending is the dominant action in the out-of-plane behavior of the web in a box-beam structure. The geometric description and nodal configuration are shown in Fig. 85b.

Assuming no interaction between the pairs of nodes 1 and 4 and 2 and 3, elementary out-of-plane beam theory can be used to form the stiffness matrix of the element (Refs. 59, 60).

$$
\begin{Bmatrix}
V_1 \\[4pt]
M_{x1} \\[4pt]
V_2 \\[4pt]
M_{x2} \\[4pt]
V_3 \\[4pt]
M_{x3} \\[4pt]
V_4 \\[4pt]
M_{x4}
\end{Bmatrix}
=
\frac{Eb^3}{12}
\begin{bmatrix}
\dfrac{12}{a^3} & \dfrac{6}{a^2} & 0 & 0 & 0 & 0 & -\dfrac{12}{a^3} & \dfrac{6}{a^2} \\[8pt]
 & \dfrac{4}{a} & 0 & 0 & 0 & 0 & -\dfrac{6}{a^2} & \dfrac{2}{a} \\[8pt]
 & & \dfrac{12}{a^3} & \dfrac{6}{a^2} & -\dfrac{12}{a^3} & \dfrac{6}{a^2} & 0 & 0 \\[8pt]
 & & & \dfrac{4}{a} & -\dfrac{6}{a^2} & \dfrac{2}{a} & 0 & 0 \\[8pt]
 & & & & \dfrac{12}{a^3} & -\dfrac{6}{a^2} & 0 & 0 \\[8pt]
 & & & & & \dfrac{4}{a} & 0 & 0 \\[8pt]
 & \text{symmetric} & & & & & \dfrac{12}{a^3} & -\dfrac{6}{a^2} \\[8pt]
 & & & & & & & \dfrac{4}{a}
\end{bmatrix}
\begin{Bmatrix}
v_1 \\[4pt]
\theta_{x1} \\[4pt]
v_2 \\[4pt]
\theta_{x2} \\[4pt]
v_3 \\[4pt]
\theta_{x3} \\[4pt]
v_4 \\[4pt]
\theta_{x4}
\end{Bmatrix}
$$

$$(5.2)$$

It should be noted that the one-way bending assumption for the out-of-plane behavior violates continuity with the deck and bottom plate elements.

5.3 Numerical Examples and Comparisons

In this section, a cantilevered beam, a simple beam, and a simple box-beam are analyzed with the use of the web element des-cribed in Section 5.2. Comparisons of analytical results are made with the solution using conventional beam theory for the cantilevered

beam and the simple beam problems, and the thin-walled elastic beam
theory for the simple box-beam problem.

The purpose of this section is to show the accuracy of the
finite element results with the use of the web element even at very
coarse discretization.

5.3.1 Cantilevered Beam Analysis

The cantilevered beam problem is shown in Fig. 86. The
structure is discretized into two different mesh schemes, each con-
sidering two types of boundary conditions at the support: fixed in
u, w with free θ_y; and fixed in u, w, and θ_y. The beam is loaded
at the tip with a concentrated load of 40 kips. The loading and
boundary condition idealizations are shown in Figs. 86a and 86b.

The finite element results for deflection and stresses are
given in Table 24. The analysis gives a good agreement with theory.
It can also be noted from the results that fixing the rotation at
the support does not affect the results to any great extent. More
important, however, is the fact that the use of a one-web element
through the depth of the beam gives just about the same accuracy
as with two elements through the depth.

5.3.2 Simply-Supported Beam Analysis

A similar comparison is made for a simply-supported beam
with a concentrated load at the center. The span length of the
beam is varied from 4d to 32d, where d is the depth of the beam.
Due to symmetry, only one-half of the structure is analyzed. Only
4 elements are used along the length to model the half span. The

purpose of this comparison is to show the behavior of the element

at various aspect ratios. Deflections are computed at midspan and

stresses are computed at 3/8 of the span for aspect ratios of 4, 8,

16 and 32. The results are listed in Table 25. The theoretical

values using classical beam theory with shear connections are shown

for comparison.

The close agreement of the analytical results, even at

very large aspect ratios, can be seen. Furthermore, good agreement

is again obtained with the use of a few number of elements.

5.3.3 Single Box-Beam Analysis

A steel box-beam composite with a reinforced concrete deck

is simply supported at two ends. The plan and elevation of the

structure is shown in Fig. 87. The experimental and theoretical

results for this problem under a symmetric and unsymmetric concen-

trated load at midspan are reported in Ref. 61. The theoretical

results were obtained by using thin-walled elastic beam theory.

Experimental results were obtained from the tests conducted at Fritz

Engineering Laboratory (Ref. 61). A comparison of normal stresses

at a midspan section among theoretical, finite elements, and test

values is made to check the accuracy of the combined elements.

The finite element model and the discretization employed

for the box-beam structure are shown in Figs. 88 and 89. Only one

element over the depth is chosen to idealize the webs. Furthermore,

one plate element is used to model the bottom plate, and three plate

elements are used to model the top deck in the transverse direction.

It should be noted that this discretization is the coarsest possible in the transverse direction. In the longitudinal direction 6 elements are employed with finer mesh sizes used near the midspan (Fig. 89). The diaphragms are also idealized by web elements.

The structure is investigated for two loading conditions: (a) a concentrated load of 18 kips at midspan and symmetric between the two webs (Fig. 90) and (b) a concentrated load of 18 kips at midspan and directly over the web (Fig. 91). The computed normal stresses at the indicated cross section are also shown in the figures. Superimposed on the stresses are the values reported in Ref. 61. Good agreement is observed between theory, finite element analysis and test results. A check of the total cross-sectional moment computed by integrating the stresses at the section result in a moment which is within 95% of the moment obtained by equilibrium.

5.4 <u>Application of the Method of Analysis to Highway Spread Box-Beam Bridges</u>

With the method of analysis presented in Section 5.2, there is no conceptual difference between the analysis of a single box-beam structure and a multi-beam bridge superstructure. As such, the method can be used directly in the analysis of spread box-beam bridges. Since the generated elements are general quadrilaterals, the method is also applicable to skew spread box-beam bridges. The accuracy of the method of analysis is demonstrated by the following comparisons with field test values.

-105-

Two comparisons are made with actual spread box-beam bridges which have been field tested. The first comparison is with the Berwick Bridge which is a 90° skew, i. e. right bridge. The second comparison is with the Brookville Bridge which has similar dimensions to the Berwick except for a skew of 45°. Bridge dimensions are shown in Fig. 92. In both cases, only one web element is used over the depth and only one plate element is used across each beam width and spacing in the finite element discretization.

5.4.1 Comparison with a Right Spread Box-Beam Bridge

The field testing of the Berwick Bridge is reported in Ref. 22. The cross-sectional dimensions of the Berwick Bridge are indicated in Fig. 92. The bridge span, center-to-center of bearing, is 66 ft., the roadway width is 28 ft. and the 48 in. prestressed concrete box-beams are equally spaced at 8'-9-3/8". The finite element discretization in the plan is shown in Fig. 93. The idealization of the cross section is shown in Fig. 94. In the analysis, the top part of the box-beam is included by adding its thickness to the corresponding plate element. The curbs and parapets are modeled by increasing the thickness of the overhang as shown in Fig. 94. Two methods of modeling the curbs and parapets are investigated. First, the thickness of the overhang is increased so that the resulting cross-sectional area is equal to the cross-sectional area of the curb and parapet with the slab. Second, the thickness of the overhang is increased so that the resulting area is equal to 1/2 the area of the curb and parapets and the full area of the slab. The second model is investigated because, by current construction

-106-

practice, the curbs are not fully integrated with the deck slab and the parapets have construction gaps along the length. It is assumed that because of this practice, the curb and parapets are only 50% effective.

The structure is loaded by the test vehicle shown in Fig. 3. The vehicle is placed at 5 positions in the transverse direction, as indicated by the lane number in Fig. 92. In the longitudinal direction, the truck is positioned so that the drive wheels are 42.6 inches to the right of midspan. This loading corresponds to the loading position that will produce the maximum moment in a simple beam of equal span under the given load configuration. This loading position also produces the maximum moment directly under the drive wheels.

Table 26 lists the distribution coefficients at section M, which is the section directly under the drive wheels for the two cases studied. Shown also for comparison are the results from the tests on the Plexiglass model reported in Ref. 32. The analytical results, based on a 50% effective curb and parapets, agree closely with the field test values. The agreement for all the beams at all load cases can be seen in Fig. 95.

The following conclusions can be made based on the above comparison:

    a) The curbs and parapets are only partially effective. A 50% effectiveness of the curb and parapet is a reasonable assumption.

b) The discretization of the structure with 6 elements along

    the length, and one element for each box-beam width and

    for each spacing gives acceptable results.

It should be noted however that the results compared are
for the overall behavior of the bridge. Finer discretization should
still be used in order to obtain critical stresses of the bridge
components.

5.4.2 Comparison with a 45° Skew Box-Beam Bridge

The section of the Brookville Bridge is superimposed on
Fig. 92 on the Berwick Bridge section. From the indicated dimensions
for each bridge at the bottom of the figure, the cross sections of
the two bridges are practically the same.

The differences between the two bridges are in the skew and
the beam size. The Brookville Bridge has a 45° (Fig. 96) and the
beams are 36 in. deep prestressed concrete box-sections. There are
also minor differences in the curb and parapet sections. Details
of the bridge can be found in Ref. 51.

The idealization of the skew box-beam structure into plate
and web elements can be seen in Fig. 97 in plan and in Fig. 98 in
section. The modeling scheme used for the Berwick Bridge is also
adopted in this study. The two methods of modeling the curb and
parapets are again used for this bridge. In both analyses, moments
are computed at Section I for interior beam C and Section E_1 for
exterior beam D.

-108-

The test vehicle (Fig. 3) is used to load the bridge at the different lane locations indicated in Fig. 99. In the longitudinal directions, the positions are as reported in Ref. 51. The longitudinal positions of the test vehicle are different for sections I and E_1, and are dependent on the direction of the vehicle. For this study, the direction of the test vehicle is from left to right of plan shown in Fig. 96. The reported longitudinal positions that produced the maximum moment response in this direction at the skew midspan are used.

Figure 99 shows the plot of the moment coefficients for beam C at beam section I against the vehicle lane locations. The moment coefficients are computed by dividing the actual beam moment with the elastic modulus (Ref. 51). The plot shows the results of the finite element analysis using fully and partially effective curbs and parapets and the reported values. A similar plot is drawn for section E_1 of the exterior beam in Fig. 100. Both figures indicate a better correlation with test values when the curbs and parapets are only partially effective.

The positioning of the vehicle in the longitudinal direction for each lane, however, is inconvenient because this position is not known initially, and may be expected to differ for different bridge configurations. A study, therefore, was conducted to determine the difference between the moment coefficients when the load is at the position which produces the maximum response and when the drive axle is at the skew midspan. The latter choice is simply a

-109-

convenience so that a consistent loading scheme for all the lanes can be adopted. The difference in the moment coefficients between the two load positions can be seen in Table 27. The smallest difference occurs when the load is directly over the beam considered for the analytical values. Compared, however, with the reported moment coefficients from field tests, the difference with the drive axle at midspan is not significant.

The conclusions made for the right spread box-beam bridge are also the conclusions for the skewed spread box-beam bridge. In addition, the load position with the drive axle at midspan may be used instead of the more exact position.

5.5 Lateral Load Distribution in Skewed Box-Beam Bridges

Load distribution factors in box-beam bridges are computed in the same manner as in I-beam bridges. In the following study the procedure of computing the maximum distribution factors for both the interior and exterior beams by loading one lane at a time and positioning the lanes across the width of the bridge and then finding the combination of lane loads that would produce the maximum distribution factor is not used. For the box-beam bridges the structure is loaded only once with the maximum number of lane loads that can be placed on a given bridge width. The vehicles are placed within the lane so that they are as close as possible towards the interior lane. The distribution factors for the interior and exterior beams are computed using this loading configuration.

The simplified procedure mentioned above is adopted for two reasons. First, the analysis of multi-beam box girder bridges involves the solution of a very large system of equations for each load configuration. With the number of bridges and skew angles that have to be considered in order to cover reasonably the range of box girder geometries, the analysis of each bridge under many individual lane loads becomes impractical. Secondly, the influence lines for moments in box girder bridges are more or less flat (Refs. 22, 51 and Figs. 95, 99). The flatness of the influence line suggests that the case with all the lanes loaded produces the maximum moment in a box-beam bridge and hence the maximum distribution factor.

In the following analyses of box girder bridges, HS20-44 standard trucks are placed on all lanes that can be placed in a given bridge width. The longitudinal positions of the trucks are such that all the drive axles fall on the skew centerline. The rear axles of the trucks are towards the obtuse angle at the supports.

5.5.1 Design of the Experiment

The selection of the analytical bridges including the determination of the variables for each bridge, is called the design of the experiment. The importance of this part in the investigation is the determination of the different widths, number of beams, span length and skew angles that will represent the general behavior of spread box-beam bridges.

The box-beams selected in this study are listed in Table 28. The 18 bridges on the list are each investigated at skew angles

of 90°, 60°, 45° and 30°. Because of the new lane width definition

in the current specifications (Ref. 3) the bridge widths considered

are different from those used in Ref. 34 for the right bridges. The

widths considered are 24 ft., 48 ft., and 72 ft. corresponding to

12 foot lane widths for 2, 4 and 6 design lanes respectively (Ref. 3).

These bridge widths are from curb to curb and do not include the over-

hang of 2 ft. on each side of the bridge. A uniform thickness of

7-1/2 inches is used for the deck slab. Curbs, parapets and dia-

phragms are not considered. One size of beam a 48/48 (Ref. 43) pre-

stressed concrete box-beam, 48" wide and 48" high, is used for all

the beams in all the bridges.

5.5.2 Load Distribution Factors in Skewed Box-Beam Bridges

The computed distribution factors for the interior box-

beams of bridges with skews of 90°, 60°, 45° and 30° are listed in

Table 28. The distribution factors for the exterior beams are

listed in Table 29. The distribution factors are computed based on

the full loading scheme, described in Section 5.5. These distri-

bution factors are plotted against the bridge S/L ratio in Figs.

101, 102 and 103 for interior beams and Figs. 104, 105 and 106 for

the exterior beams.

The following observations can be made for the loading

considered (Figs. 101 to 106):

1) The effect of skew is to significantly reduce the

distribution factor for the interior and exterior

beams.

-112-

2) There is a monotonic decrease in the distribution factors with decreasing skew angle.

3) The reduction factor is largest at shorter span lengths for interior beams and at longer span lengths for exterior beams (for example see Figs. 101 and 104). The reason for this behavior is primarily the increased participation of the exterior beams at longer spans.

The significant reduction in the distribution factors because of the skew can be attributed to the principal bending of the bridge being in the direction of the skew and not in the direction of the span. The cross-sectional geometry of the bridge is also such that there is a better lateral distribution of the loads and consequently a better participation of all the beams.

The larger reduction in the distribution factors at shorter span lengths for the interior beams can be attributed to the fact that at large skews some of the wheels of the vehicular load are off the bridge or very near the supports. This reduction, however, is considerably larger than is typical of a corresponding prestressed concrete I-beam bridge.

It is not possible though to make a general conclusion for the load distribution behavior of the exterior beams. The loading scheme as described in Section 5.5 produces the maximum moment response for the most interior beam and therefore can not be expected to produce the maximum moment response for the exterior beams.

5.6 Proposed Lateral Distribution Provisions

A simplified method for the determination of live-load distribution factors for the interior beams of spread box-beam bridges is presented in this section. The process in the development of this design procedure is similar to the prestressed concrete I-beam analysis. Because of the limited number of bridges and the limited scope of the loading, only a tentative design recommendation is made. The simplified equation, within the specified limits, conservatively predicts the distribution factors for the skew bridges investigated.

The live load bending moment in the interior beams of skewed spread box-beam bridges may be determined by applying to the beams the fraction of the wheel load specified by the following formula:

$$DF_{\emptyset} = DF_{90} \left(1 - \frac{PCTR_{(Box)}}{100}\right) \qquad (5.1)$$

where

$$PCTR_{(Box)} = \frac{5000 \cot \emptyset}{L + 64}$$

and

DF_{90} = distribution factor for the interior beam of a right bridge with the same spacing and span length.

$DF_{\emptyset}$ = the distribution factor for the interior beam of the bridge with skew angle $\emptyset$.

The above equation is limited to the following bridge dimensions:

$$24' \leq W_C \leq 72'$$

$$42' \leq L \leq 128'$$

The plot of $DF_\emptyset/DF_{90}$ using the equation for the 34 and 128 ft. span is shown in Fig. 107. A comparison of the equation with the measured values is given in Ref. 12.

6. SUMMARY, CONCLUSIONS, AND RECOMMENDATIONS FOR FUTURE RESEARCH

6.1 Summary

The lateral load distribution behavior of skew I-beam and box-beam highway bridges has been presented. The technique employed was the finite element method. Live load distribution factors were computed for 120 skew bridges with prestressed concrete I-beams and for 72 skew bridges with prestressed concrete box-beams. The bridges were subjected to design HS20-44 vehicular loadings. From the results, simplified design procedures for the determination of live-load moments in the interior and exterior beams of skew bridges were developed.

In the method of analysis, plate and beam finite elements were used to model the bridge structure. Quadrilateral plate elements with in-plane and out-of-plane behavior represented the deck slab of the bridge and the top and bottom plate of the box-beams. Eccentric beam elements represented the I-beams, and web finite elements modeled the webs of the box-beams. The general concepts and the structural idealizations with the use of the finite element method were described in Chapter 1.

The in-plane and out-of-plane behavior of the quadrilateral plates as skew plates representing the deck slab were presented in Chapter 2. The accuracy of the finite elements used for the deck

slab was verified through comparisons with available solutions and test data.

In Chapter 3, the eccentric beam finite elements were introduced. The plate elements of Chapter 2 were then combined with the beam elements to model plates with eccentric stiffeners. The method was then applied to highway bridges with I-beams. The effects of curbs, parapets and diaphragms on lateral load distribution were also investigated. The applicability of the method of analysis to multi-span continuous bridges was demonstrated. The validity of the modeling and the overall analysis were verified by the results of the comparisons with four field tested I-beam bridges.

In Chapter 4, the load distribution analyses of the skew bridges with prestressed concrete I-beams were presented. Load distribution factors were determined for interior and exterior beams of the bridges under the critical loading pattern of HS20-44 vehicular loads. The behavior of the load distribution factors with skew and the major bridge parameters were illustrated. Based upon the results, a simplified design procedure for the determination of load distribution factors for I-beam bridges with skew was developed.

The skew bridges with prestressed concrete box-beams were analyzed in Chapter 5. Load distribution factors were determined for the interior and exterior box-beams based on a full load of HS20 trucks. The behavior of the beam distribution factors with the skew and the bridge parameters was demonstrated. The validity of the model and the method of analysis was shown through comparisons

-116-

with two field-tested spread box-beam bridges. A simplified design procedure for the determination of load distribution factors for box-beam bridges with skew was developed.

6.2 Conclusions

The finite element method has proven to be efficient and accurate in the analysis of skewed beam-slab structures. The applicability of the method for a load distribution analysis has been demonstrated for bridges with I-beams or with box-beams.

The following conclusions are made for the load distribution study:

For the prestressed concrete I-beam bridges,

1. The effect of skew is generally to reduce the distribution factors for the interior beams when compared to a right bridge of equal span and beam spacing. The distribution factors for the exterior beams are increased by a small amount for the bridges with beam spacing to span ratio less than 1/8.

2. The reduction in the distribution factor is minimal from 90° skew to 60° skew but becomes significant at skews beyond 45°. The reduction is influenced to a large degree by (a) beam spacing to span length ratio, and (b) bridge curb-to-curb width to span length ratio.

-117-

3. The amount of reduction can be predicted by the trigonometric function in the form presented in Section 4.5.

4. The effect of the curbs and parapets is to reduce the load carried by the interior beams and to increase the load carried by the exterior beams. However, for wider bridges, this effect is considerably diminished. Also the curbs and parapets may be considered only 50% effective based on the construction practice of not fully integrating the curbs and parapets with the deck slab.

5. The effect of the diaphragms is to distribute the load more uniformly to the beams of the bridge. However, for bridges which are fully loaded, this effect is not significant. For all practical purposes, one line of diaphragms at midspan is quite effective in distributing a given load compared to several lines of diaphragms along the span.

6. The effect of continuity is to distribute the load more efficiently to the different beams in a multi-span bridge. Based on the findings, strong consideration should be given to the design of multi-span bridges with distribution factors for continuous beam-slab structures.

For the prestressed concrete box-beam bridges,

1. The effect of the skew is to significantly reduce the distribution factors for the interior and exterior beams when compared to a right bridge of equal span and spacing. It should be noted, however, that this behavior is based only on a fully loaded bridge with the loads placed as close as possible towards the middle of the bridge width.

2. The amount of reduction can be predicted by the trigonometric function in the form presented in Section 5.6.

6.3 Recommendations for Future Studies

The analysis procedure developed in this research is applicable to beam-slab bridges, with or without skew. The following areas are recommended for future research:

1. Load distribution in skewed beam-slab bridges with curbs and parapets.

2. Load distribution in skewed beam-slab bridges with diaphragms perpendicular to the beam or in the direction of the skew.

3. Load distribution in beam-slab bridges with non-parallel skews.

4. Load distribution in composite steel I-beam bridges.

5. Load distribution in multi-span continuous

    beam slab bridges.

The above areas can be investigated with the analytical

procedures developed and presented herein.

TABLE 1

IN-PLANE DISPLACEMENTS AND STRESSES IN
A SQUARE PLATE UNDER UNIFORM EDGE LOADING (Fig. 10a)

Node	Quantity[1]	Q8D11	CST[2] (Ref. 52)	Exact
5	u	1.66667	1.66667	1.66667
	v	0.	0.	0.
	σ_x	1.0	0.99995	1.0
	σ_y	0.	0.00149	0.
	τ_{xy}	0.	0.00161	0.
9	u	3.33333	3.33333	3.33333
	v	0.25	0.25	0.25
	σ_x	1.0	0.99368	1.0
	σ_y	0.	0.00065	0.
	τ_{xy}	0.	0.00015	0.

[1] u, v displacements in inches, σ_x, σ_y, τ_{xy} stresses in ksi.

[2] .1% solution accuracy specified.

TABLE 2

IN-PLANE DISPLACEMENTS AND STRESSES IN
A SQUARE PLATE UNDER IN-PLANE SHEAR (Fig.10b)

Quantity[1]	Q8D11	CST[2] (Ref. 52)	Exact
σ_x	0.	0.00083	0.
σ_y	0.	0.00093	0.
τ_{xy}	0.13333	0.13284	0.13333
σ_{11}, σ_{22}, σ_{12}	0.13333	0.13196	0.13333
γ_{xy}	0.1022×10^{-3}	0.1138×10^{-3}	0.1023×10^{-3}

[1] stresses in ksi.

[2] .1% solution accuracy specified.

TABLE 3

DISPLACEMENTS AND STRESSES IN A SKEW PLATE
UNDER UNIFORM EDGE LOADING (Fig. 11)

u - Displacements(in.)			v - Displacements(in.)		
Node	Q8D11	CST	Node	Q8D11	CST
1	0.	0.	1	-0.000306	-0.000308
2	0.	0.	2	0.	0.
3	0.	0.	3	0.000306	0.000301
4	0.001667	0.001657	4	0.000657	0.000647
5	0.0001667	0.001658	5	0.000962	0.000960
6	0.001667	0.001694	6	0.001268	0.001241
7	0.003333	0.003314	7	0.001619	0.001605
8	0.003333	0.003339	8	0.001924	0.001889
9	0.003333	0.003371	9	0.002230	0.002163

σ_x Stresses(ksi)			σ_y Stresses(ksi)		
Node	Q8D11	CST	Node	Q8D11	CST
1	1.0	0.995	1	0.	0.
2	1.0	0.995	2	0.	0.
3	1.0	1.005	3	0.	0.
4	1.0	0.995	4	0.	0.
5	1.0	1.002	5	0.	0.
6	1.0	1.011	6	0.	0.
7	1.0	1.002	7	0.	0.
8	1.0	1.008	8	0.	0.
9	1.0	1.007	9	0.	0.

TABLE 4

MIDSPAN DISPLACEMENT OF A SKEW PLATE
UNDER IN-PLANE CONCENTRATED LOAD (Fig. 12)

Finite Element Analysis	Displacement x 10^{-4} ft.
Q8D8[1]	11.40
CST[2]	19.58
Q8D11(3)	30.44
Q8D11(2)	51.49
LSE [1]	54.51

[1]Refs. 59, 60
[2]Ref. 52

TABLE 5

NORMAL STRESS AND DEFLECTION IN A
SIMPLY-SUPPORTED BEAM WITH INCLINED FACES (Fig. 13)

	Vertical Displacement at A x P/Et			Normal Stress at B x P/dt		
Mesh	Q8D8[1]	Q8D11	Ref. 53	Q8D8	Q8D11	Ref. 53
5 x 2	9.44	14.34	15.21	1.55	1.73	2.54
5 x 4	10.09	13.58	17.27	1.67	2.52	2.96

[1]From Ref. 53

TABLE 6

CENTER DEFLECTION OF A SQUARE PLATE WITH FIXED SUPPORTS

Multiplier PL^2/D

Source	2 x 2	4 x 4	8 x 8	10 x 10	16 x 16
ACM	.00592	.00613	.00580	--	.00568
Q19	.00521	.00515	.00546	.00551	--
EXACT	(Ref. 55)		.00560		

TABLE 7

CENTER DEFLECTION OF A SQUARE PLATE WITH SIMPLE SUPPORTS

Multiplier PL^2/D

Source	2 x 2	4 x 4	8 x 8	10 x 10	16 x 16
ACM	0.01378	0.01233	0.01133	--	0.01167
Q19	0.00975	0.01106	0.01145	0.01150	0.01159
EXACT	(Ref. 55)		0.01160		

TABLE 8

RHOMBIC PLATE UNDER CONCENTRATED LOAD
TWO SIDES SIMPLY SUPPORTED, $\varphi = 45^{\circ}$ (Fig.28)

Method		w $\times Pa^2/D$	$M_{max.}$ $\times P$	$M_{min.}$ $\times P$
Finite Difference[1]	4 x 8	0.0117	0.331	0.199
Finite Difference[1]	6 x 8	0.0117	0.370	0.257
Experiment[1]		0.0099	0.354	0.254
Finite Element	8 x 8	0.0107	0.363	0.253

[1]Ref. 37

$$D = \frac{Et^3}{12(1-\nu^2)}$$

TABLE 9

MOMENTS IN A SKEW PLATE UNDER UNIFORM LOAD

Pt	Moment (in-lb) in	Multiplier x 10^5			
		Ref. 48	Discretization		
			(1)	(2)	(3)
A	M_u^1	0.906	0.897	0.896	
	M_{uv}^1	0.270	0.285	0.286	
	M_I	0.980	0.975	0.981	
	M_{II}	0.068	0.058	0.056	
B	M_x	0.976	0.964	0.965	0.968
	M_y	0.019	0.010	0.010	0.012
	M_{xy}	0.188	0.205	0.207	0.206
	M_I	1.01	1.01	1.01	1.01
	M_{II}	0.027	0.032	0.032	0.030
E	M_x	0.210	0.487*	0.368	0.309
	M_y	-0.213	-0.160*	-0.245	-0.202
	M_{xy}	0.131	0.336*	0.195	0.248
	M_I	0.238	0.631*	0.425	0.410
	M_{II}	-0.238	-0.303*	-0.302	-0.302

*At center of plate element.

[1]M_u, M_{uv} are in the direction of the skew.

-127-

TABLE 10

MOMENTS IN A SKEW PLATE UNDER CONCENTRATED LOAD

Pt	Moment (in-lb) in	Multiplier x 10^5			
			Discretization		
		Ref. 48	(1)	(2)	(3)
A	$M_u{}^1$	0.453	0.461	0.457	
	$M_{uv}{}^1$	0.134	0.125	0.125	
B	M_x	0.684	0.667	0.658	0.643
	M_y	0.262	0.240	0.231	0.221
	M_{xy}	0.122	0.106	0.108	0.104
E	M_x	0.068	0.143	0.122	0.104
	M_y	0.100	0.082	0.117	0.094
	M_{xy}	0.068	0.115	0.113	0.130

[1] M_u, M_{uv} are in the direction of the skew.

TABLE 11

MOMENT COEFFICIENTS AND REACTIONS IN A 45°
SKEW BRIDGE WITH CHANGE IN BOUNDARY CONDITIONS

Beam	Moment Coefficients x L x P		Reactions at Left Support x P	
	S.S.[1]	Skew S.S.[2]	S.S.[1]	Skew S.S.[2]
A	0.00232	0.0233	0.0614	0.0600
B	0.0437	0.0439	0.0371	0.0412
C	0.0922	0.0918	0.1085	0..028
D	0.0437	0.0439	0.2545	0.2254
E	0.00232	0.0233	0.0385	0.0706

[1]Simply supported.

[2]Simply supported and constrained to rotate about
skew line of support, $\beta = 45°$.

TABLE 12

LOAD DISTRIBUTION COEFFICIENTS - BRIDGE 3[1]

	Ratio of Bending Moments (%)	
	Interior Girders	Exterior Girders
Field Test	60	40
Analytical Results	59	41

[1]Ref. 6

TABLE 13

MOMENT PERCENTAGES

Bridge		Σ Beam Moment	Beam Moment/Σ Beam Moment		
		Truck Moment	Interior	Center	Exterior
2B	Field Test (Ref. 24)	89.30	34.0	32.0	34.0
	Finite Element (composite)	93.57	32.6	34.0	33.2
	Finite Element (non-composite)	92.13	33.2	33.8	33.0
3B	Field Test (Ref. 24)	92.10	33.8	33.4	29.2
	Finite Element (composite)	94.50	32.7	34.3	33.0
	Finite Element (non-composite)	83.95	33.2	33.8	33.0

TABLE 14

LOAD DISTRIBUTION FACTORS IN LEHIGHTON BRIDGE WITH AND WITHOUT DIAPHRAGMS - CASE A[1]

L = 71'-6"   S = 6'-9"

Loaded Lanes	Beam	Without Diaphragms		With Diaphragms Partially Effective		Diaphragms in Shear Only	Diaphragms Fully Effective
		Analytic	Field Test	Analytic	Field Test	Analytic	Analytic
1	A	0.79	0.71	0.81	0.75	0.79	0.80
	B	0.69	0.69	0.61	0.64	0.69	0.58
	C	0.64	0.58	0.51	0.53	0.64	0.45
	D	0.62	0.62	0.50	0.59	0.62	0.45
	E	0.68	0.64	0.61	0.54	0.68	0.58
	F	0.83	0.85	0.83	0.87	0.83	0.82
2	A	0.85	0.81	0.94	0.88	0.85	0.99
	B	1.01	0.99	0.96	0.98	1.01	0.94
	C	1.07	0.98	0.92	0.94	1.07	0.84
	D	1.04	1.06	0.92	1.02	1.04	0.84
	E	1.09	1.02	1.02	0.87	1.09	0.98
	F	1.03	1.08	1.10	1.14	1.03	1.15
3	A	0.85	0.81	0.94	0.88	0.85	0.99
	B	1.03	1.01	1.01	1.05	1.03	1.00
	C	1.20	1.10	1.11	1.06	1.20	1.06
	D	1.18	1.20	1.13	1.18	1.18	1.11
	E	1.13	1.08	1.11	0.96	1.13	1.09
	F	1.02	1.07	1.08	1.15	1.02	1.13

[1]Design Lane = 12'-0", leftmost lane starts at beam A.

TABLE 15

LOAD DISTRIBUTION FACTORS IN LEHIGHTON BRIDGE WITH AND WITHOUT DIAPHRAGMS - CASE B[1]

L = 71'-6"   S = 6'-9"

Loaded Lanes	Beam	Without Diaphragms		With Diaphragms Partially Effective		Diaphragms in Shear Only	Diaphragms Fully Effective
		Analytic	Field Test	Analytic	Field Test	Analytic	Analytic
1	A	0.95	0.84	0.93	0.86	0.95	0.90
	B	0.69	0.69	0.63	0.65	0.69	0.61
	C	0.64	0.58	0.51	0.53	0.64	0.45
	D	0.62	0.63	0.51	0.59	0.63	0.45
	E	0.68	0.64	0.60	0.53	0.68	0.56
	F	0.73	0.77	0.75	0.79	0.73	0.76
2	A	1.09	0.99	1.16	1.05	1.09	1.19
	B	1.11	1.08	1.04	1.06	1.11	1.01
	C	1.09	1.00	0.93	0.95	1.09	0.84
	D	1.07	1.08	0.92	1.05	1.07	0.84
	E	0.97	0.92	0.94	0.79	0.97	0.92
	F	0.85	0.93	0.92	0.98	0.85	0.98
3	A	1.06	1.00	1.12	1.05	1.06	1.16
	B	1.18	1.17	1.15	1.16	1.18	1.14
	C	1.25	1.17	1.18	1.13	1.25	1.13
	D	1.21	1.23	1.12	1.23	1.21	1.06
	E	0.99	0.96	0.99	0.86	0.00	0.99
	F	0.84	0.91	0.89	0.97	0.84	0.92

[1] Design Lane = 12'-0", leftmost lane starts at overhang.

TABLE 16

LOAD DISTRIBUTION FACTORS IN BARTONSVILLE BRIDGE WITH AND WITHOUT CURBS, PARAPETS AND DIAPHRAGMS

L = 68'-6"   S = 8'-0"

No. of Loaded Lanes	Beam	Live Load Distribution Factors					
		(1)[a]	(2)[b]	(3)[c]	(4)[d]	(5)[e]	(6)[f]
1	A	0.92	0.92	0.94	0.94	0.80	0.94
	B	0.85	0.84	0.71	0.70	0.72	0.75
	C	0.84	0.82	0.68	0.66	0.76	0.72
2	A	0.97	1.00	1.08	1.10	0.85	1.06
	B	1.30	1.28	1.18	1.17	1.04	1.21
	C	1.38	1.35	1.20	1.18	1.27	1.24

[a] beams and slab only.

[b] beams and slab with curbs and parapet

[c] beams and slab with diaphragms

[d] beams and slab with curbs, parapets and diaphragms

[e] field test results with curbs, parapets and diaphragms

[f] beams and slab with with only 20% effective diaphragms

TABLE 17

LOAD DISTRIBUTION FACTORS IN A 36 FT. WIDE BRIDGE WITH DIAPHRAGMS

$$L = 71'-6'' \qquad S = 7'-2''$$

Beam	One Loaded Lane				
	w/o Diaphragms	Diaphragm Locations			
		at L/2	at L/3	at L/4	at L/5
A	0.84	0.84	0.84	0.86	0.83
B	0.76	0.64	0.71	0.69	0.66
C	0.72	0.59	0.66	0.62	0.59

Beam	Two Loaded Lanes				
	w/o Diaphragms	Diaphragm Locations			
		at L/2	at L/3	at L/4	at L/5
A	0.92	0.94	0.96	1.00	0.97
B	1.13	1.04	1.08	1.08	1.04
C	1.19	1.06	1.11	1.08	1.04

Beam	Three Loaded Lanes				
	w/o Diaphragms	Diaphragm Locations			
		at L/2	at L/3	at L/4	at L/5
A	0.90	0.90	0.92	0.96	0.92
B	1.16	1.08	1.13	1.14	1.09
C	1.34	1.25	1.29	1.28	1.23

TABLE 18

MOMENT COEFFICIENTS[1] IN A FOUR-SPAN CONTINUOUS BRIDGE

Beam	Static Load Test		Vehicular Load Test	
	Analytic	Test[2]	Analytic	Test[2]
A	19.53	20.0	17.44	16.0
B	30.47	29.0	32.56	33.0
C	30.47	29.0	32.56	31.0
D	19.53	22.0	17.44	19.0

[1]All values in percent of theoretical single beam moment.
[2]From Ref. 24

TABLE 19

MOMENT COEFFICIENTS[1] IN A FOUR-SPAN CONTINUOUS BRIDGE
WITH CHANGES IN BOUNDARY CONDITIONS

Beam	Static Load			Vehicular Load		
	Simply Supported	Continuous	Fixed	Simply Supported	Continuous	Fixed
A	20.49	19.53	17.11	21.55	17.44	13.19
B	29.51	30.47	32.89	28.45	32.56	36.81
C	29.51	30.47	32.89	28.45	32.56	36.81
D	20.49	19.53	17.11	21.45	17.44	13.19

[1]All values in percent of theoretical single beam moment.

TABLE 20

LOAD DISTRIBUTION FACTORS IN A SIX-BEAM CONTINUOUS BRIDGE

L = 75'-100'-75'

S = 7'-2"

Number of Loaded Lanes	Beam	Distribution Factors	
		At Midspan	At Supports
1	A	0.780	0.785
	B	0.706	0.720
	C	0.664	0.700
2	A	0.882	0.833
	B	1.061	1.011
	C	1.107	1.165
3	A	0.884	0.855
	B	1.121	1.146
	C	1.268	1.308

TABLE 21

LIST OF BRIDGES ANALYZED

Bridge No.	Width (ft.)	Number of Beams	Spacing (in.)	Length (ft.)	Beam Size	S/L
1	24.00	6	57.60	120.00	AASHO-VI	.0400
2	24.00	6	57.60	72.00	24/42	.0667
3	24.00	6	57.60	38.40	20/30	.1250
4	24.00	5	72.00	120.00	AASHO-VI	.0500
5	24.00	5	72.00	60.00	20/39	.1000
6	24.00	5	72.00	42.00	20/30	.1429
7	24.00	4	96.00	120.00	AASHO-VI	.0667
8	24.00	4	96.00	64.00	24/45	.1250
9	24.00	4	96.00	40.00	20/30	.2000
10	48.00	11	57.60	120.00	AASHO-VI	.0400
11	48.00	11	57.60	84.00	24/48	.0571
12	48.00	11	57.60	48.00	20/30	.1000
13	48.00	9	72.00	105.00	28/63	.0571
14	48.00	9	72.00	60.00	20/39	.1000
15	48.00	9	72.00	42.00	20/30	.1429
16	48.00	6	115.20	96.00	AASHO-VI	.1000
17	48.00	6	115.20	57.60	24/45	.1667
18	48.00	6	115.20	48.00	20/33	.2000
19	72.00	16	57.60	120.00	ASSHO-VI	.0400
20	72.00	16	57.60	57.60	20/36	.0833
21	72.00	16	57.60	38.40	AASHO-I	.1250
22	72.00	14	66.50	110.80	AASHO-VI	.0500
23	72.00	14	66.50	66.50	24/42	.0833
24	72.00	14	66.50	38.80	AASHO-I	.1429
25	72.00	12	78.50	114.50	AASHO-VI	.0571
26	72.00	12	78.50	65.50	24/42	.1000
27	72.00	12	78.50	39.30	20/30	.1667
28	72.00	9	108.00	108.00	AASHO-VI	.0833
29	72.00	9	108.00	54.00	24/42	.1667
30	72.00	9	108.00	45.00	24/36	.2000

TABLE 22

MAXIMUM DISTRIBUTION FACTORS - INTERIOR BEAMS

Bridge No.	*NL	***NLL	90°	NLL	60°	NLL	45°	NLL	30°
1	2	2	.81	2	.79	2	.77	2	.71
2	2	2	.84	2	.81	2	.77	2	.66
3	2	2	.96	2	.94	2	.93	2	.86
4	2	2	.96	2	.92	2	.88	2	.82
5	2	2	1.05	2	.99	2	.92	2	.78
6	2	2	1.17	2	1.07	2	.95	2	.76
7	2	2	1.23	2	1.20	2	1.18	2	1.08
8	2	2	1.30	2	1.24	2	1.17	2	.99
9	2	2	1.32	2	1.23	2	1.14	2	.88
10	4	4	.94	4	.91	4	.87	4	.79
11	4	4	.94	4	.90	4	.87	4	.75
12	4	2	1.03	3	.98	3	.94	3	.87
13	4	4	1.17	4	1.13	4	1.09	4	.97
14	4	4	1.20	4	1.14	4	1.08	4	.89
15	4	4	1.24	3	1.13	3	1.07	3	.83
16	4	4	1.84	4	1.79	4	1.74	4	1.59
17	4	4	1.83	4	1.77	4	1.70	4	1.45
18	4	4	1.86	4	1.72	4	1.58	3	1.24
19	6	5	.94	5	.92	5	.90	5	.84
20	6	4	.95	4	.91	4	.87	5	.75
21	6	4	.97	4	.91	4	.96	5	.72
22	6	5	1.07	5	1.05	5	1.04	5	.98
23	6	4	1.07	4	1.04	4	1.01	5	.89
24	6	4	1.09	4	1.02	5	.96	5	.77
25	6	5	1.23	5	1.21	5	1.19	5	1.11
26	6	4	1.24	5	1.20	5	1.16	5	1.03
27	6	4	1.30	4	1.21	5	1.12	5	.89
28	6	5	1.72	5	1.68	5	1.65	6	1.51
29	6	4	1.74	5	1.68	5	1.61	5	1.33
30	6	4	1.77	5	1.68	5	1.60	5	1.23

*Number of Lanes
**Number of Loaded Lanes

TABLE 23

MAXIMUM DISTRIBUTION FACTORS - EXTERIOR BEAMS

Bridge No.	*NL	***NLL	NUMBER OF LOADED LANES AND SKEW ANGLE 90°	NLL	60°	NLL	45°	NLL	30°
1	2	2	.69	2	.70	2	.70	2	.72
2	3	2	.67	2	.67	2	.67	2	.64
3	2	2	.56	1	.57	1	.57	2	.58
4	2	2	.80	2	.81	2	.82	2	.83
5	2	2	.75	2	.77	2	.78	2	.73
6	2	2	.73	2	.73	2	.72	2	.62
7	2	2	1.01	2	1.02	2	1.02	2	1.01
8	2	2	.95	2	.95	2	.94	2	.88
9	2	2	.87	2	.87	2	.86	2	.74
10	4	2	.71	2	.72	2	.73	3	.73
11	4	4	.68	2	.68	2	.68	4	.65
12	4	1	.62	1	.61	1	.61	2	.59
13	4	2	.83	2	.83	2	.84	4	.83
14	4	2	.78	2	.76	2	.76	4	.70
15	4	2	.72	2	.74	4	.71	4	.62
16	4	2	1.10	2	1.10	2	1.11	4	1.09
17	4	2	1.02	2	1.01	2	1.00	4	.92
18	4	2	1.08	2	1.03	4	.99	4	.85
19	6	2	.70	2	.71	2	.72	3	.72
20	6	6	.65	2	.64	2	.63	2	.58
21	6	1	.61	1	.60	2	.60	2	.53
22	6	2	.78	2	.78	2	.79	2	.78
23	6	2	.74	2	.72	2	.73	2	.67
24	6	1	.68	2	.66	2	.67	6	.58
25	6	2	.88	2	.89	2	.91	3	.91
26	6	2	.83	2	.85	2	.86	6	.80
27	6	1	.74	2	.75	2	.75	2	.63
28	6	2	1.09	2	1.10	2	1.11	3	1.09
29	6	2	.97	2	.96	2	.95	6	.86
30	6	2	.95	2	.93	2	.91	6	.80

*Number of Lanes
**Number of Loaded Lanes

-139-

TABLE 24

CANTILEVER BEAM WITH CONCENTRATED LOAD
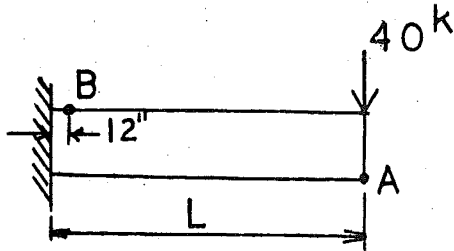
$E = 30,000$ ksi

$= 0.25$

$b = 1.0"$

$d = 12.0"$

$L = 48.0"$

Mesh (Fig. 86)	Boundary Condition	Deflection at A (in In.)	Normal Stress at B (in ksi)
1 x 4	Simple Supports	0.3279	60.0
	Fixed Supports	0.3283	60.0
2 x 4	Simple Supports	0.3416	60.97
	Fixed Supports	0.3428	61.48
Ref. 59		0.3558	60.0

TABLE 25

SIMPLY SUPPORTED BEAM WITH CONCENTRATED LOAD
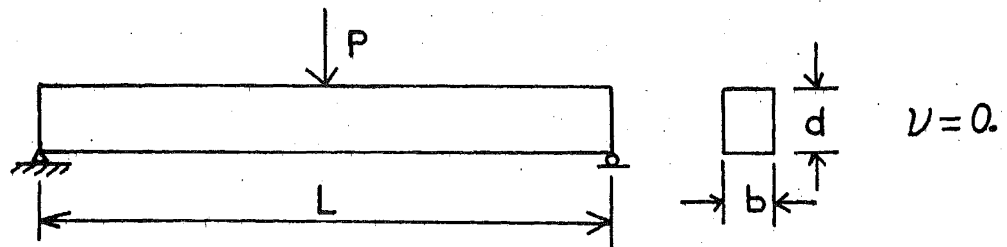
Span L [1]	Averaged Vertical Displacement at Midspan x P/Ed			Stress at 3/8 Span (bottom face) x P/bd		
	Beam Theory	Finite Element	% of Theory	Beam Theory	Finite Element	% of Theory
4d	18.19	18.36	99.00	4.5	4.5	100
8d	132.59	130.61	99.00	9.0	9.0	100
16d	1033.39	1016.57	98.34	18.0	18.0	100
32d	8210.99	8080.42	98.41	36.0	36.0	100

[1]All discretizations into 1 x 4 mesh

TABLE 26

DISTRIBUTION COEFFICIENTS BOX-BEAM BRIDGE - SECTION M

(BERWICK BRIDGE)

Lane	Beam	Distribution Coefficients (%)		
		Field Test[1]	Finite Element	Plexiglass Model[2]
1	A	43.82	42.79	---
	B	30.95	29.75	---
	C	15.02	17.53	---
	D	10.21	9.93	---
2	A	33.00	32.41	---
	B	31.06	30.27	---
	C	20.85	21.51	---
	D	15.09	15.82	---
3	A	21.12	23.27	25.5
	B	29.00	26.73	24.5
	C	28.88	26.73	24.5
	D	21.12	23.27	25.5

[1] Ref. 22

[2] Ref. 32

TABLE 27

MAXIMUM MOMENT COEFFICIENTS
45° SKEW BOX-BEAM BRIDGE - SECTION I
(BROOKVILLE BRIDGE)

Lane	Moment Coefficients (ft.-in.^{2})			
	(1)	(2)	(3)	(4)
1	0.028	0.029	0.031	0.027
2	0.034	0.031	0.03.	0.032
3	0.030	0.029	0.030	0.026
4	0.019	0.024	0.023	0.016
5	0.012	0.018	0.016	0.013

[1] Field tests (Ref. 51)

[2] Curb and Parapet fully effective

[3] Curb and Parapet partially effective

[4] Case (3) with drive axle at midspan

TABLE 28

LIST OF SPREAD BOX-BEAM BRIDGES

Bridge No.	Width (ft.)	Number of Beams	Spacing (in.)	Length (ft.)	Beam Size	S/L
1	24.00	3	122.50	40.83	3-48/48	.2500
2	24.00	3	122.50	71.46	3-48/48	.1430
3	24.00	3	122.50	122.50	3-48/48	.0830
4	24.00	4	81.67	34.03	4-48/48	.2000
5	24.00	4	81.67	47.64	4-48/48	.1430
6	24.00	4	81.67	102.08	4-48/48	.0670
7	48.00	5	133.25	44.42	5-48/48	.2500
8	48.00	5	133.25	88.83	5-48/48	.1250
9	48.00	5	133.25	11.04	5-48/48	.1000
10	48.00	7	88.83	37.01	7-48/48	.2000
11	48.00	7	88.83	59.22	7-48/48	.1250
12	48.00	7	88.83	111.03	7-48/48	.0670
13	72.00	8	117.29	39.10	8-48/48	.2500
14	72.00	8	117.29	78.19	8-48/48	.1250
15	72.00	8	117.29	97.74	8-48/48	.1000
16	72.00	9	102.62	42.75	9-48/48	.2000
17	72.00	9	102.62	68.42	9-48/48	.1250
18	72.00	9	102.62	128.25	9-48/48	.0670

TABLE 29

MAXIMUM DISTRIBUTION FACTORS - INTERIOR BOX-BEAMS

Bridge No.	*NL	**NLL	NUMBER OF LOADED LANES AND SKEW ANGLE							
			90°	NLL	60°	NLL	45°	NLL	30°	
1	2	2	1.73	2	1.45	2	1.09	2	.53	
2	2	2	1.61	2	1.38	2	1.04	2	.47	
3	2	2	1.56	2	1.27	2	1.01	2	.66	
4	2	2	1.15	2	.95	2	.70	2	.38	
5	2	2	1.06	2	.91	2	.65	2	.30	
6	2	2	1.01	2	.87	2	.68	2	.40	
7	4	4	2.16	4	1.77	4	1.20	4	.47	
8	4	4	1.93	4	1.56	4	1.03	4	.32	
9	4	4	1.89	4	1.49	4	1.00	4	.41	
10	4	4	1.47	4	1.09	4	.74	4	.30	
11	4	4	1.33	4	1.01	4	.62	4	.26	
12	4	4	1.22	4	.86	4	.54	4	.24	
13	6	6	1.87	6	1.55	6	1.03	6	.46	
14	6	6	1.80	6	1.37	6	.82	6	.32	
15	6	6	1.76	6	1.27	6	.75	6	.27	
16	6	6	1.63	6	1.25	6	.77	6	.33	
17	6	6	1.55	6	1.13	6	.66	6	.26	
18	6	6	1.49	6	.85	6	.50	6	.24	

*Number of Lanes

**Number of Loaded Lanes

TABLE 30

MAXIMUM DISTRIBUTION FACTORS - EXTERIOR BOX-BEAMS

Bridge No.	*NL	**NLL	90°	NLL	60°	NLL	45°	NLL	30°
1	2	2	1.17	2	1.01	2	.69	2	.24
2	2	2	1.29	2	1.12	2	.73	2	.23
3	2	2	1.27	2	1.03	2	.65	2	.20
4	2	2	.90	2	.68	2	.42	2	.12
5	2	2	.96	2	.77	2	.47	2	.13
6	2	2	.99	2	.79	2	.46	2	.08
7	4	4	1.17	4	1.00	4	.67	4	.26
8	4	4	1.40	4	1.09	4	.59	4	.17
9	4	4	1.43	4	1.06	4	.53	4	.11
10	4	4	.89	4	.70	4	.46	4	.16
11	4	4	.99	4	.75	4	.44	4	.19
12	4	4	1.10	4	.75	4	.44	4	.20
13	6	6	1.01	6	.88	6	.58	6	.24
14	6	6	1.20	6	.92	6	.58	6	.29
15	6	6	1.26	6	.90	6	.55	6	.28
16	6	6	.93	6	.76	6	.49	6	.21
17	6	6	1.04	6	.75	6	.46	6	.24
18	6	6	1.14	6	.56	6	.32	6	.18

*Number of Lanes

**Number of Loaded Lanes
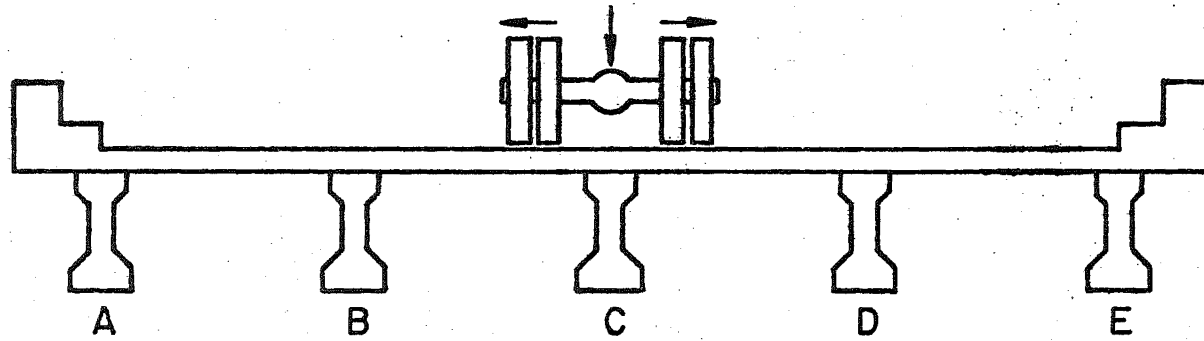
(a)　Prestressed Concrete I-beam Bridge
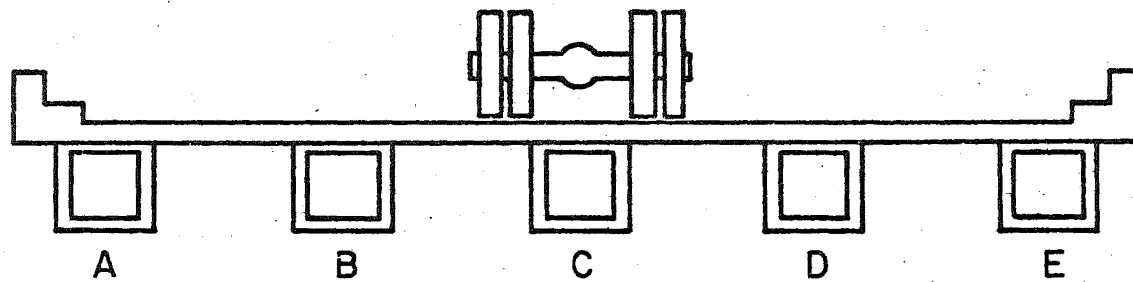
(b)　Prestressed Concrete Spread Box-Beam Bridge

Fig. 1　Beam-Slab Bridge Cross Section
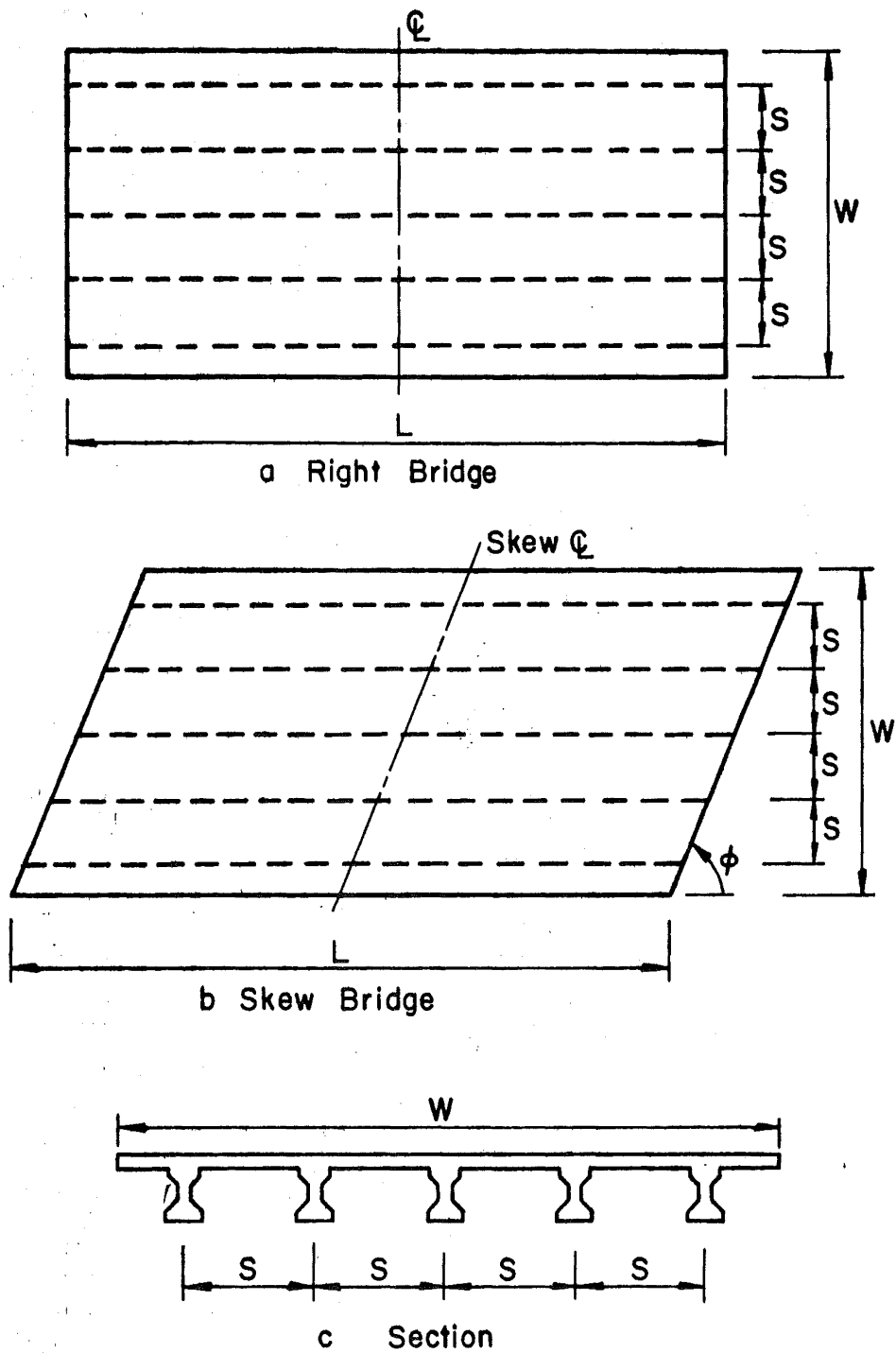
Fig. 2   Plan and Cross Section of a Beam-Slab Bridge

Axle Loads: 32 k   32 k   8 k

HS 20-44 Design Load Vehicle

Axle Loads: 32.5k   32.3 k   10.3 k

Test Vehicle
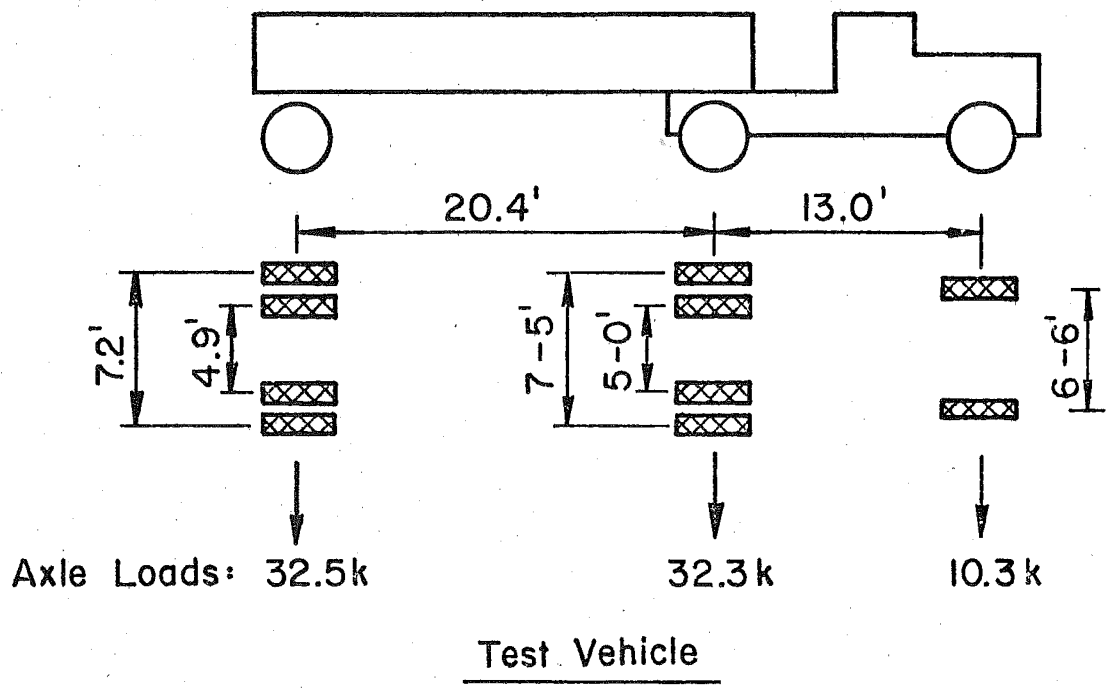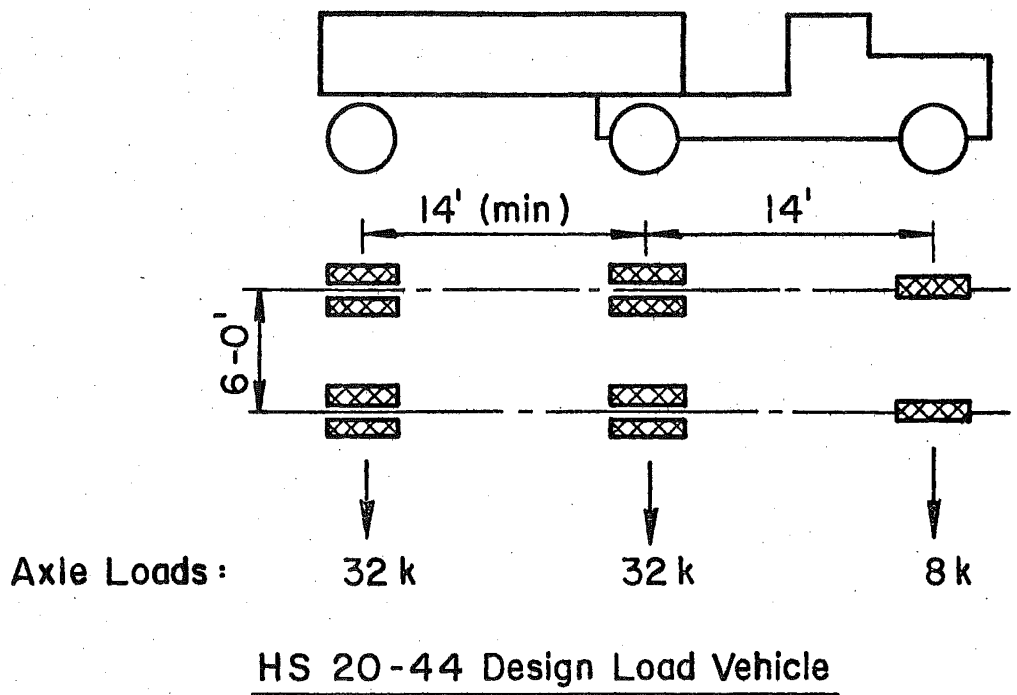
Fig. 3 Vehicular Loadings
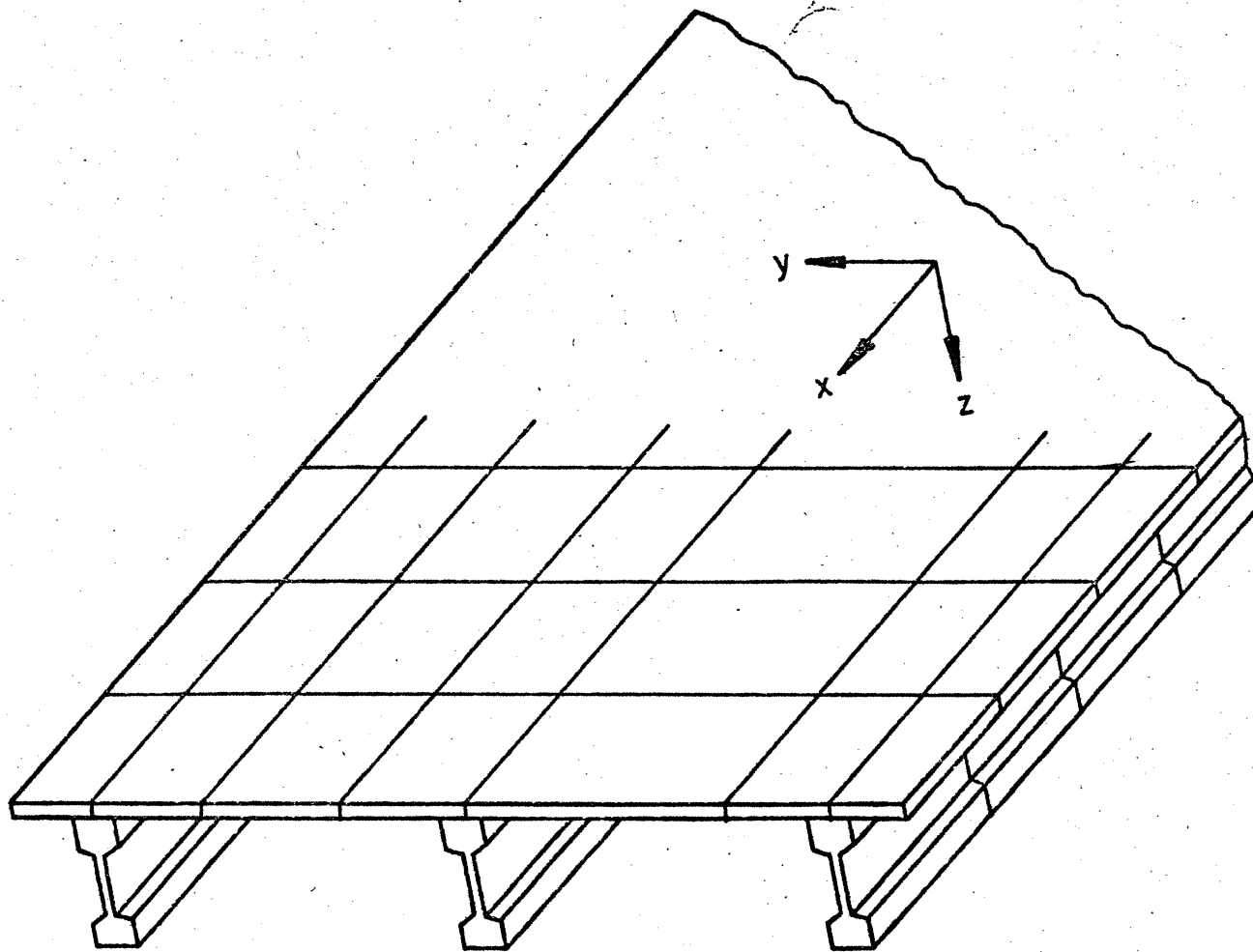
Fig. 4 Finite Element Discretization of a Prestressed Concrete I-Beam Bridge
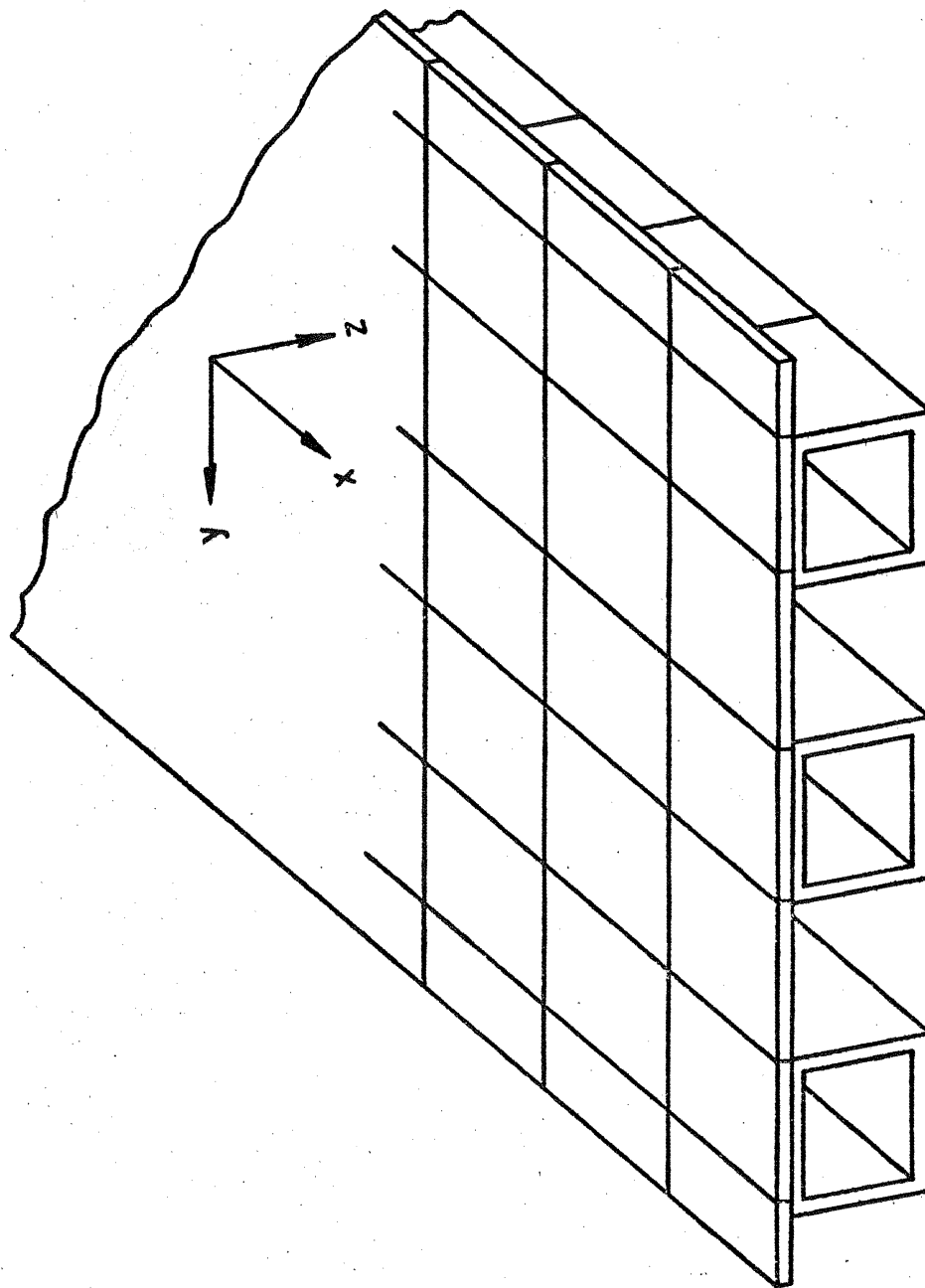
Fig. 5 Finite Element Discretization of a Prestressed Concrete Spread Box—Beam Bridge
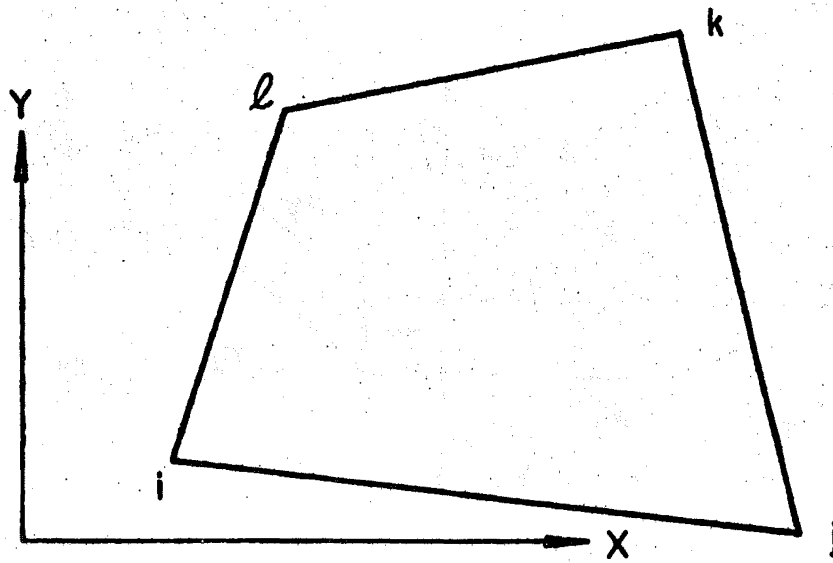
(a) Quadrilateral Plate Element
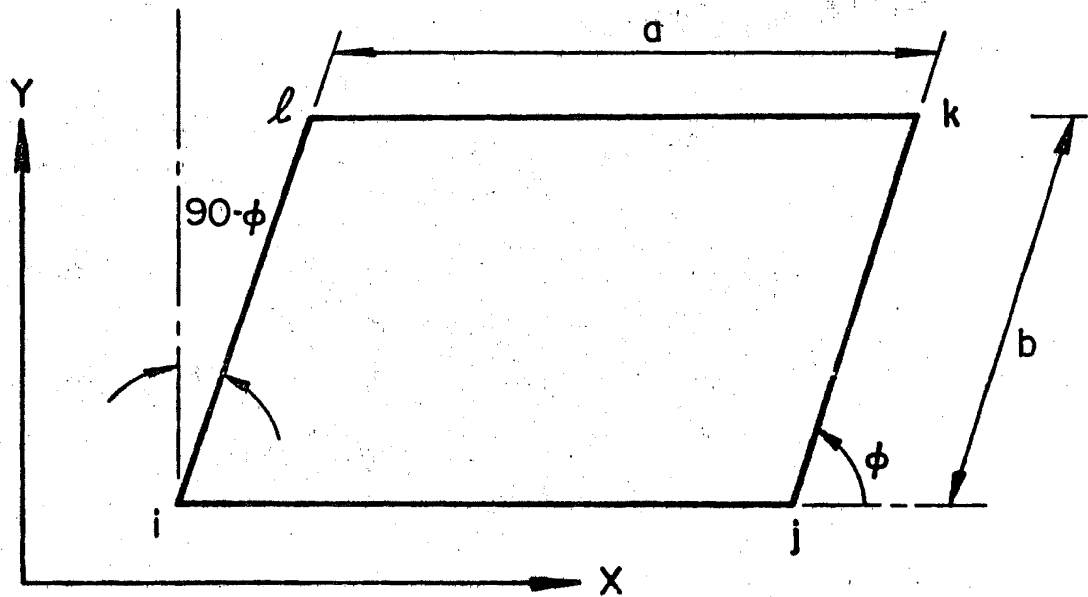
(b) Skew Plate Element

Fig. 6 Plate Finite Elements

Stresses
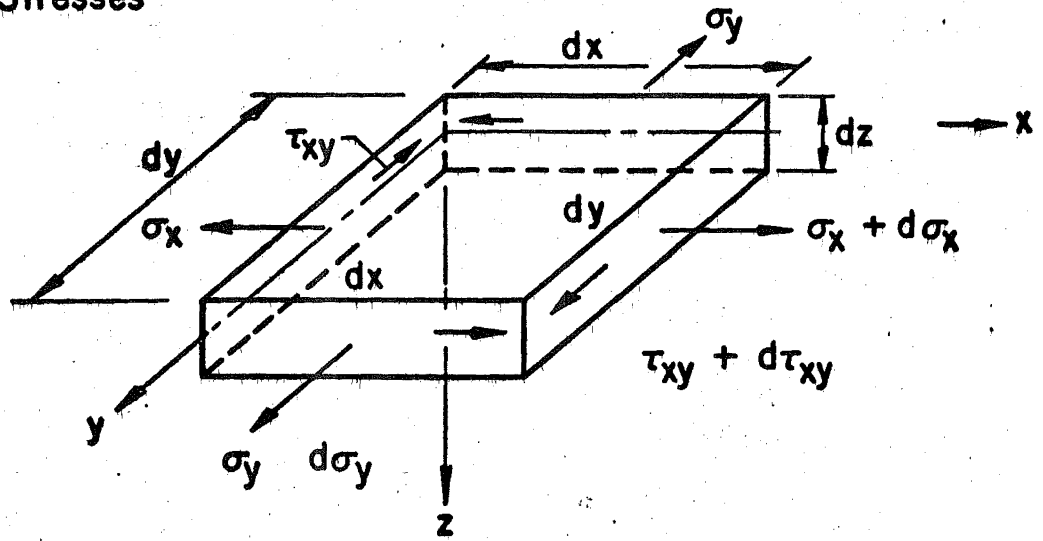
In - Plane Forces
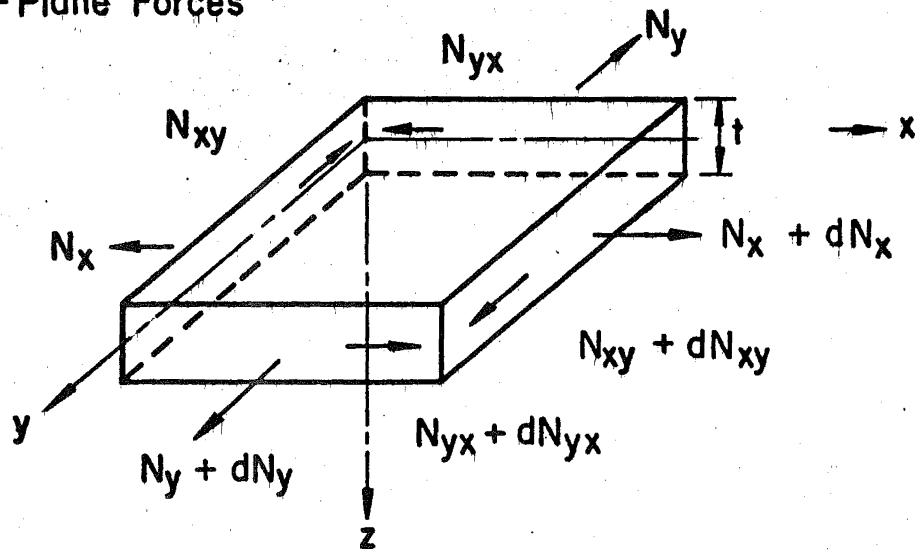
Fig. 7 In-Plane Stresses and Forces
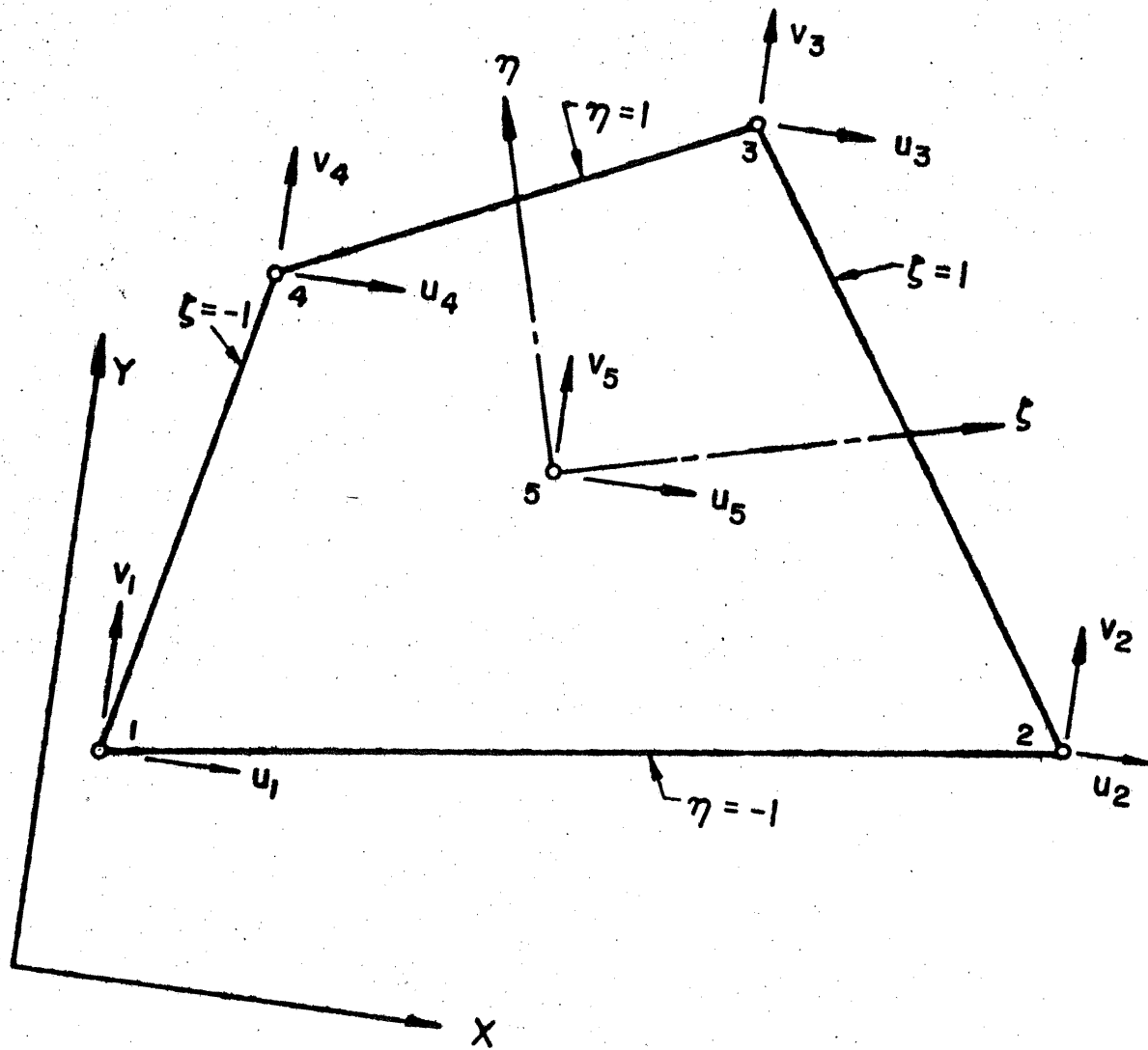
Fig. 8 A General Quadrilateral In-Plane Element,
Coordinate System and Associated Degrees
of Freedom
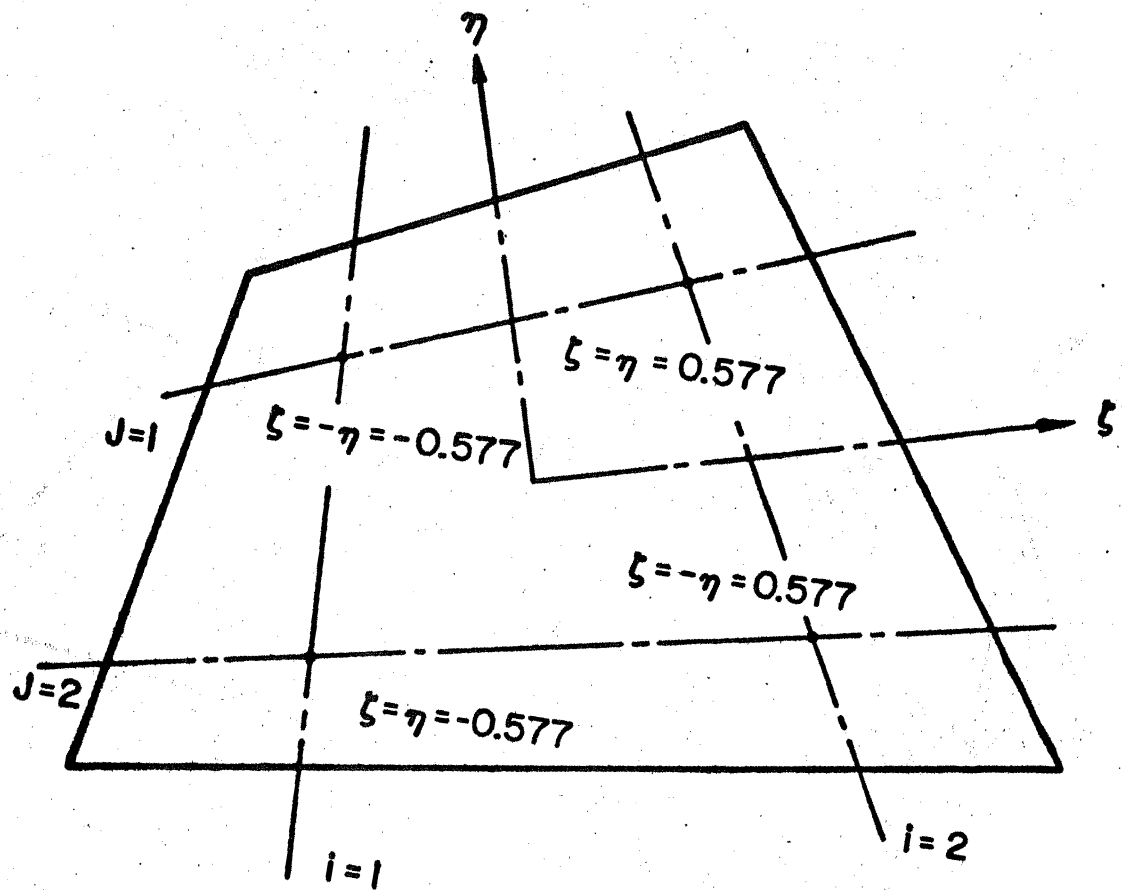
Fig. 9 2 x 2 Gaussian Quadrature for the Numerical
Integration of the Quadrilateral Finite Element
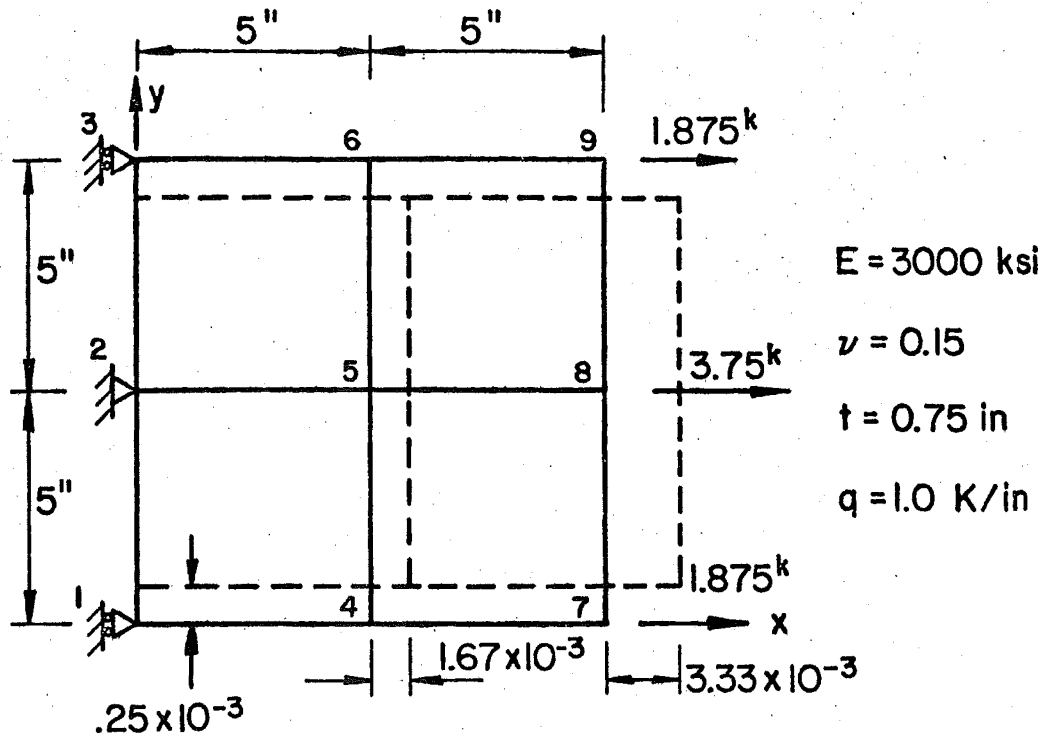
a. Normal Loads
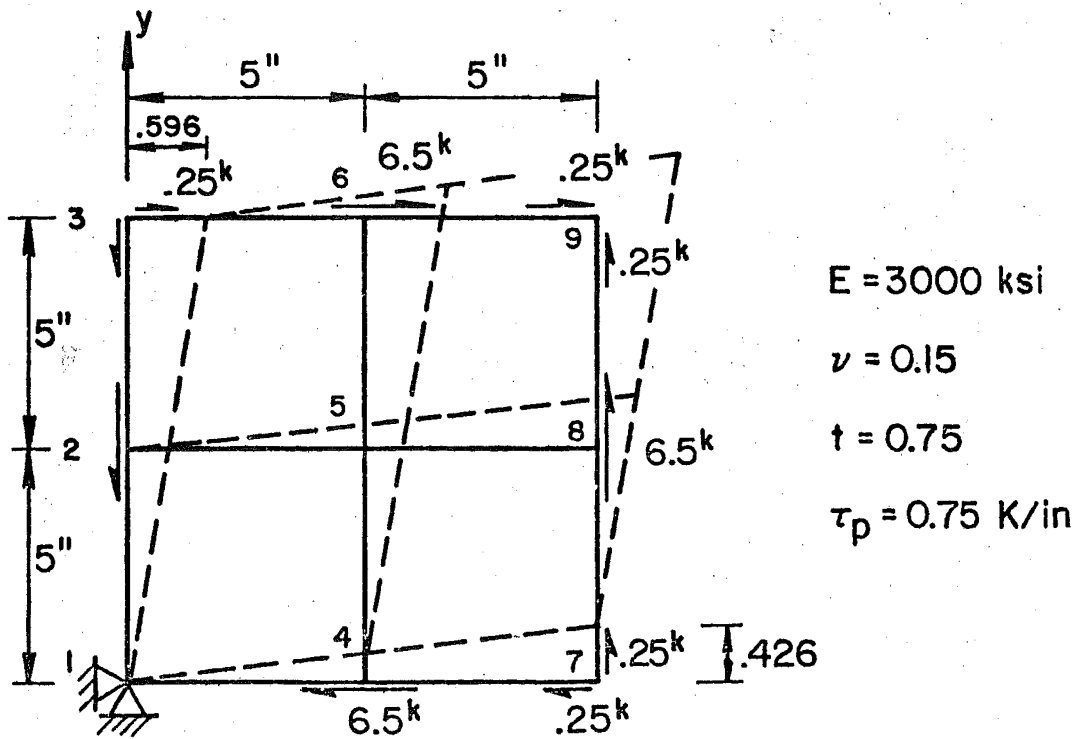
b. Shear Loads

Fig. 10 Rectangular Plate Under Uniform In-Plane Edge Loadings

-156-

20"

.75 K/in

60°

10"

.75 K/in

E = 3000 ksi   u = 0.15   t = ¾"
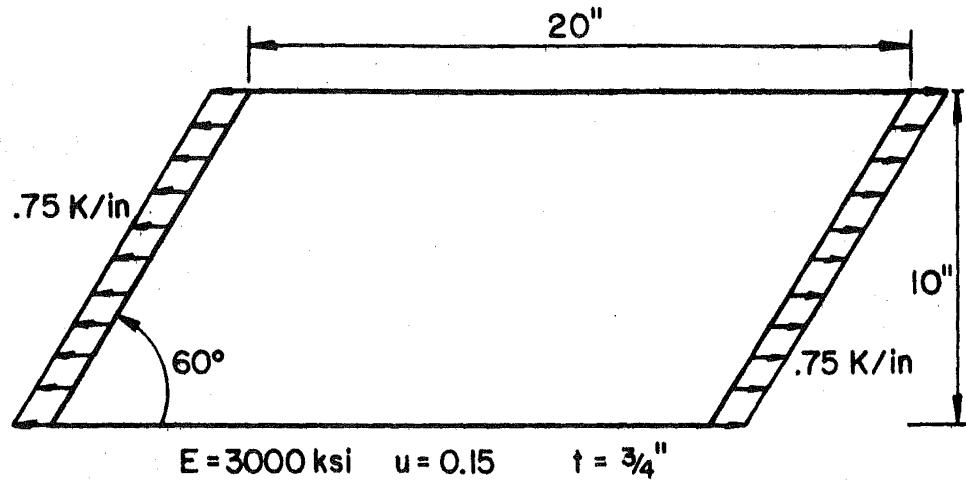
a.   Plate Dimension and Properties

y

1.875^k

5"

3.75^k

5"

60°

1.875^k

x

5"   5"
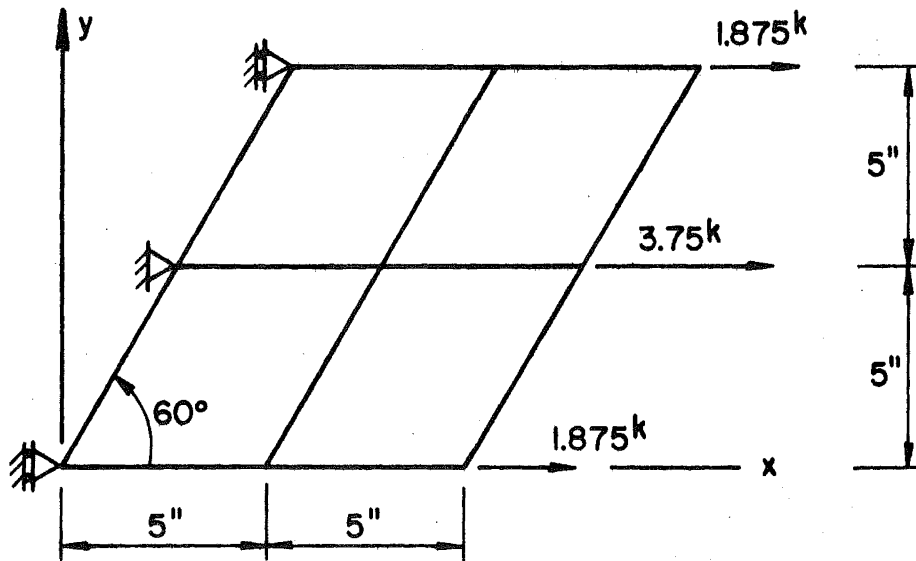
b.   Idealization and Modeling

Fig.   11   Skew Plate under Uniform In-Plane Edge Loading

-157-

$P_1 = 100^K$ $P_2 = 100^K$

9.33'

60'   30°   X

E = 432,000 KSF
$v = .15$
$t = 1.0$

Discretization To Triangular Elements
(CST)

Discretization To Parallelogram Elements
(Q8DII)
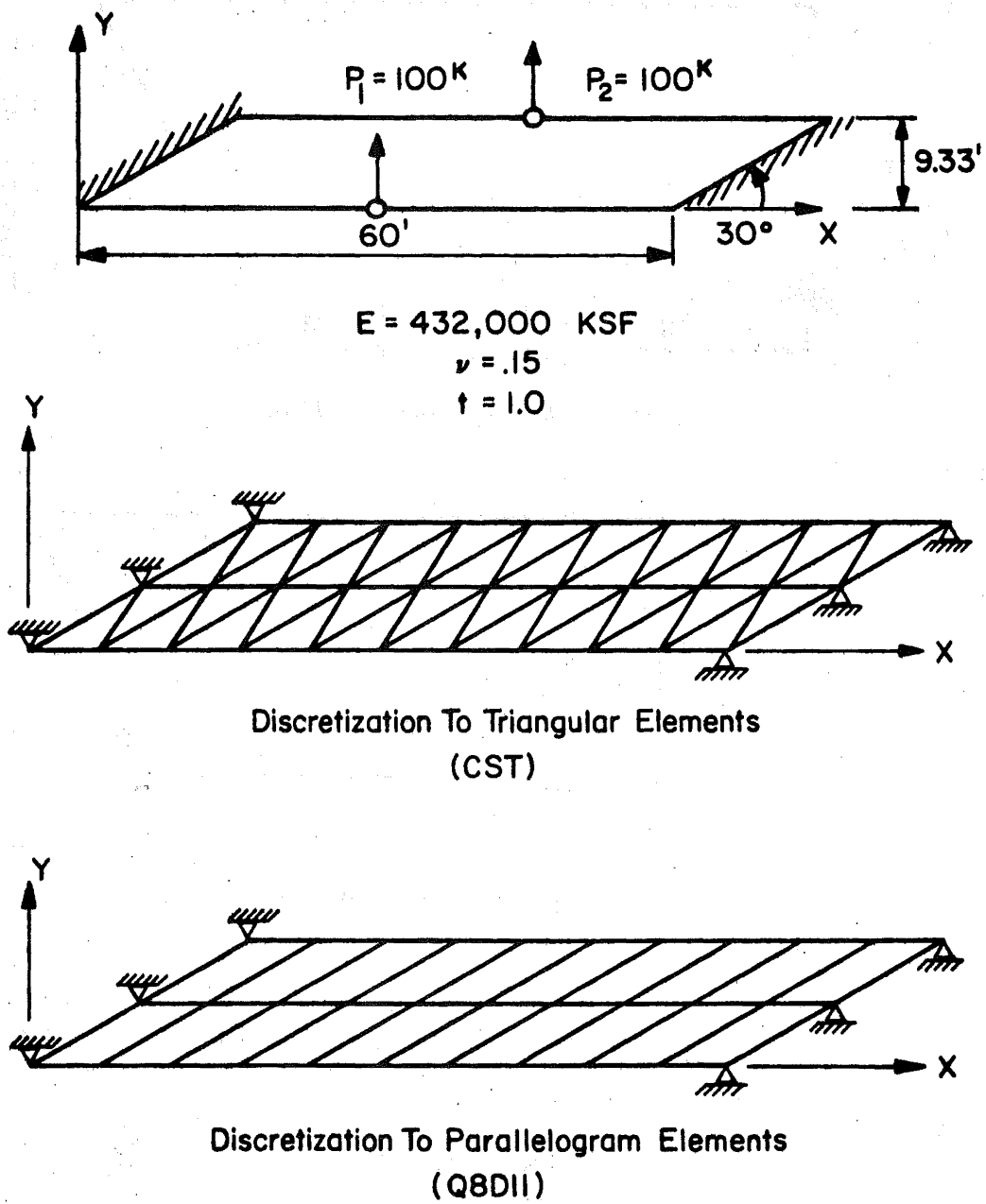
Fig.   12   Skew Plate Under In-Plane Concentrated Loads
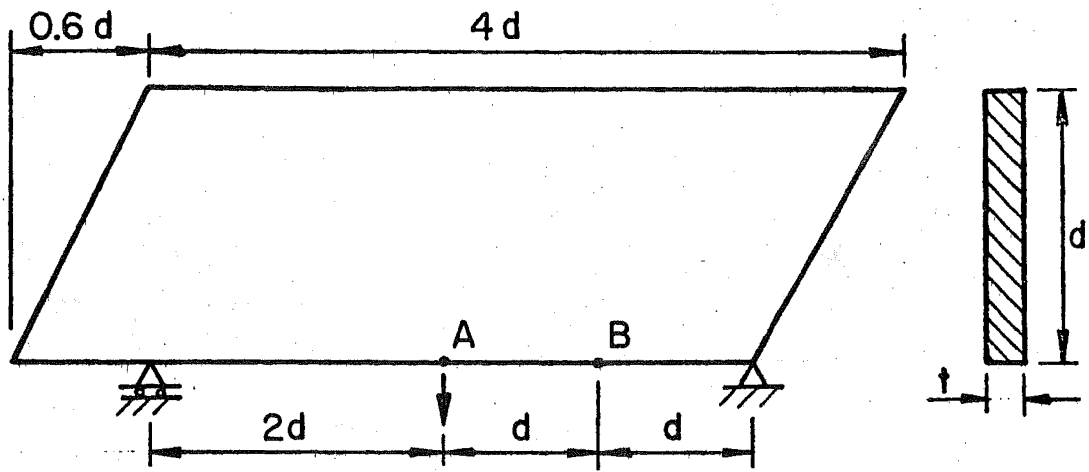
a. Structure and Loading
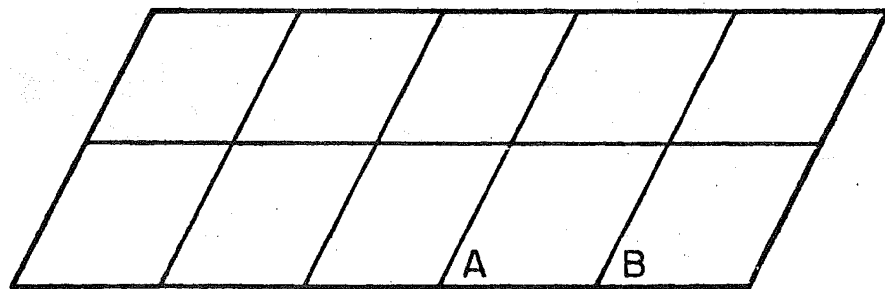
b. 2 x 5 Discretization
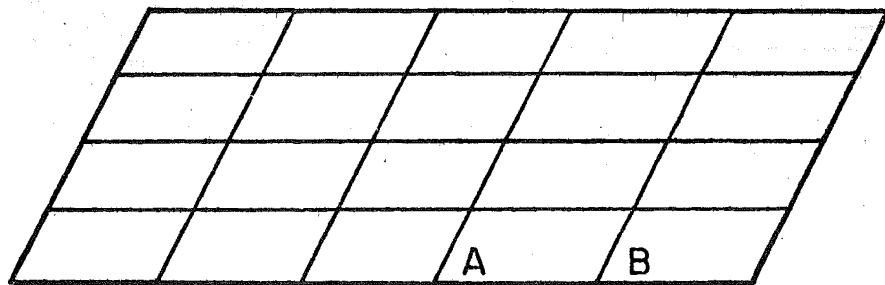
c. 4 x 5 Discretization

Fig. 13   Simply Supported Beam with Inclined Faces

-159-
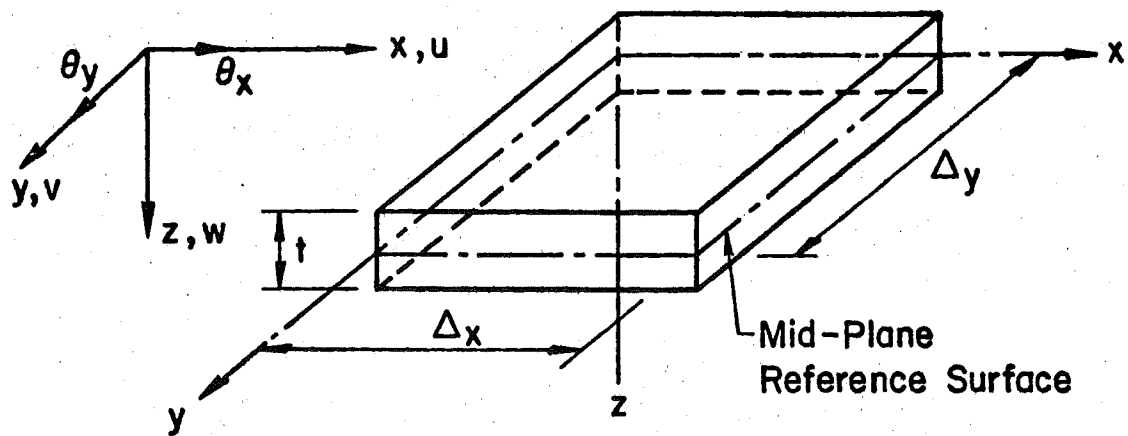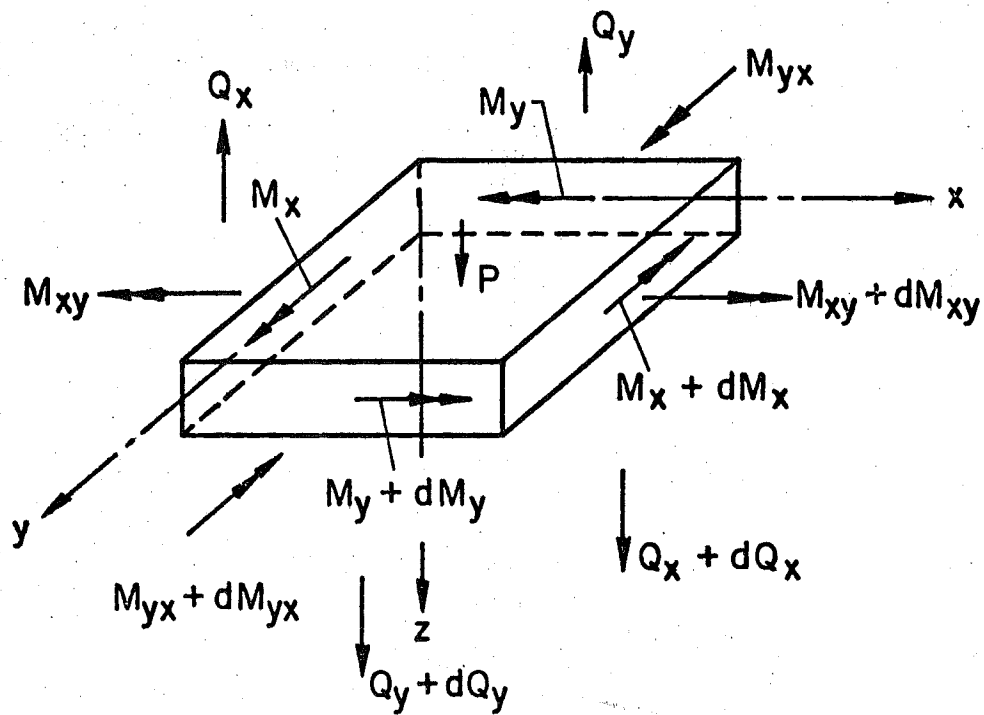
a. Displacements

b. Stress Resultants

Fig. 14 Plate Bending Stresses and Displacements
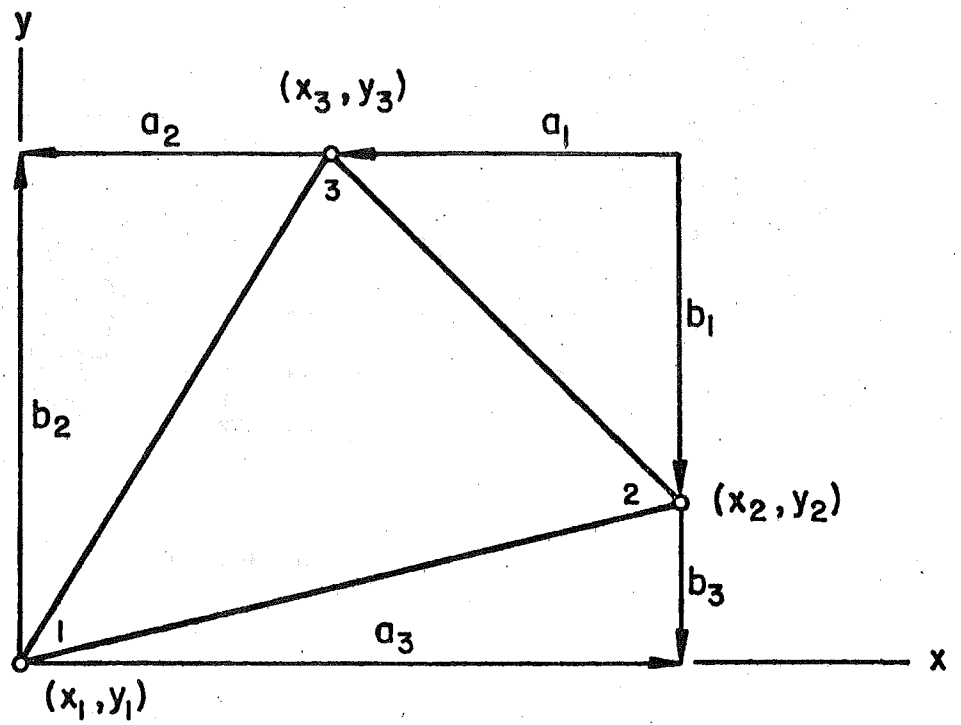
Fig. 15   Projected Dimensions
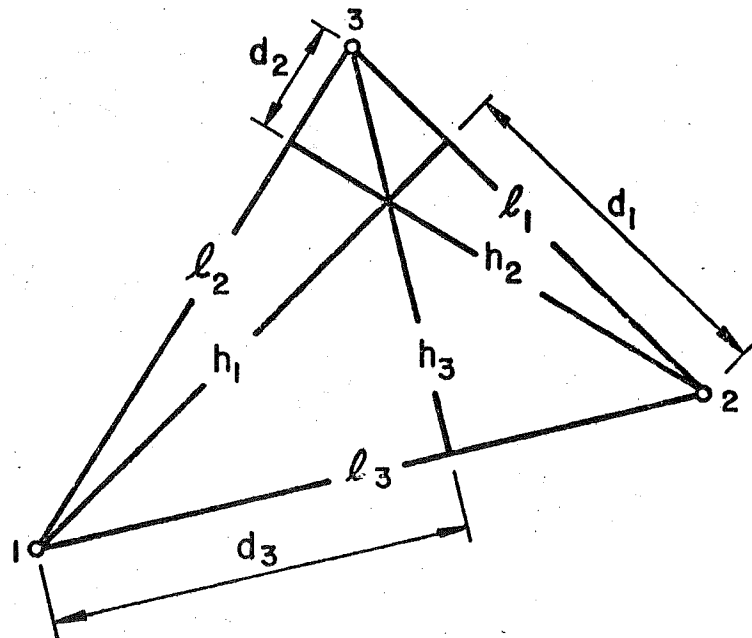
Fig. 16   Intrinsic Dimensions
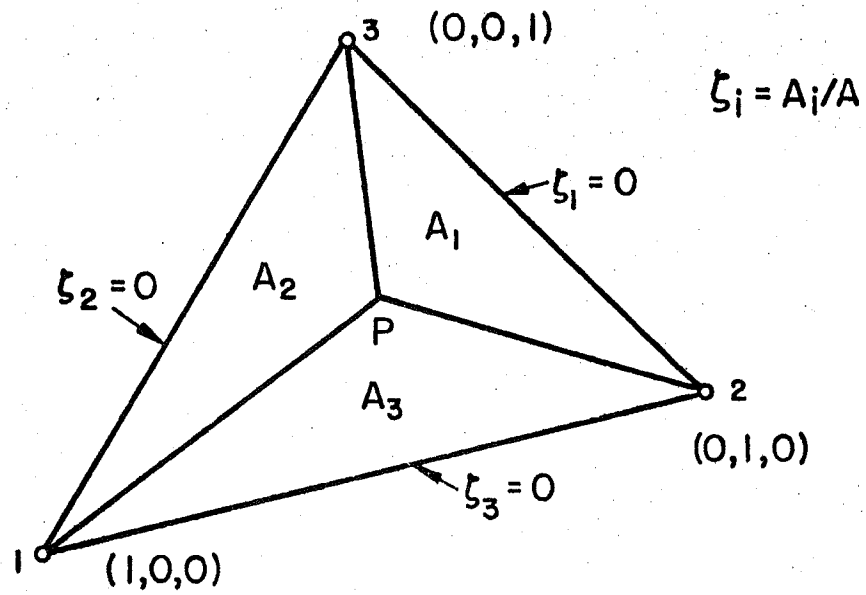
Fig. 17   Natural Coordinate System
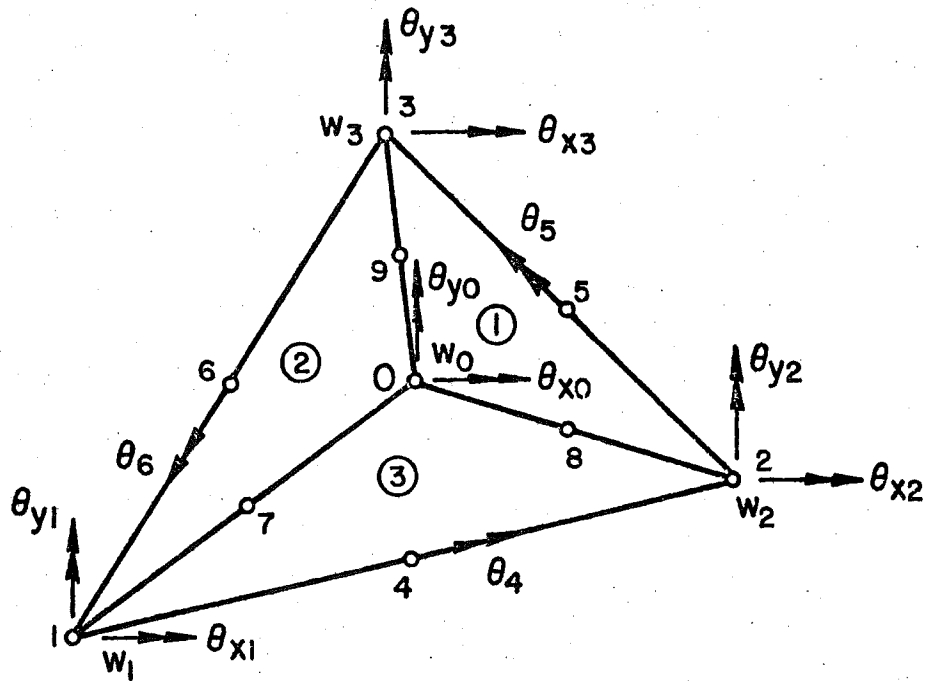
Fig. 18   Nodal Degrees of Freedom
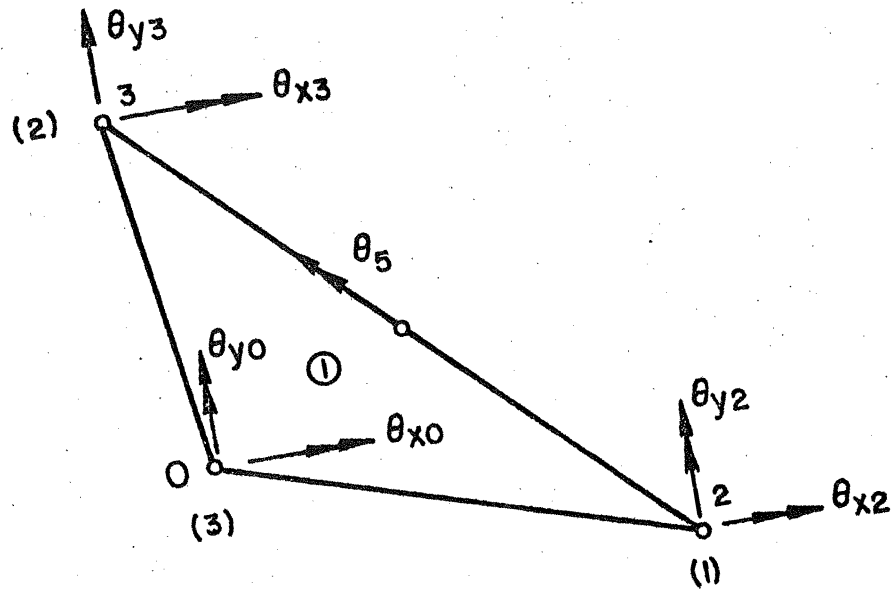
Fig. 19 Subelement Displacement Components
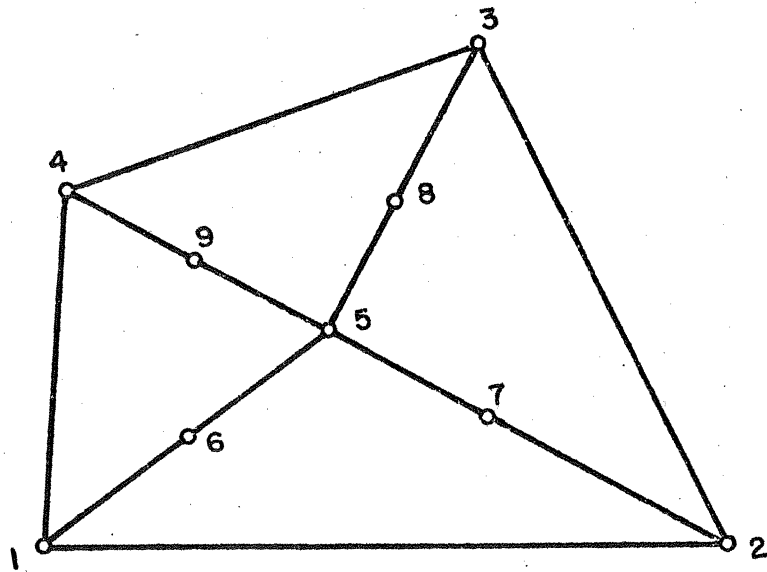
Fig. 20 Assembled Triangular Elements

Case 1
    Concentrated load at center
    Fixed supports

Case 2
    Concentrated load at ceter
    Simply supported

Case 3
    Uniform load, simply supported

a)
Support On All Sides

Uniform load
Skew angle ϕ varied

b)
Support On 4 Sides

Case 1
    Uniform load
    Skew angle ϕ varied

Case 2
    Concentrated load at center
    $\phi = 45°$

c)
Simple Supports On 2 Sides

Case 1
    Uniform load
    $\phi = 30°$, $b/L_\phi = 0.40$

Case 2
    Concentrated load
    $\phi = 30°$, $b/L_\phi = 0.40$

Case 3
    Uniform load
    $b/L_\phi = 0.5$, ϕ varied

d)
Simple Supports 2 Sides

Fig. 21 Numerical Examples and Comparisons for Plate Loading

-164-
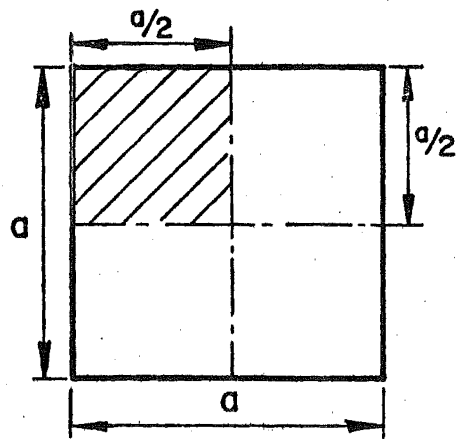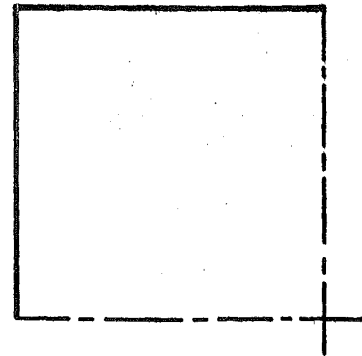
a. Square Plate

b. 2x2
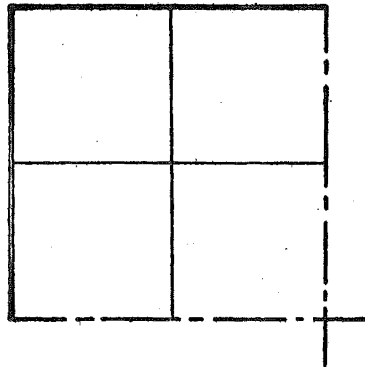
c. 4x4
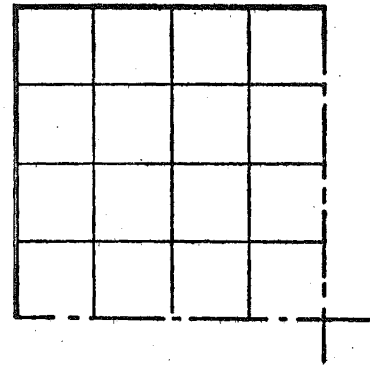
d. 8x8
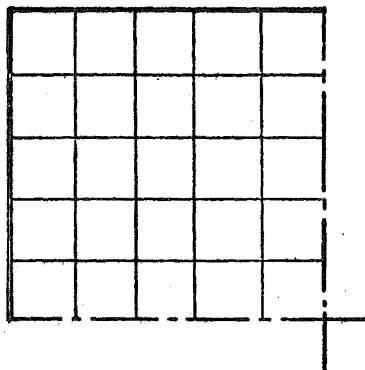
e. 10x10
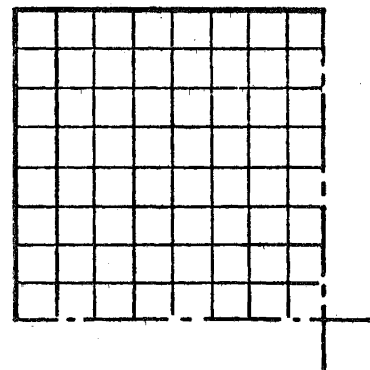
f. 16x16

Fig. 22 Fully Supported Square Plate and Discretizations
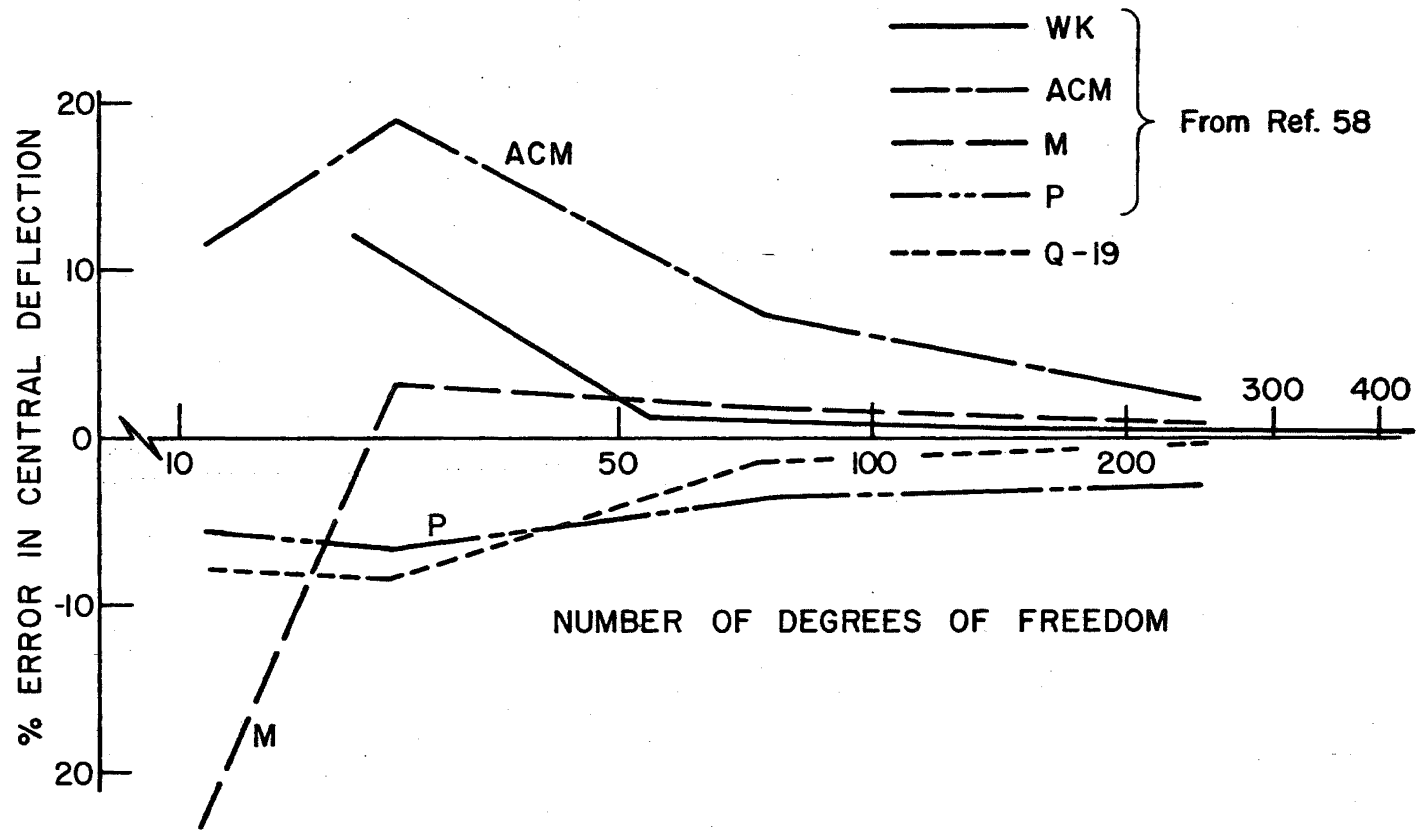
Fig. 23 Percent Error in Central Deflection Versus Number of Degrees of Freedom - Fixed Supports with Concentrated Load at Center

% ERROR IN CENTRAL DEFLECTION
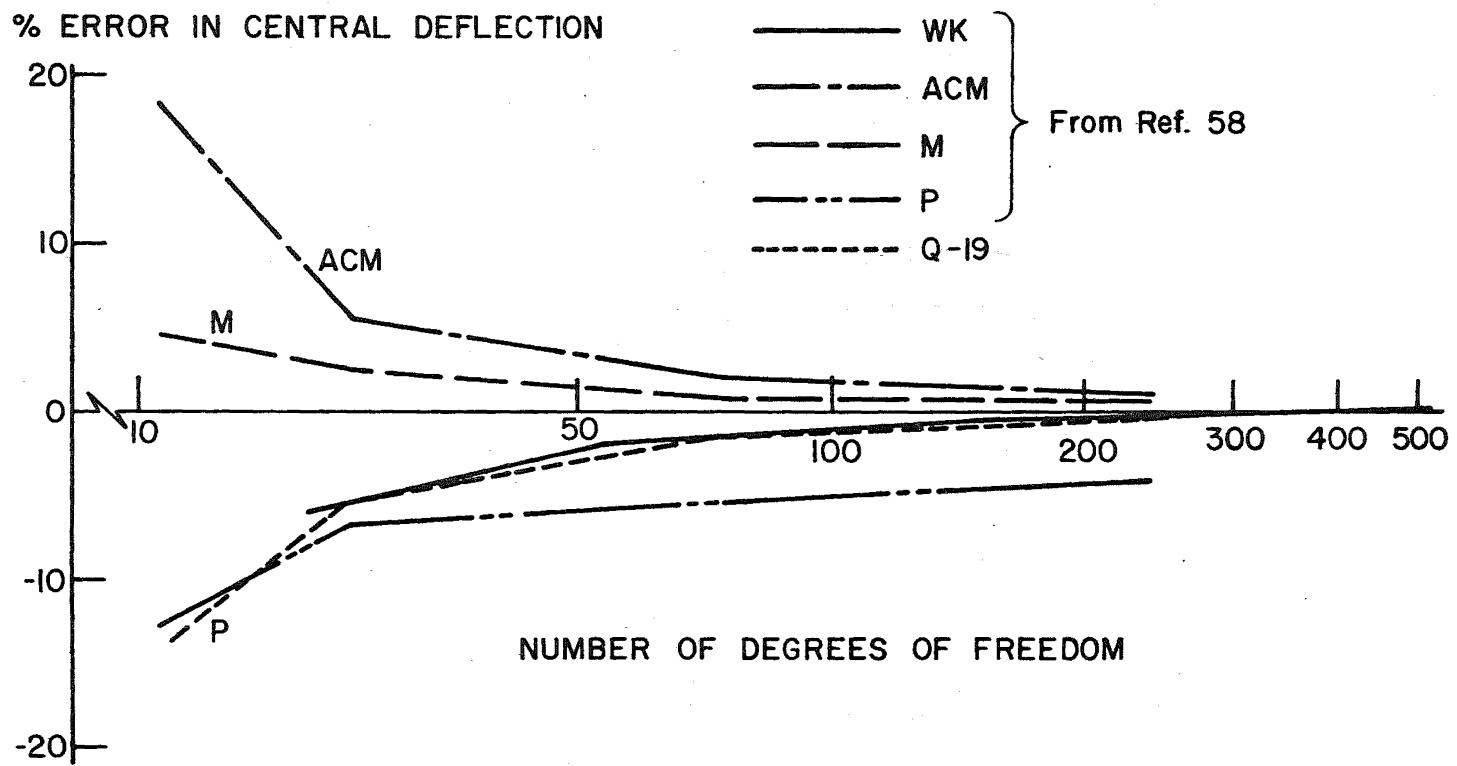
Fig. 24 Percent Error in Central Deflection Versus Number of Degrees of Freedom - Simple Supports with Concentrated Load at Center.
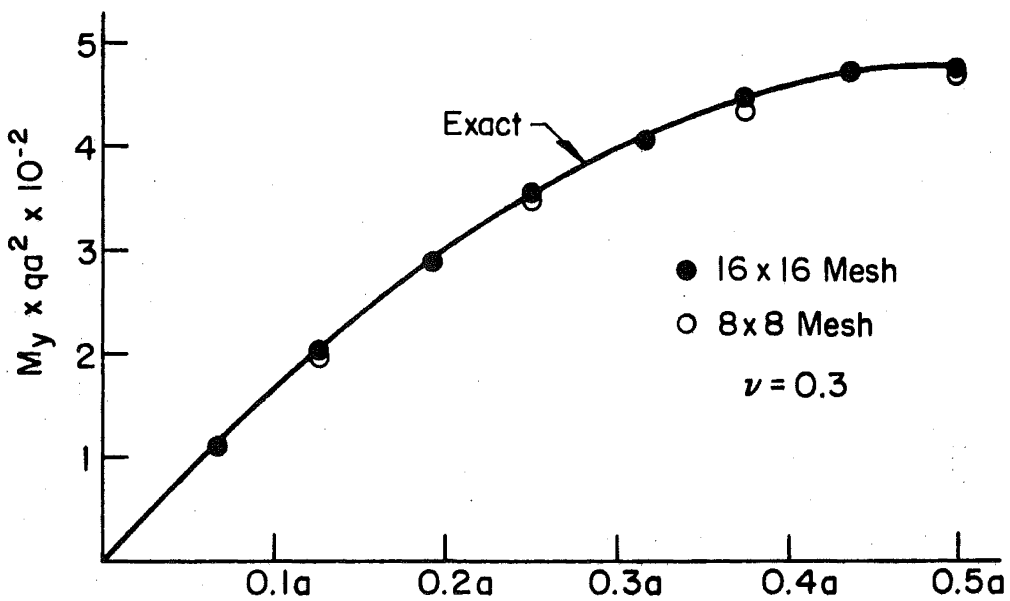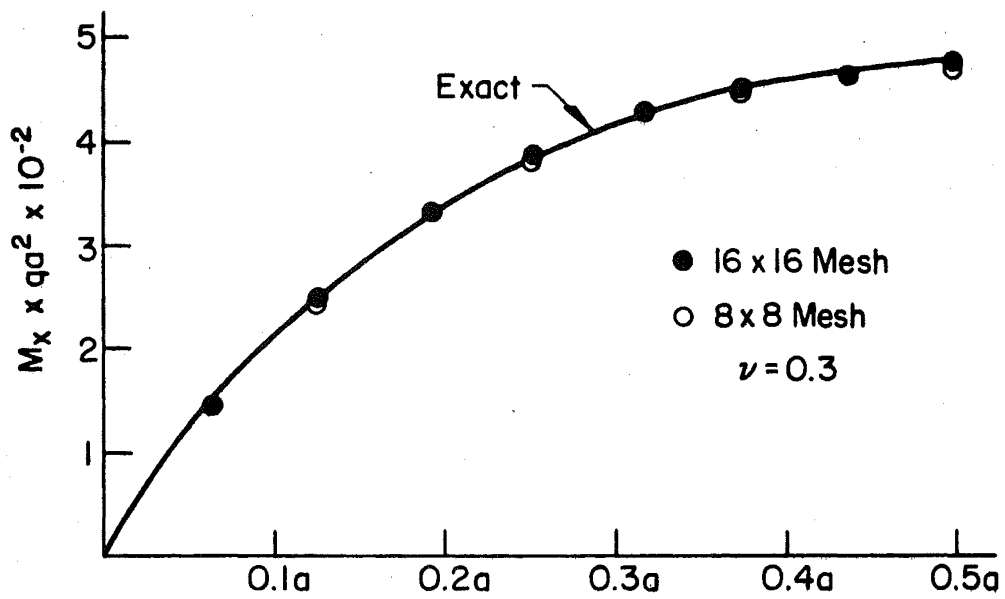
Fig. 25 Bending Moments M_x and M_y in a Simply Supported
Square Plate - Uniform Load
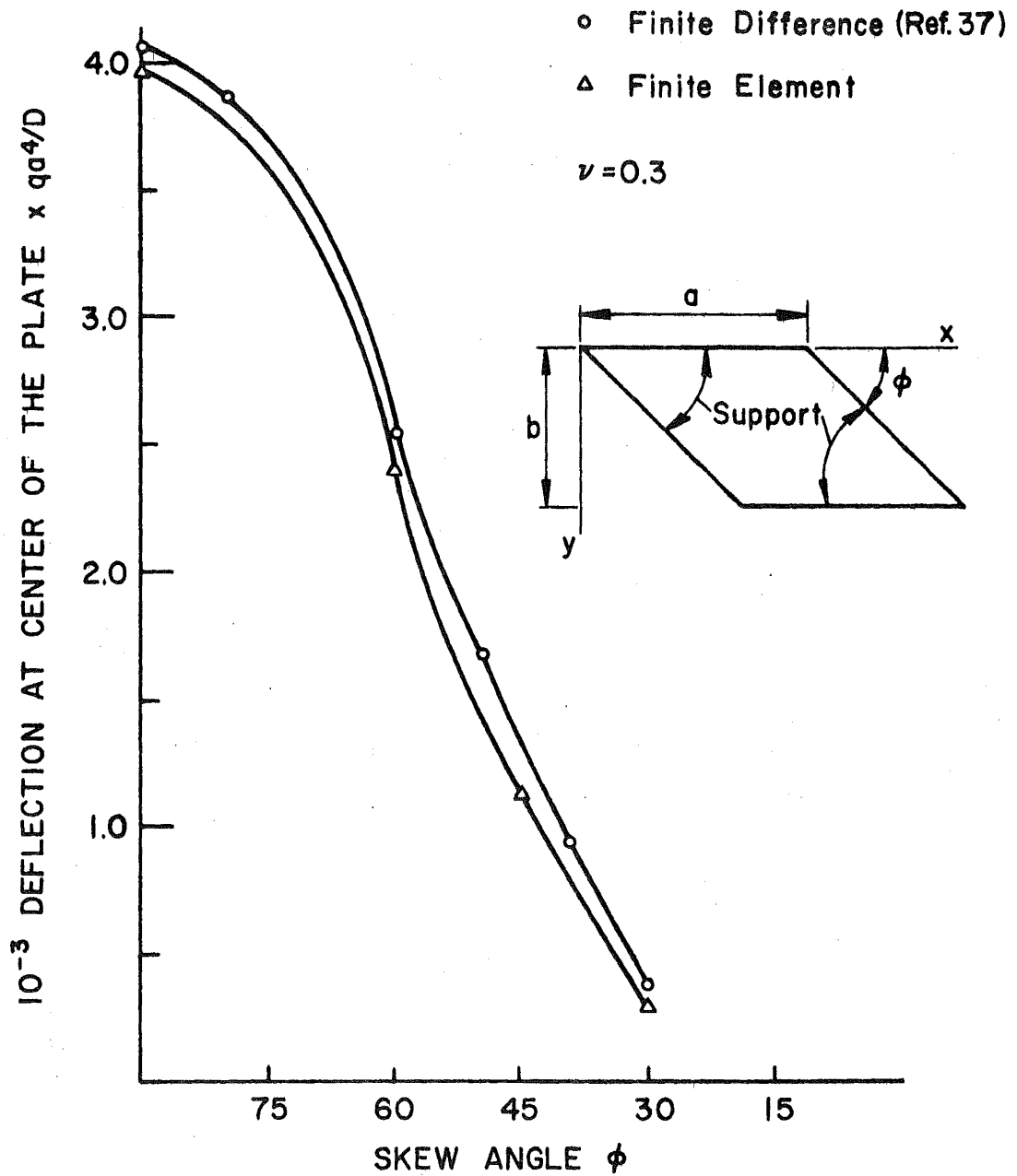
Fig. 26 Deflection at the Center of a Simply Supported
Rhombic Plate - Uniform Load
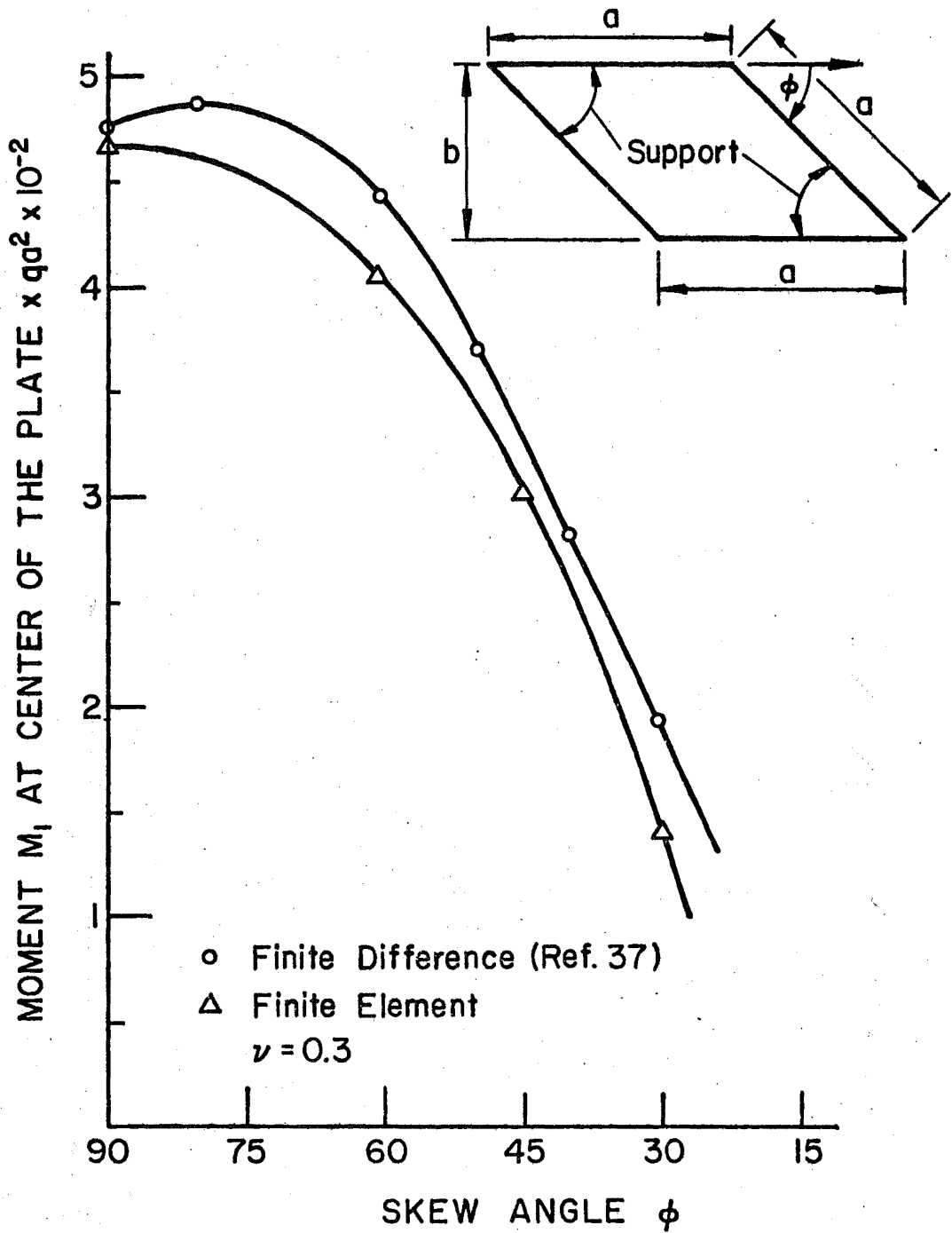
Fig. 27 Principal Moment M_1 at Center of a Simply
Supported Rhombic Plate — Uniform Load
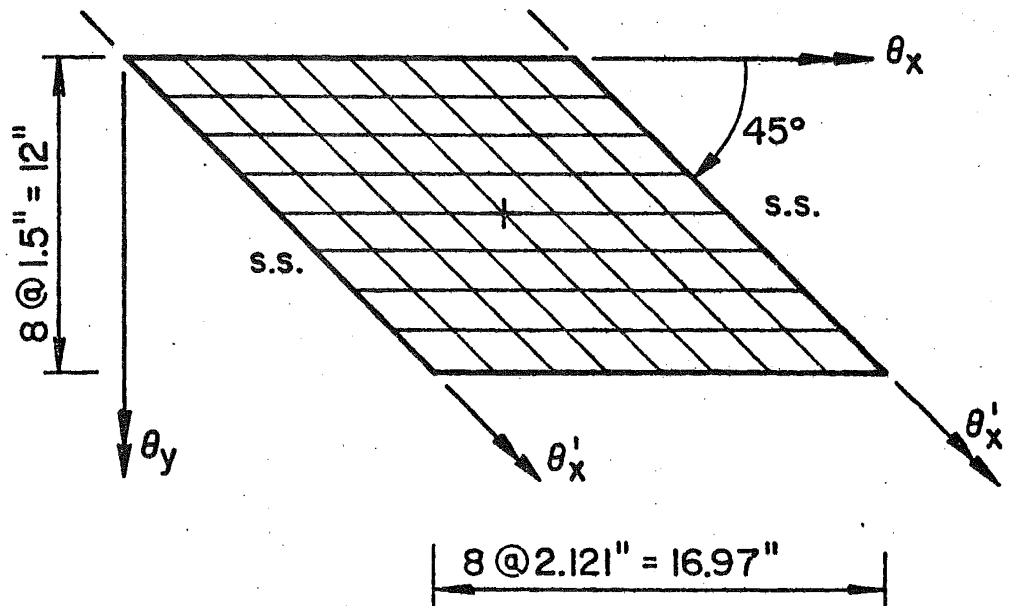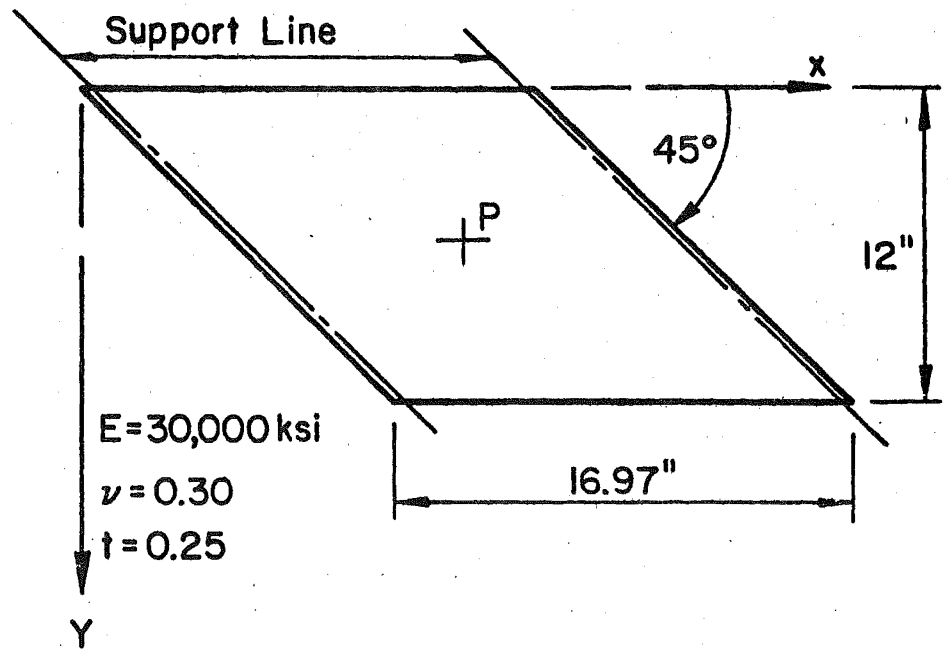
Fig. 28   Skew Steel Plate, Two Sides Simply Supported -
Concentrated Load at Center

$E = 1.0665 \times 10^6 \ \text{lb/in}^2$ $\ell_\phi = 100 \ \text{in}$

$\nu = 0.215$ $\phi = 60°$
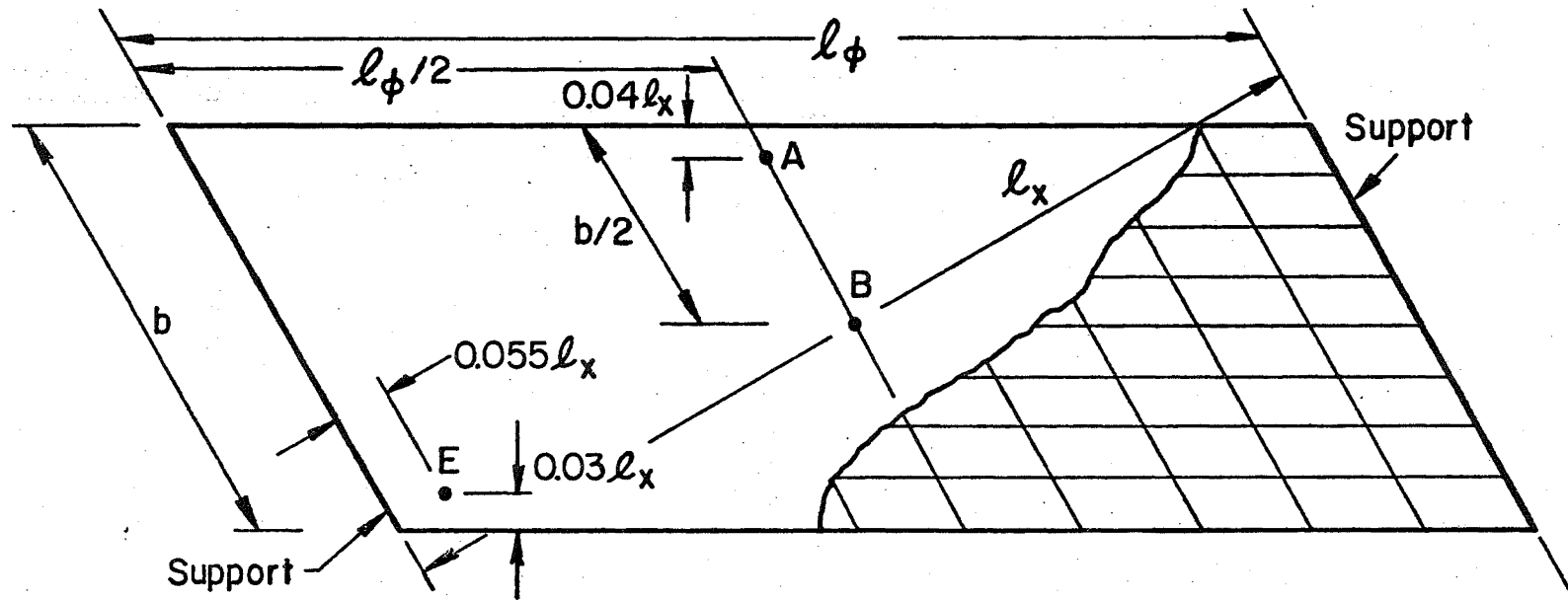
$t = 3.47$ $\ell_x = 86.66 \ \text{in}$

$b = 40.0 \ \text{in}$

Fig. 29   Skew Slab Model (Ref. 48) and Discretization Scheme 1
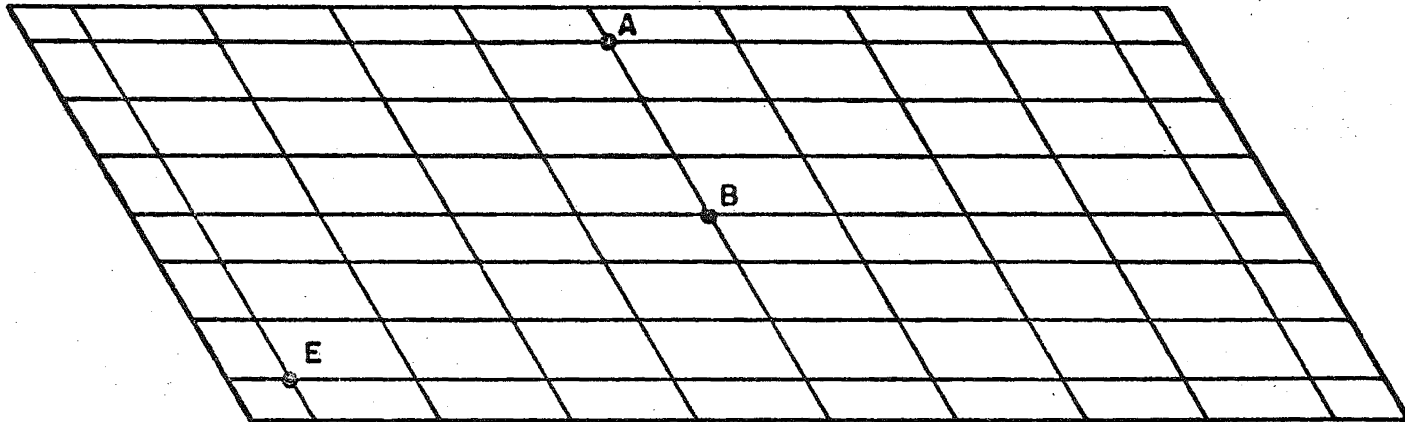
Discretization Scheme 2
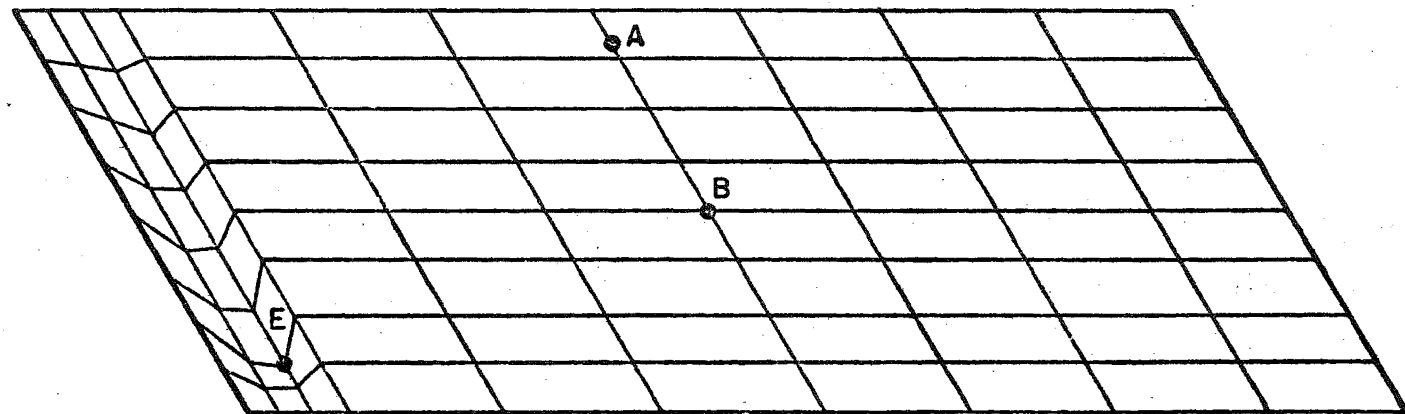
Discretization Scheme 3

Fig. 30   Skew Slab Model Discretization Schemes 2 and 3
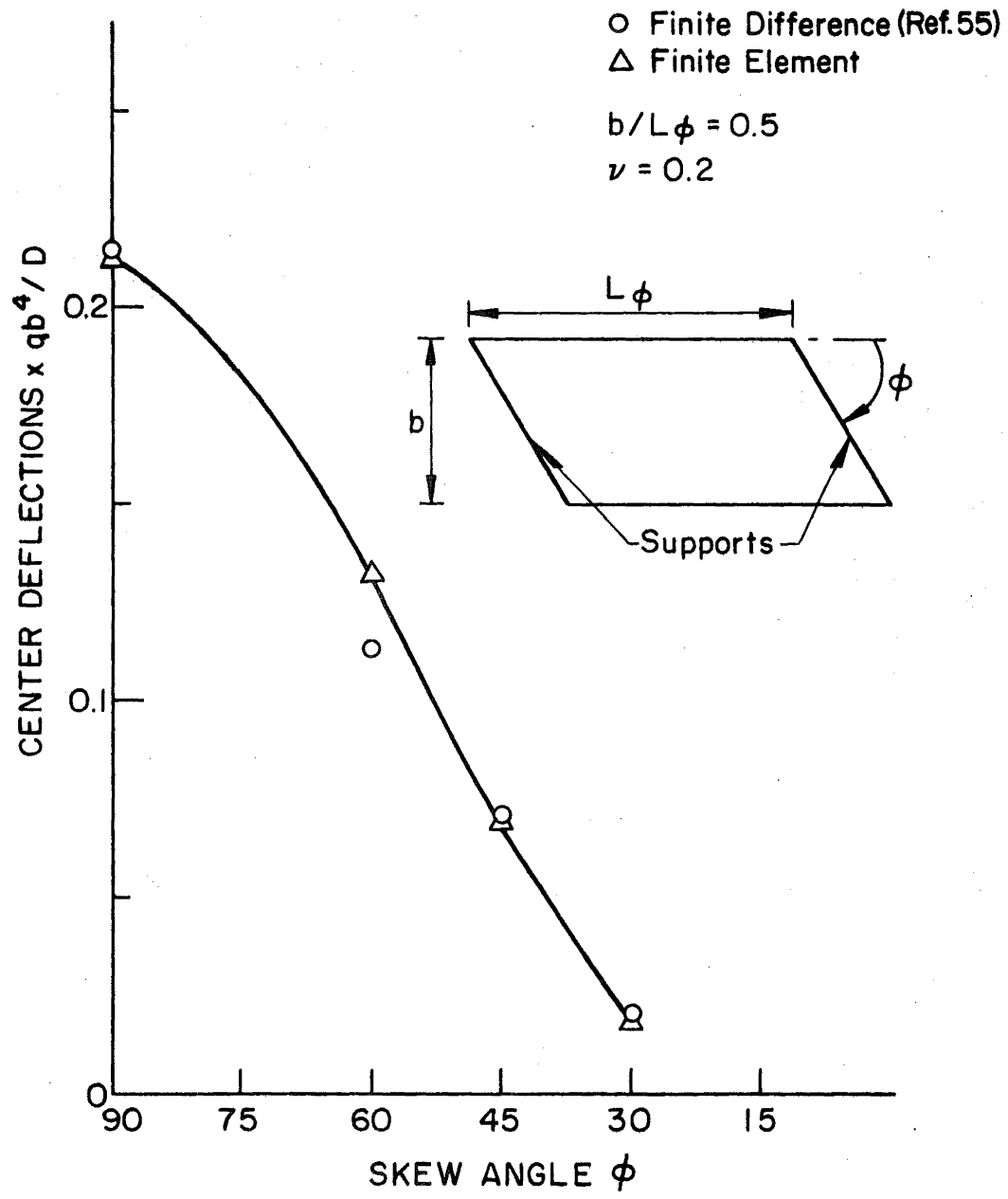
Fig. 31 Deflection of a Skew Plate, Two sides Simply
Supported - Uniform Loads
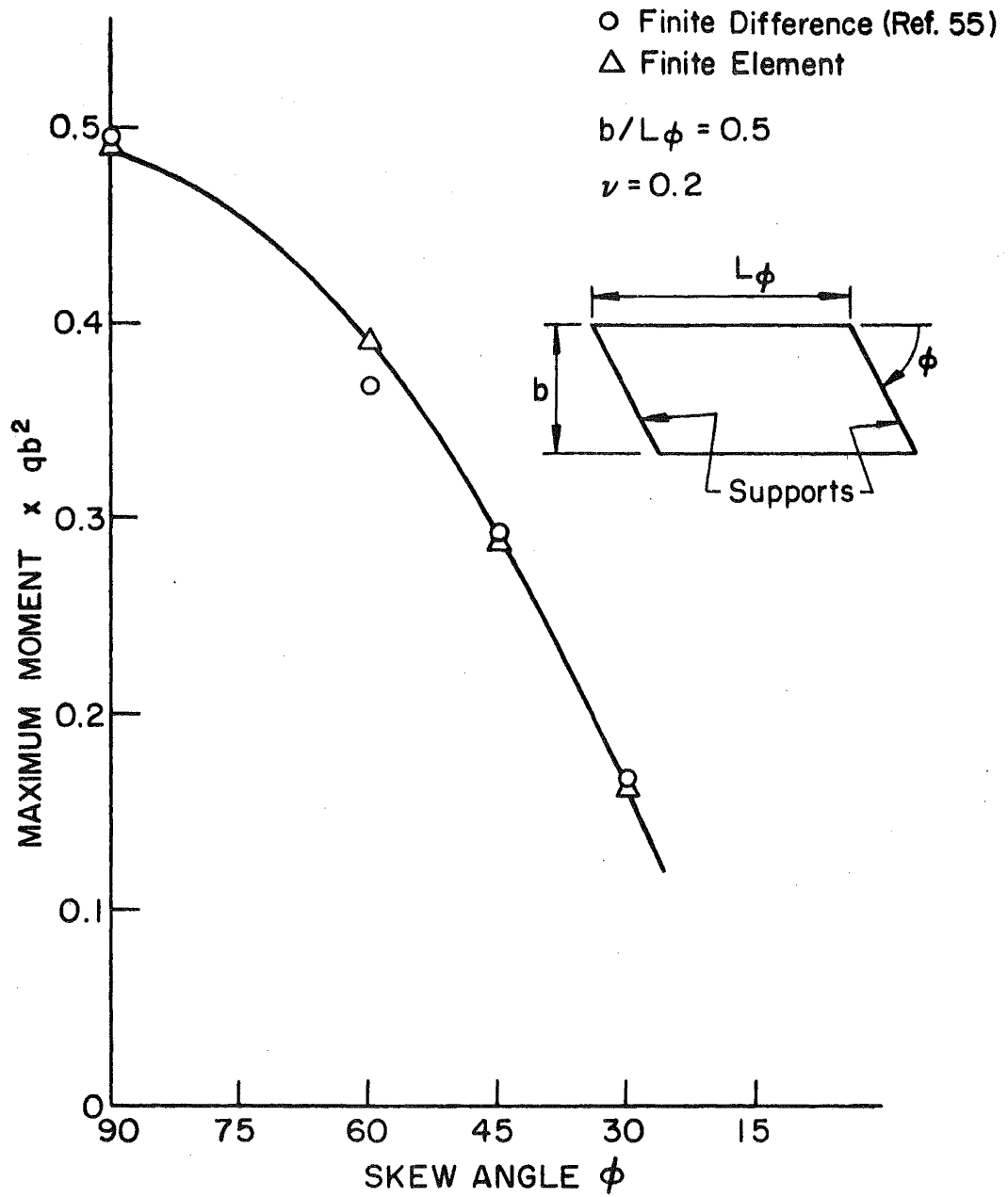
Fig. 32 Maximum Moment in a Skew Plate, Two Sides Simply Supported - Uniform Load
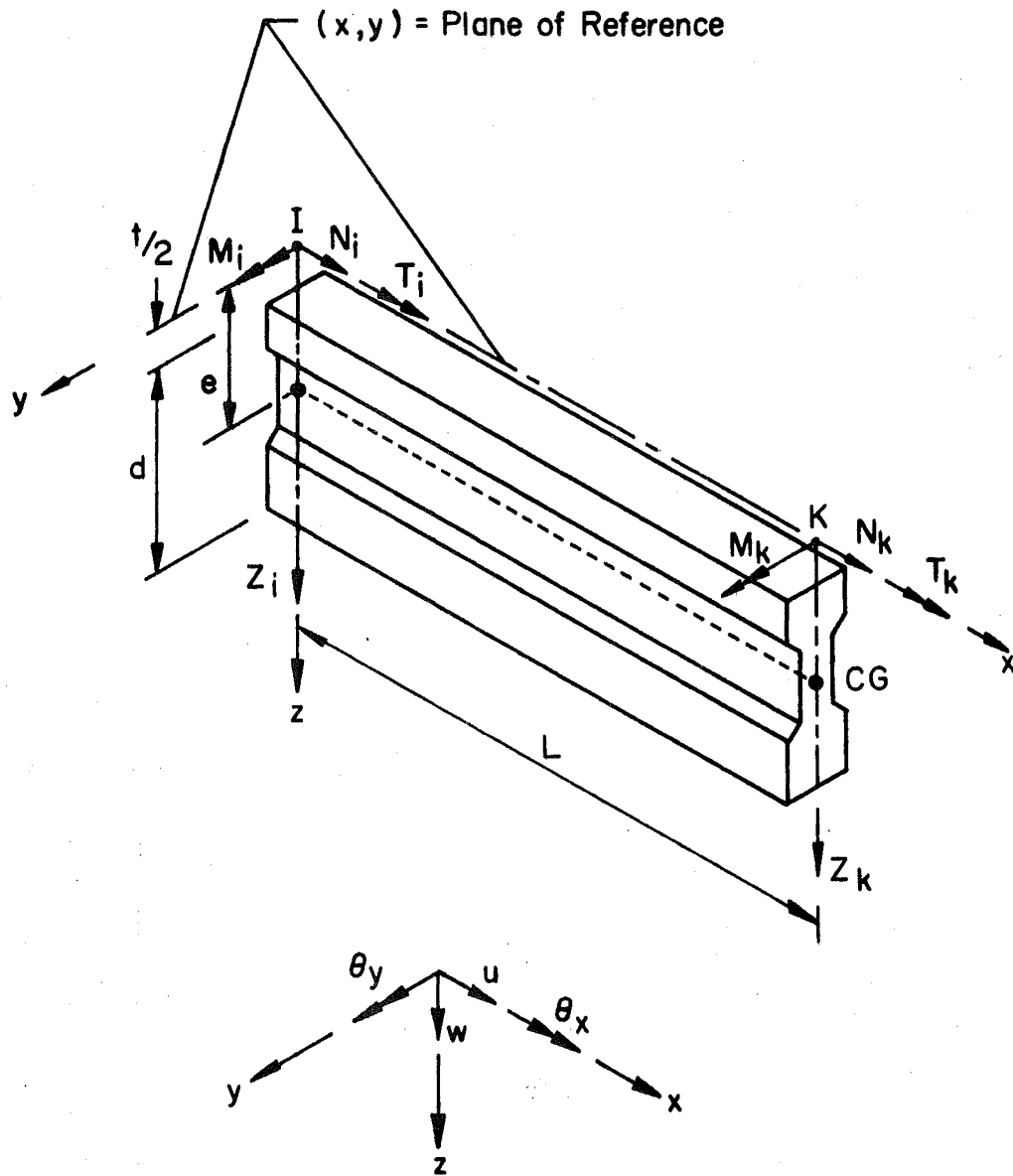
Fig. 33 A Stiffener Finite Element with Associated
Degrees of Freedom and Nodal Forces
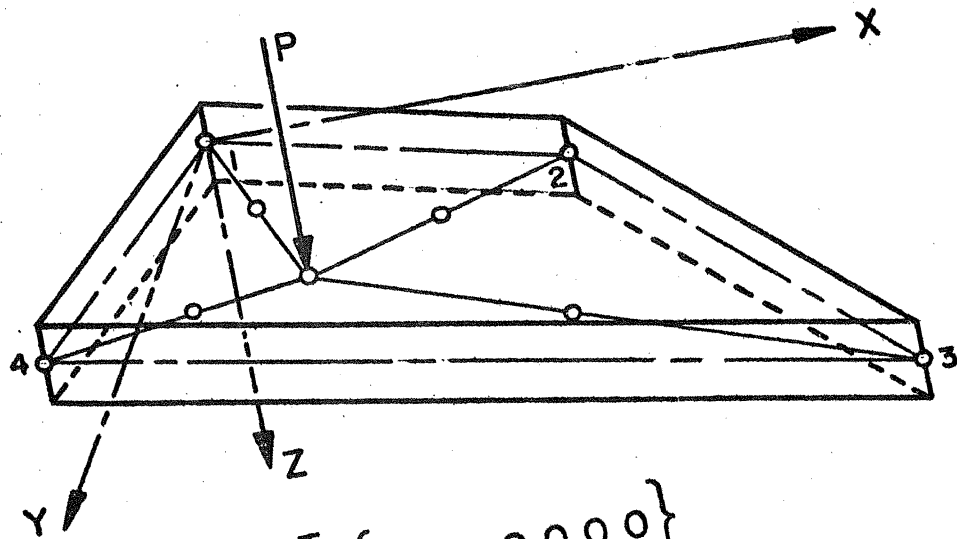
$$\{F_I\}^T = \{P\ 0\ 0\ 0\ 0\ 0\}$$
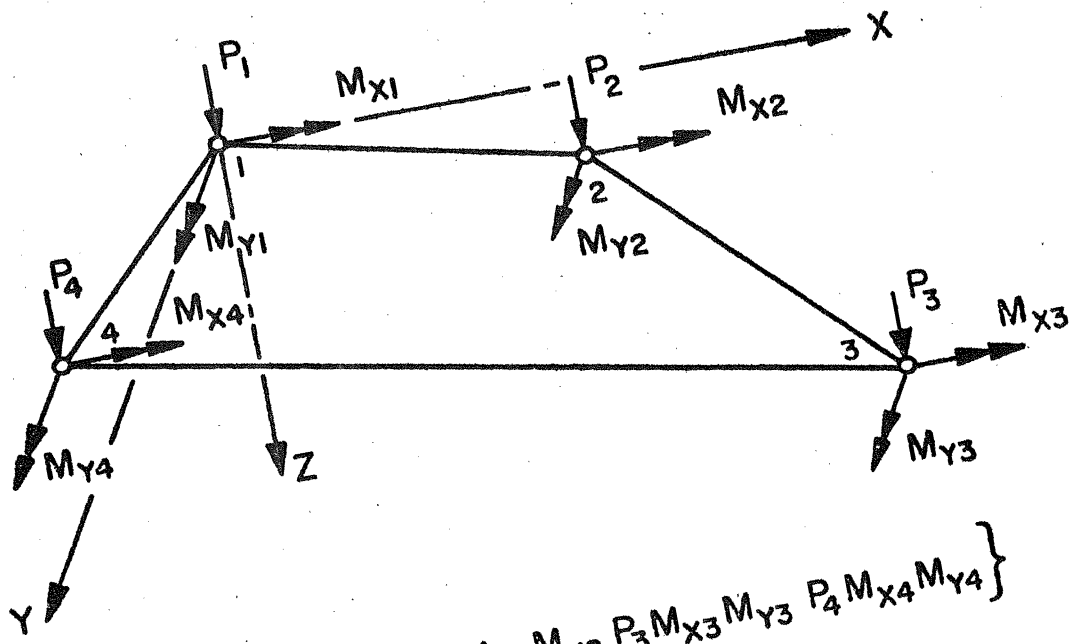
$$\{F_E\}^T = \{P_1 M_{X1} M_{Y1}\ P_2 M_{X2} M_{Y2}\ P_3 M_{X3} M_{Y3}\ P_4 M_{X4} M_{Y4}\}$$

Fig. 34 Equivalent Force Vector $\{F_E\}$ Due to Concentrated Load P Normal to the Element

-177-
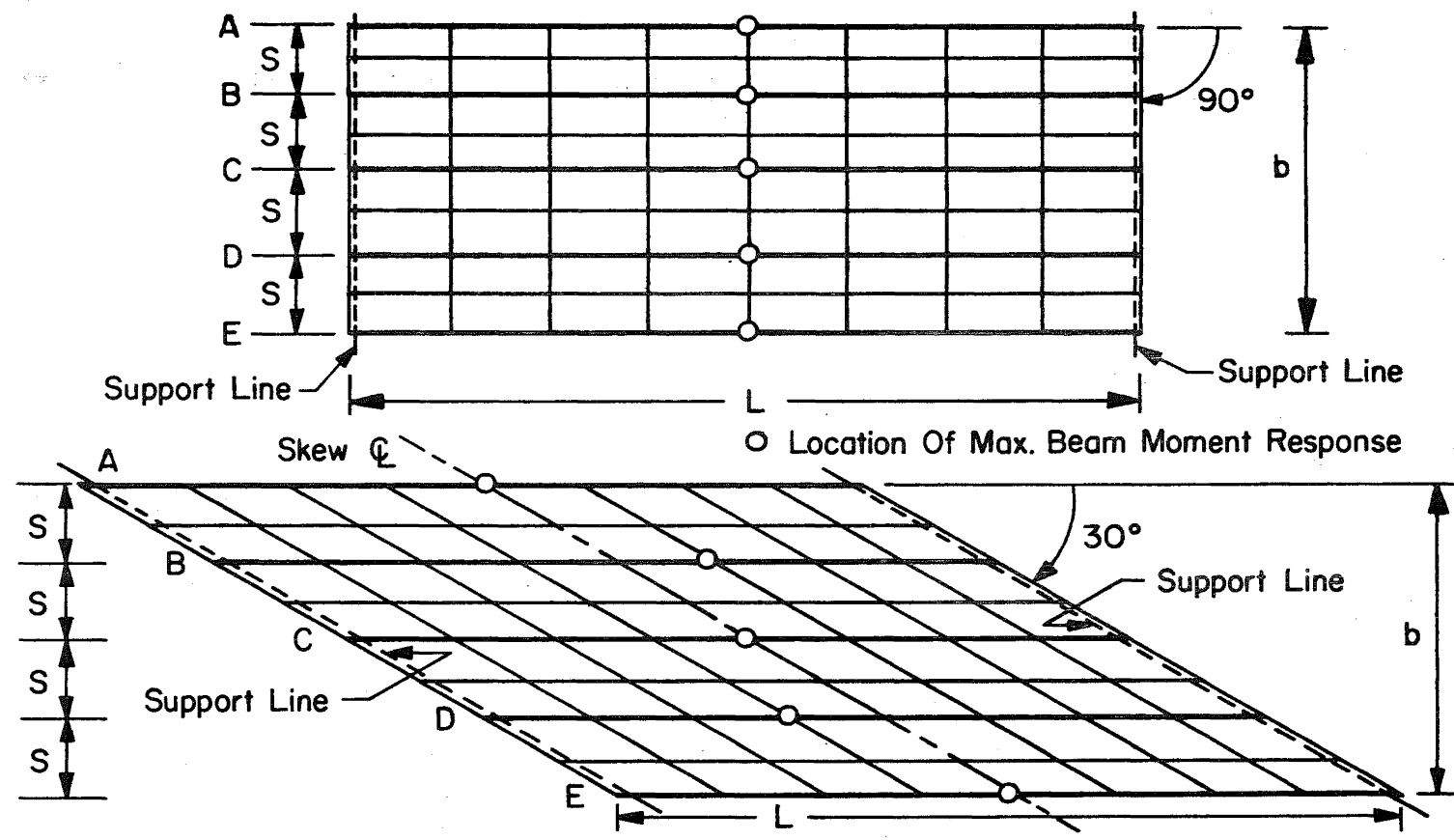
Fig. 35 Location of the Maximum Beam Moment Response in a $90°$ Skew Bridge (Right Bridge) and a $30°$ Skew Bridge - Concentrated Load at Midspan of Beam C
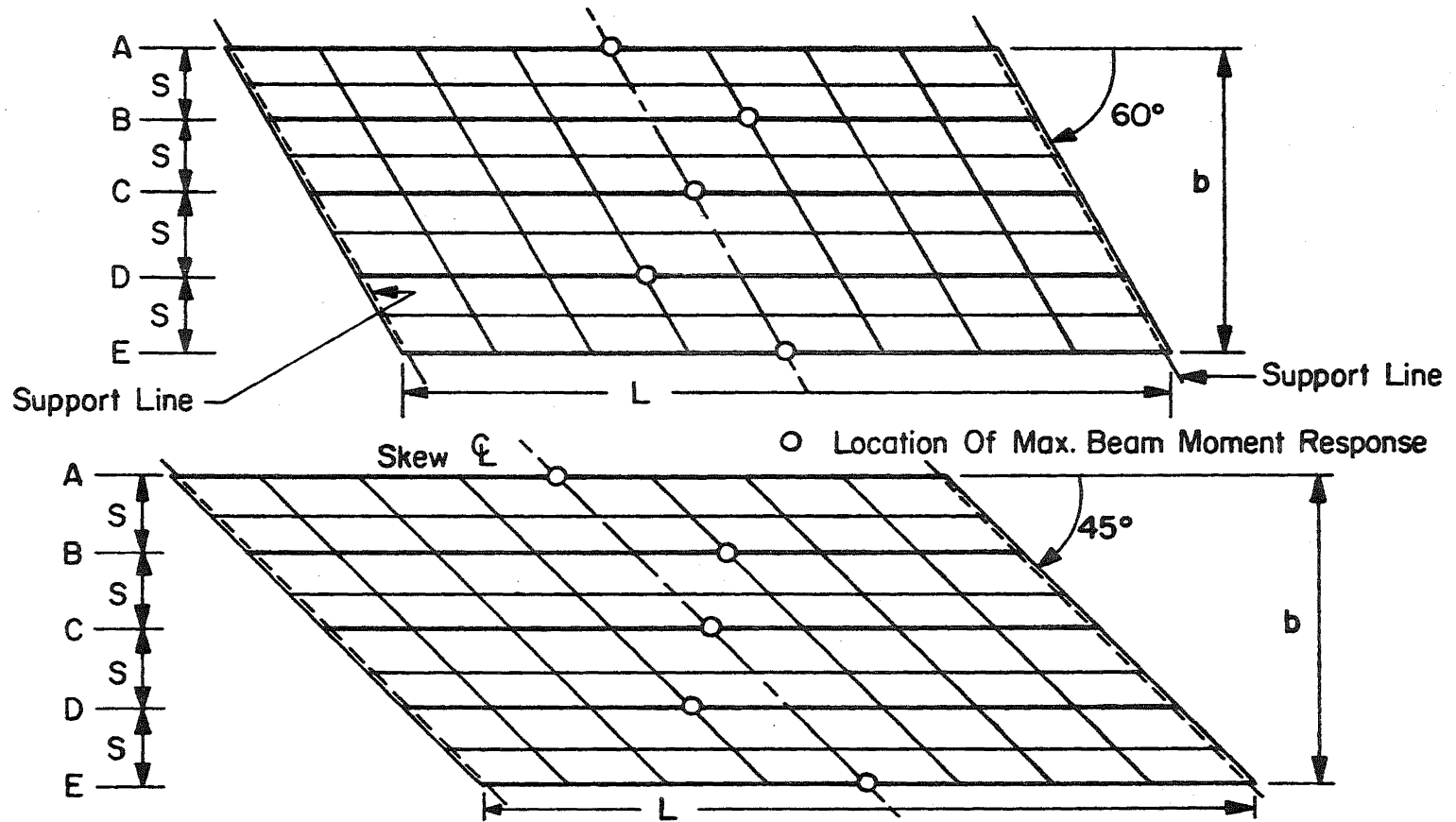
Fig. 36 Location of the Maximum Beam Moment Response in a 60° Skew Bridge and a 45° Skew Bridge - Concentrated Load at Midspan of Beam C
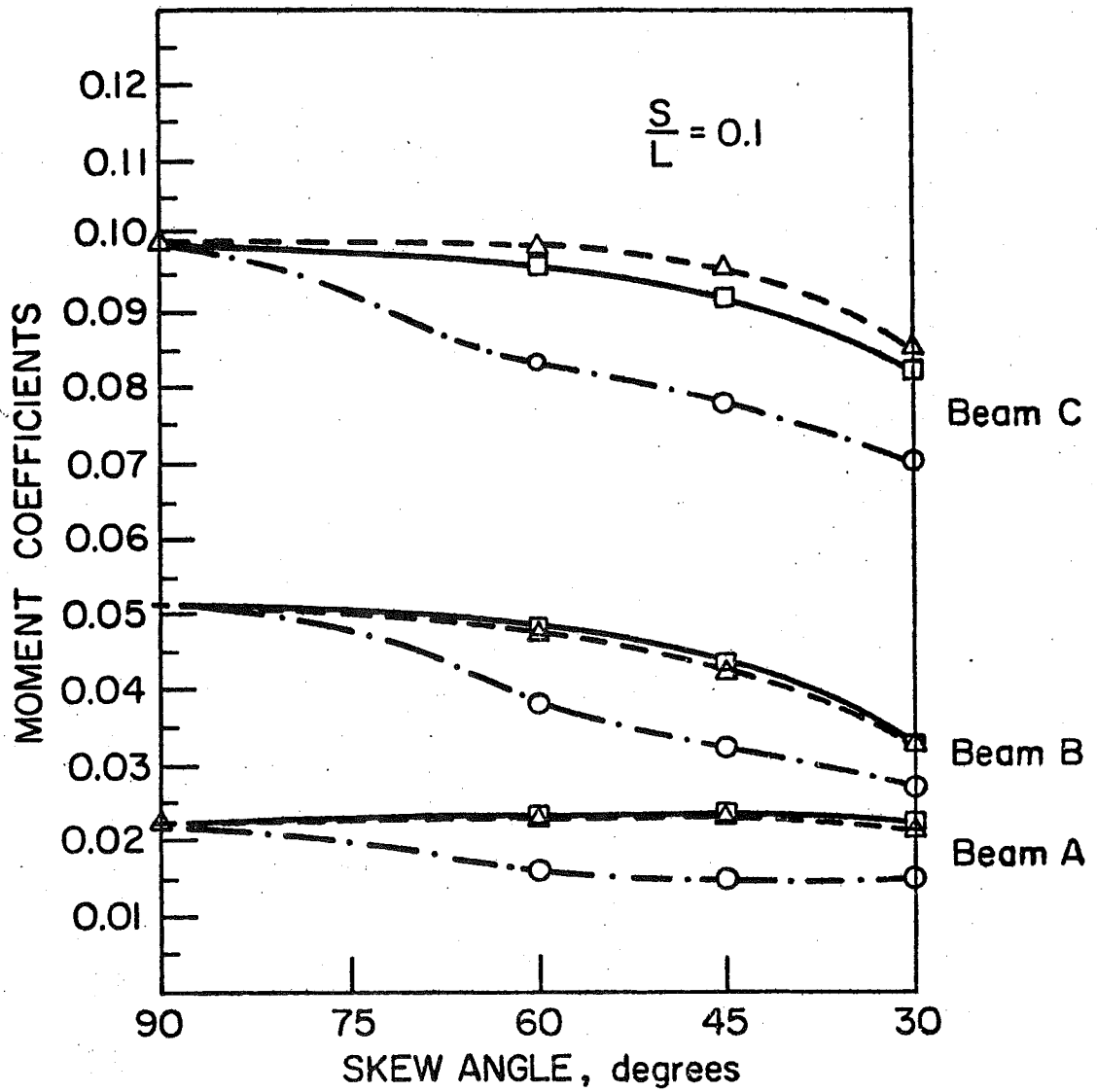
Fig. 37 Moment Coefficients in a 5-Beam Bridge Neglecting
the Eccentricity of the Beams to the Slab

-180-
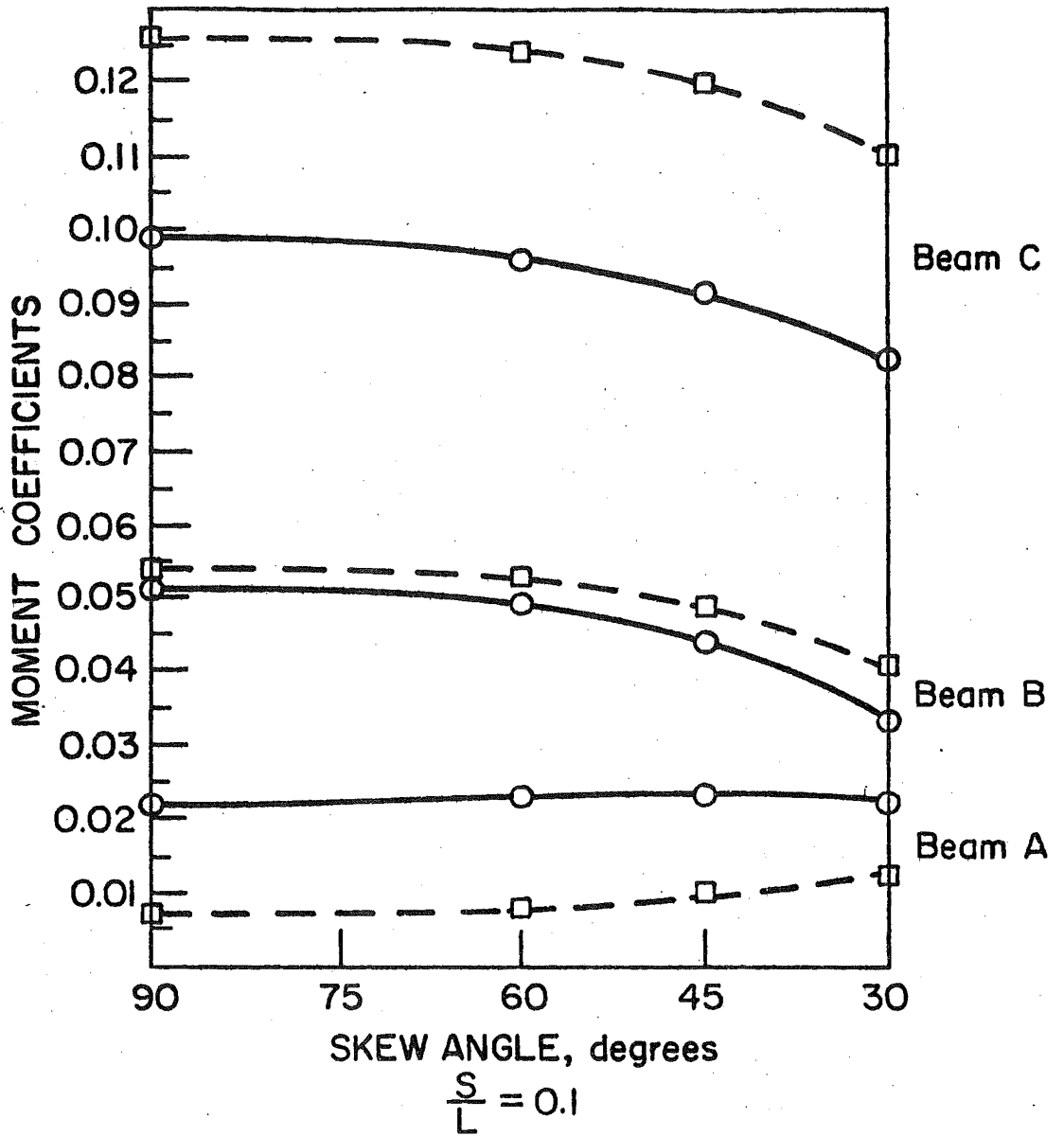
Fig. 38   Moment Coefficients in a 5-Beam Bridge Including
the Beam Eccentricity and Torsional Rigidity

● Load Points
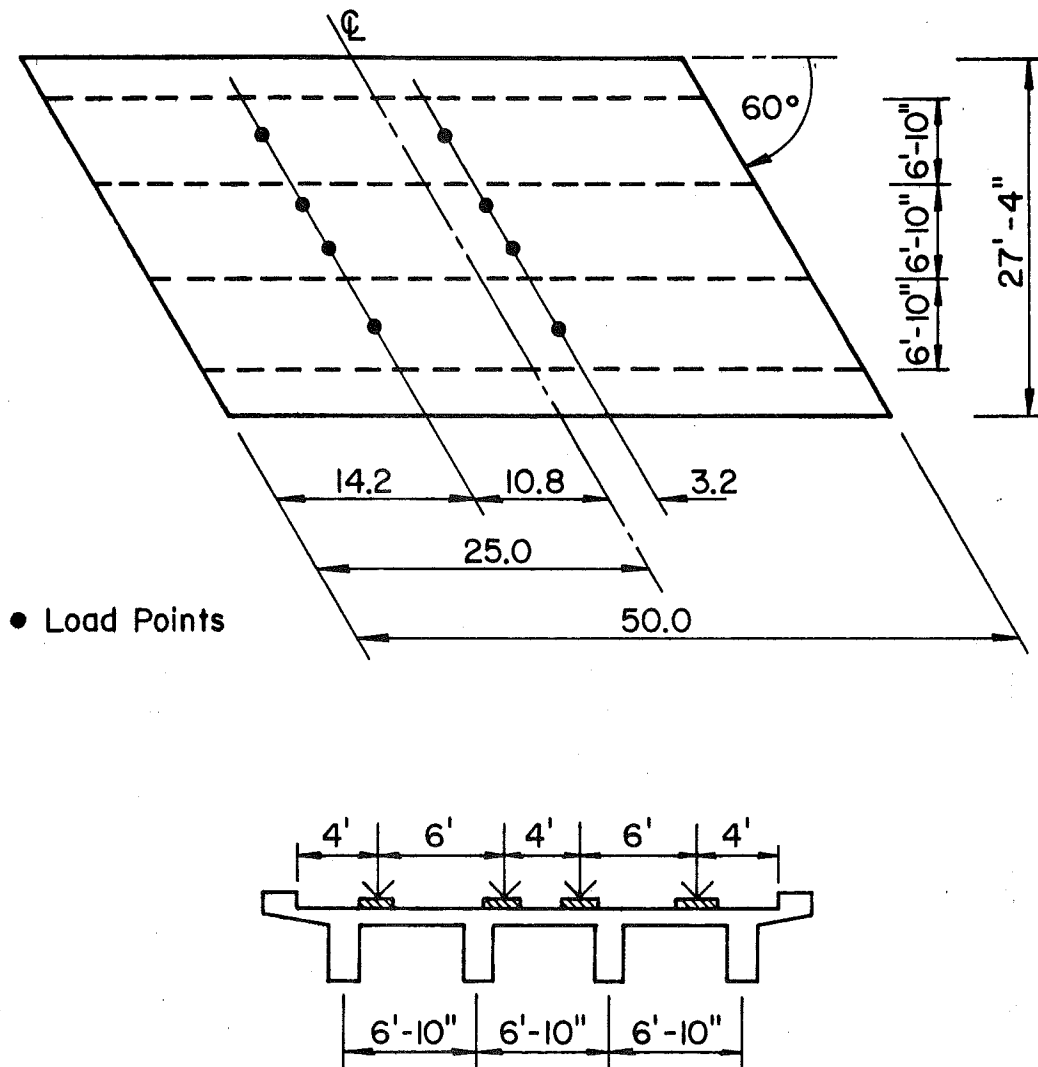
Fig. 39 Static Load Test of Bridge 3 (Ref. 6)

Plan and Discretization

| Interior Beam |
| Center Beam |
| Exterior Beam |

2'
2'-6"
4 @ 2'-6"
3'

2'
5'-0"
5'-0"
3'

15'-0"

12 @ 4'-2" = 50'-0"

15'-0"

3'-0"   5'-0"   5'-0"   2'-0"

⅞" bolts (4'-2" o.c.)
1'-0"
#3 Bars at 1'-6" Ctrs.
No Crown
6½"
1½"

6"
#5 Bars at 5" Ctrs.
⅞" Rivets
12" ℄ 20.7
3"
1½"
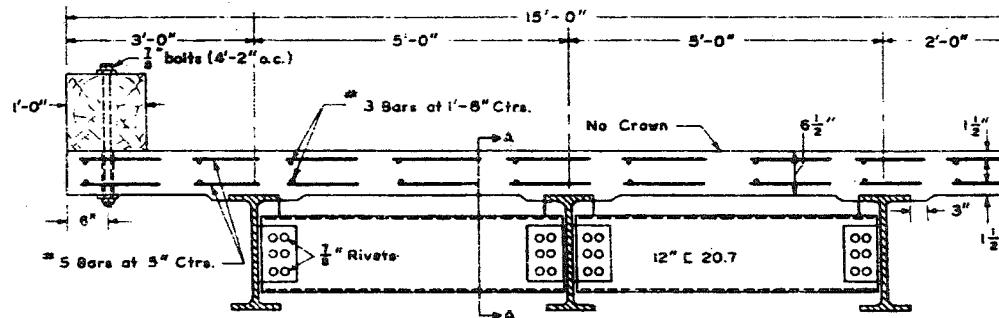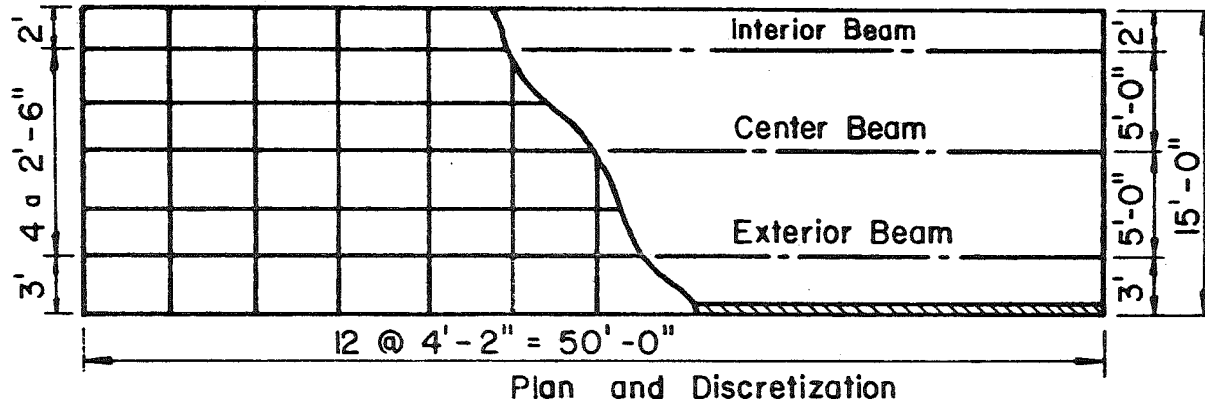
Beam Properties

Bridge	Beam Size	I_x (In^4) w/Coverplate
2B	w18 x 50	1040
3B	w18 x 60	1176

Fig. 40 AASHO Test Bridge (Ref. 24)
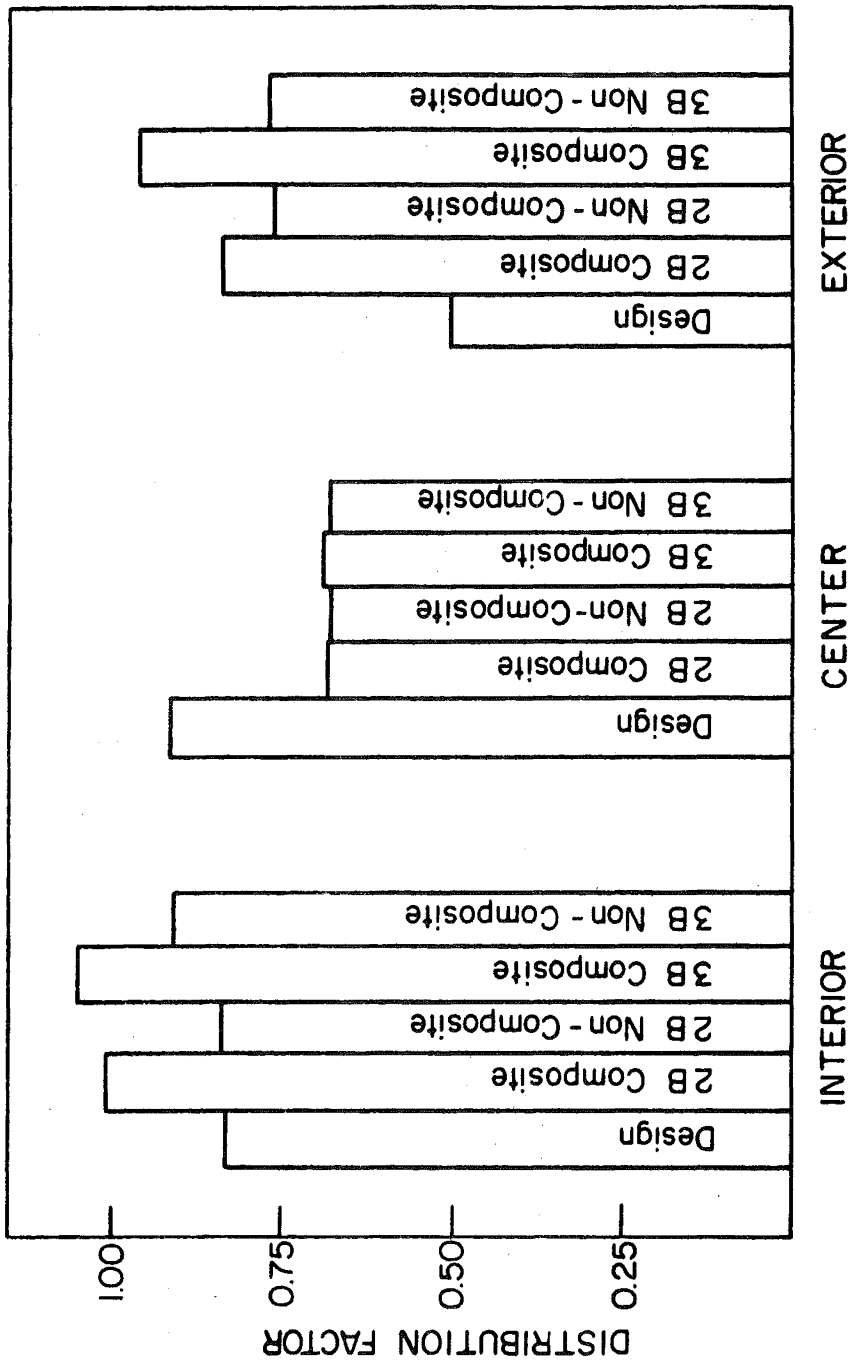
Fig. 41   Distribution Factors for Interior, Center and Exterior Bridge Beams - AASHO Test Bridge
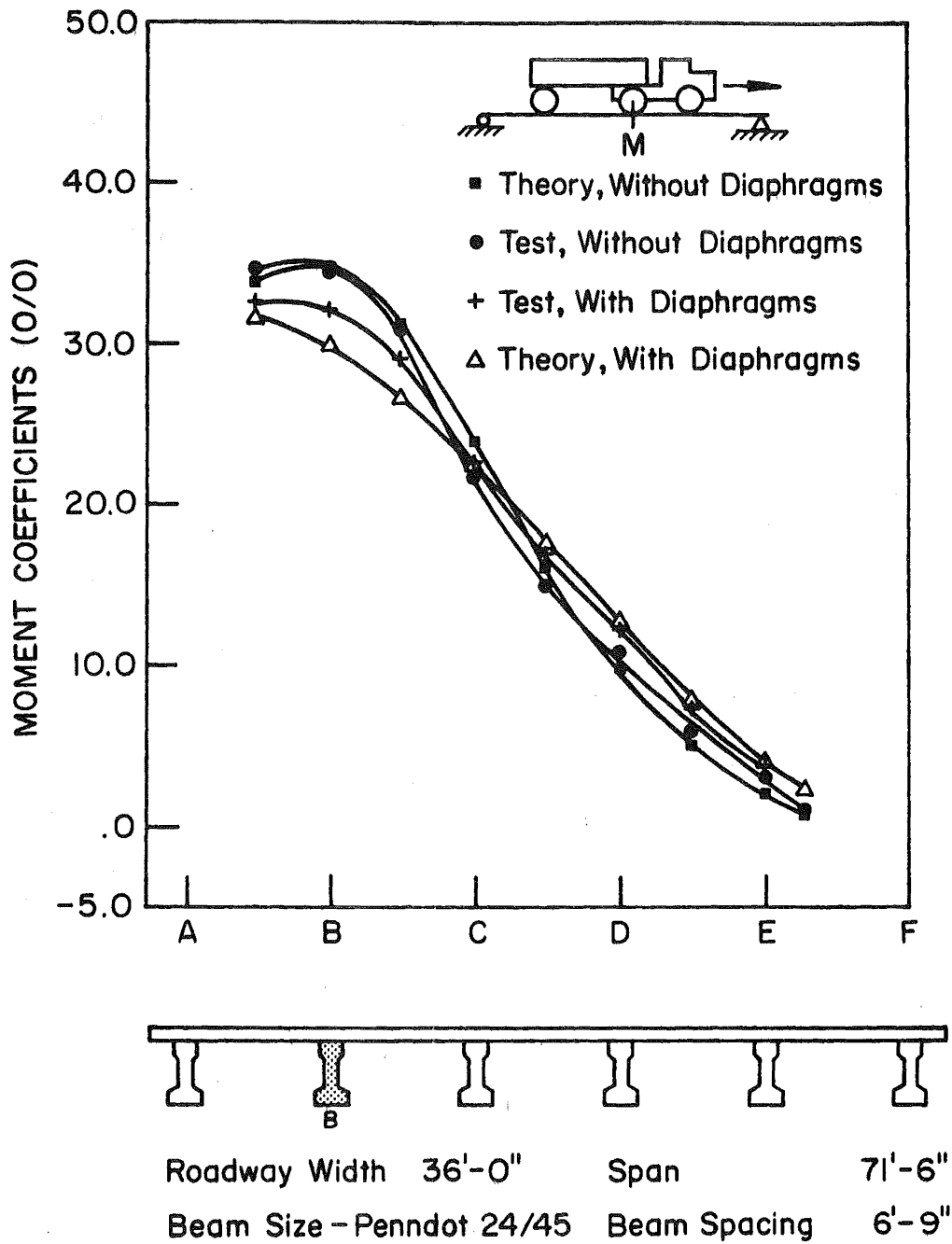
Fig. 42 Influence Lines for Moments - Lehighton Bridge
With and Without Diaphragms, Beam B
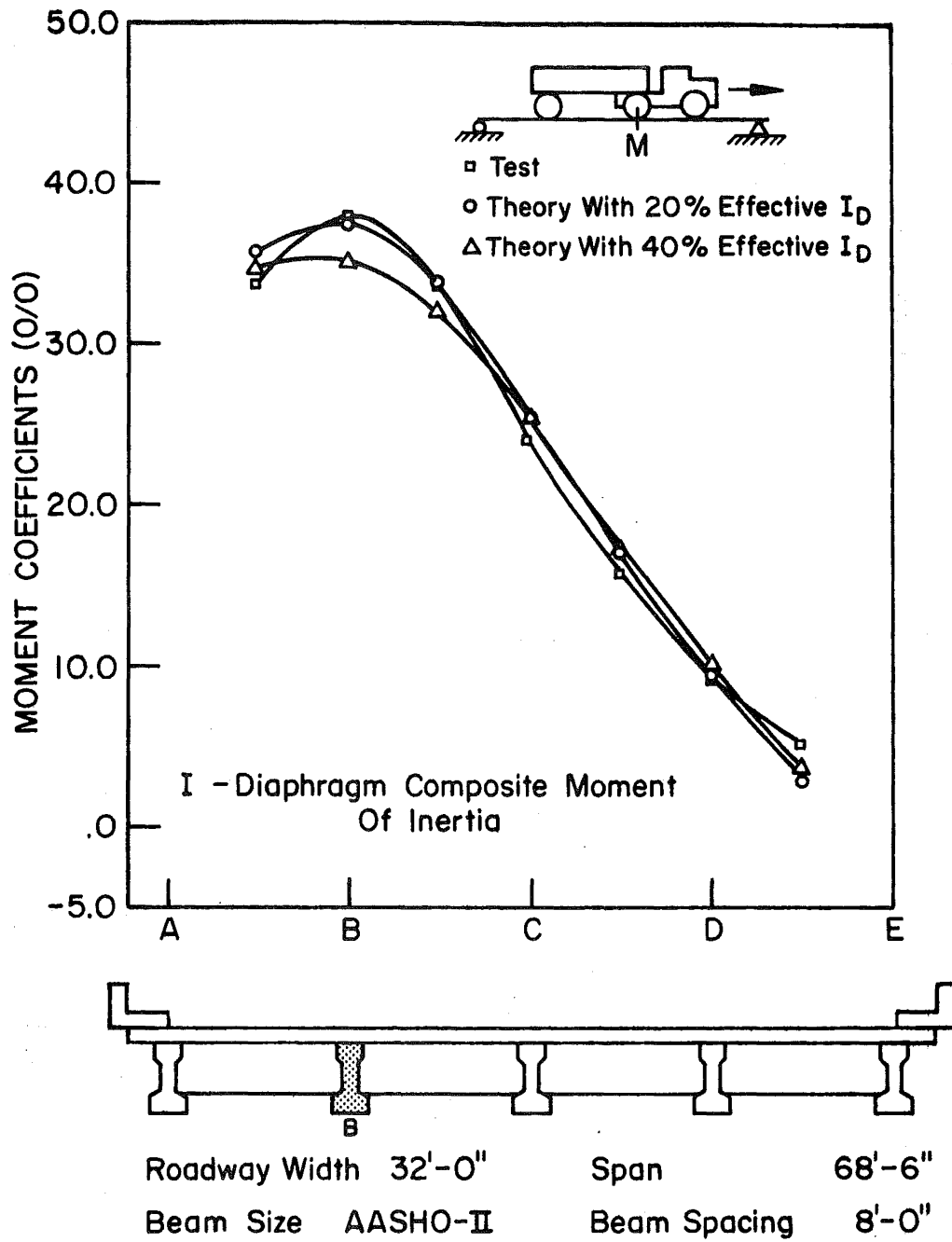
Fig. 43 Influence Lines for Moment - Bartonsville Bridge
with Partially Effective Diaphragms, Beam B
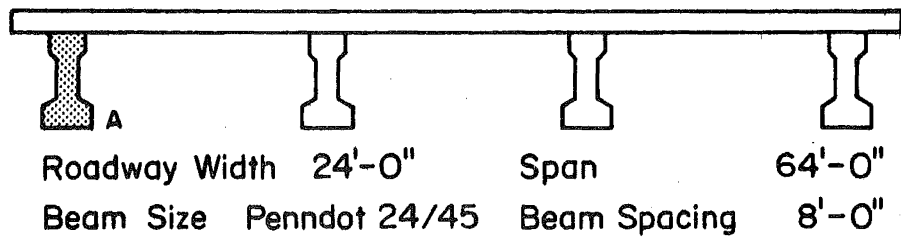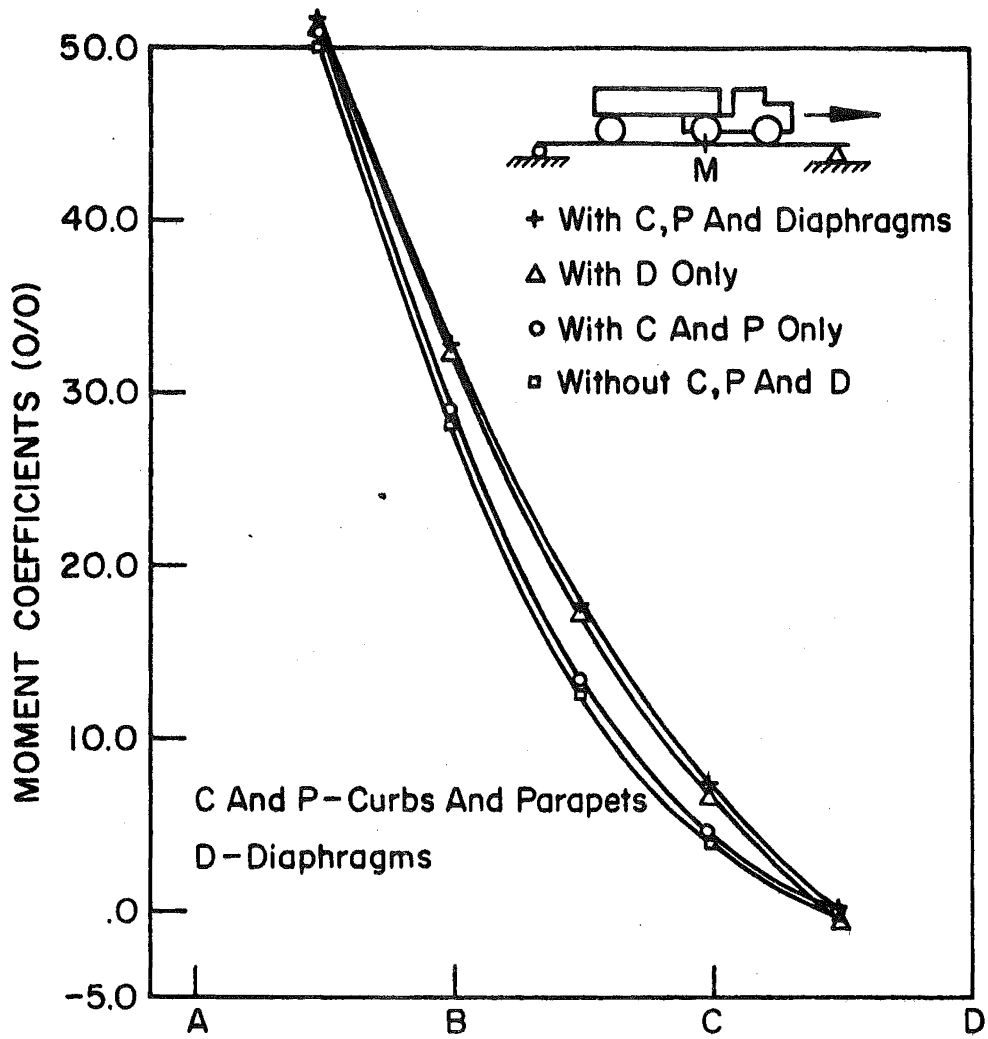
Fig. 44 Influence Lines for Moment, Beam A - 4-Beam
Bridge
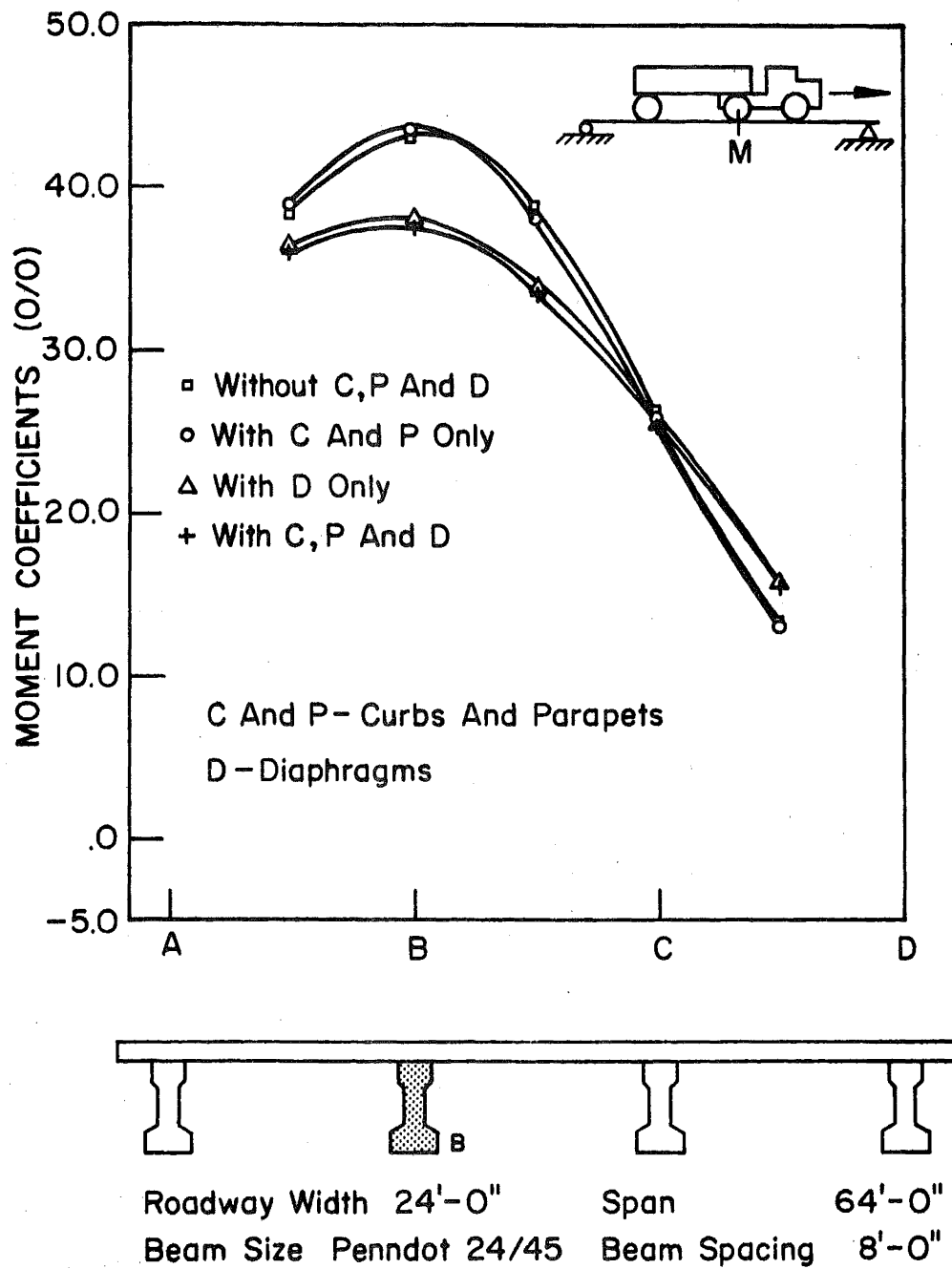
Fig. 45 Influence Lines for Moments, Beam B - 4-Beam
Bridge
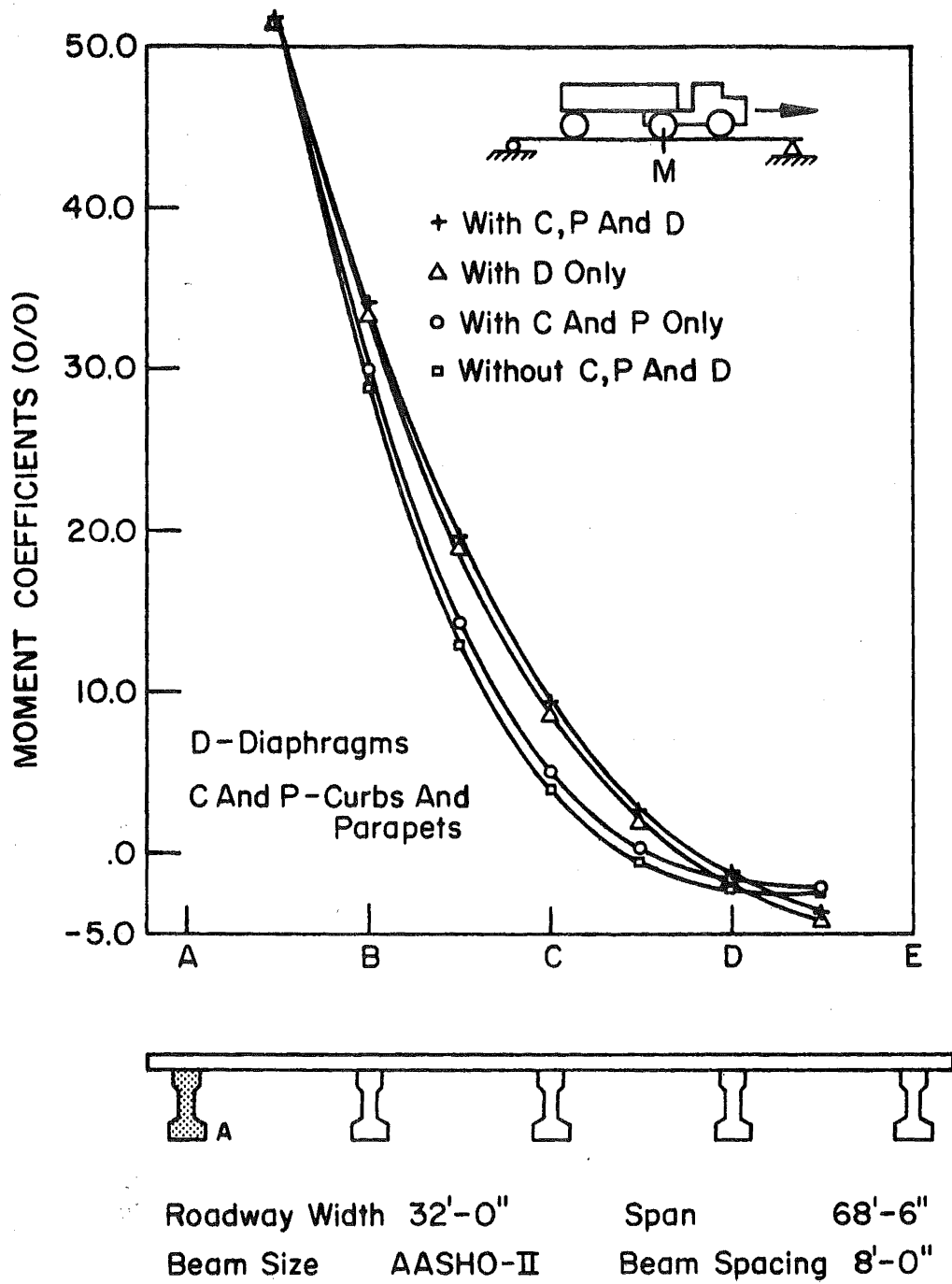
Fig. 46 Influence Lines for Moments, Beam A - 5-Beam
Bridge
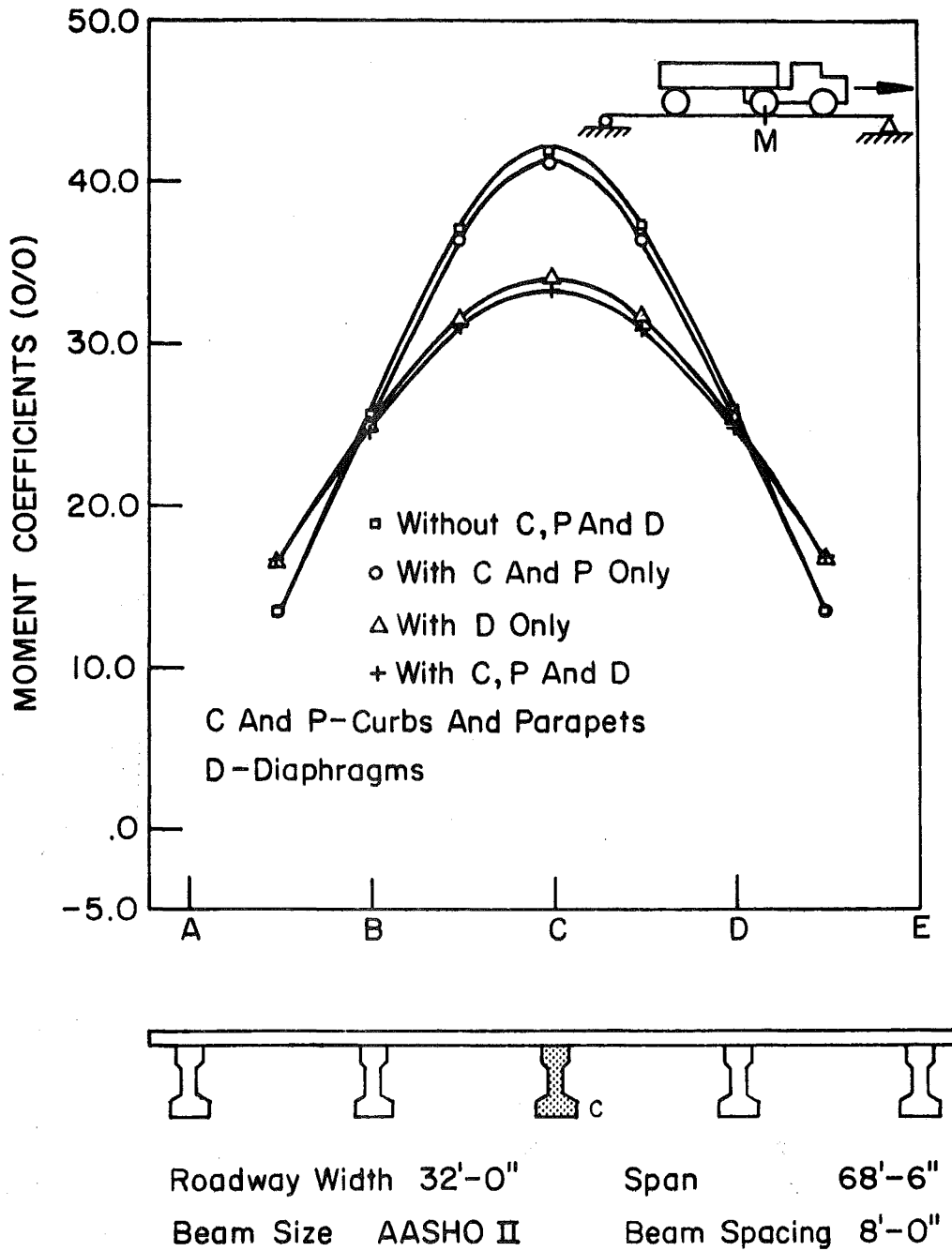
Fig. 47 Influence Lines for Moments, Beam C - 5-Beam Bridge
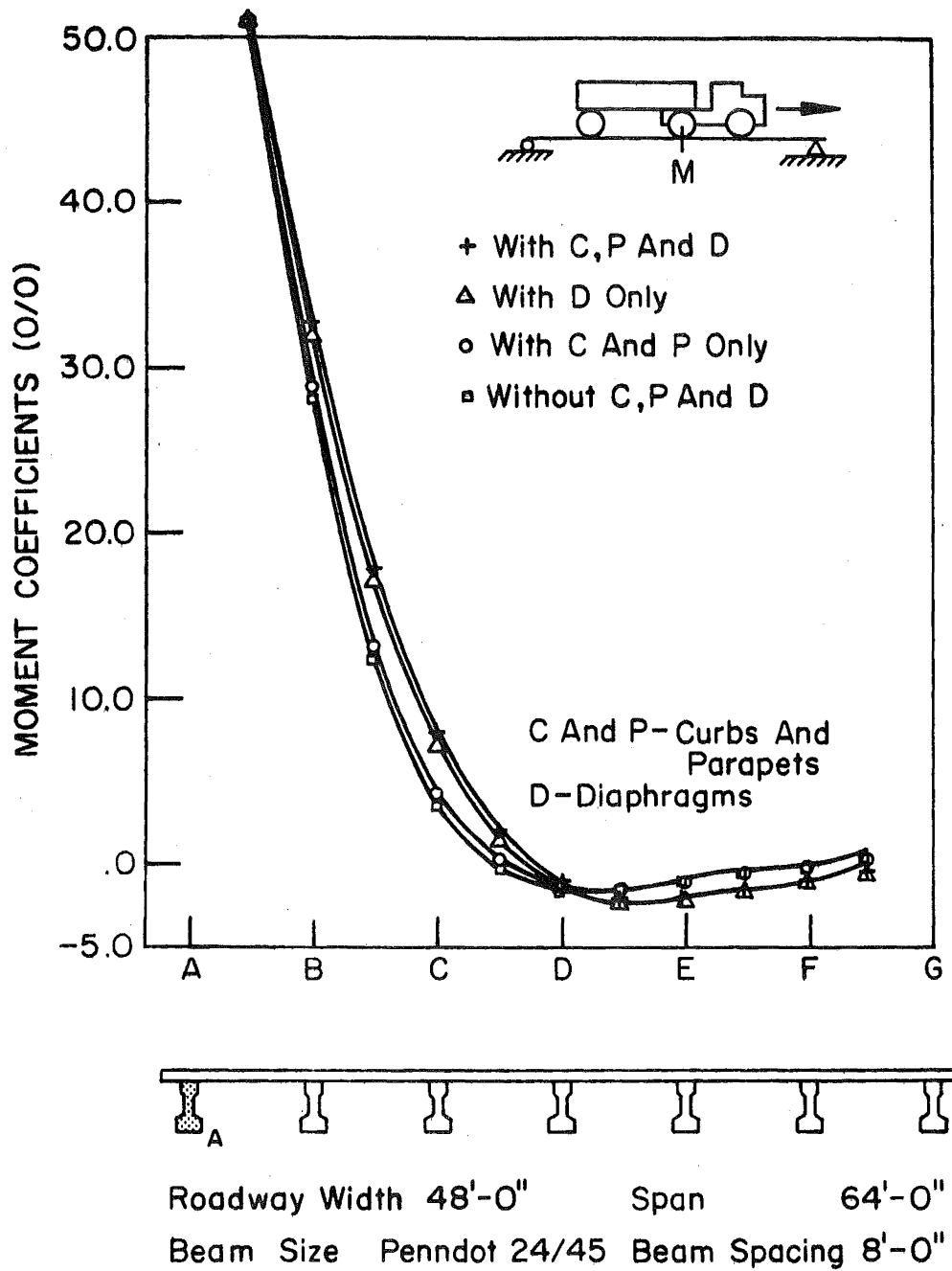
Fig. 48 Influence Lines for Moments, Beam A - 7-Beam Bridge
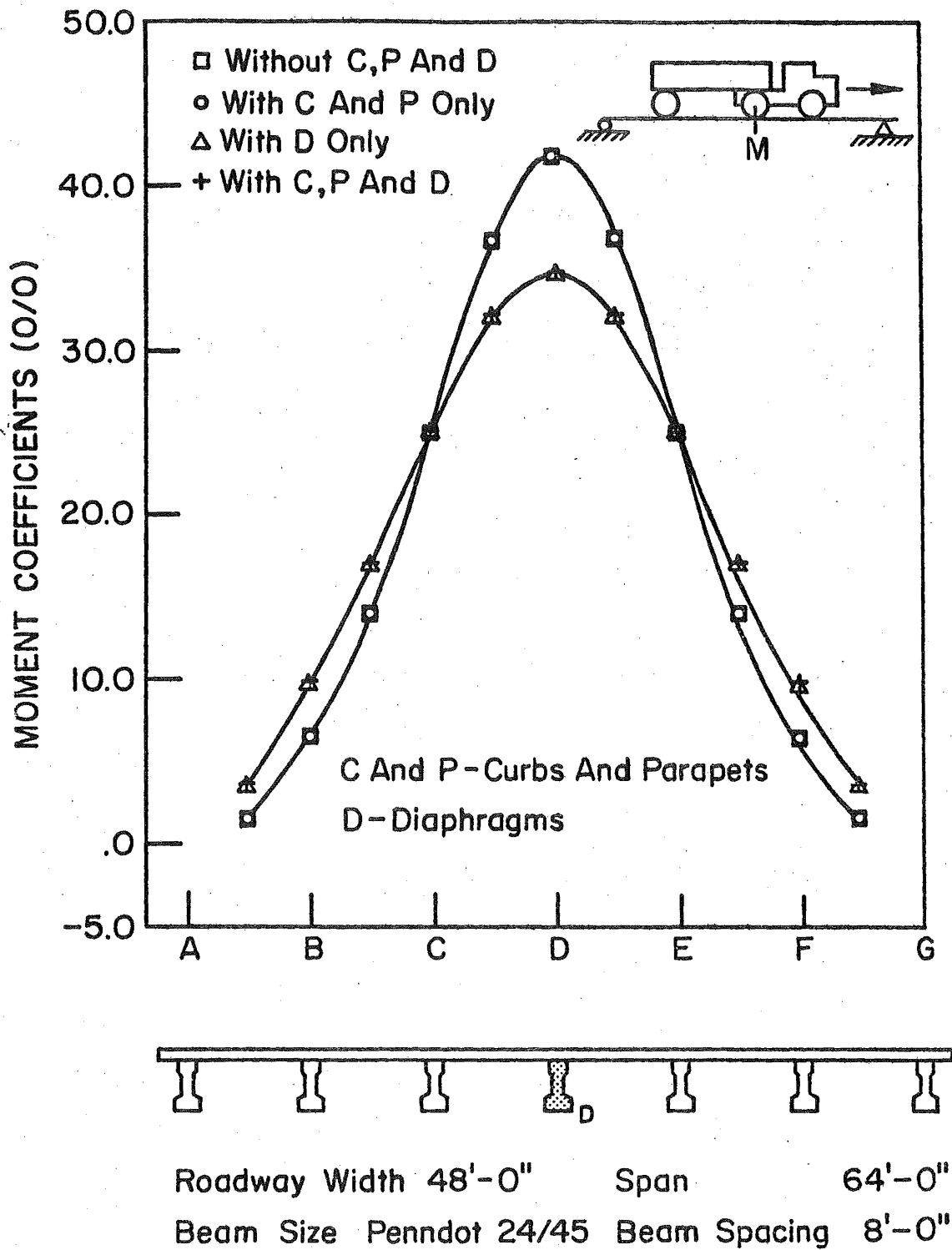
Fig. 49   Influence Lines for Moments, Beam D - 7-Beam Bridge
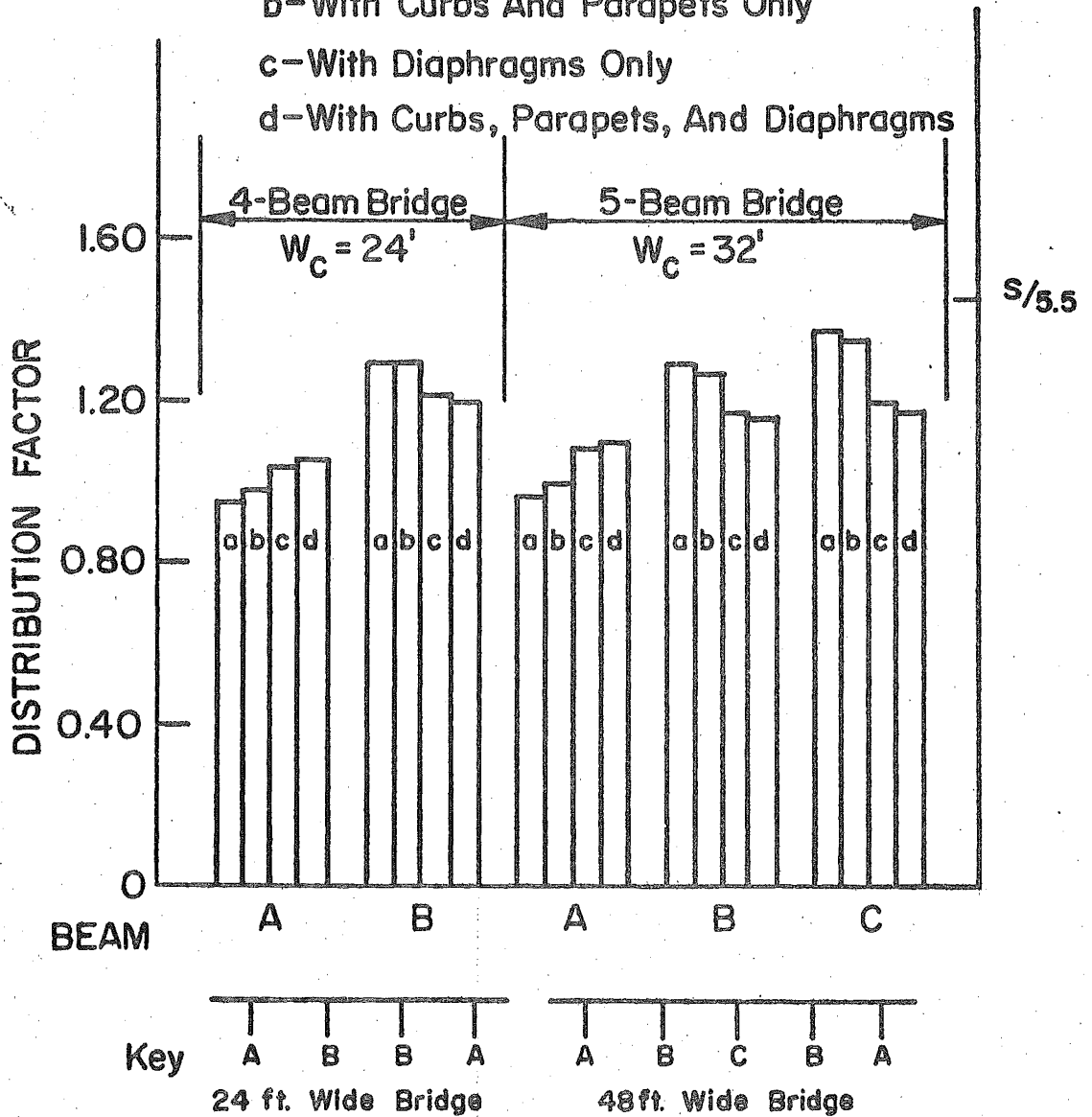
Fig. 50 Distribution Factors for the 4-Beam and 5-Beam Bridges
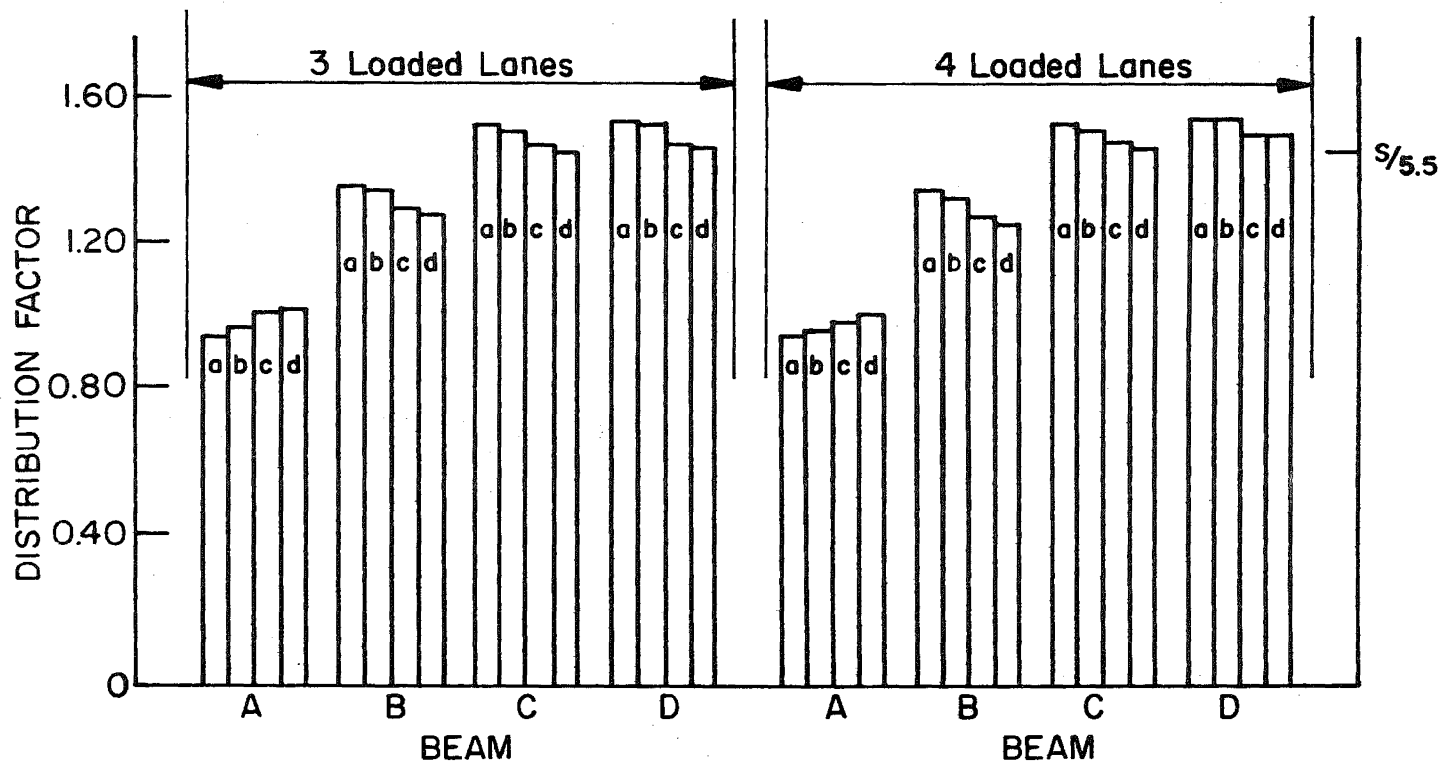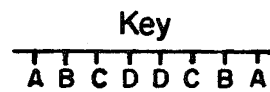
Fig. 51 Distribution Factors for the 7-Beam Bridge

No Diaphragms

$L = 71'0"$

Diaphragm At $L/2$

$L/2$ $L/2$

Diaphragms At $L/3$

$L/3$ $L/3$ $L/3$

Diaphragms At $L/4$

$L/4$ $L/4$ $L/4$ $L/4$

Diaphragms At $L/5$

$L/5$ $L/5$ $L/5$ $L/5$ $L/5$
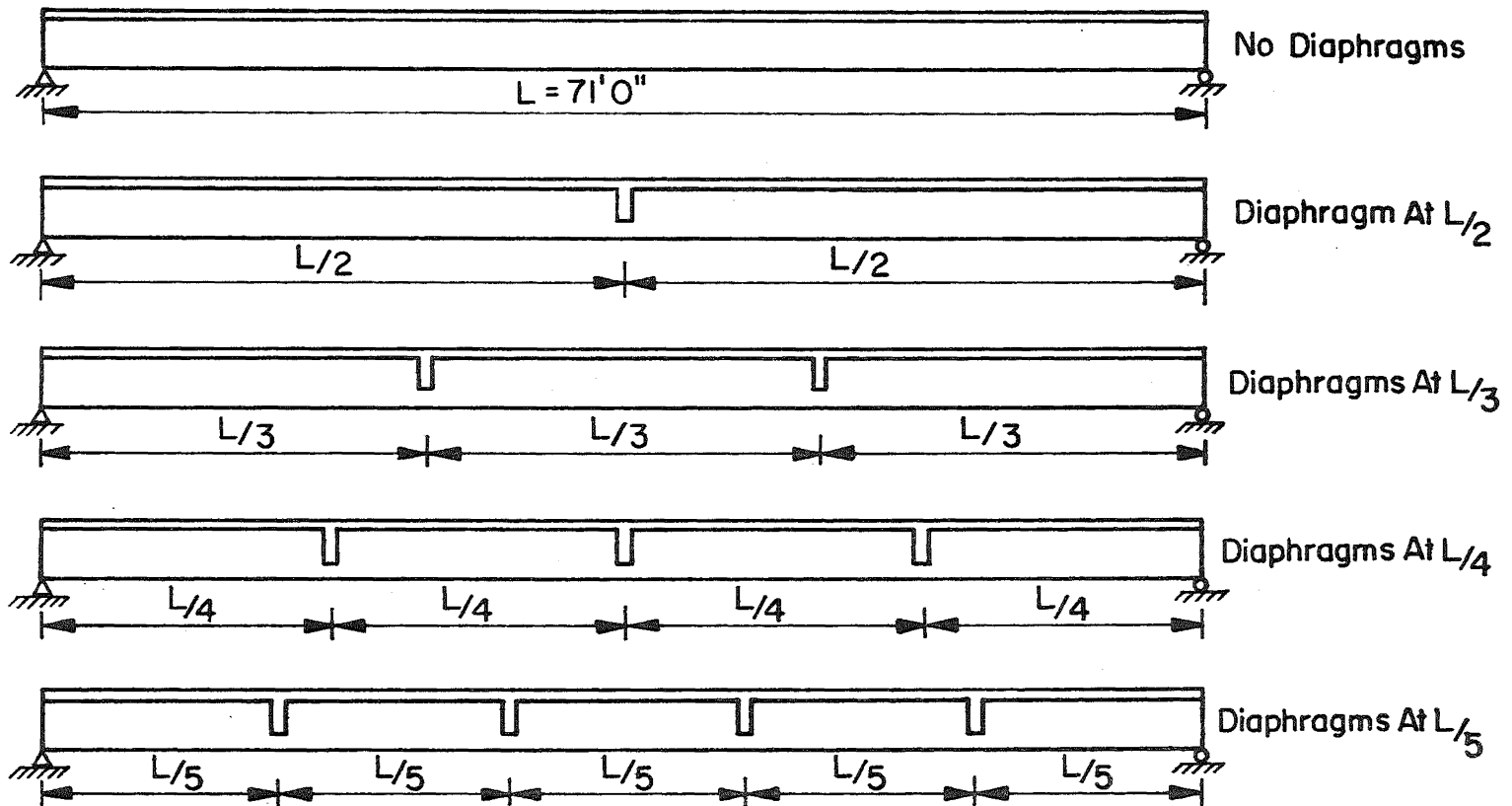
Fig. 52 Diaphragm Locations in the 6-Beam Bridge, 71 ft. Span
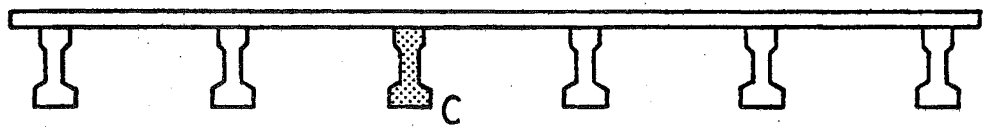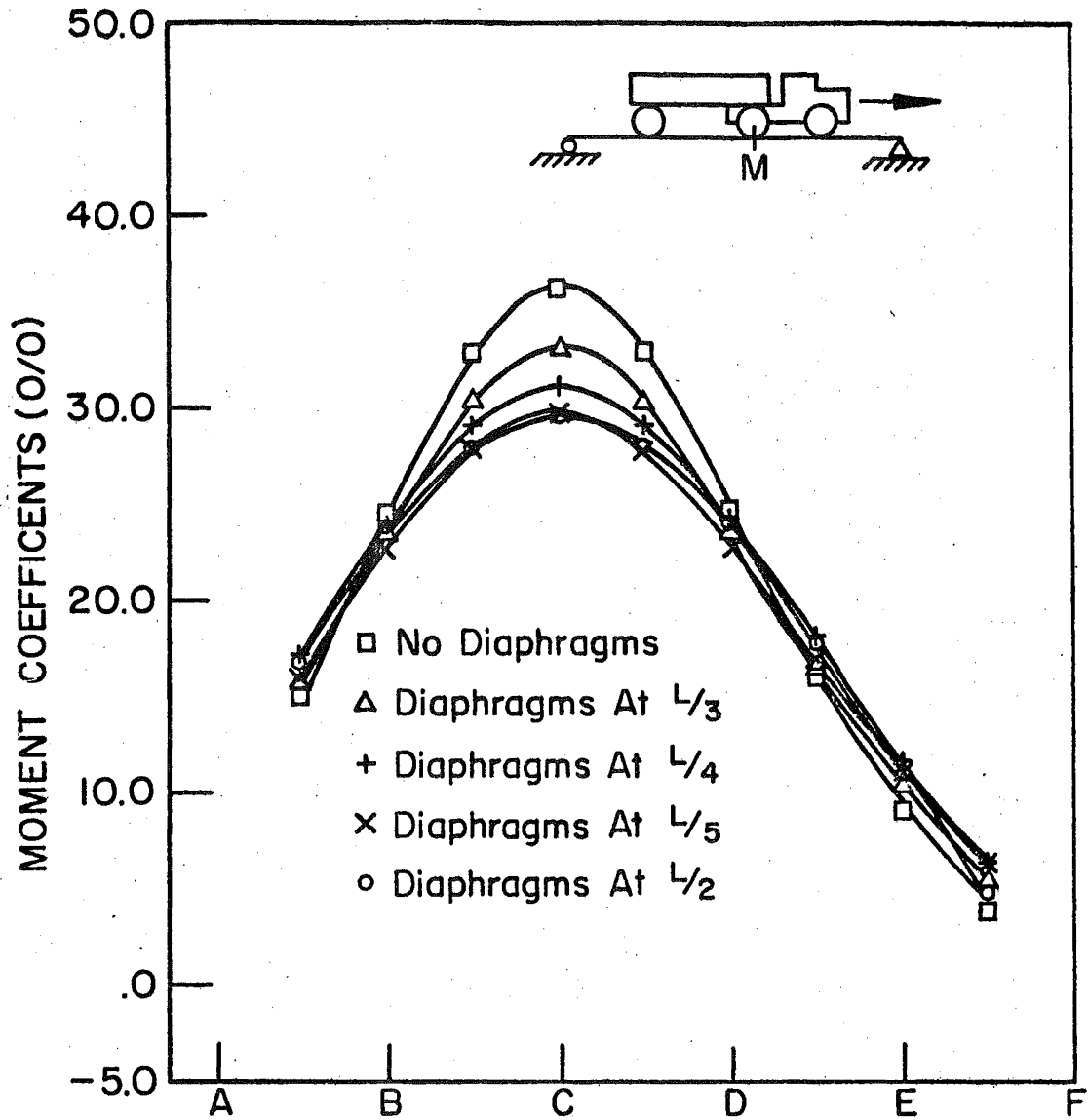
Fig. 53 Influence Lines for Moment, Beam C - With and
Without Diaphragms

-196-
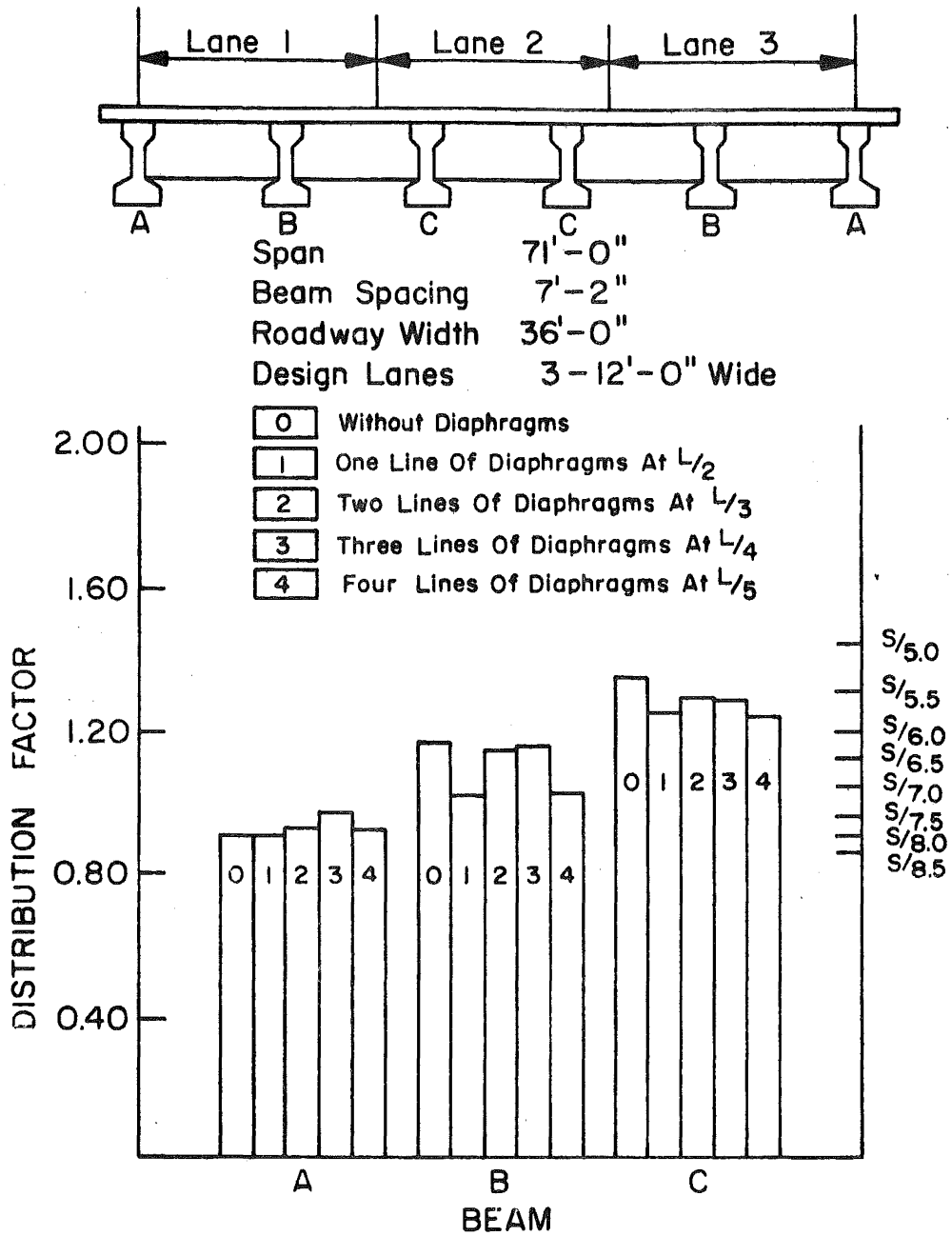
Fig. 54 Distribution Factors in the 6-Beam Bridge With
and Without Diaphragms
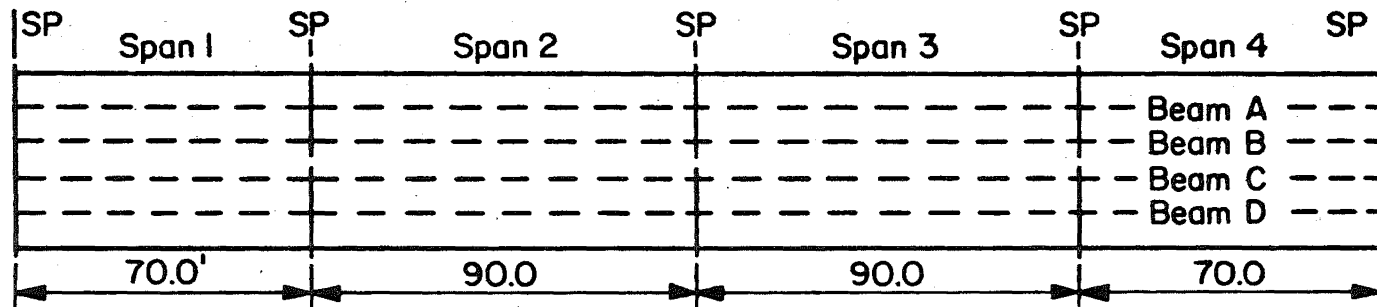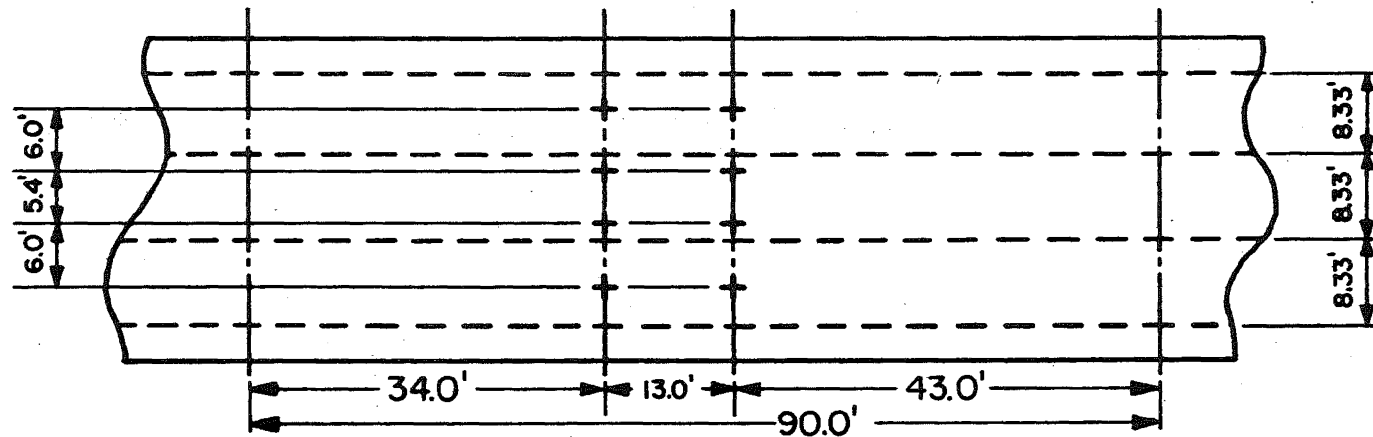
Fig. 55 4-Span Continuous, Steel Composite Bridge with Static Loading on Span 2
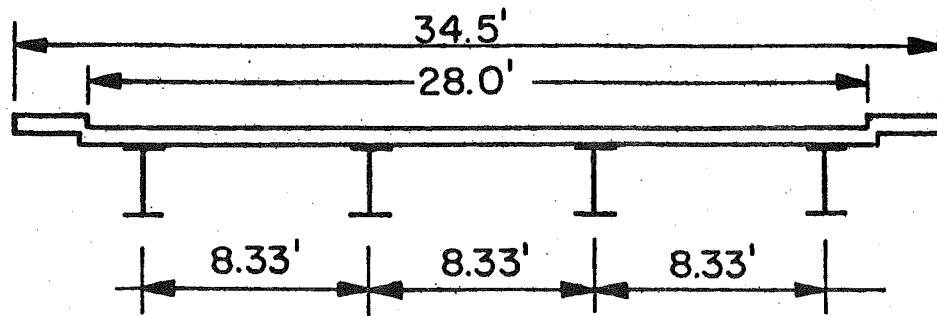
(a) Cross Section
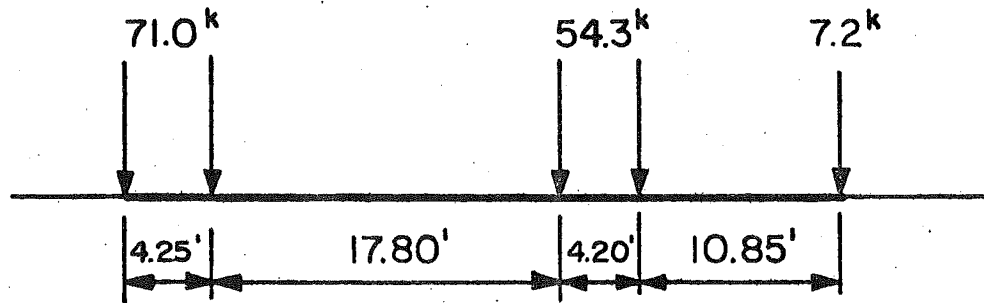
(b) UT-HS40 Axle Loads
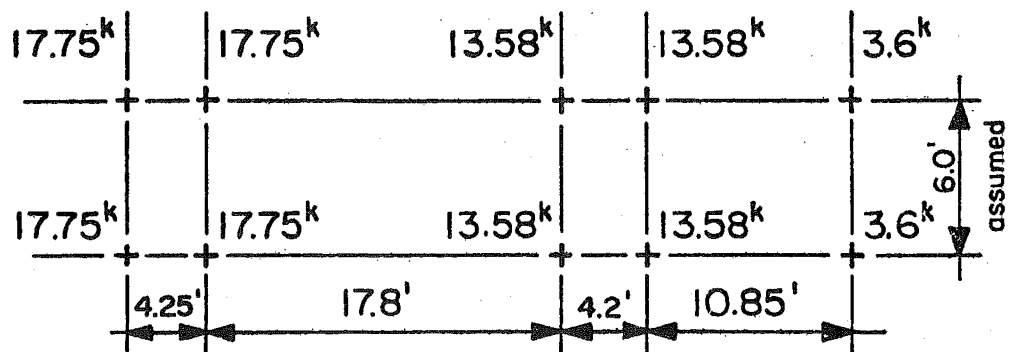
(c) Idealized Load Points

Fig. 56 Cross Section, Test Vehicle and Load Point
Idealization - 4-Span Continuous Bridge (Ref. 6)

-199-
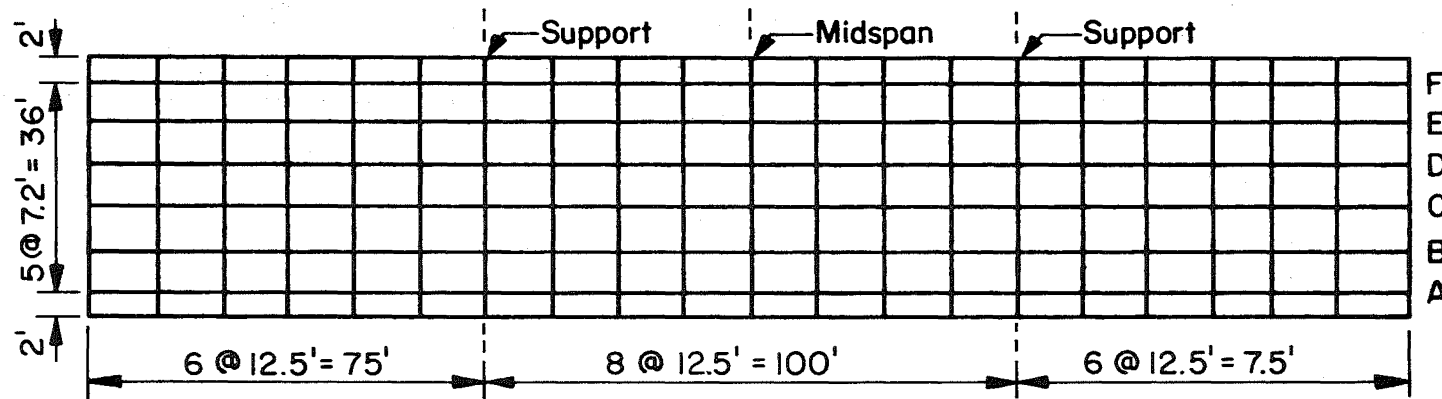
a) Plan And Discretization
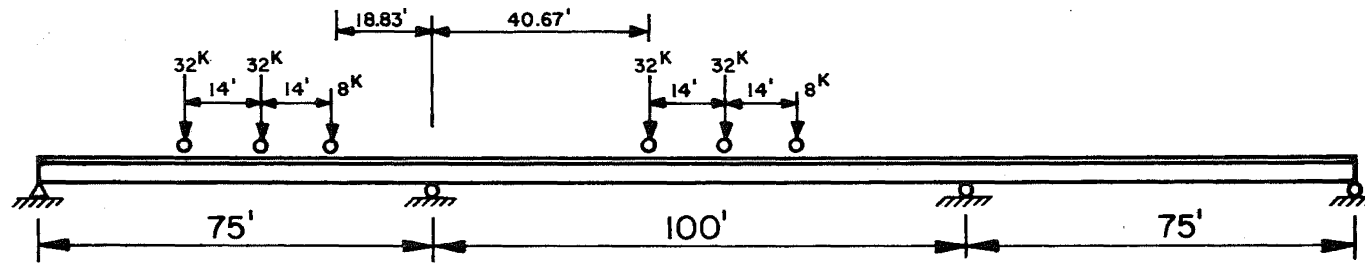
b) Elevation And Loading

Fig. 57 3-Span, 6-Beams, Continuous, Prestressed Concrete I-Beam Bridge, Discretization and Loading
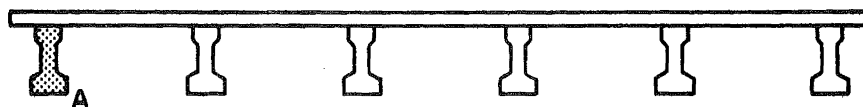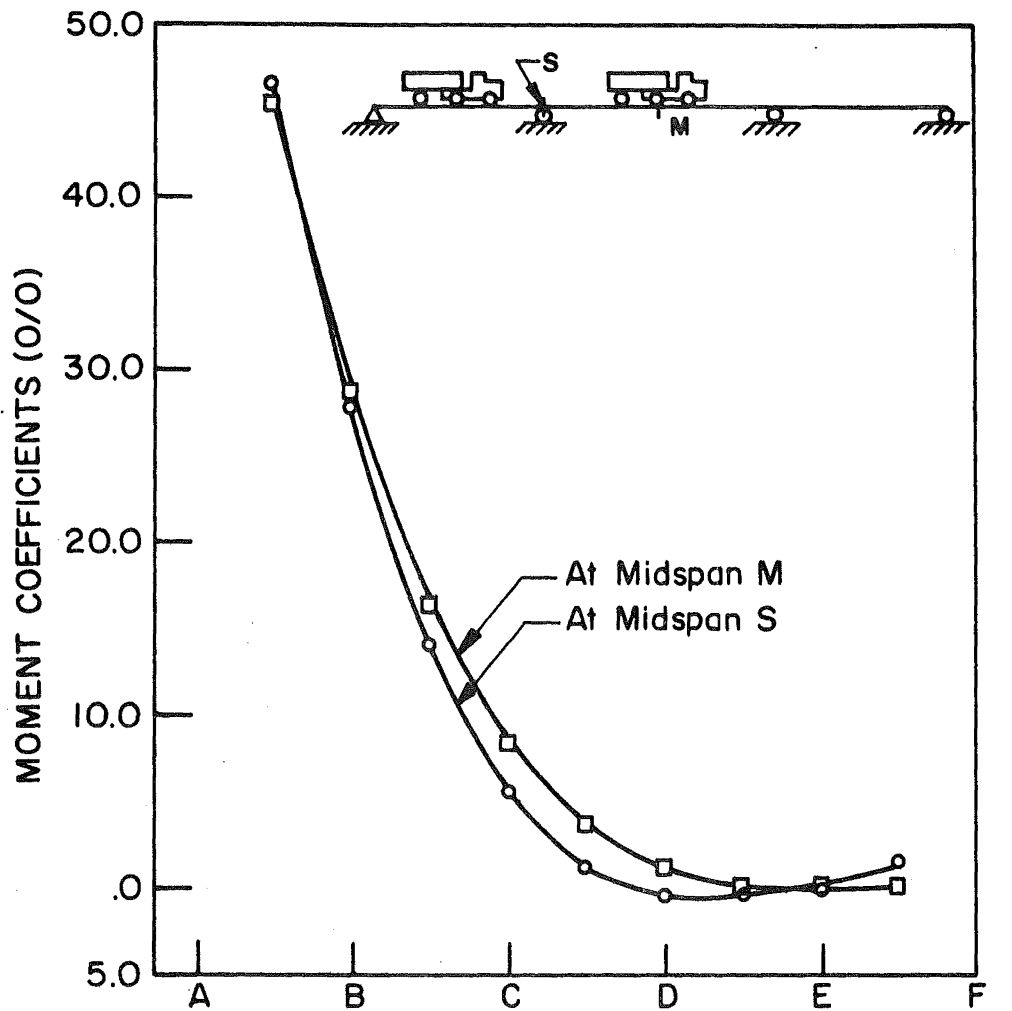
Fig. 58 Influence Lines for Moments at Midspan and
Support, 6-Beam Continuous Bridge - Beam A

-201-
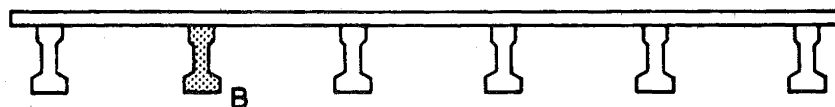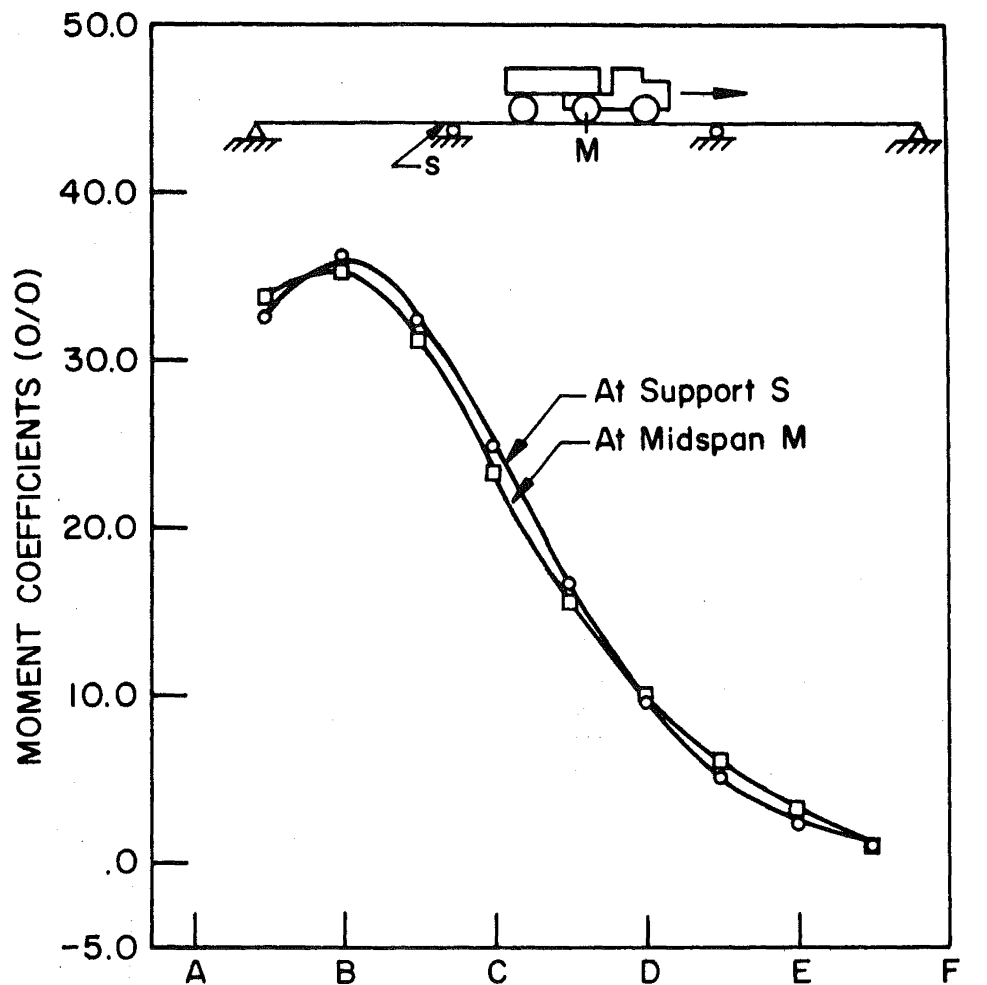
Fig. 59 Influence Lines for Moments at Midspan and
Supports, 6-Beam Continuous Bridge - Beam B
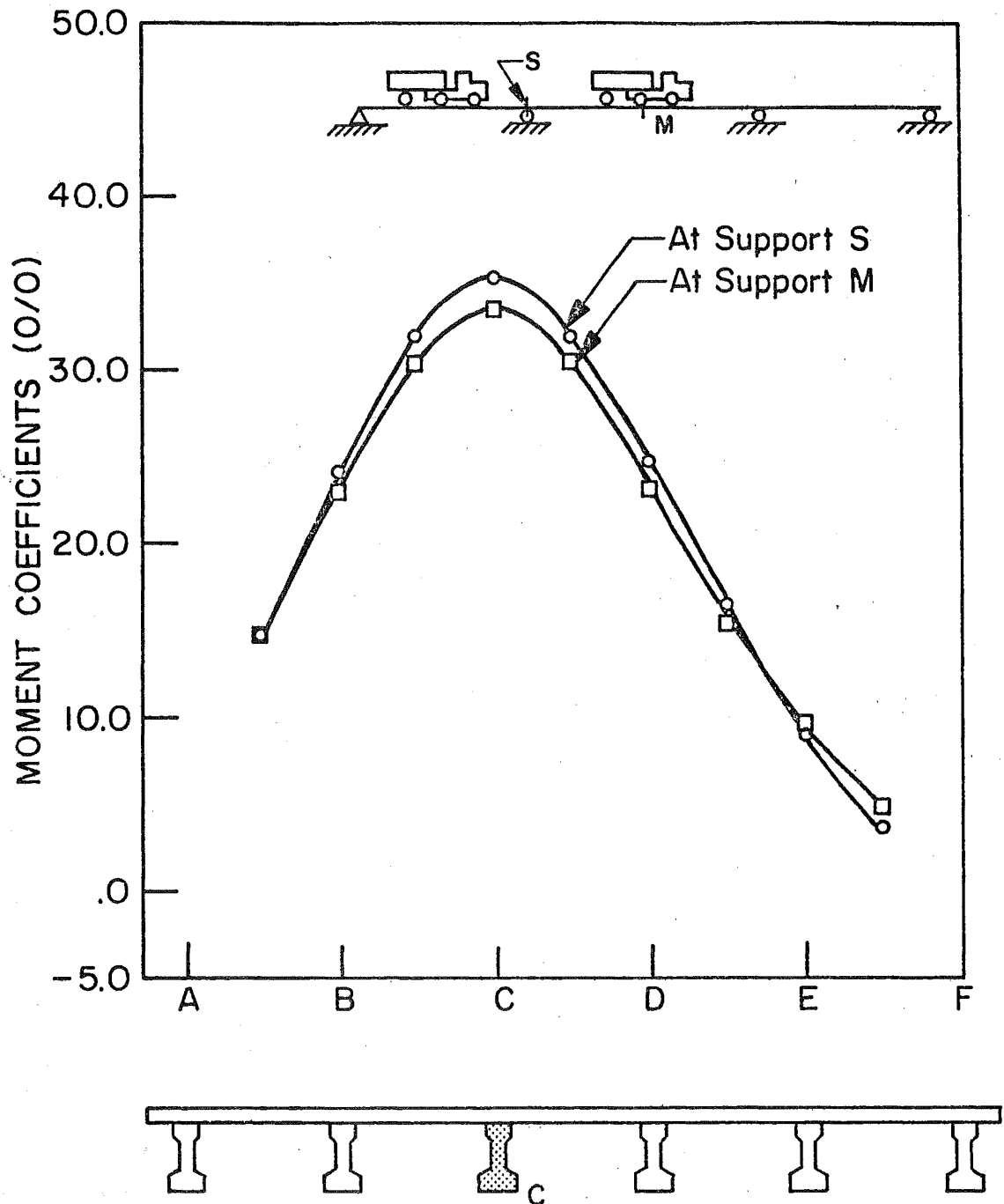
Fig. 60   Influence Lines for Moments at Midspan and Support,
6-Beam Continuous Bridge - Beam C
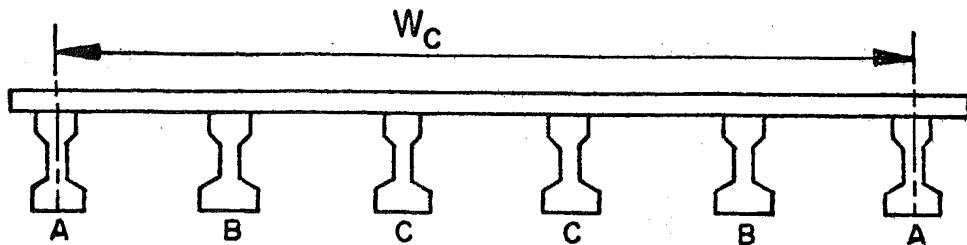
Span: 75'-100'-75'
Beam Spacing: 7'-2 ½"
Roadway Width: 36'-0"
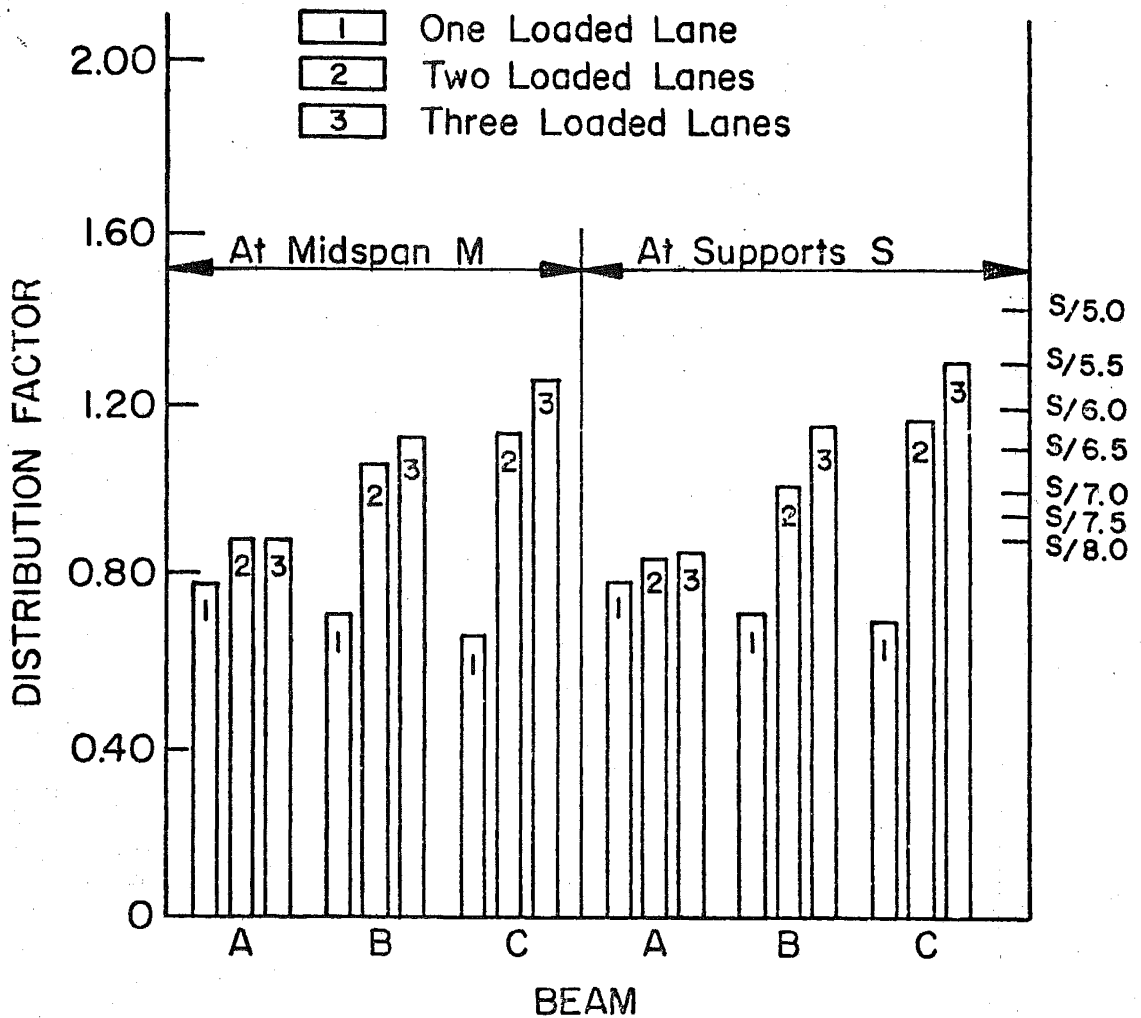
Fig. 61 Distribution Factors for Live Load Moments at
Midspan and Supports - 6-Beam Continuous Bridge

$2'-0'' \leq X_1 \leq 4'-0''$

(a) One Lane

$2'-0'' \leq X_1, X_2, X_3 \leq 4'-0''$
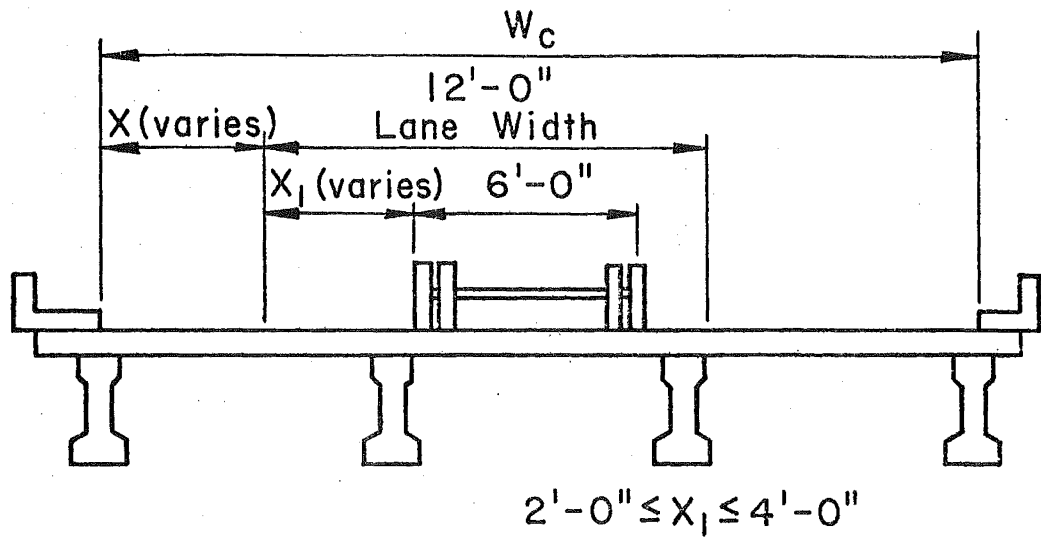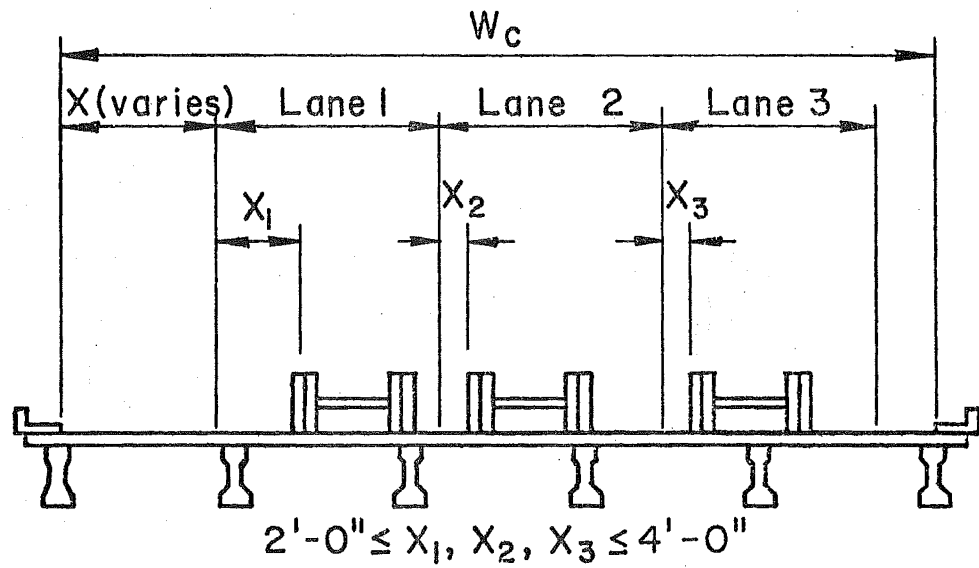
(b) Two Lanes

Fig. 62 Design Traffic Lanes
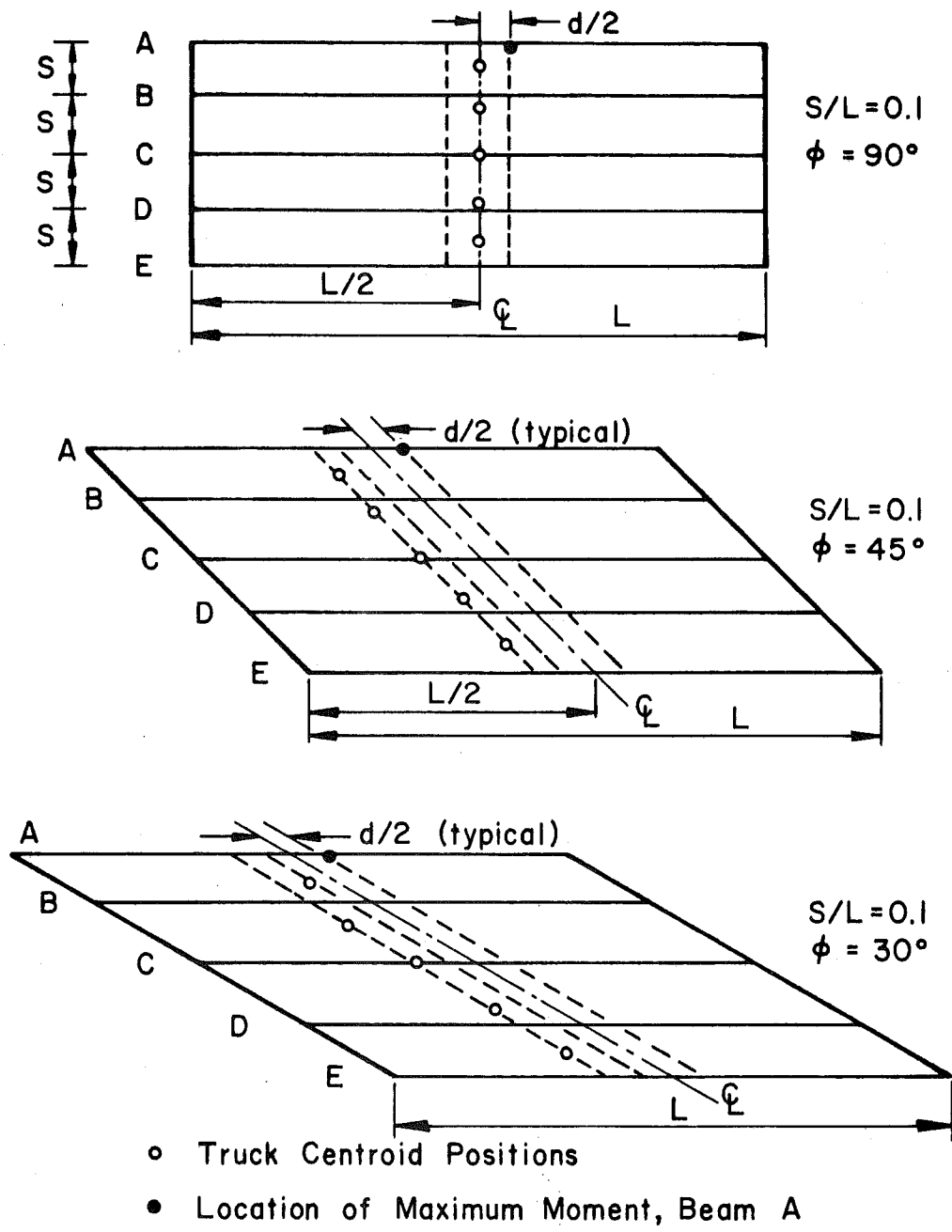
Fig. 63 Load Positions and Locations of Maximum Moment
REsponse - Beam A
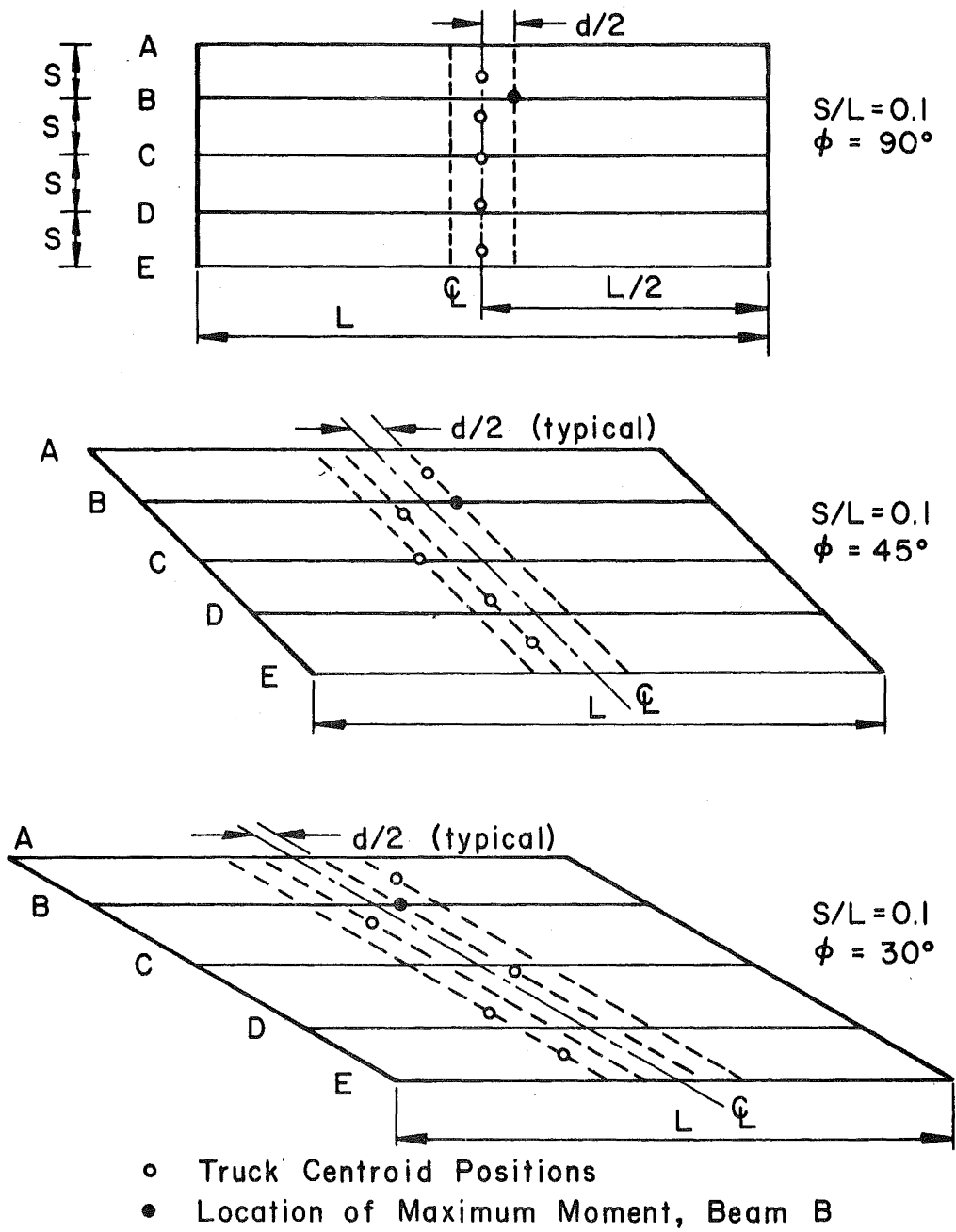
Fig.   64   Load Positions and Location of Maximum Moment
Response - Beam B
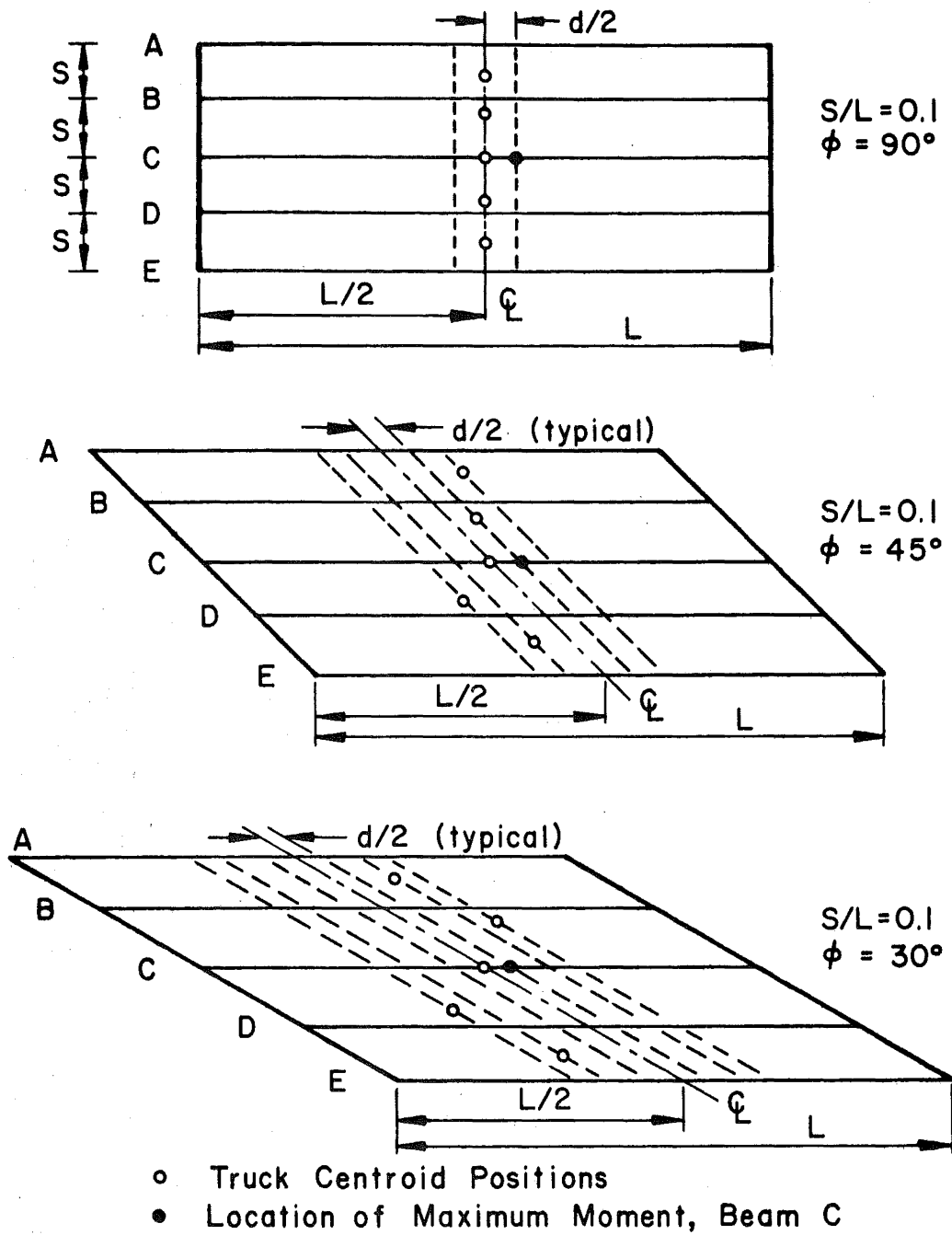
Fig. 65 Load Positions and Location of Maximum Moment
Response - Beam C
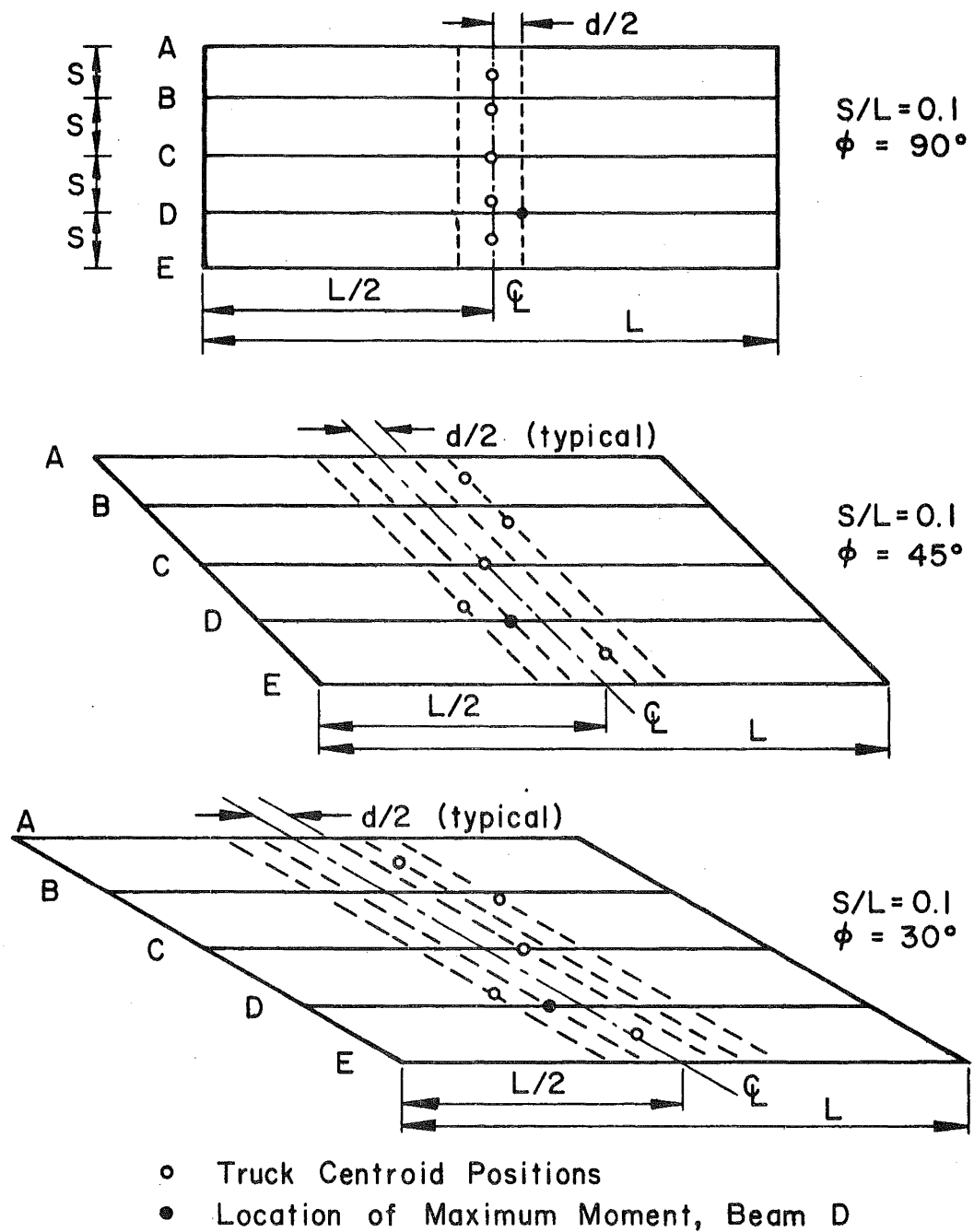
Fig. 66 Load Positions and Location of Maximum Moment
Response - Beam D
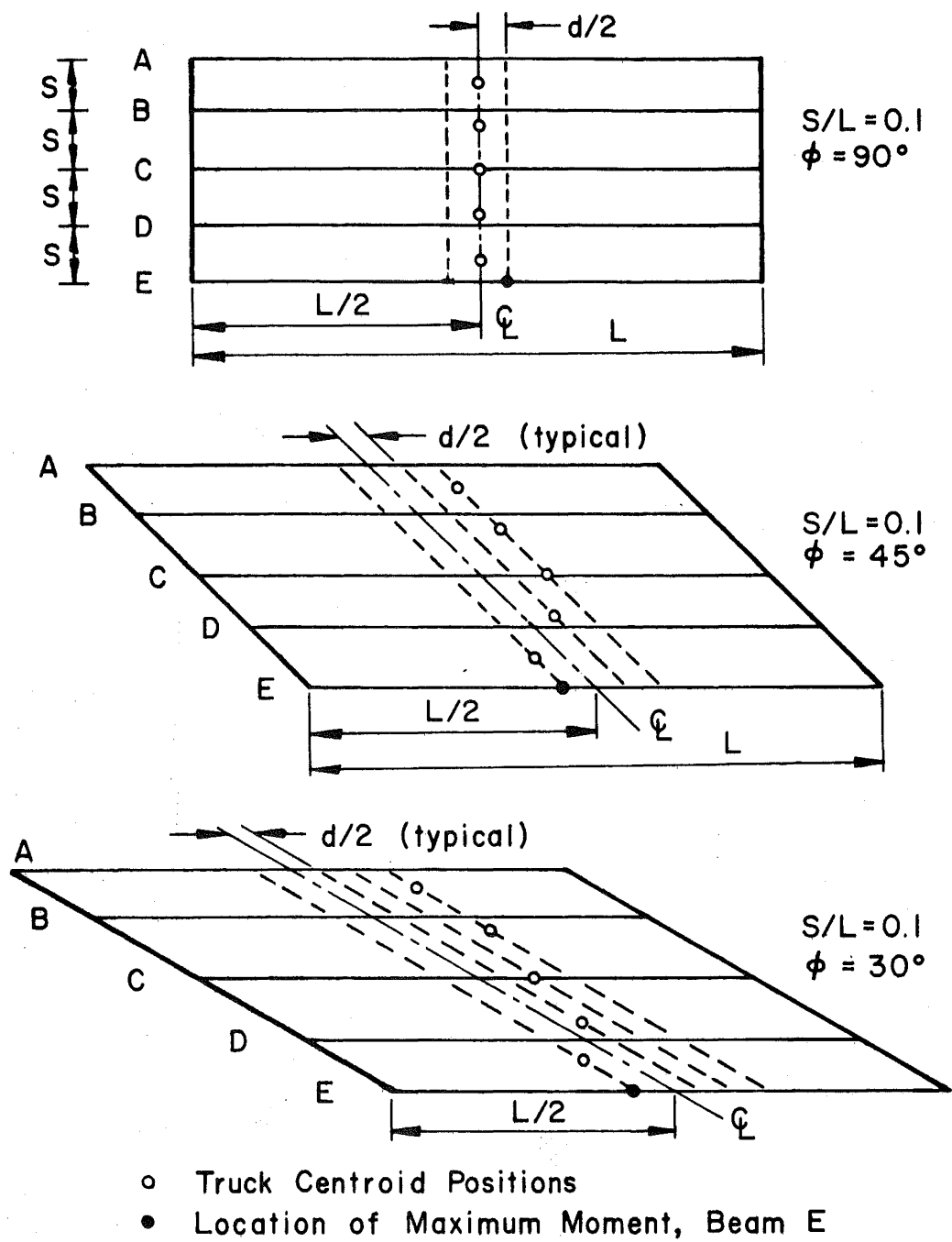
Fig. 67 Load Positions and Location of Maximum Moment
Response - Beam E
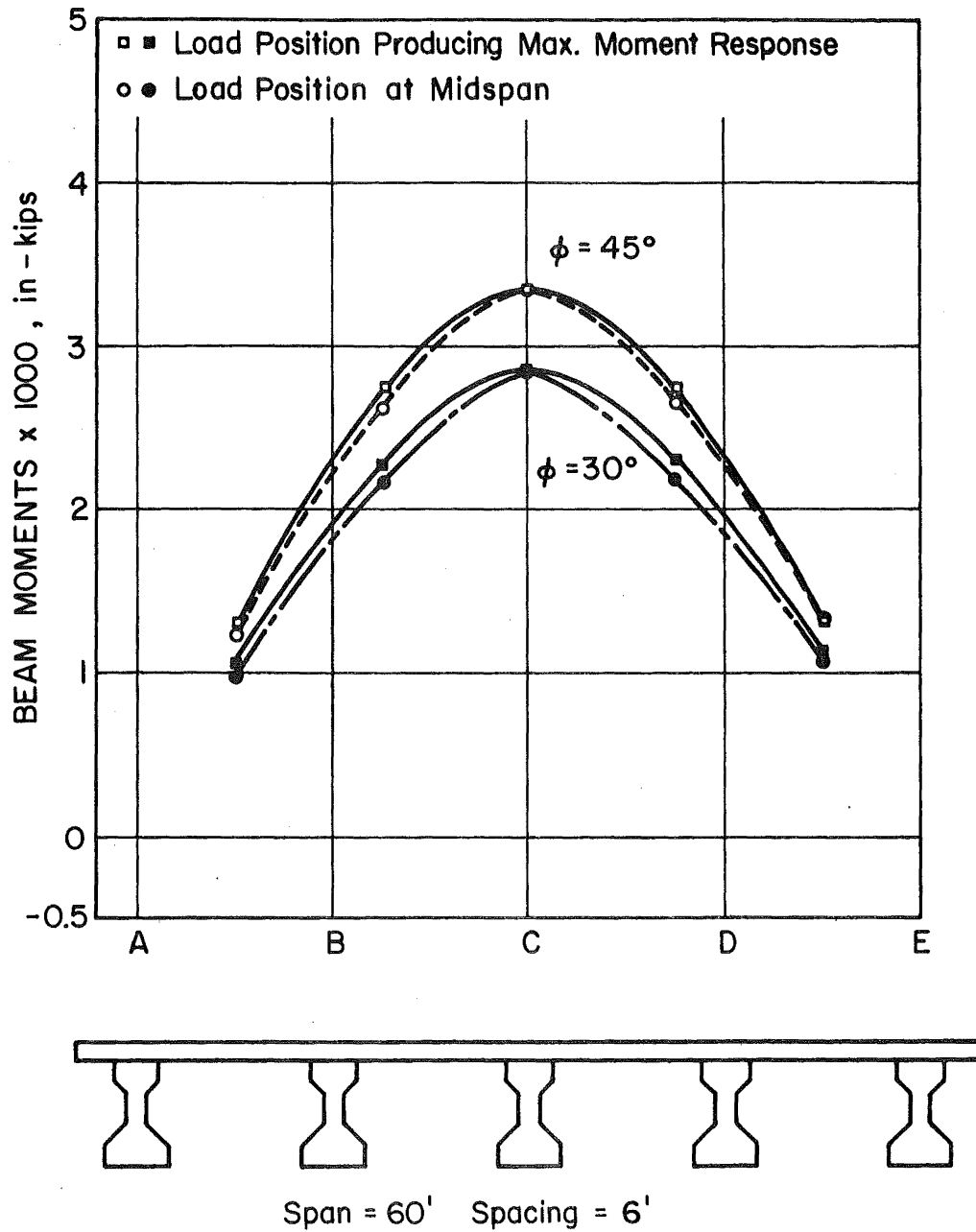
Fig. 68   Influence Lines for Moment, 45° and 30° Skew
          Bridges - Beam C
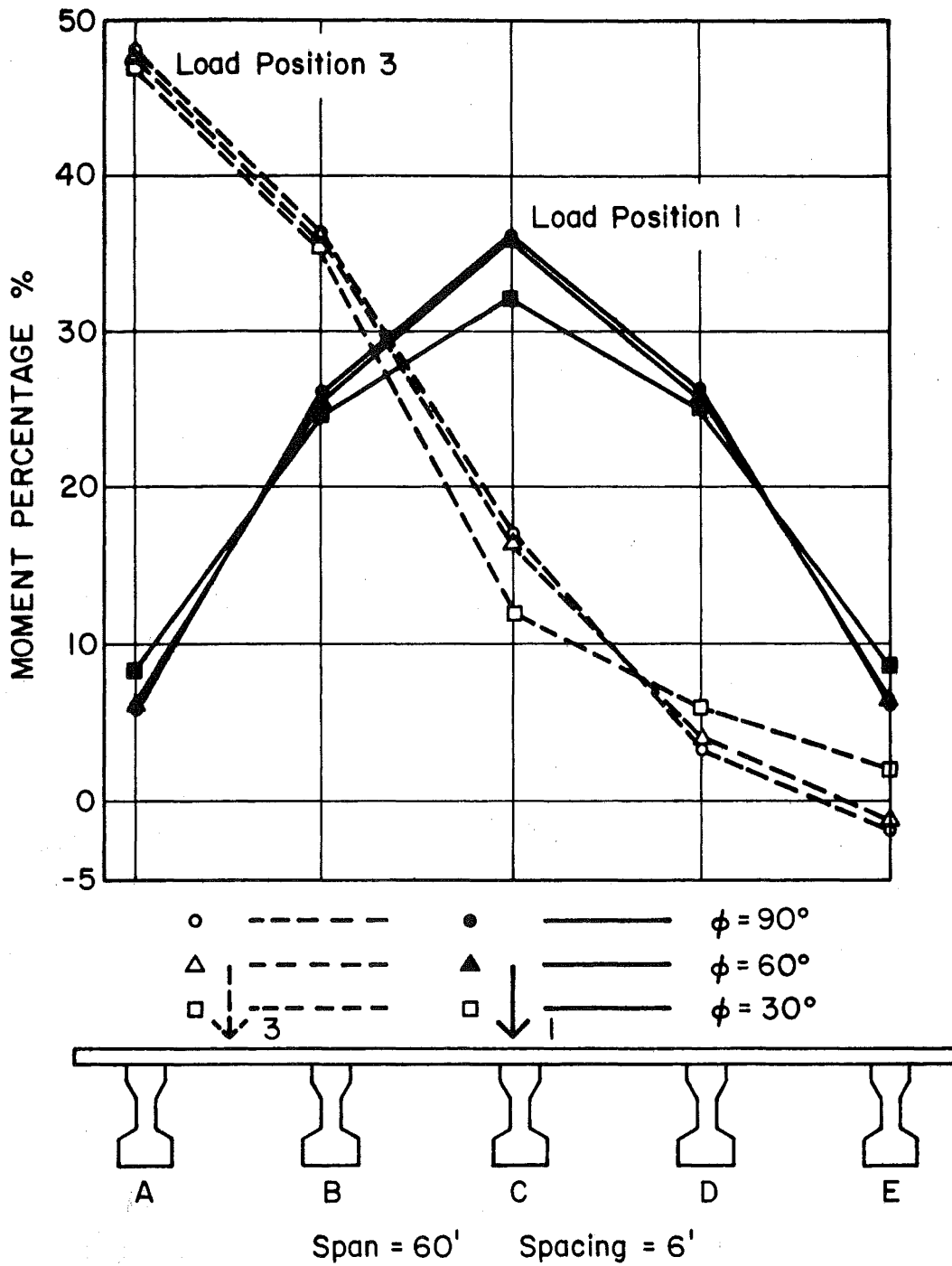
Fig. 69   Lateral Distribution of a Truck Load: Truck
Centroid on Beam C and Between Beams A and B

-212-
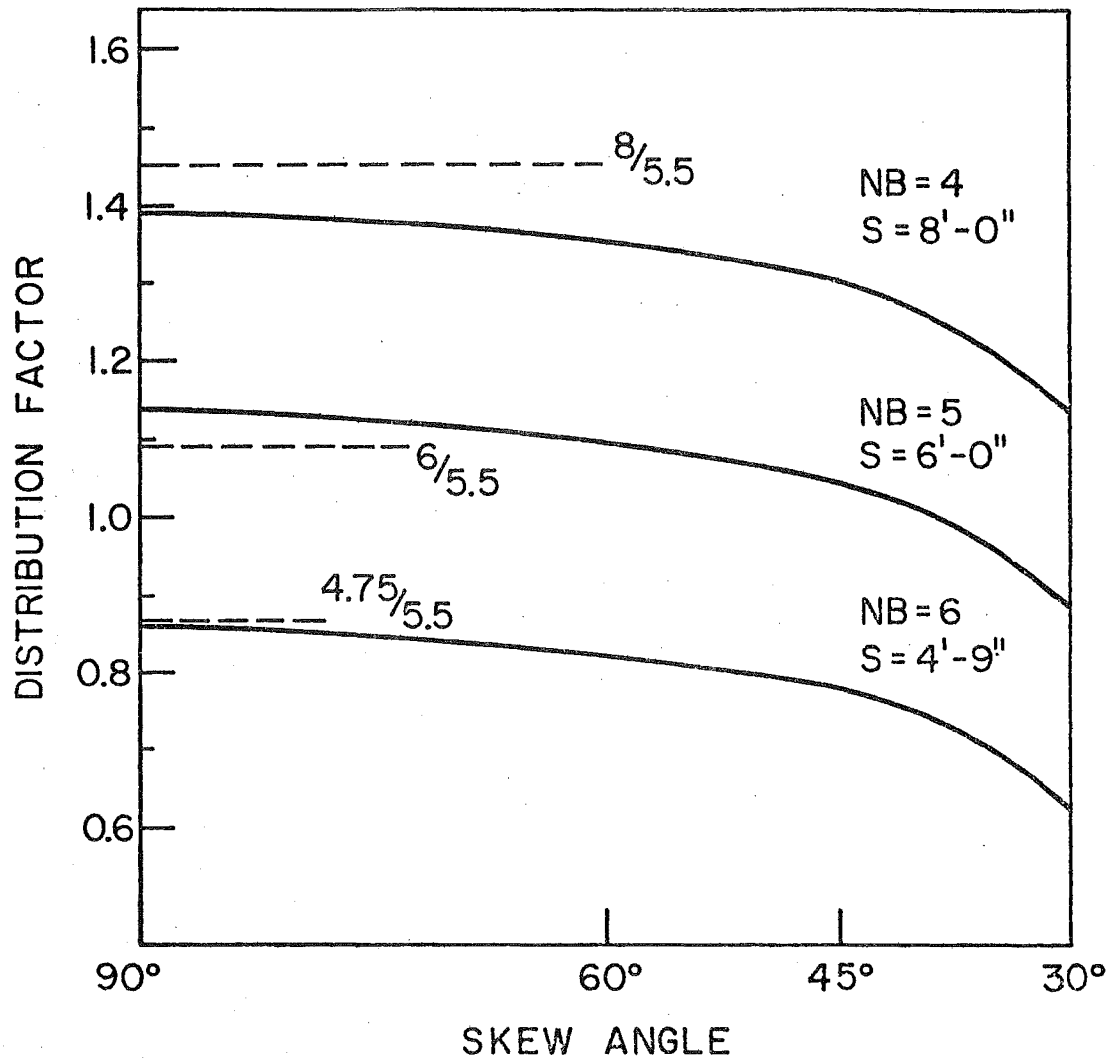
Fig. 70 Live Load Distribution Factors in the 24 ft. Wide
60 ft. Span Skew Bridges with Varying Number of Beams
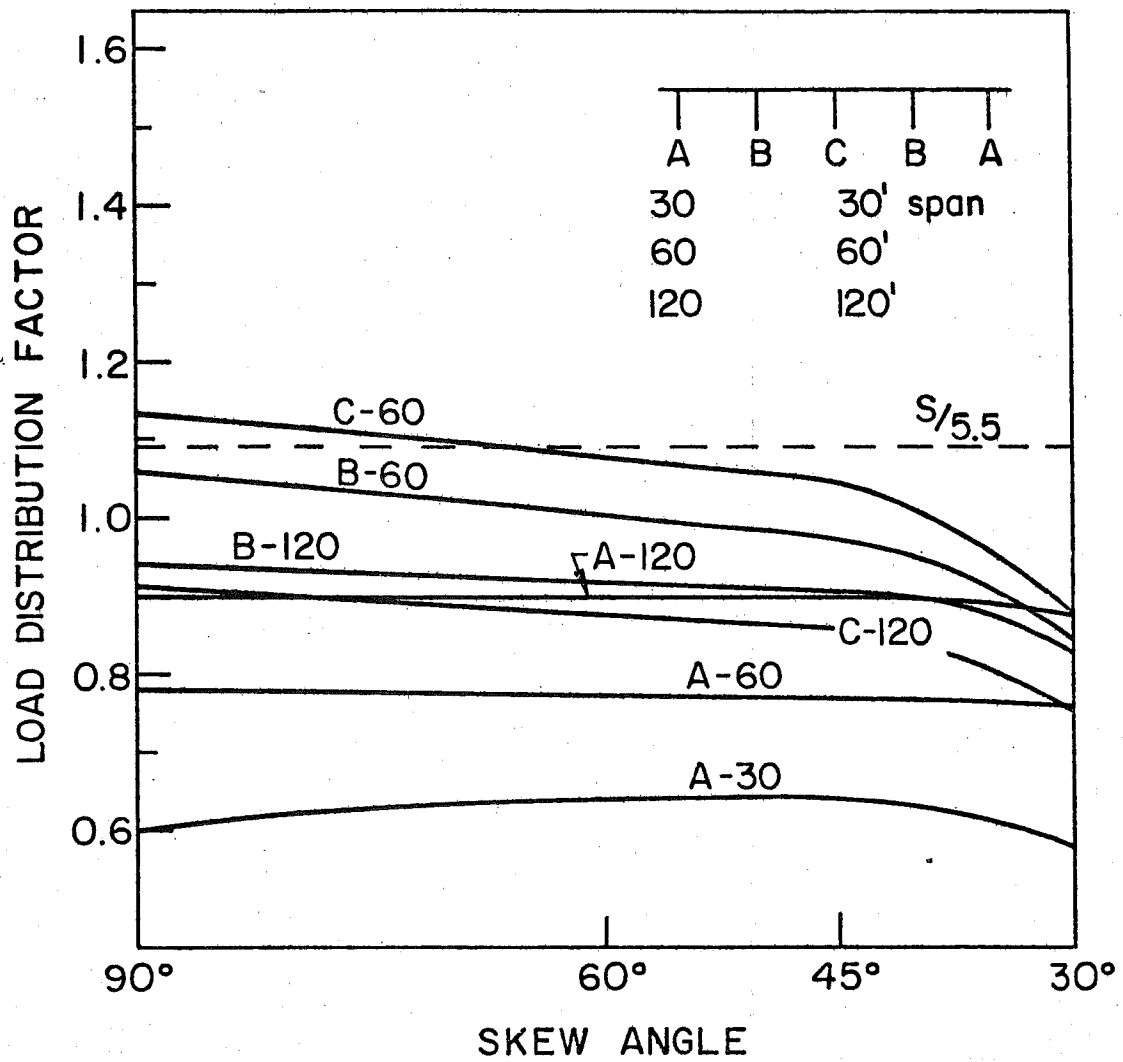
Fig. 71 Live Load Distribution Factors in the 24 ft.
Wide Skew Bridges, 5 Beams with Varying Span
Length

-214-
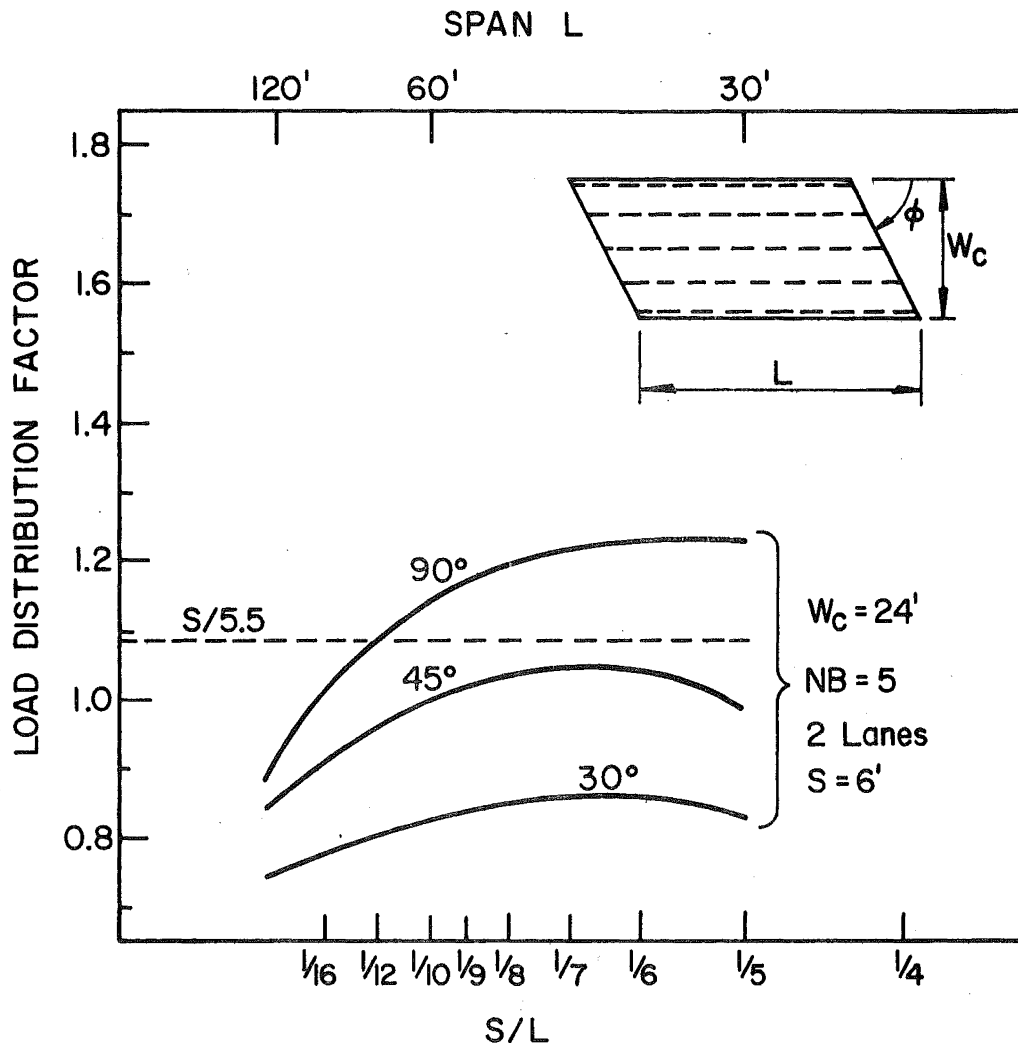
Fig. 72 Live Load Distribution Factors in the 24 ft.
Wide Skew Bridge with 5 Beams
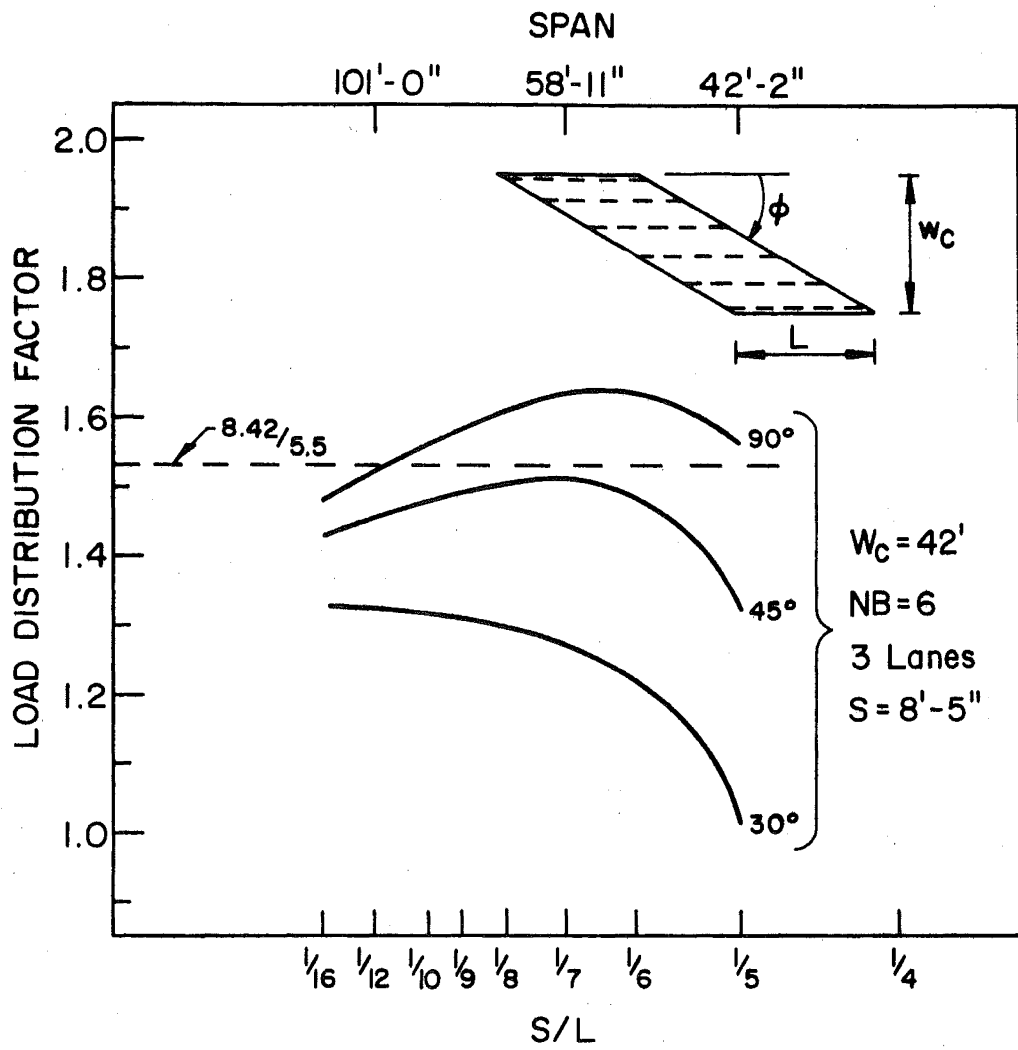
Fig. 73 Live Load Distribution Factors in the 42 ft.
Wide Skew Bridges with 6 Beams
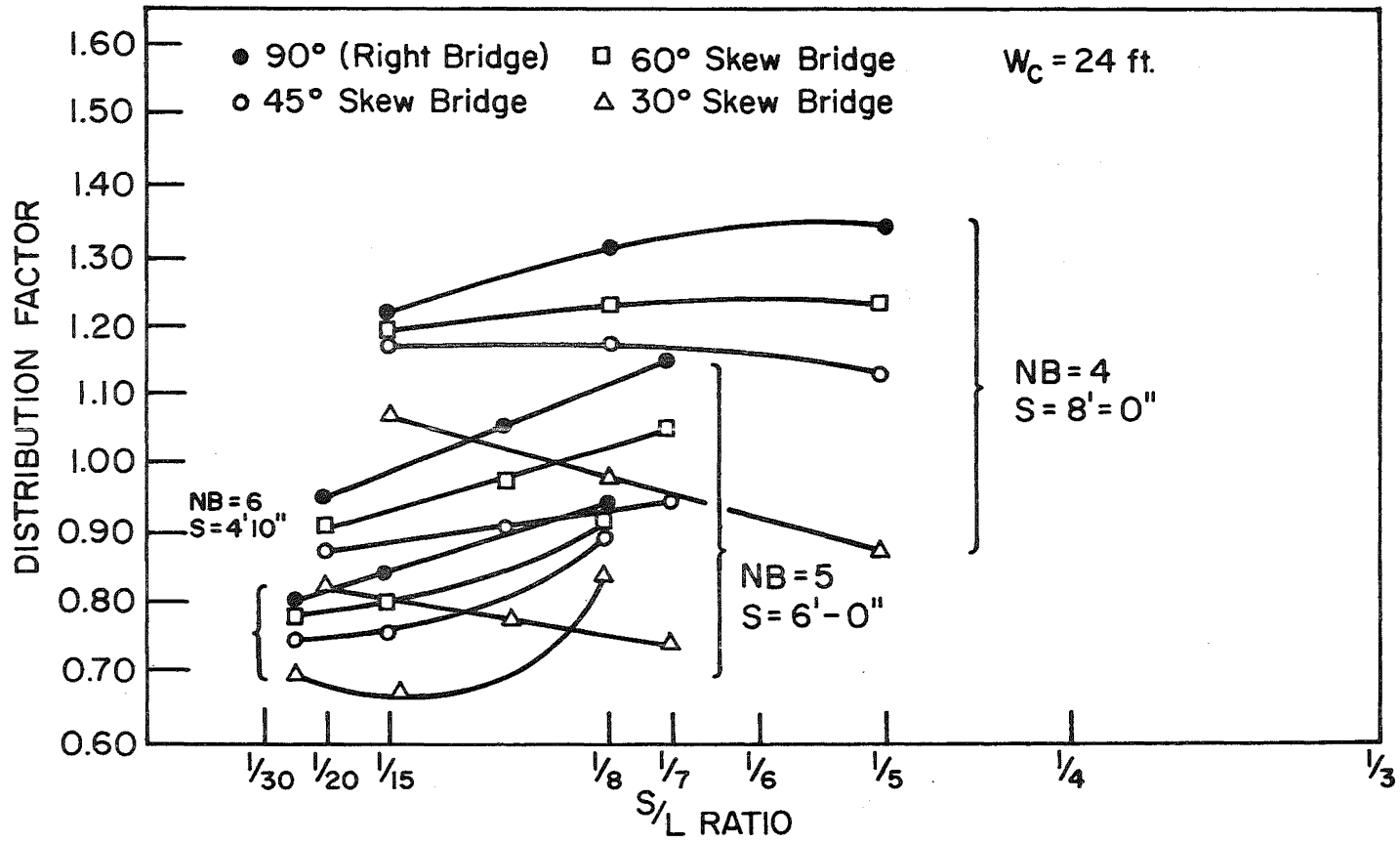
Fig. 74 Distribution Factors for Interior Beams - 24 ft. Wide Bridges
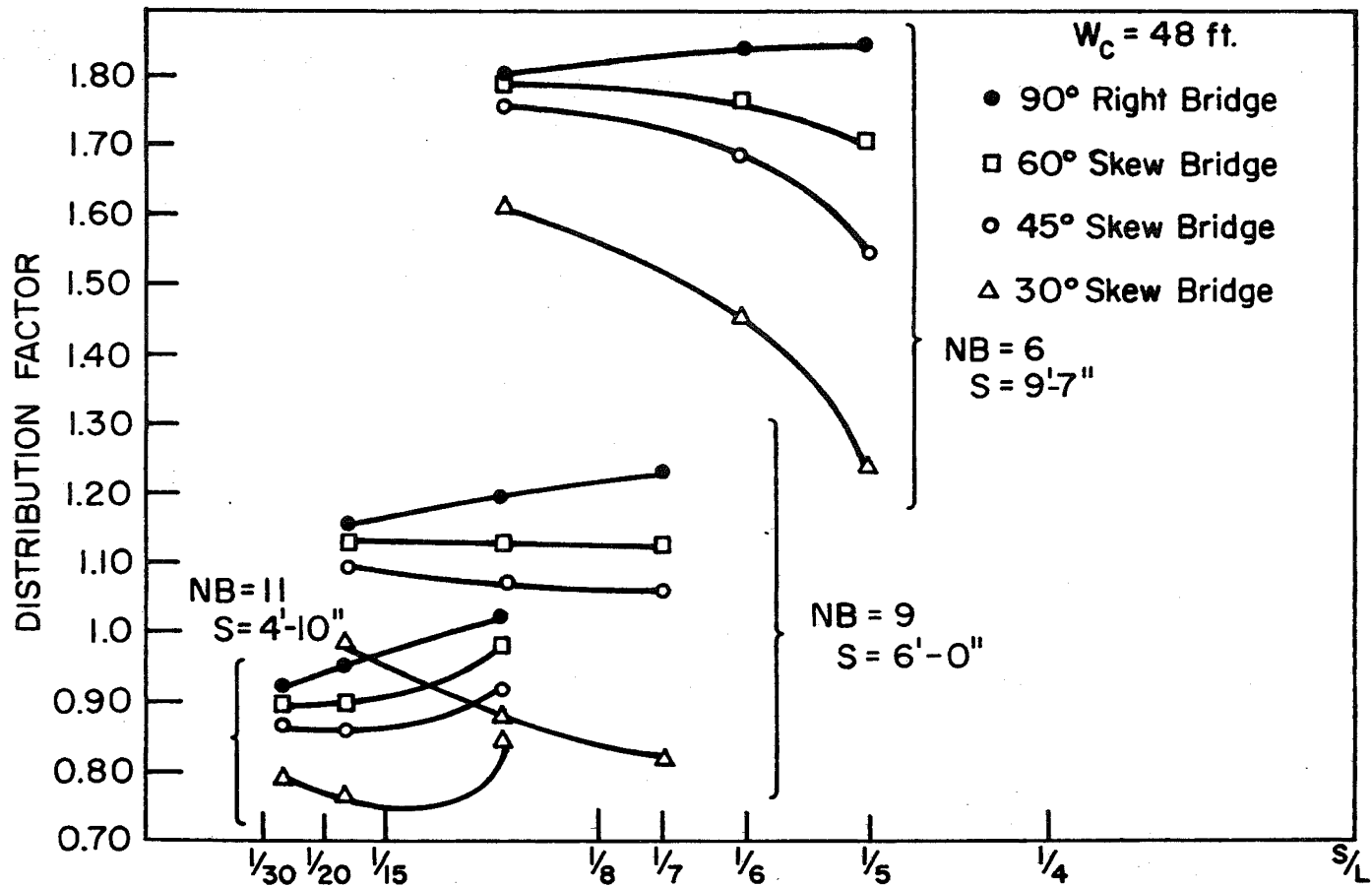
Fig. 75 Distribution Factors for Interior Beams - 48 ft. Wide Bridges
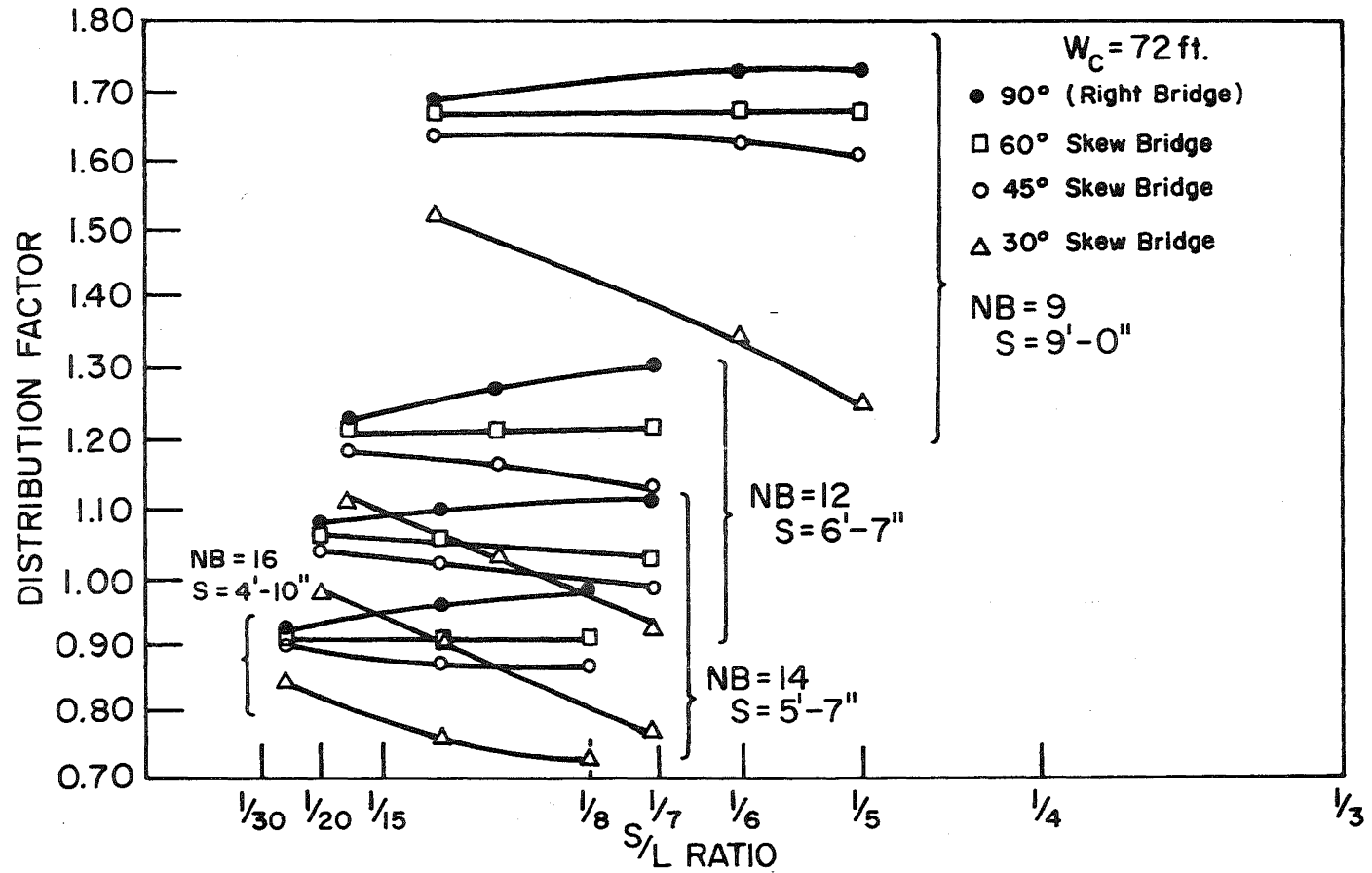
Fig. 76 Distribution Factors for Interior Beams 72 ft. Wide Bridges
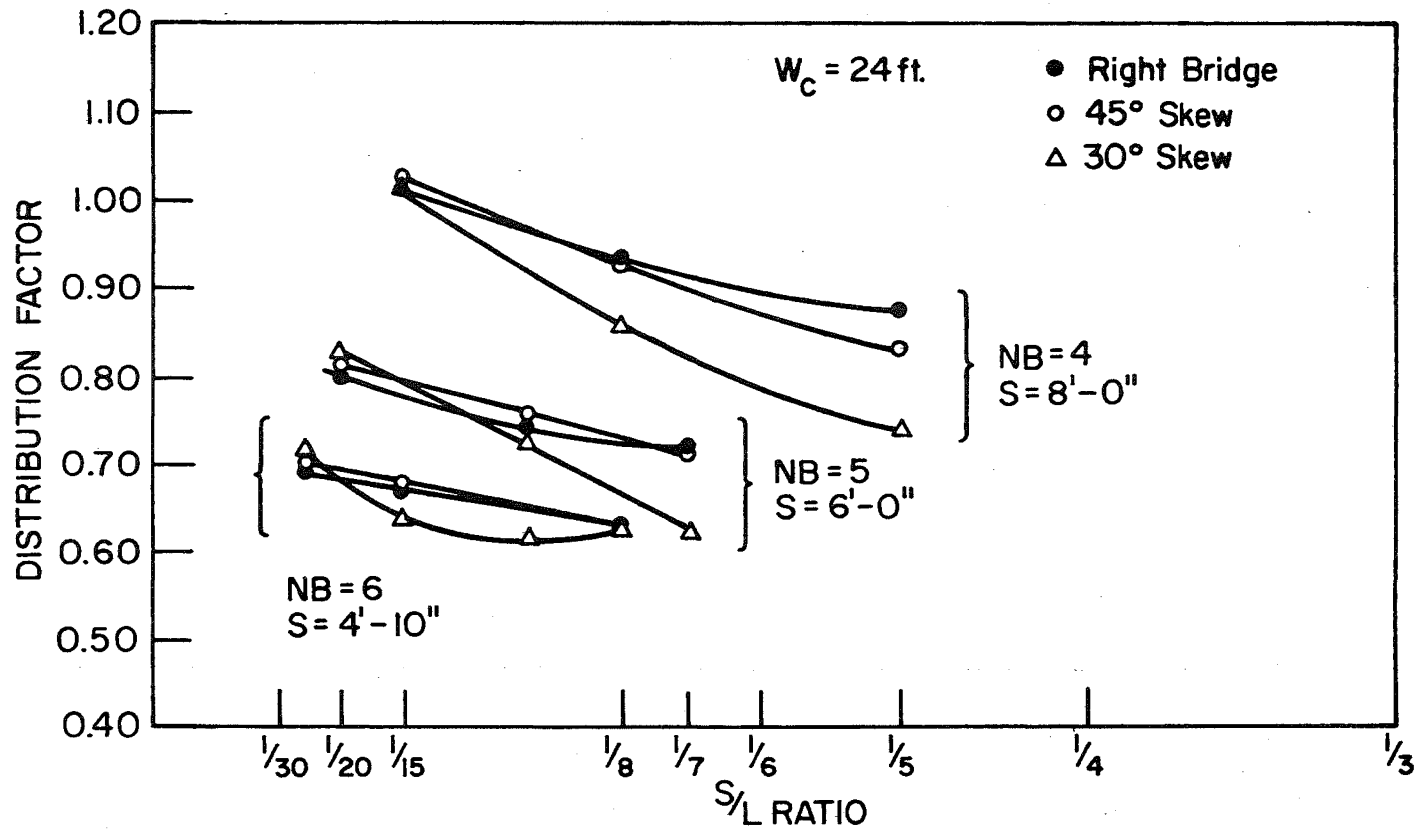
Fig. 77 Distribution Factors for Exterior Beams - 24 ft. Wide Bridges
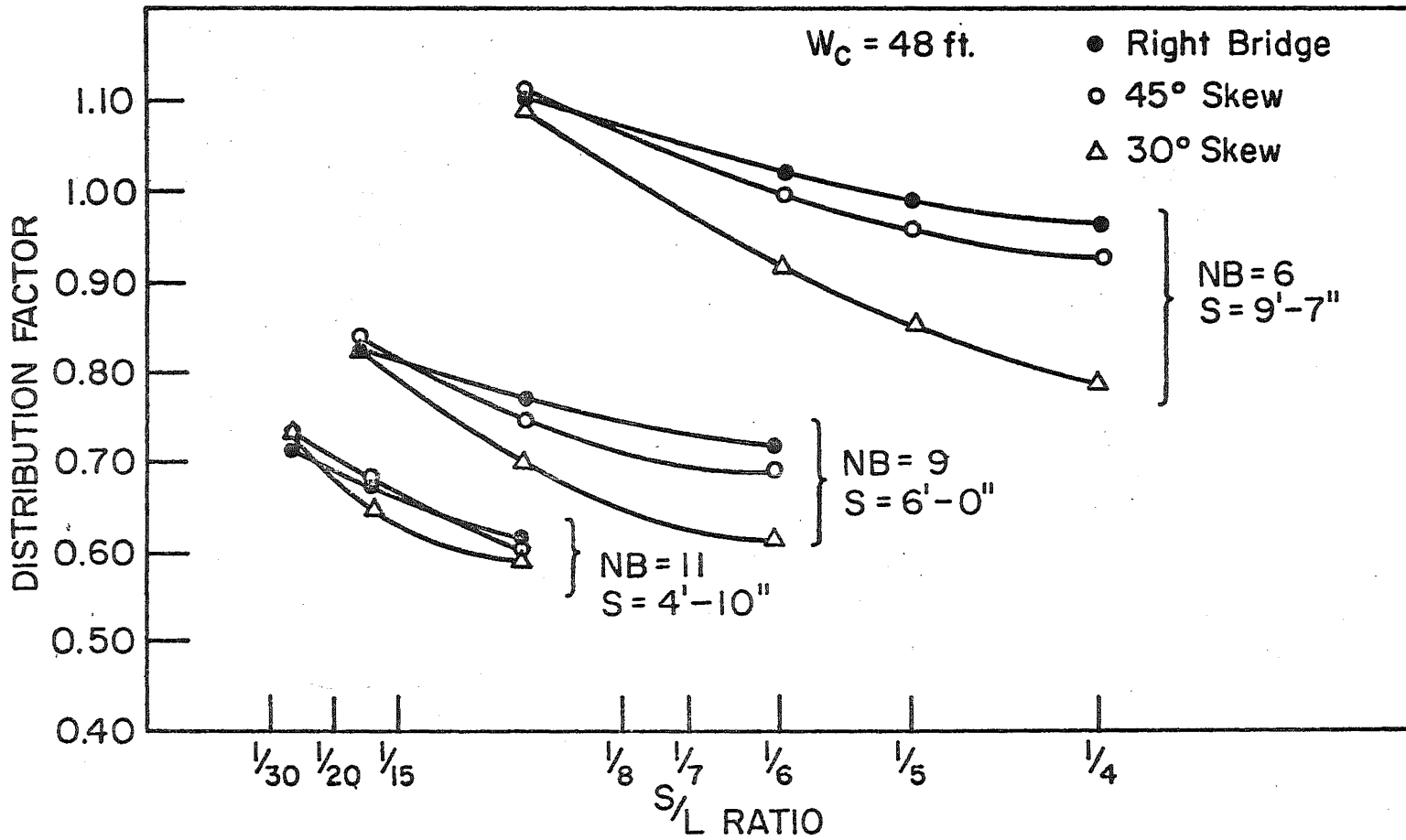
Fig. 78 Distribution Factors for Exterior Beams - 48 ft. Wide Bridges
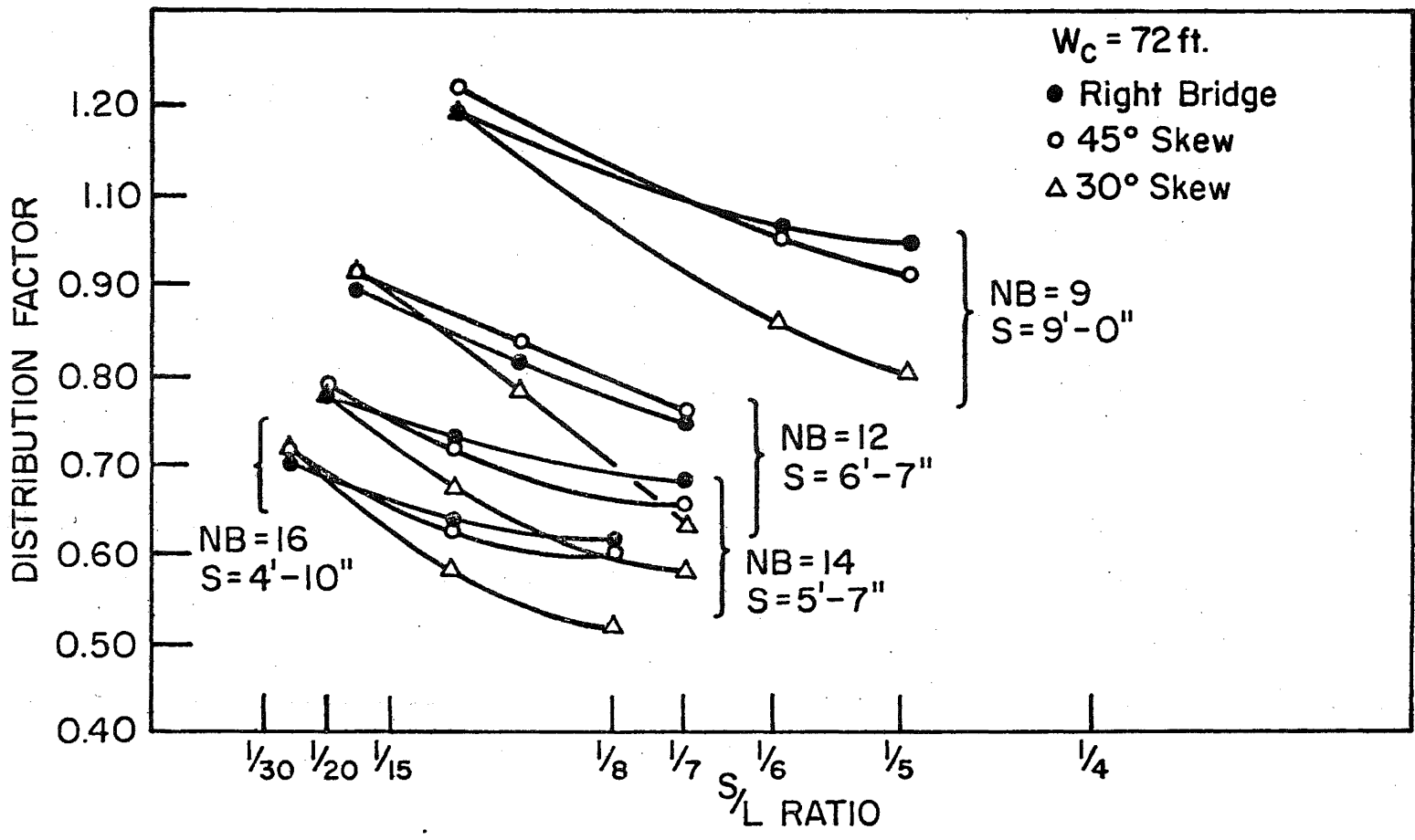
Fig. 79 Distribution Factors for Exterior Beams - 72 ft. Wide Bridges
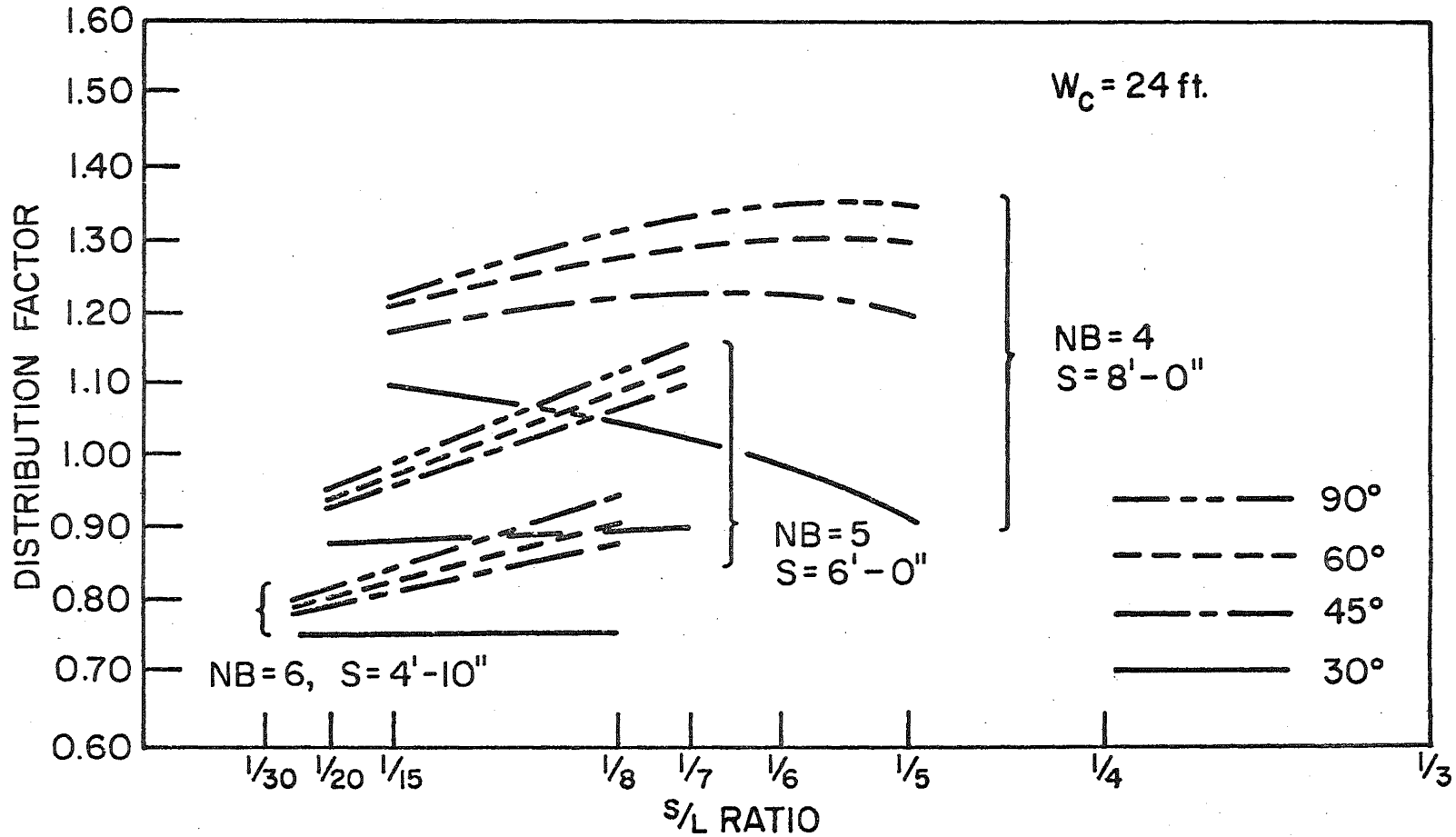
Fig. 80 Analytically Developed Distribution Factors for Interior Beams -
24 ft. Wide Bridges
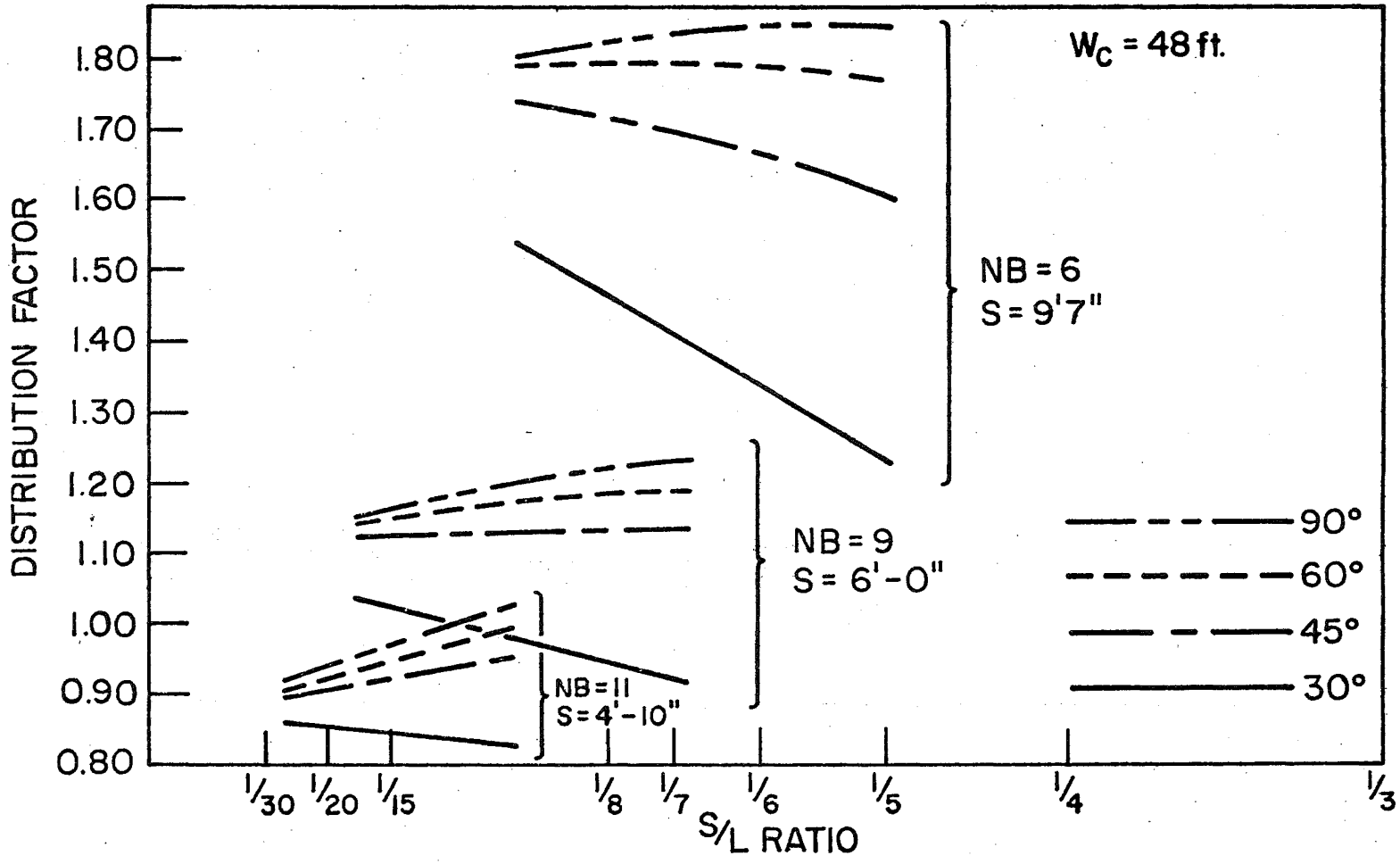
Fig. 81 Analytically Developed Distribution Factors - 48 ft. Wide Bridges
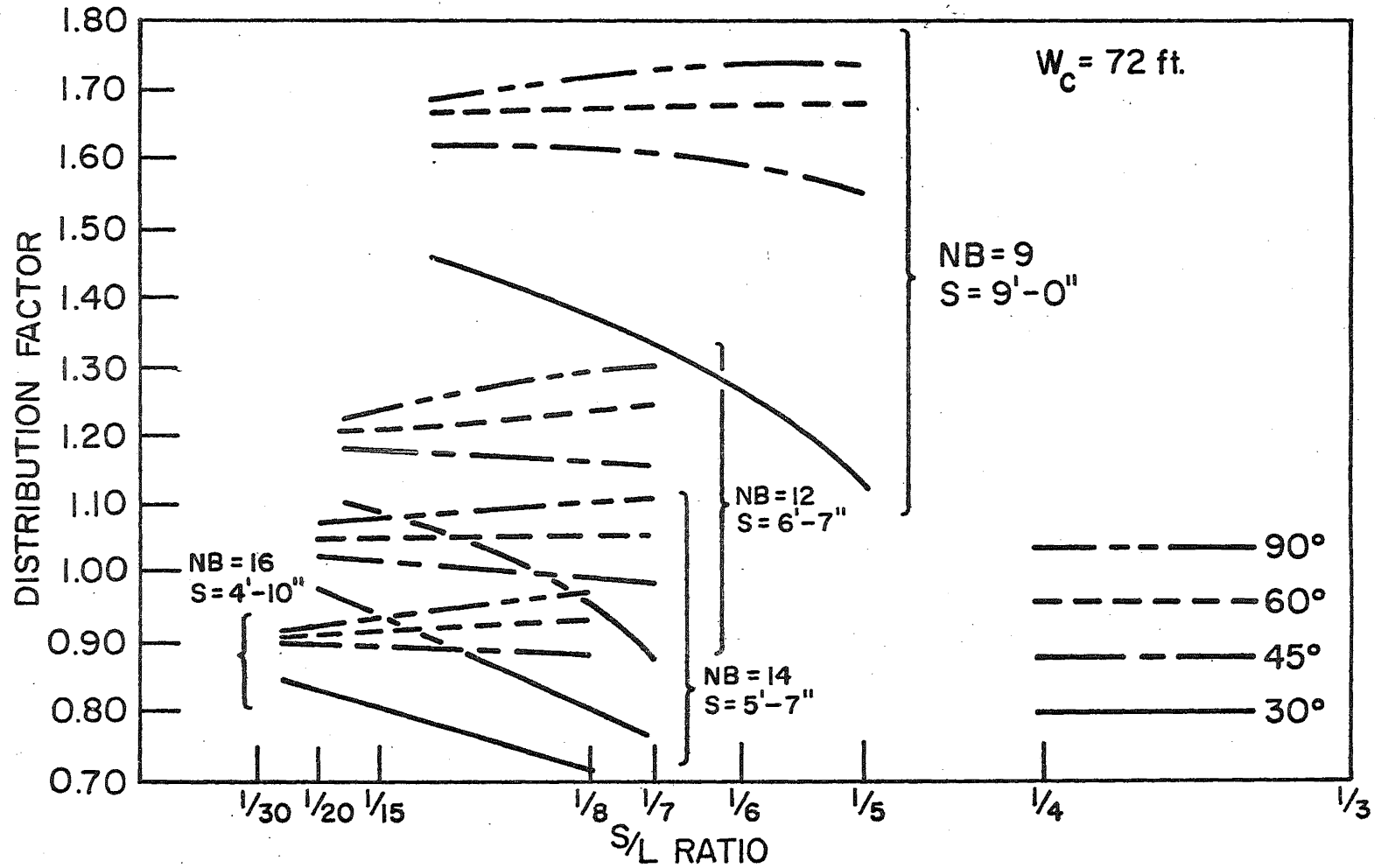
Fig. 82 Analytically Developed Distribution Factors - 72 ft. Wide Bridges
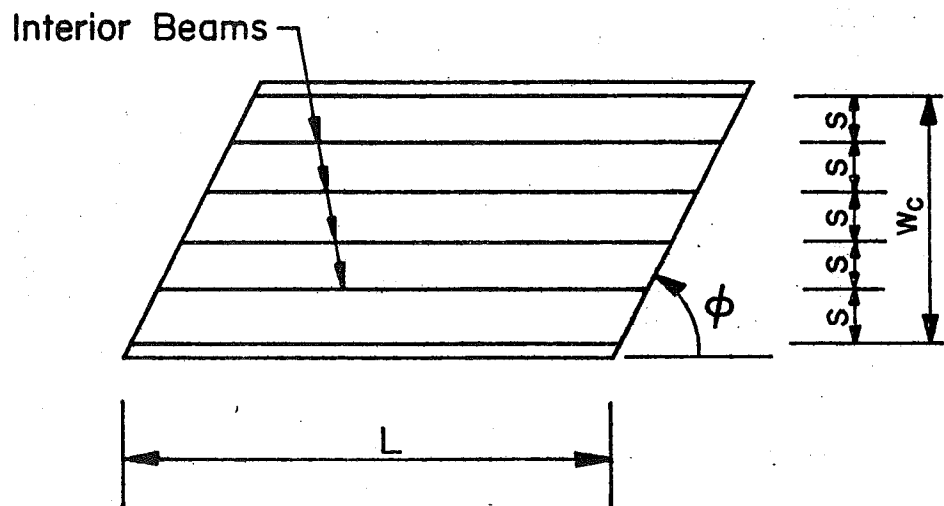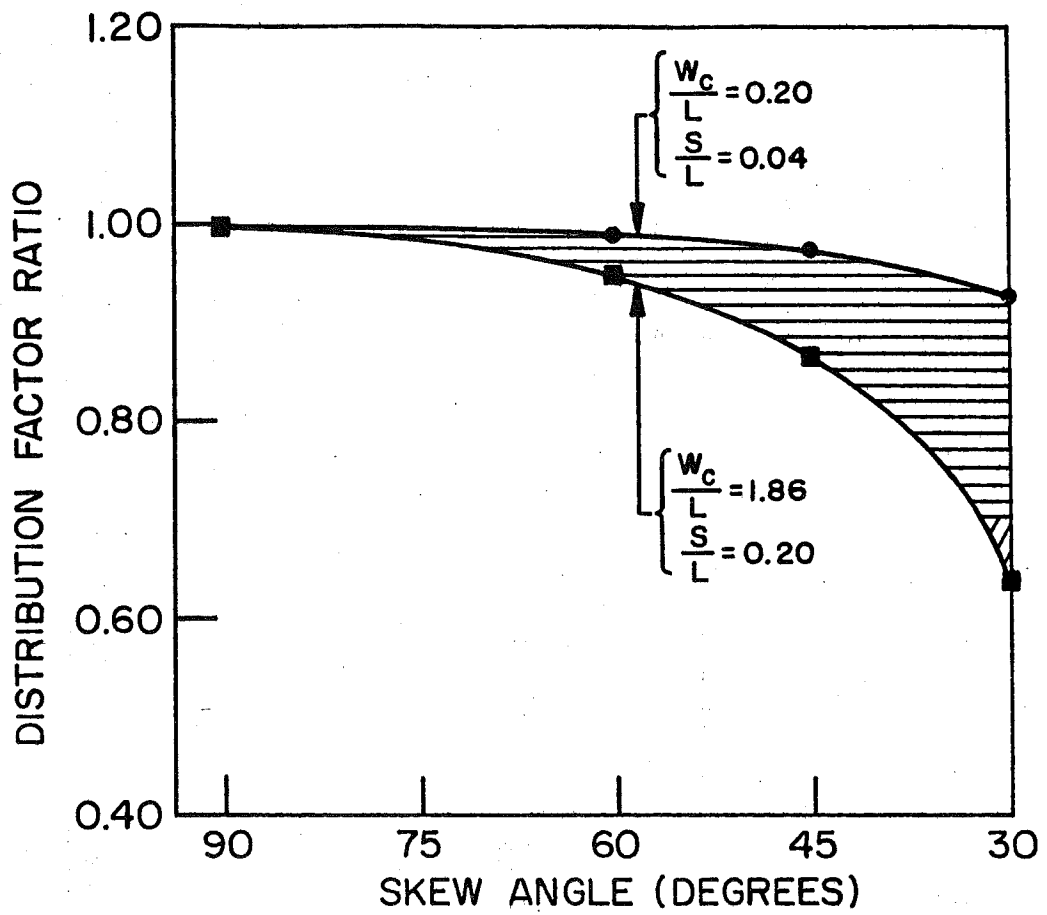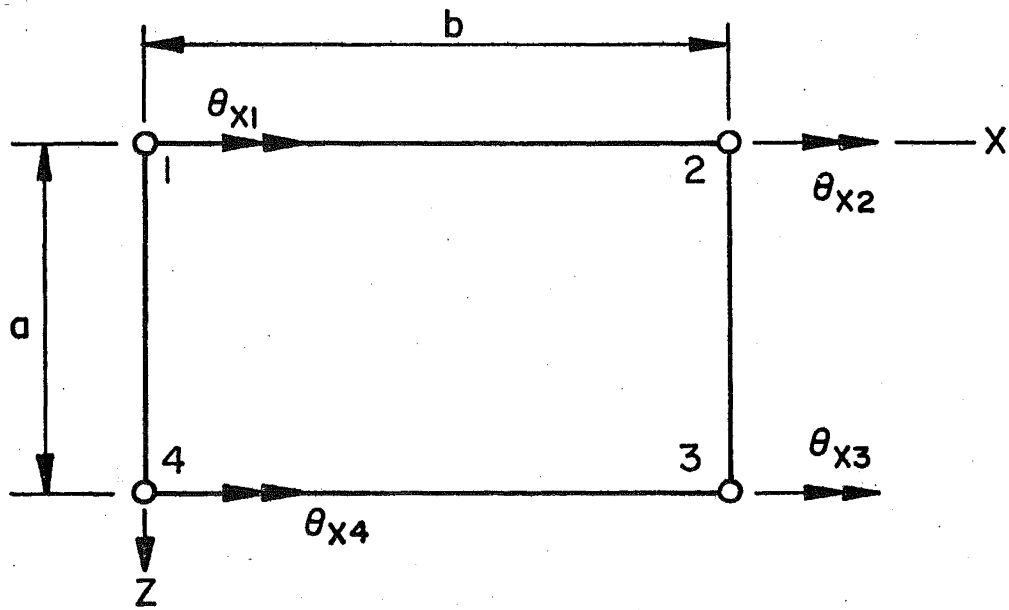
Fig. 83   Interior Beam Distribution Factor Ratio
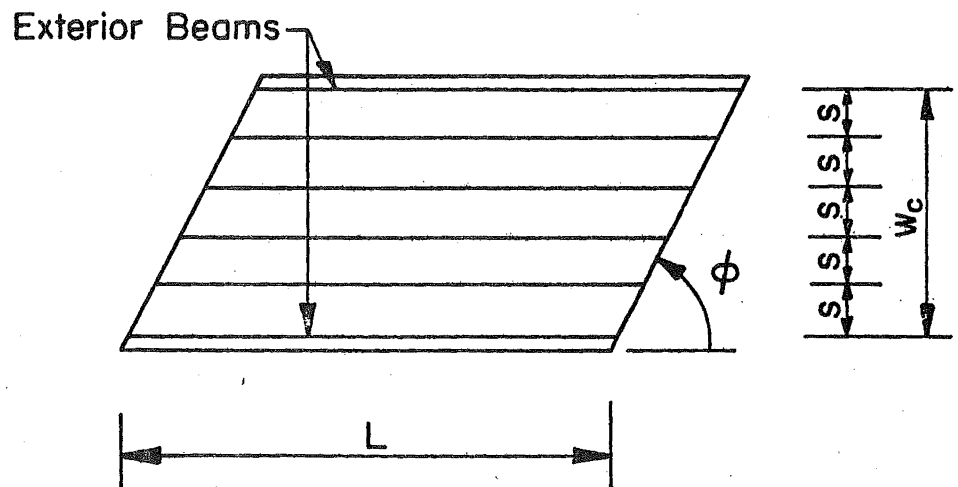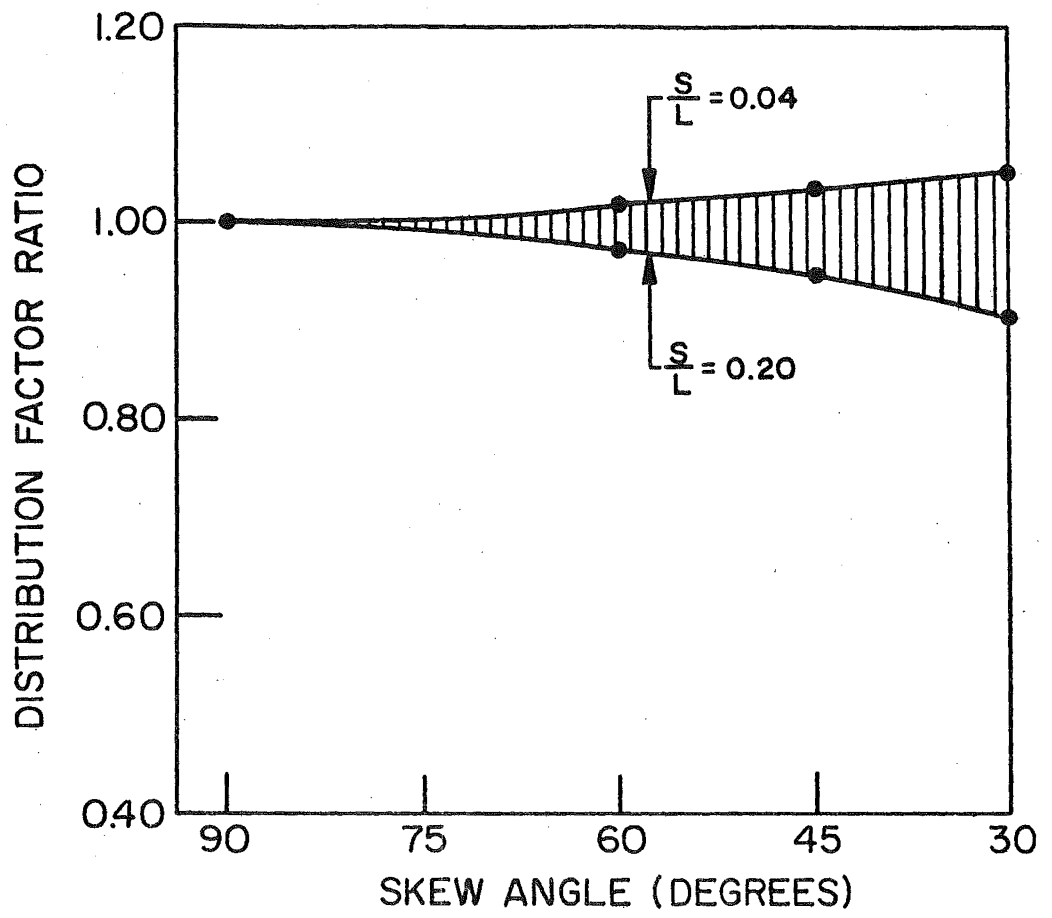
Fig. 84   Exterior Beams Distribution Factor Ratio
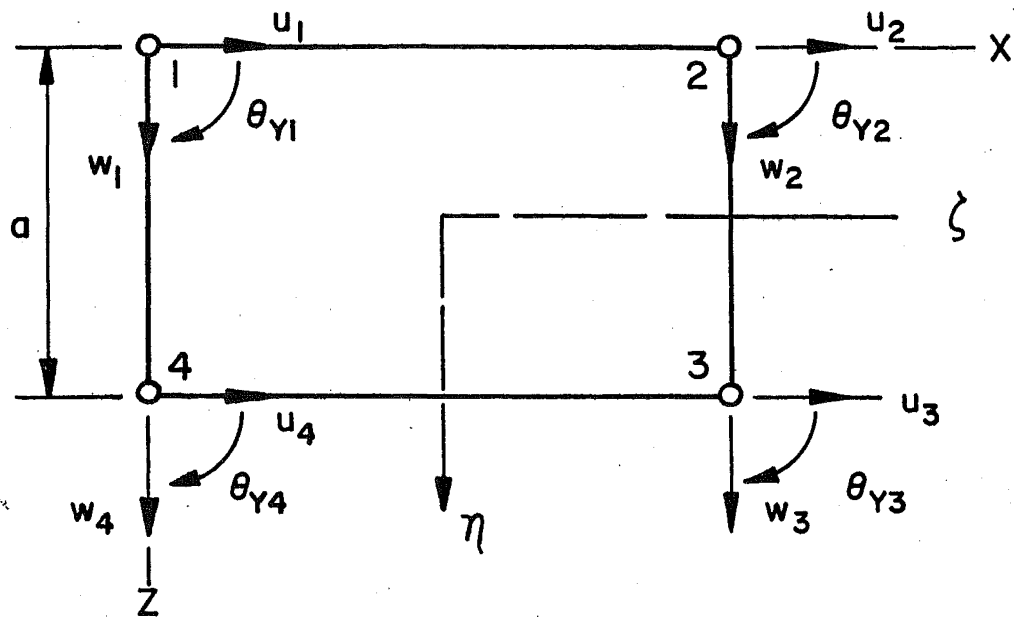
(a) In Plane Degrees Of Freedom

(b) Out Of Plane Degrees Of Freedom

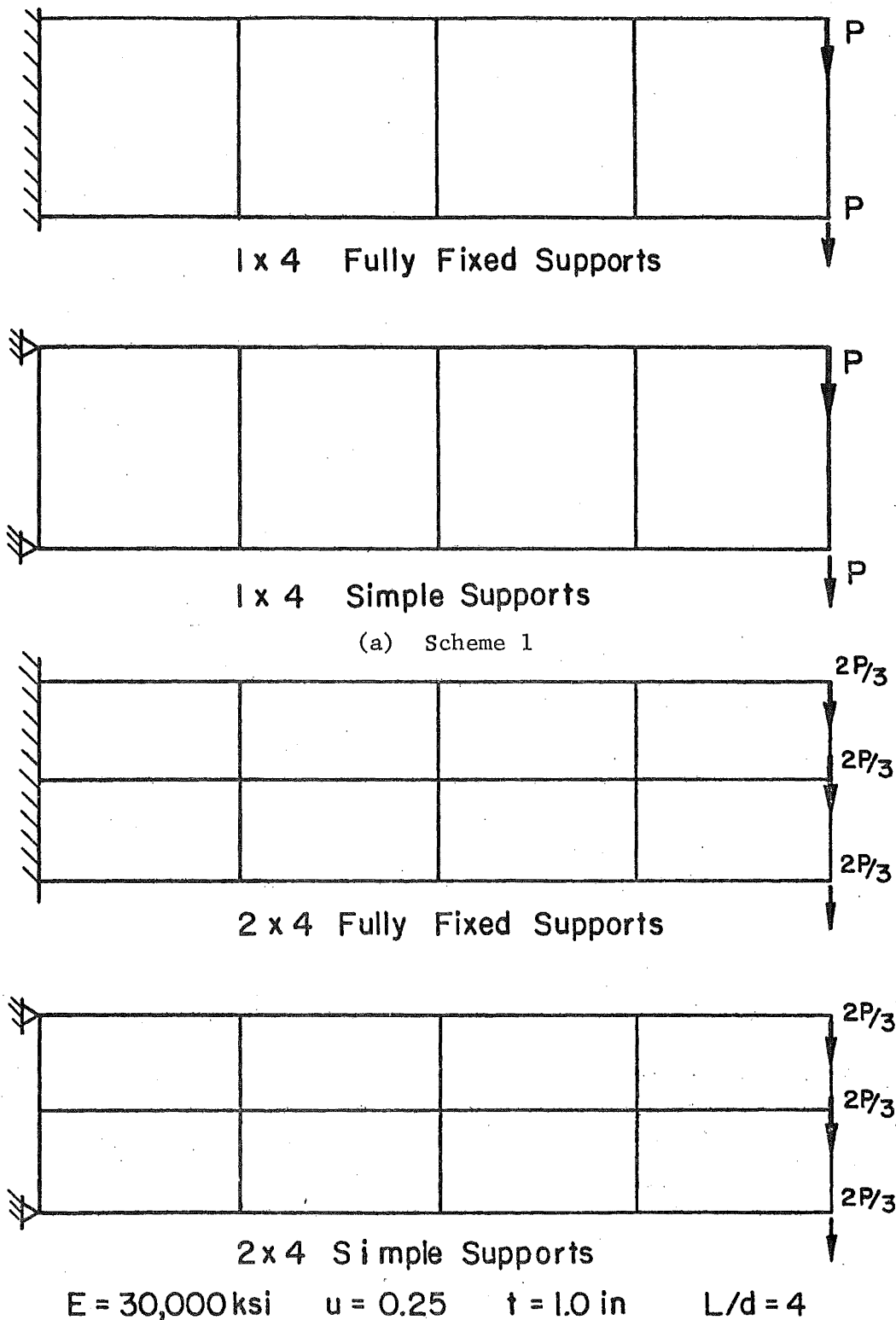Fig. 85 Web Finite Element Degrees of Freedom

1 x 4   Fully Fixed Supports

1 x 4   Simple Supports

(a)   Scheme 1

2 x 4 Fully Fixed Supports

2 x 4 Simple Supports

E = 30,000 ksi   u = 0.25   t = 1.0 in   L/d = 4

(b)   Scheme 2

Fig. 86   Cantilever Beam Discretization and Modeling Schemes
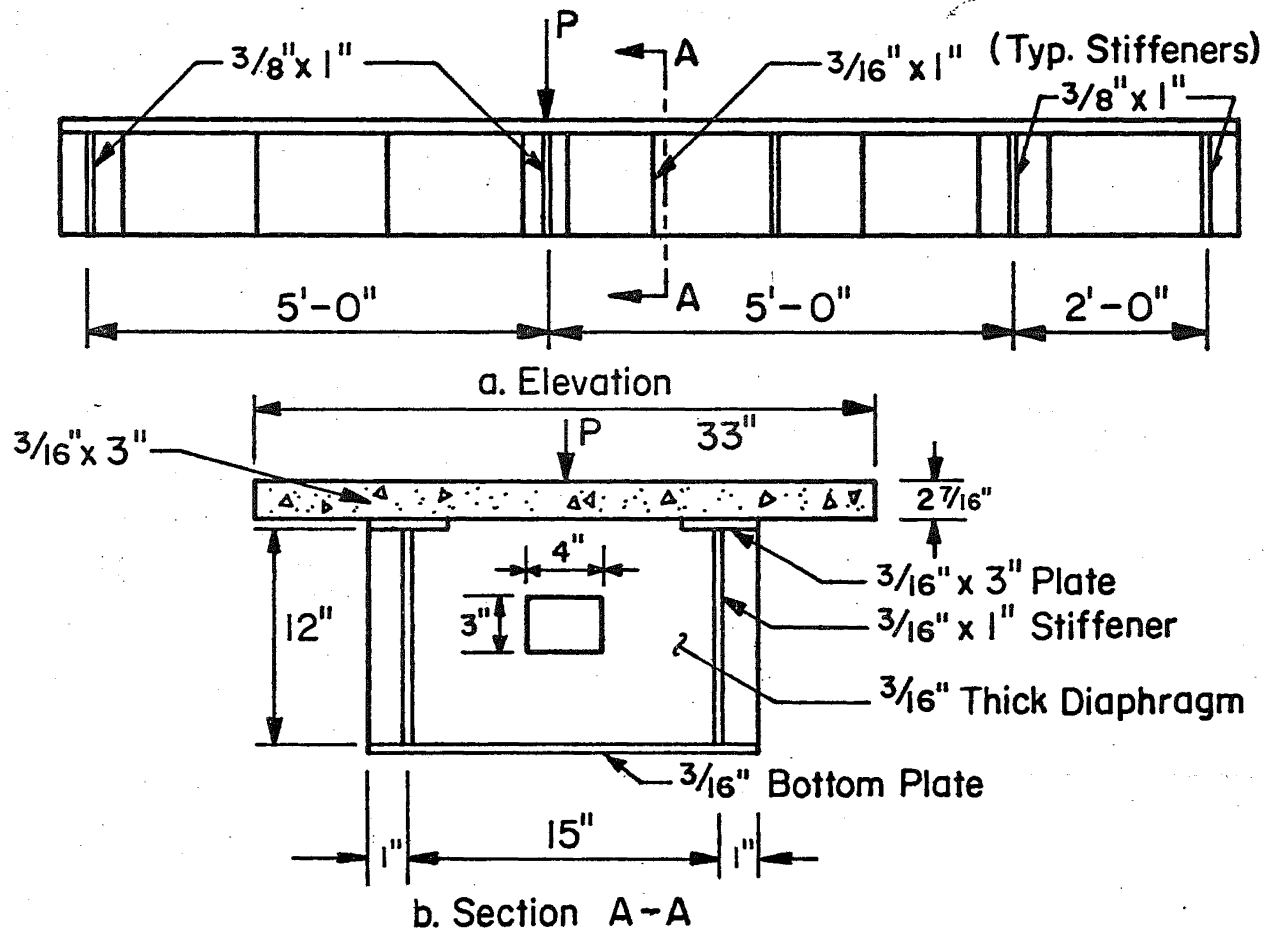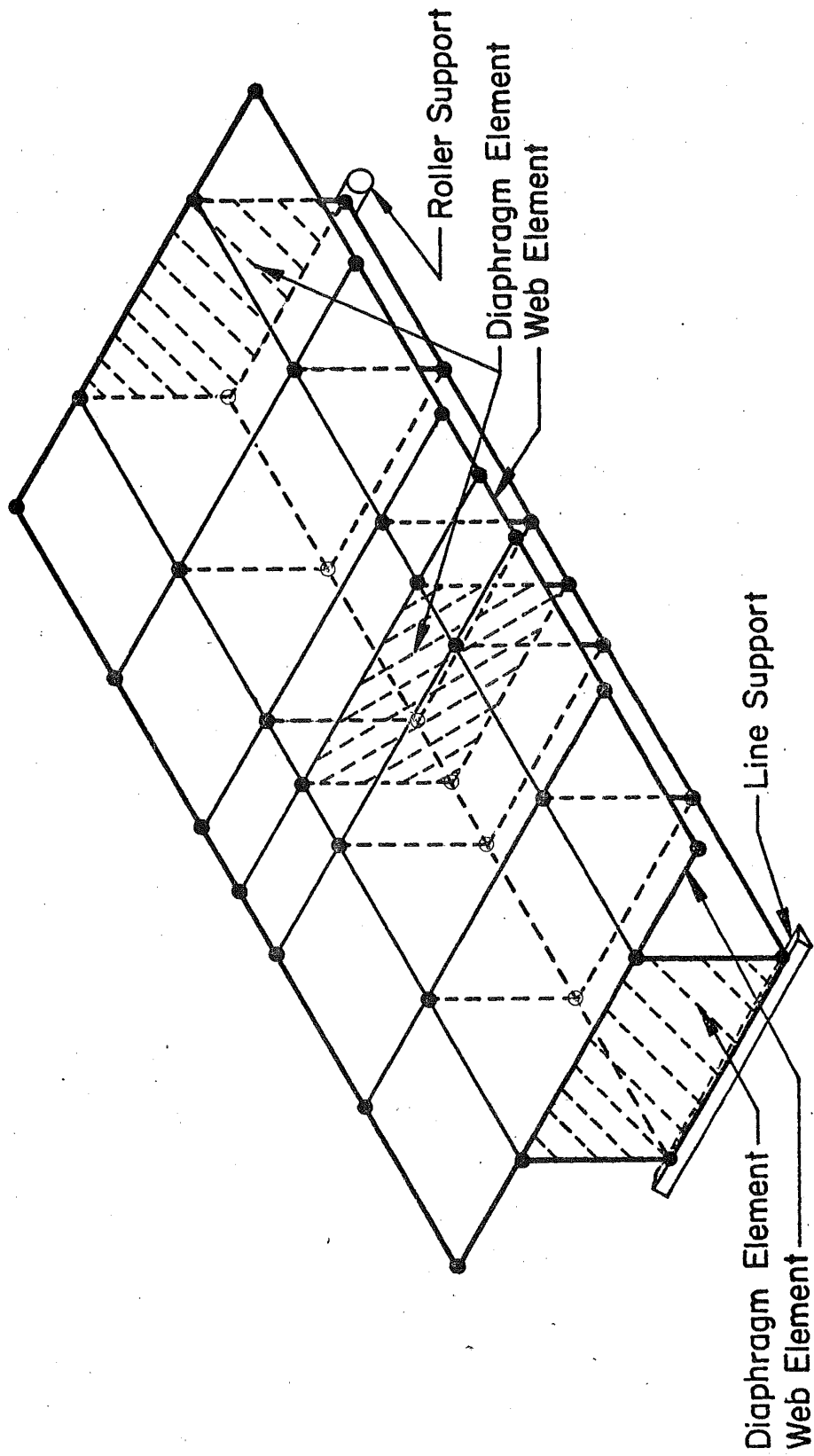
Fig. 87 Composite Steel Box-Beam, Elevation and Section

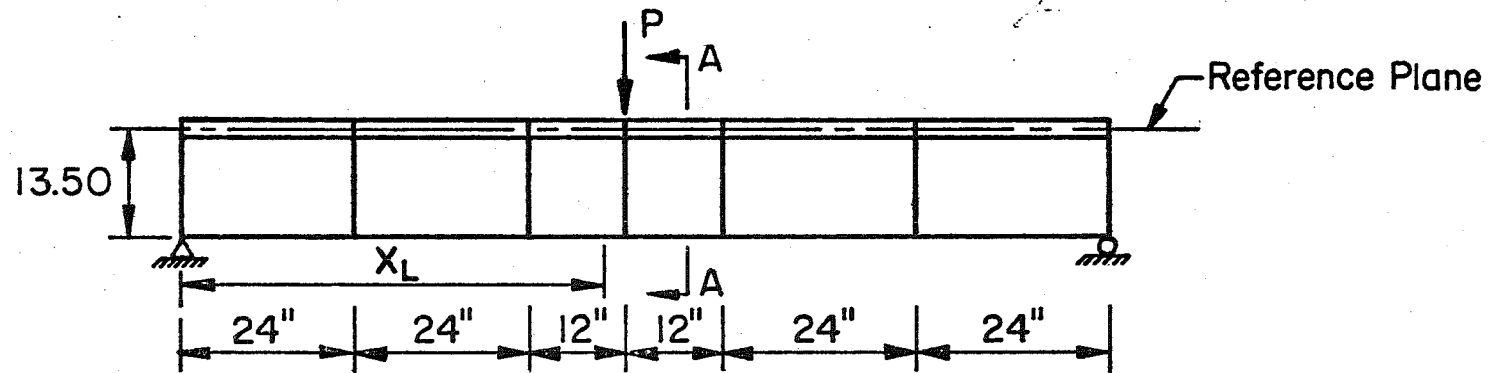Fig. 88 Composite Box-Beam, Structural Idealization

Roller Support

Diaphragm Element
Web Element

Line Support

Diaphragm Element
Web Element
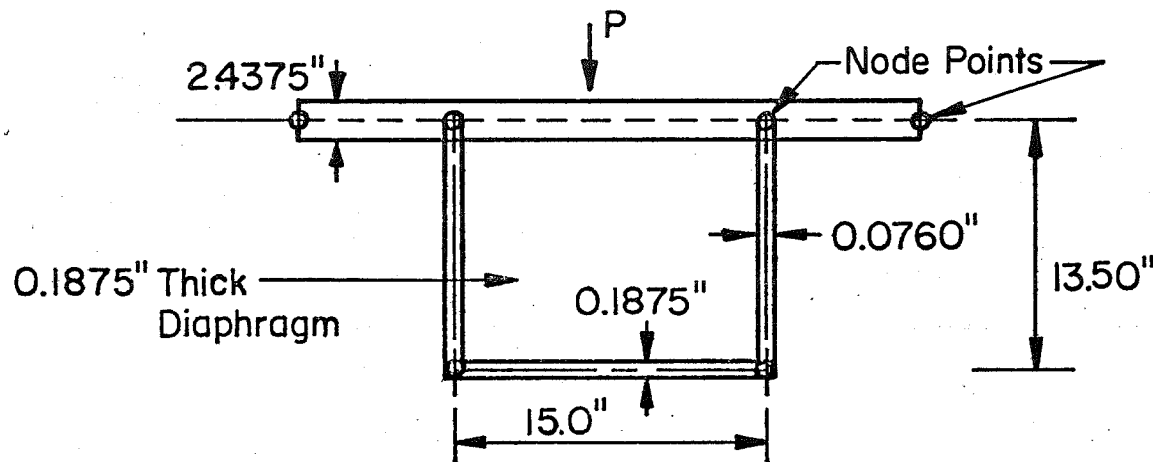
a. Discretization Along Length

$E_C = 3.700 \times 10^3$ ksi
$E_S = 29.600 \times 10^3$ ksi

$\mu_C = .15$
$\mu_S = .25$

b. Discretization At Cross Section (Section A-A)

Fig. 89   Composite Box-Beam Finite Element Mesh

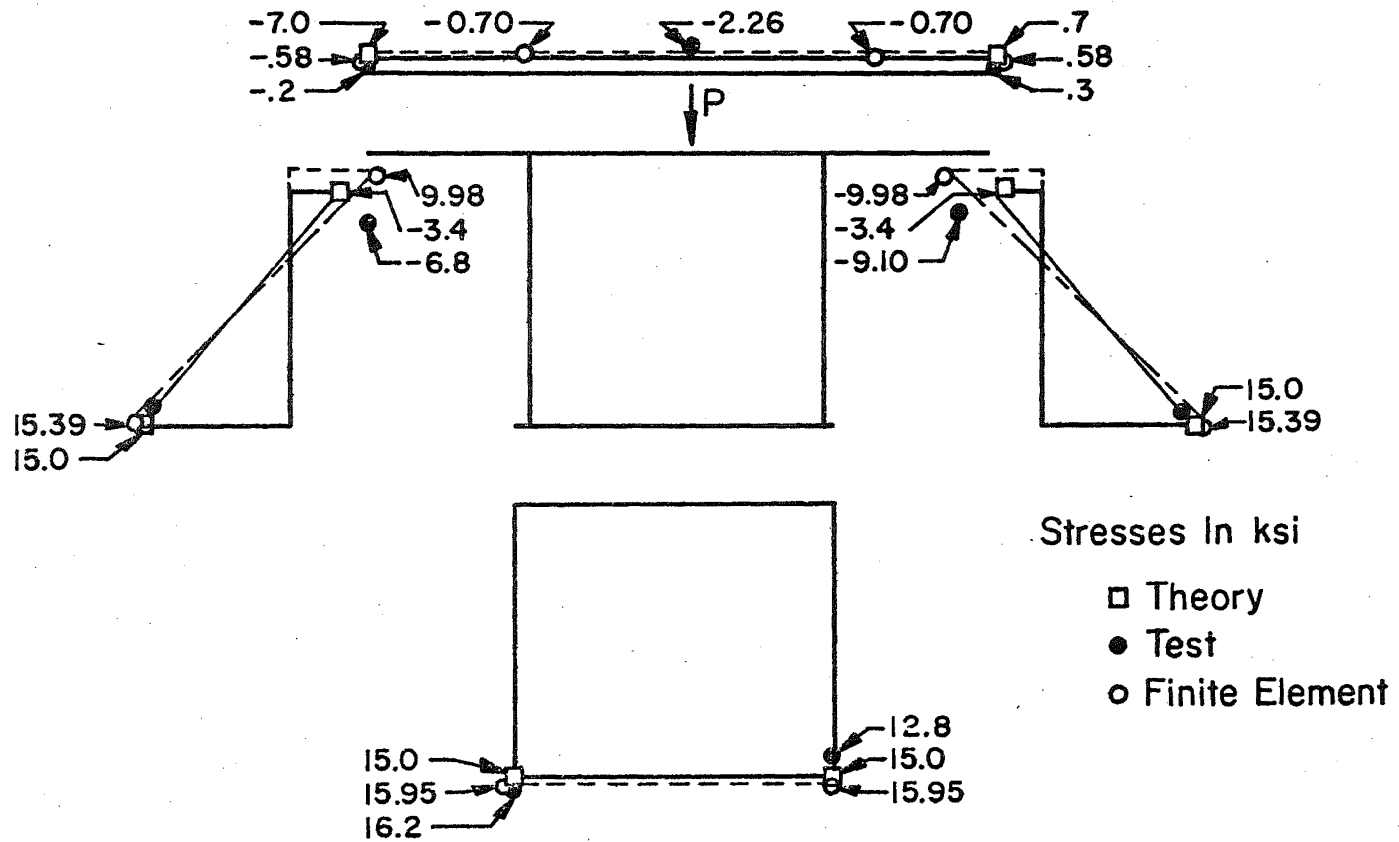Fig. 90 Normal Stresses at Midspan, Symmetric Loading
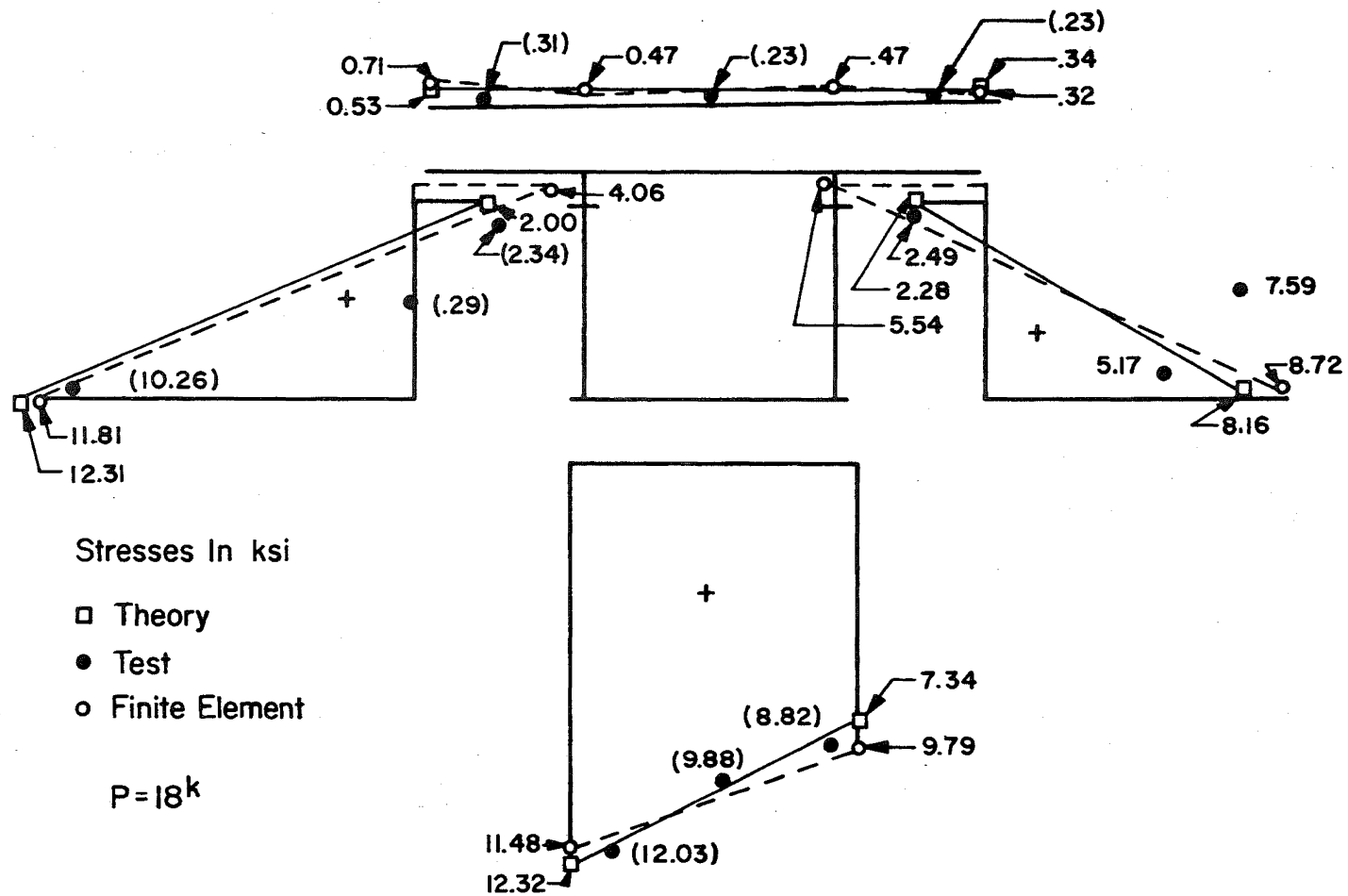
Fig. 91 Normal Stresses at Midspan - Unsymmetric Loading

Stresses In ksi

□ Theory
● Test
○ Finite Element

$P = 18^k$
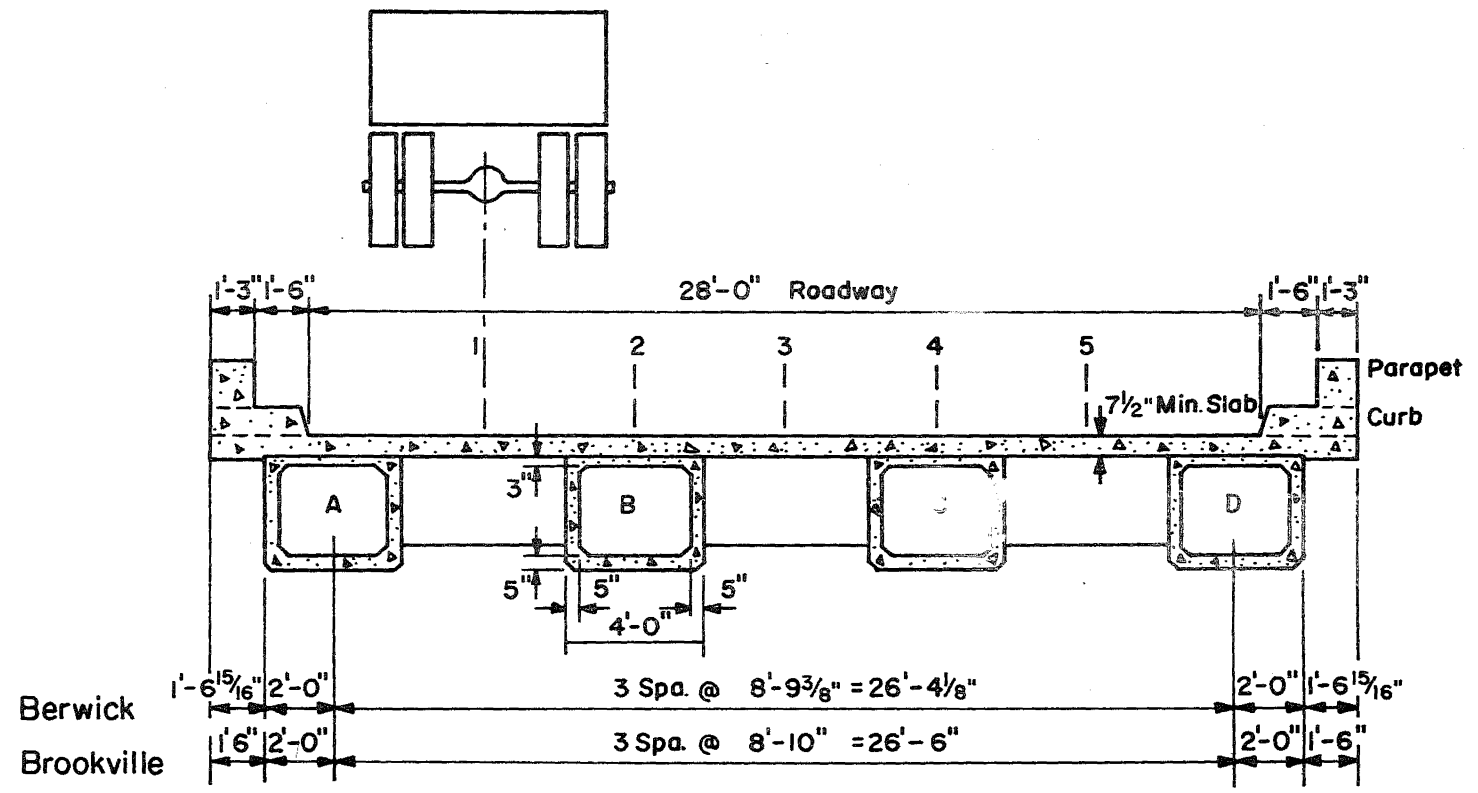
Fig. 92 Cross Section of the Berwick and Brookville Bridge
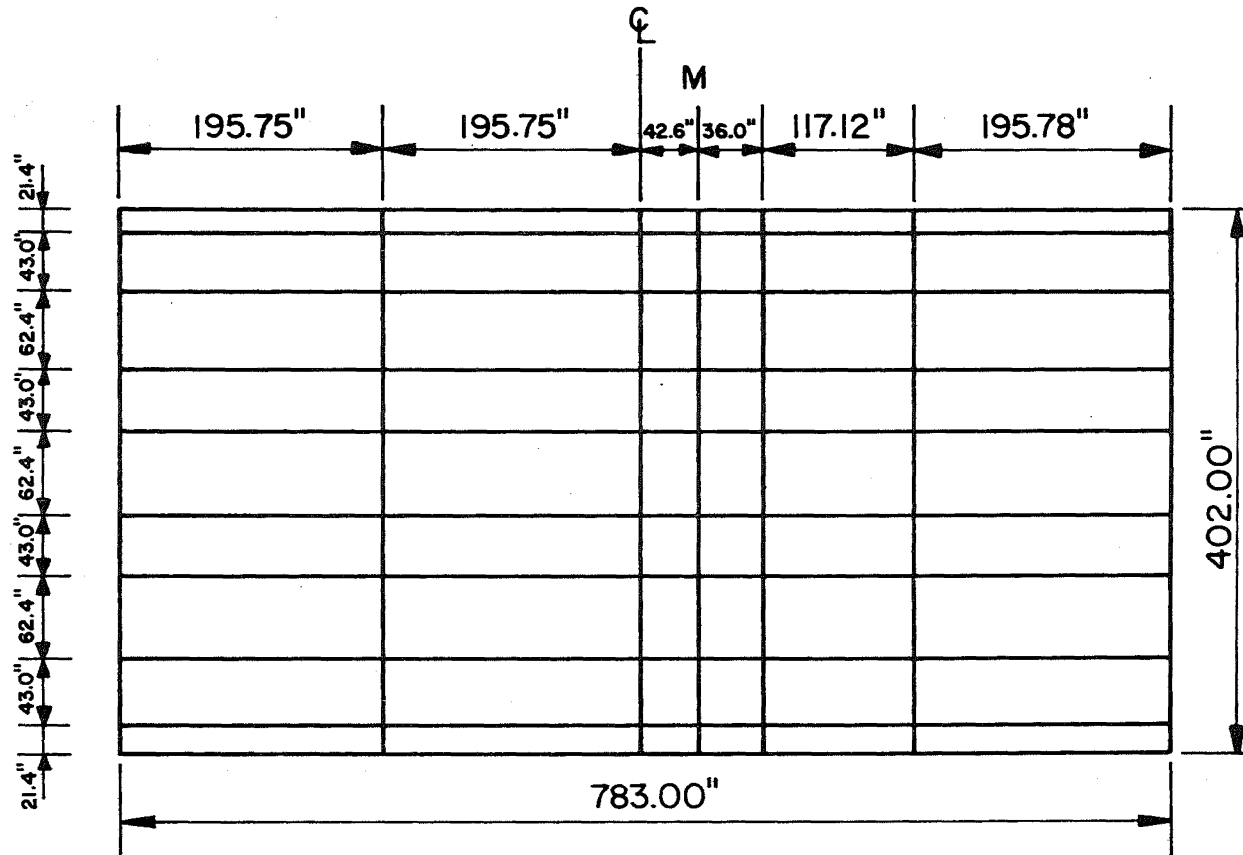
Fig. 93 Finite Element Mesh - Berwick Bridge
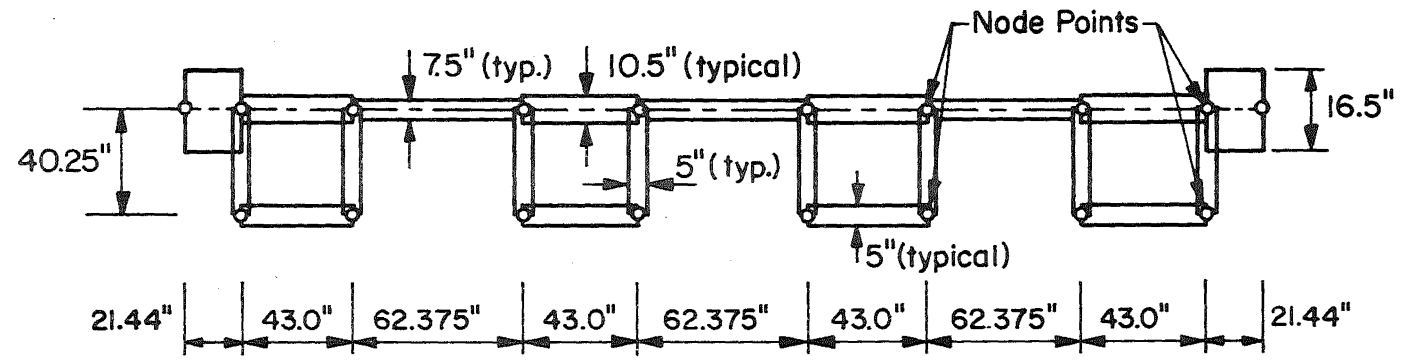
Fig. 94 Idealization of the Cross Section - Berwick Bridge
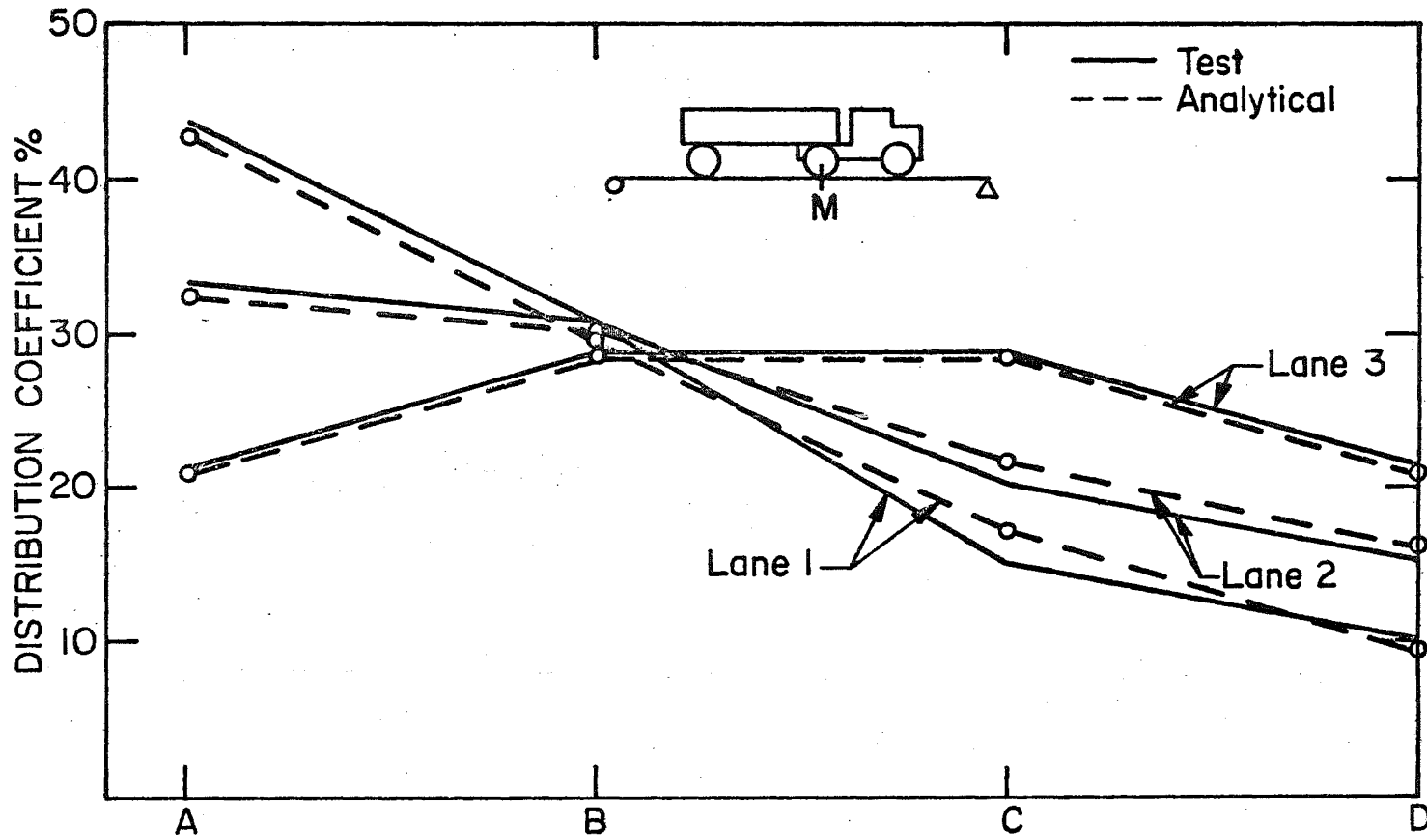
Fig. 95 Distribution Coefficient at Section M - Berwick Bridge
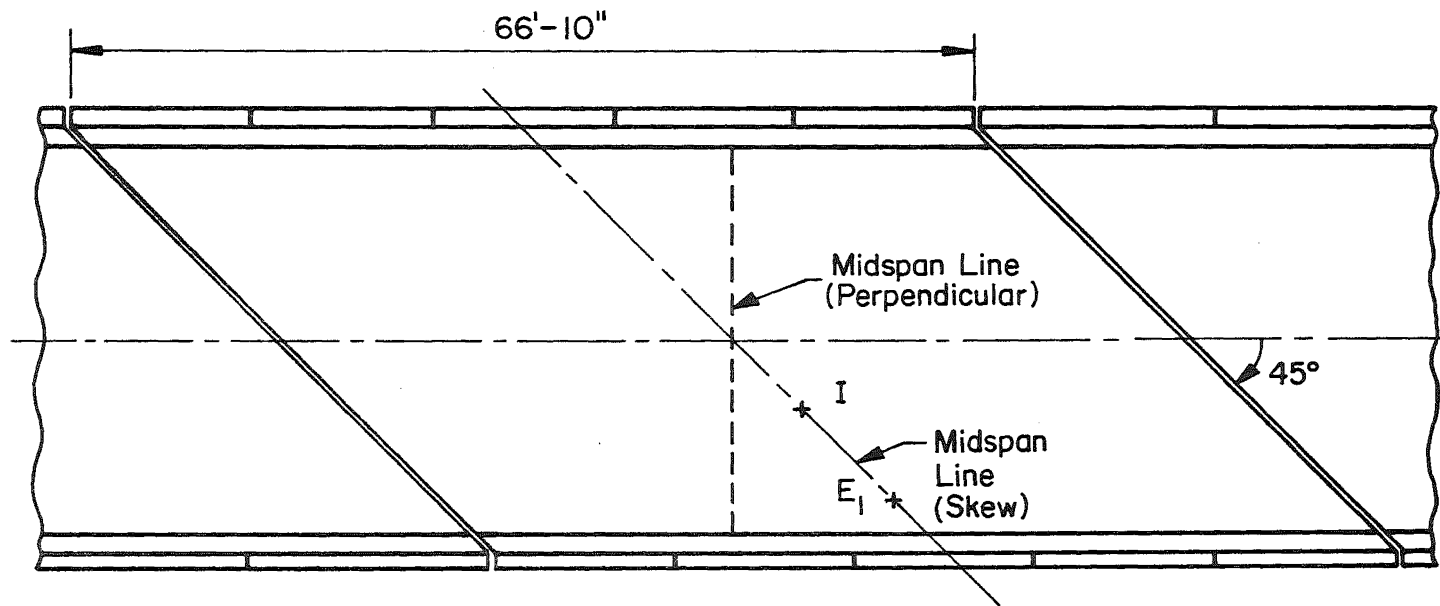
Fig. 96 Plan of the 45° Skew Spread Box-Beam Bridge - Brookville Bridge

Finite Element Discretization
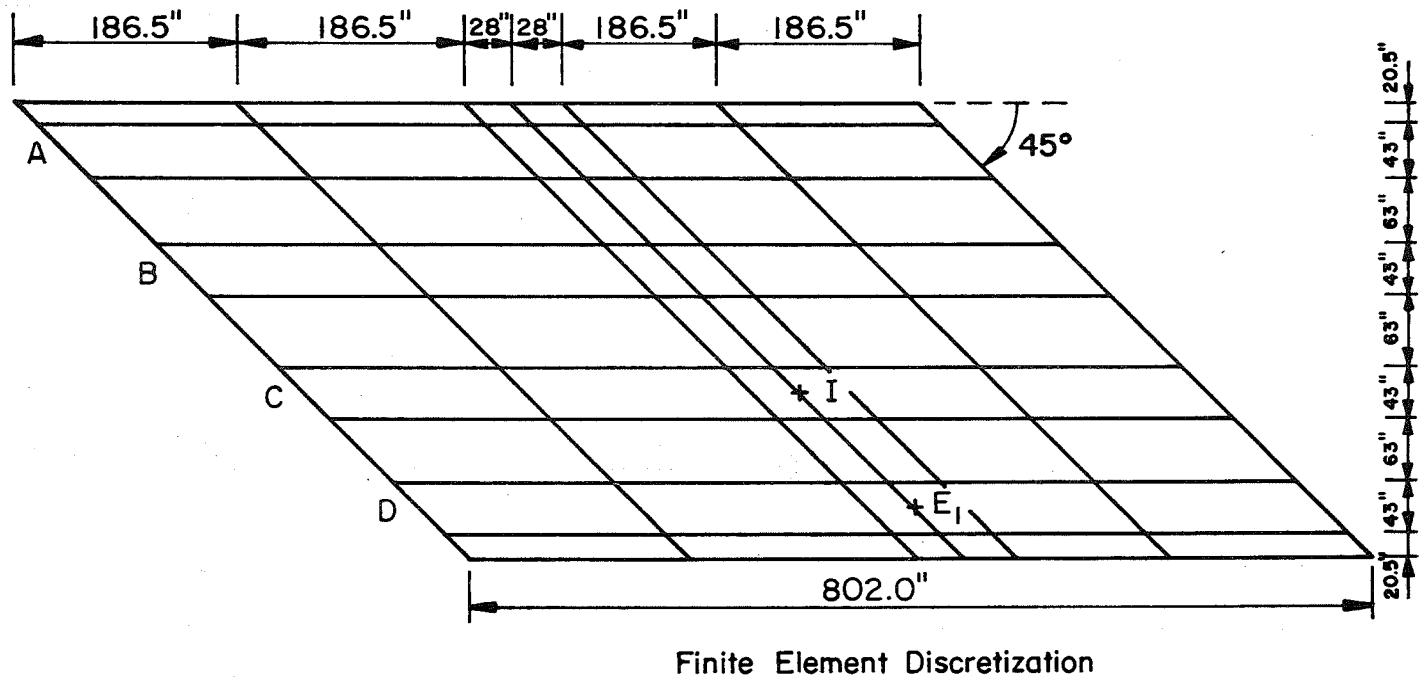
Fig. 97   Finite Element Mesh - Brookville Bridge
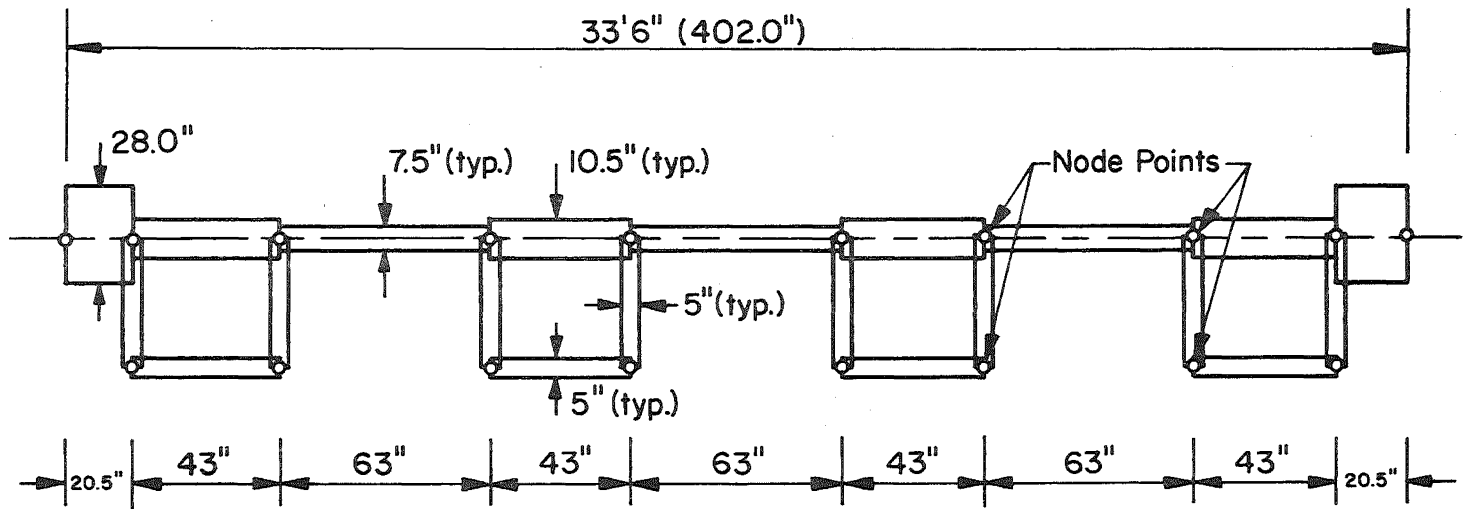
Fig. 98 Idealization of the Cross Section - Brookville Bridge
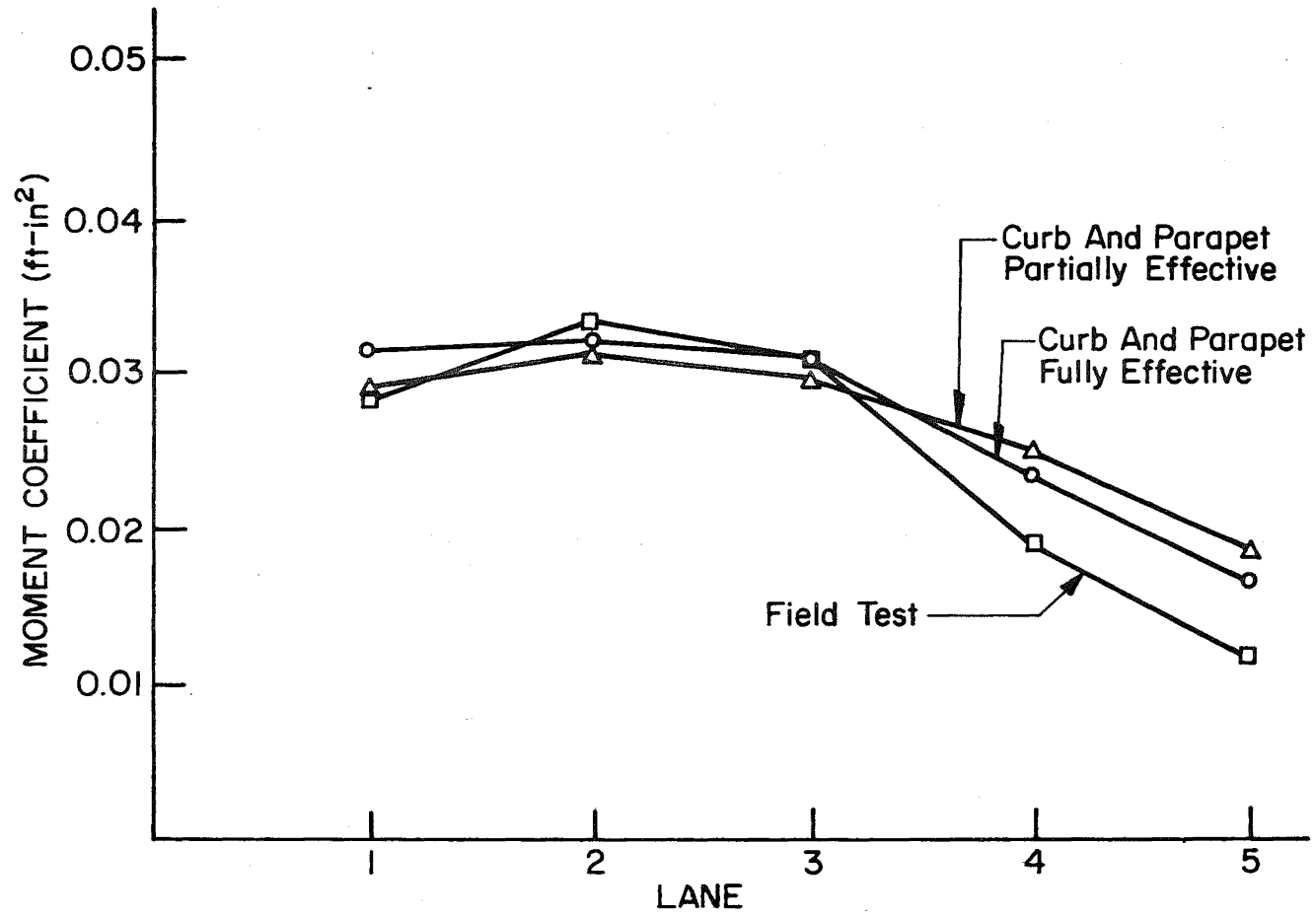
Fig. 99 Influence Moment Coefficients, Beam C - Brookville Bridge
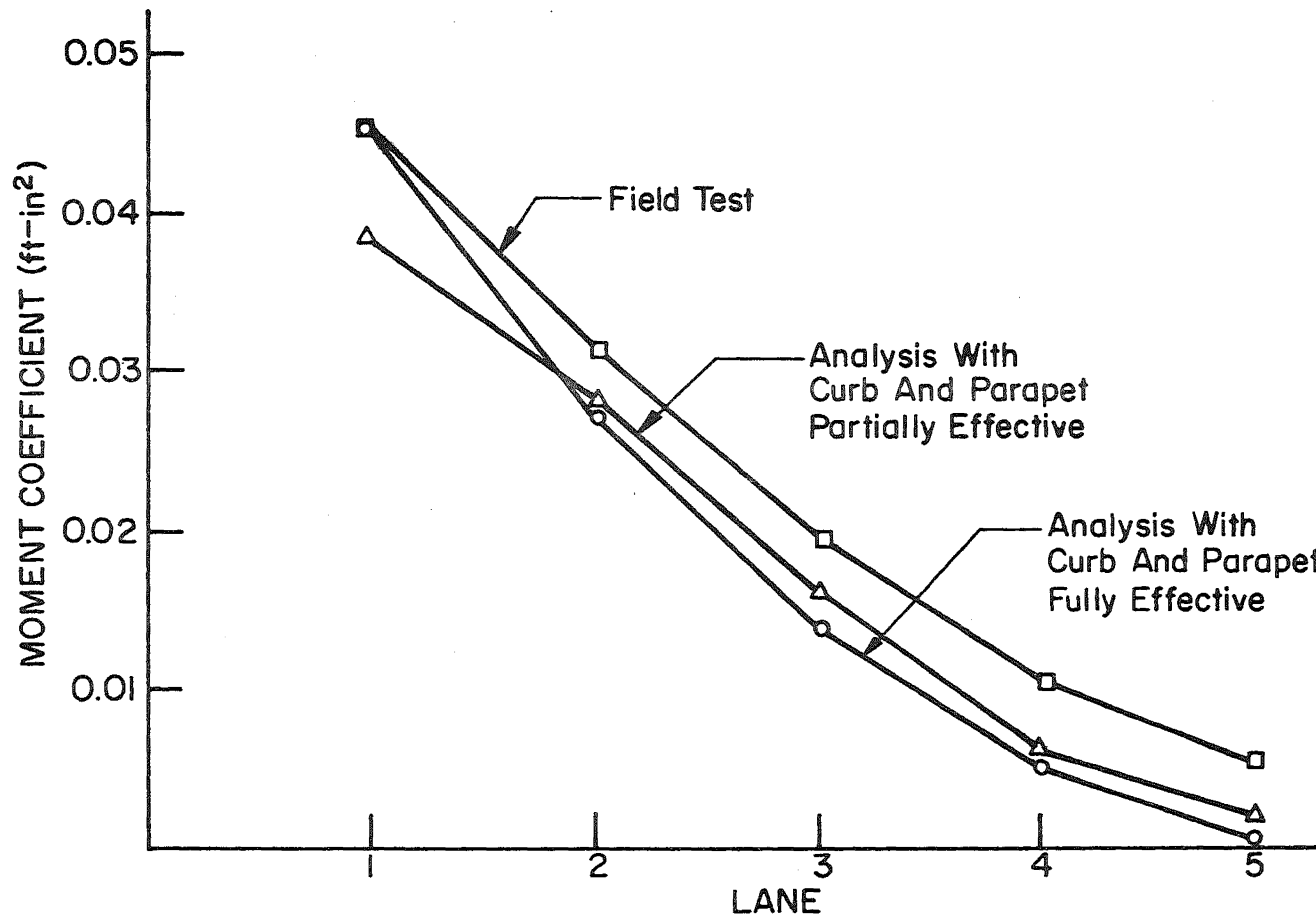
Fig. 100 Influence Moment Coefficients, Beam D - Brookville Bridge
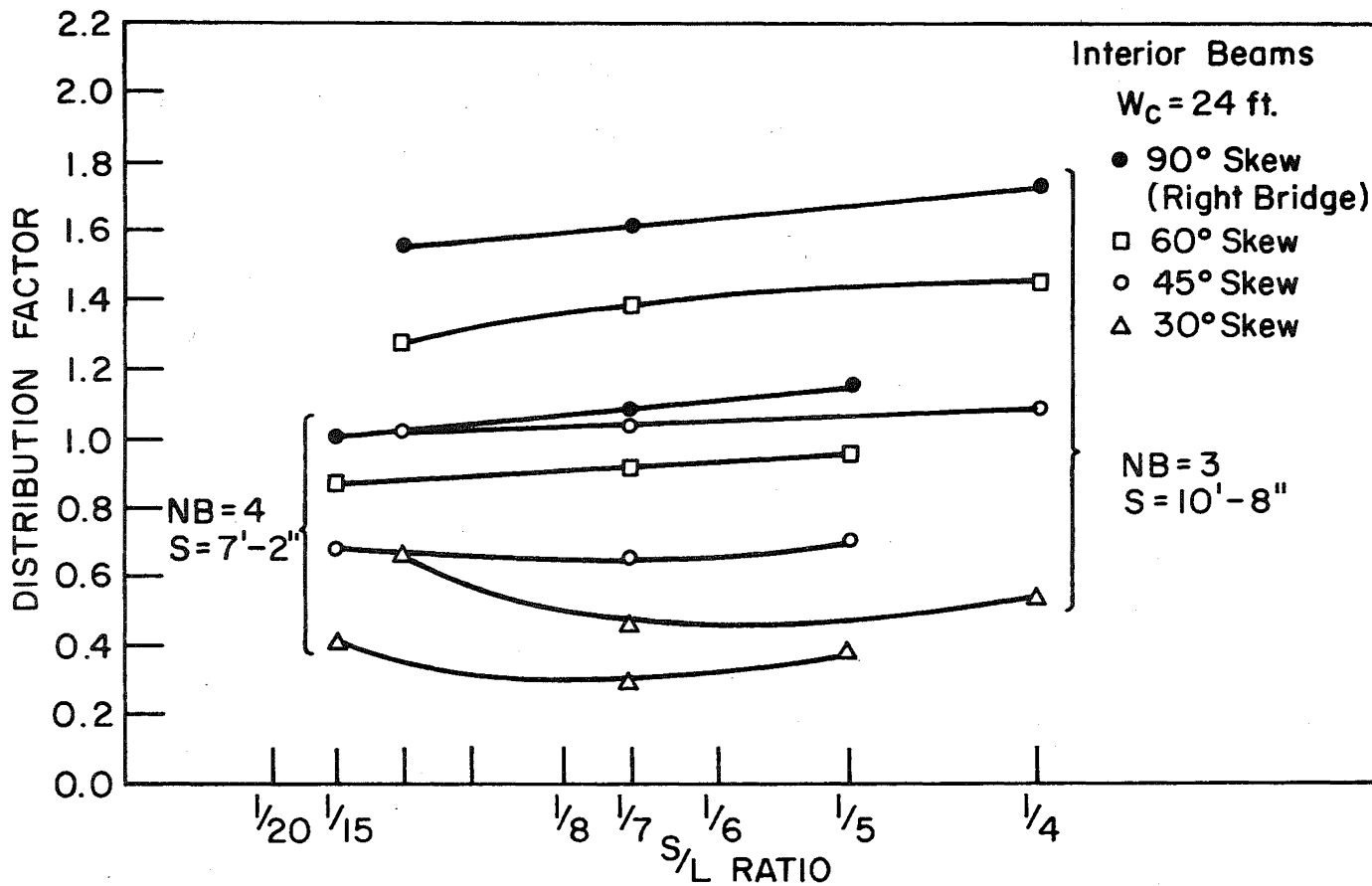
Fig. 101 Maximum Interior Beam Distribution Factors, Skew Box-Beam Bridges, W_c = 24 ft.
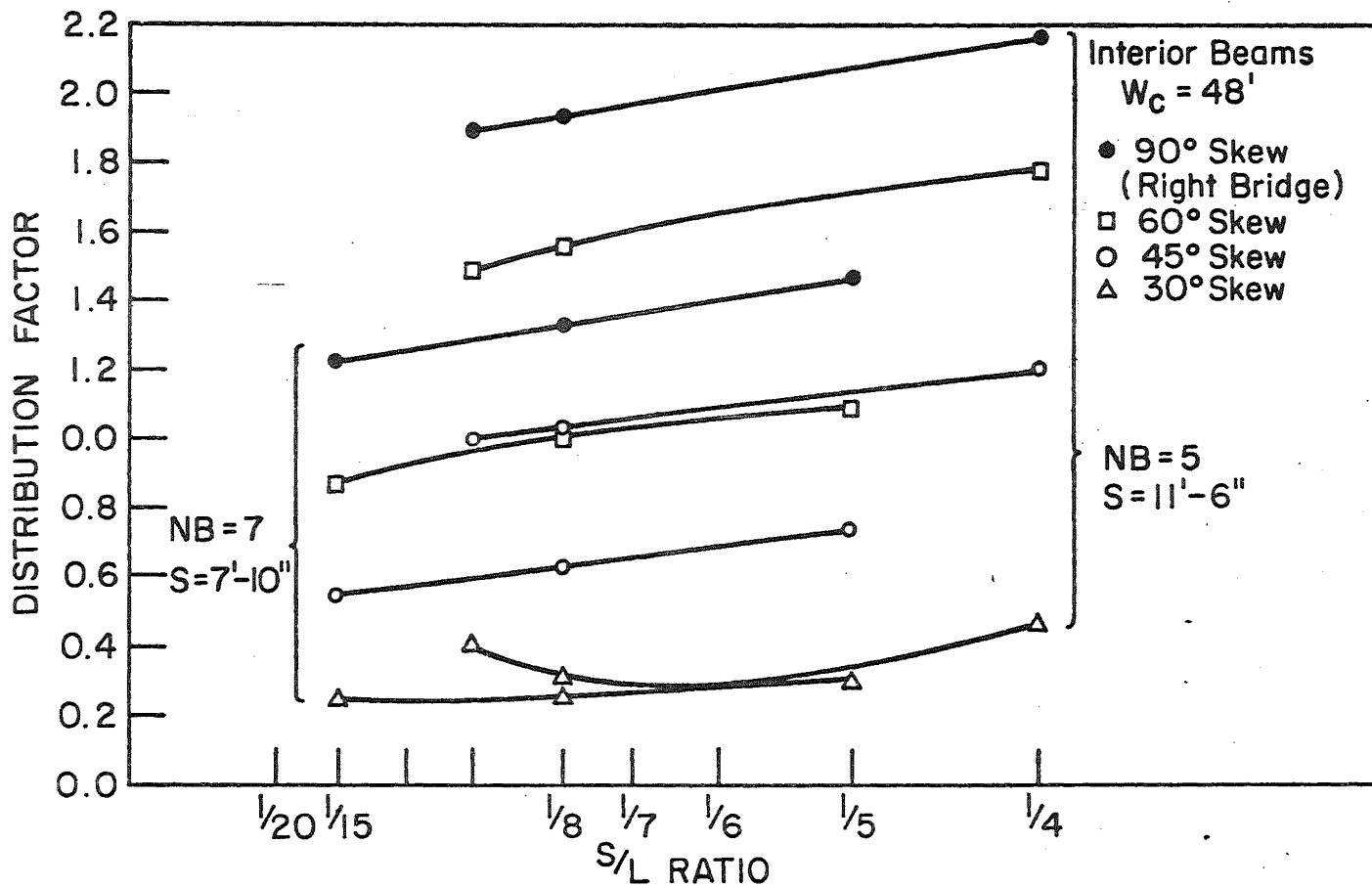
Fig. 102 Maximum Interior Beam Distribution Factors, Skew Box-Beam Bridges,
W_c = 48 ft.
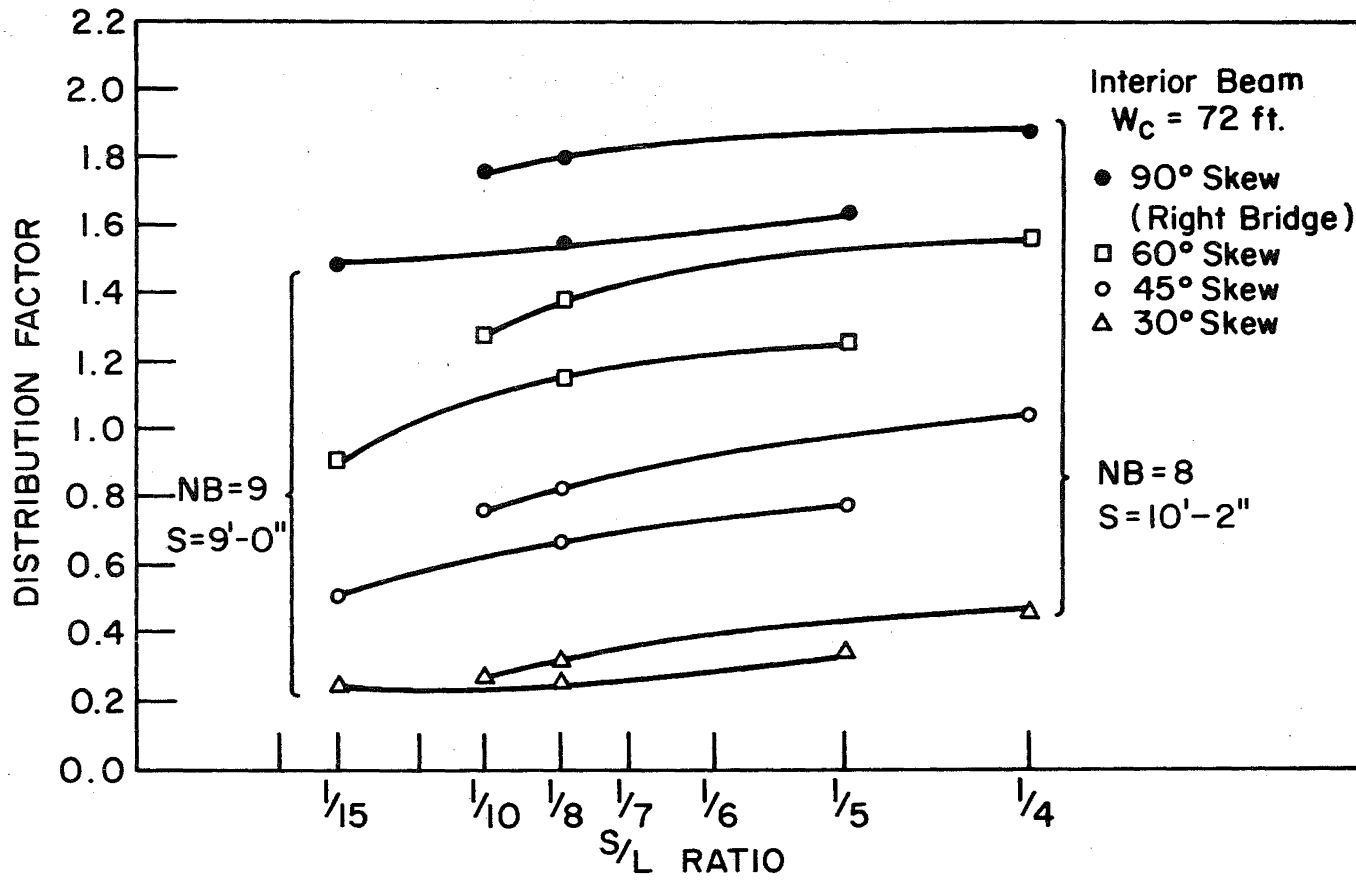
Fig. 103 Maximum Interior Beam Distribution Factors, Skew Box-Beam Bridges, W_c = 72 ft.
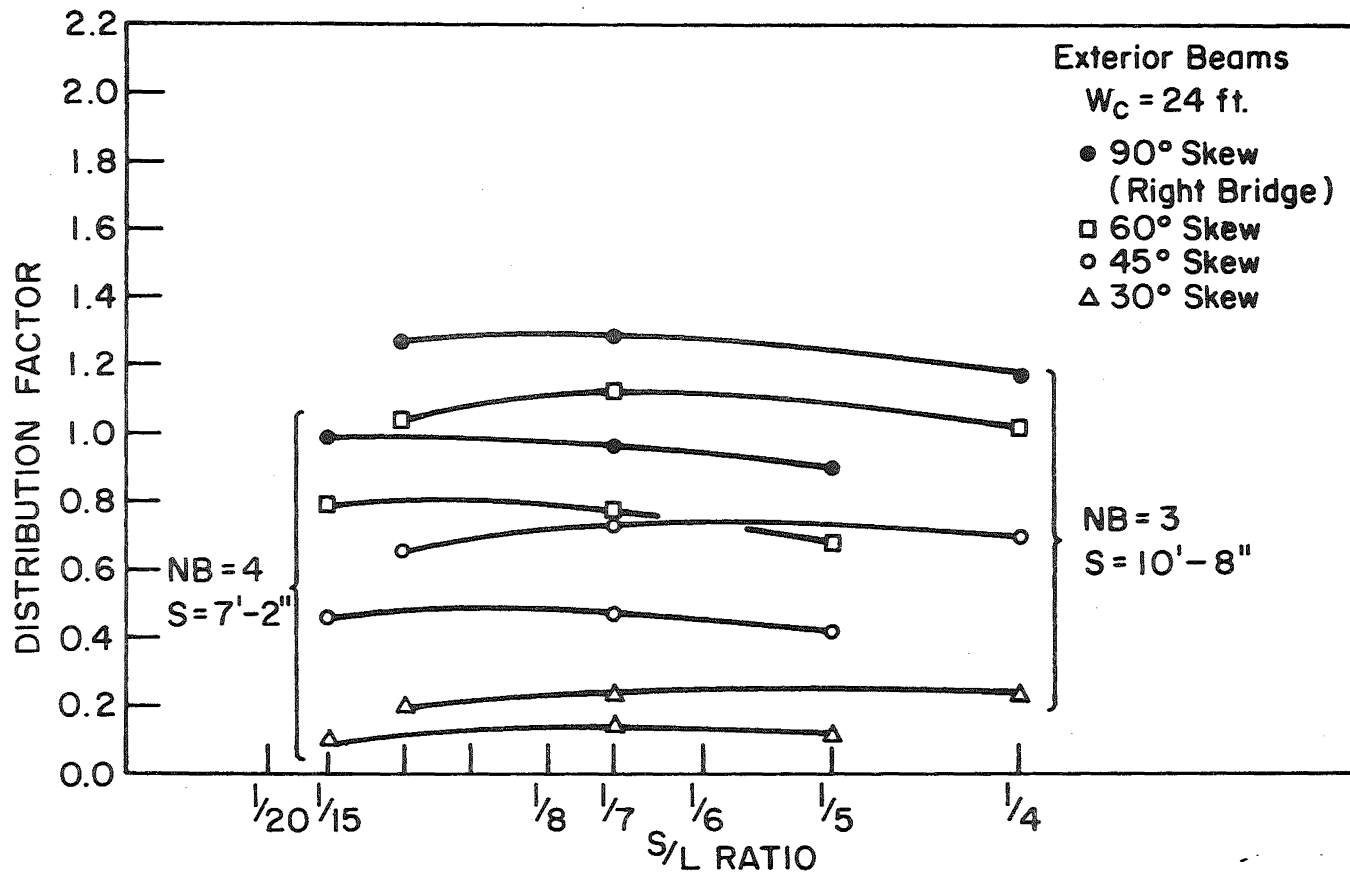
Fig. 104 Exterior Beam Distribution Factors, Skew Box-Beam Bridge, W_c = 24 ft.
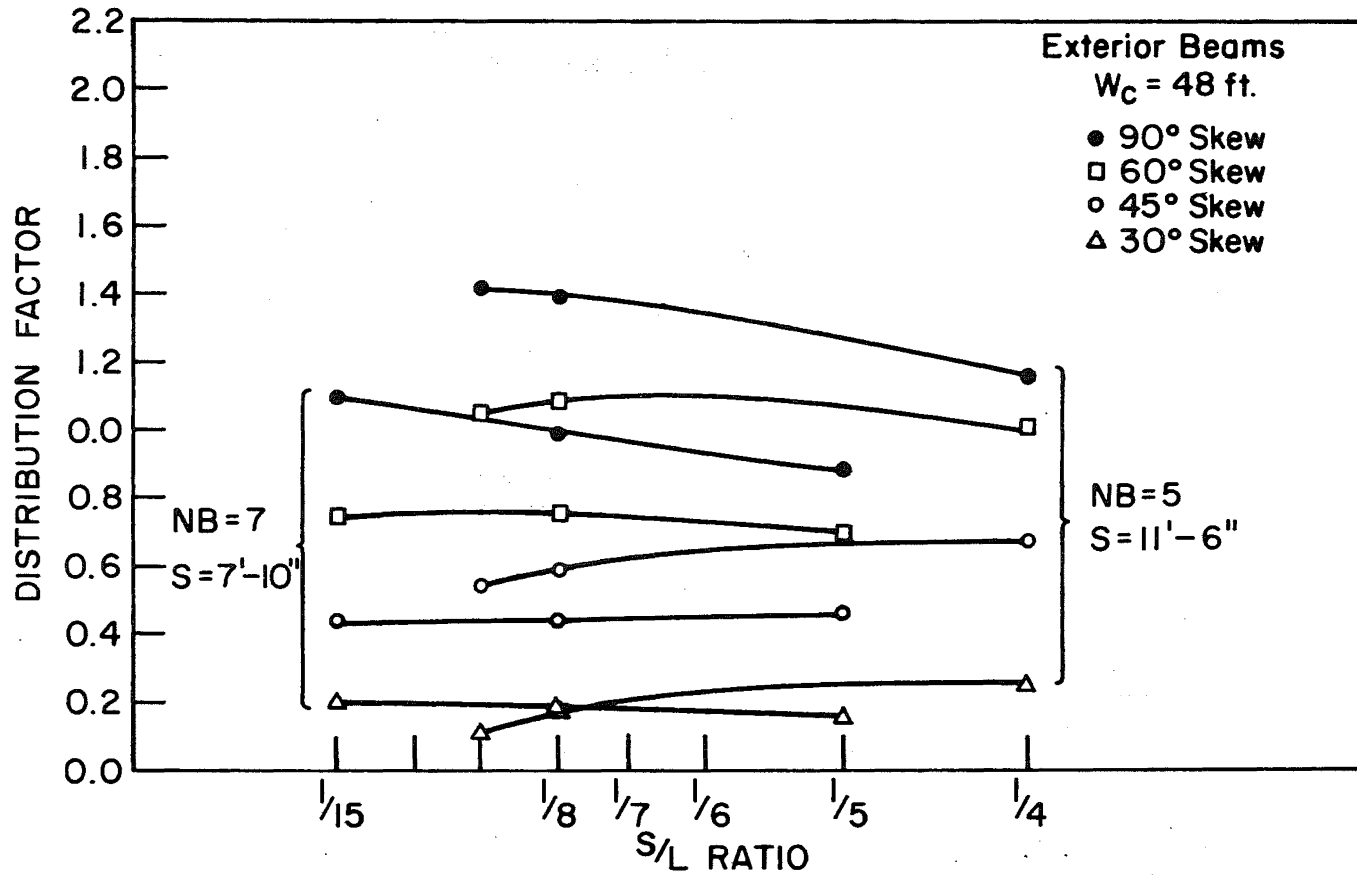
Fig. 105 Exterior Beam Distribution Factors, Skew Box-Beam Bridge, W_c = 48 ft.
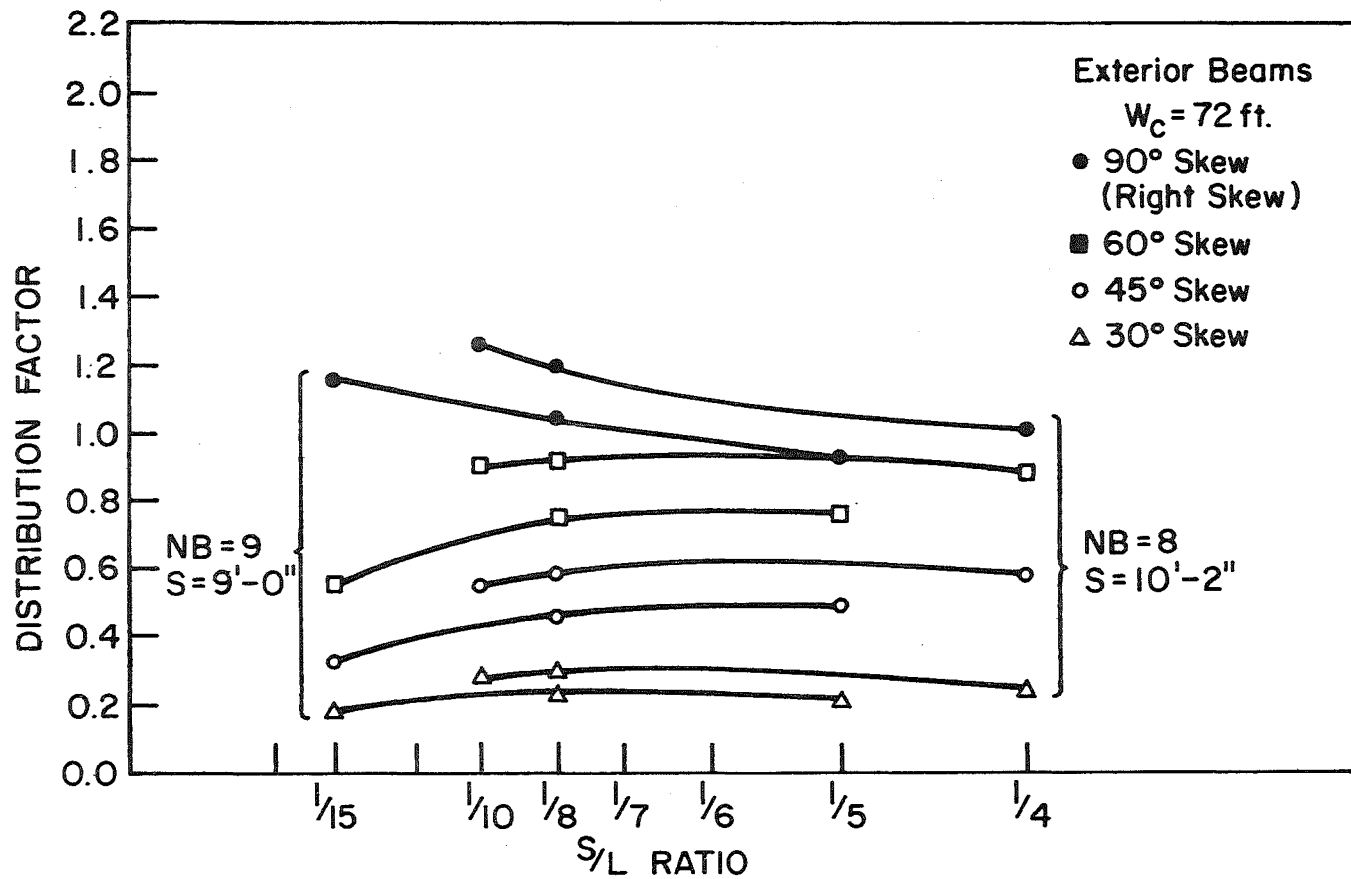
Fig. 106 Exterior Beam Distribution Factors, Skew Box-Beam Bridge, W_c = 72 ft.
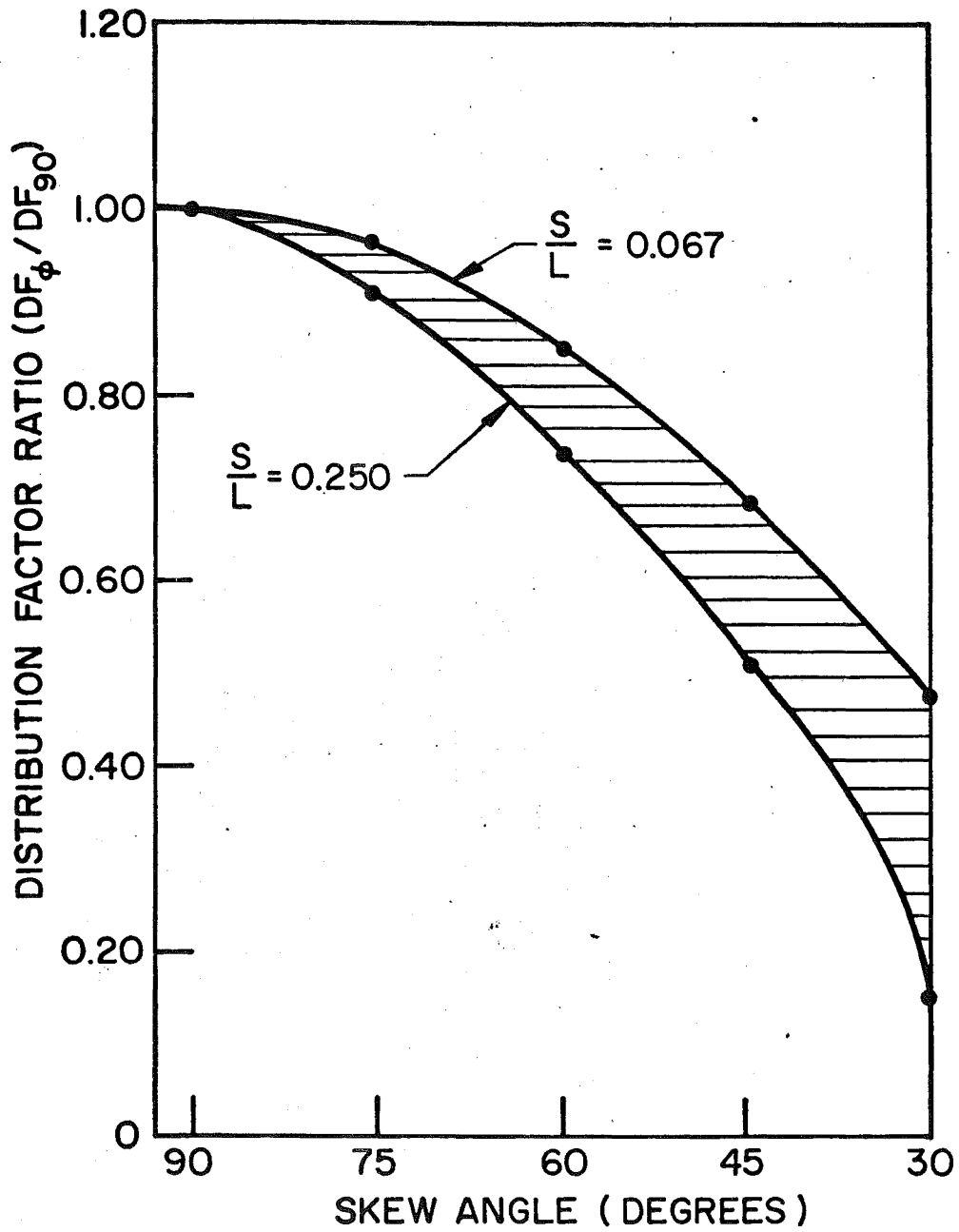
Fig. 107   Interior Box-Beam Distribution Factor Ratio with
the Equivalent Right Bridge

9. REFERENCES

1. American Association of State Highway Officials,
        STANDARD SPECIFICATIONS FOR HIGHWAY BRIDGES,
        10th Edition, Washington, D. C., 1971.

2. American Association of State Highway Officials,
        STANDARD SPECIFICATIONS FOR HIGHWAY BRIDGES,
        11th Edition, Washington, D. C., 1973.

3. American Association of State Highway and Transportation
   Officials,
        STANDARD SPECIFICATIONS FOR HIGHWAY BRIDGES,
        Interim Specifications, Washington, D. C., 1974.

4. American Concrete Institute Committee 318,
        BUILDING CODE REQUIREMENTS FOR REINFORCED CONCRETE,
        American Concrete Institute 318-71, Detroit,
        Michigan, 1971.

5. Bogner, F. K., Fox, R. L. and Schmidt, L. A.
        THE GENERATION OF INTERELEMENT COMPATIBLE STIFFNESS AND
        MASS MATRICES BY THE USE OF INTERPOLATION FORMULAS,
        Proc. Conference on Matrix Methods in Structural Mechanics,
        Wright Patterson Air Force Base, Dayton, Ohio, October
        1965.

6. Burdette, E. G. and Goodpasture, D. W.
   FINAL REPORT ON FULL SCALE BRIDGE TESTING: AN EVALUATION
        OF BRIDGE DESIGN CRITERIA, Department of Civil Engineering,
        University of Tennessee, December 1971.

7. Chen, Chiou-Horng and VanHorn, D. A.
        STATIC AND DYNAMIC FLEXURAL BEHAVIOR OF A PRESTRESSED
        CONCRETE I-BEAM BRIDGE - BARTONSVILLE BRIDGE, Fritz
        Engineering Laboratory Report No. 349.2, January 1971.

8. Chen, Chiou-Horng and VanHorn, D. A.
        STRUCTURAL BEHAVIOR OF A PRESTRESSED CONCRETE I-BEAM
        BRIDGE - LEHIGHTON BRIDGE, Fritz Engineering Laboratory
        Report No. 349.4, October 1971.

9. Chen, T. Y., Siess, C. P. and Newmark, N. M.
        MOMENTS IN SIMPLY-SUPPORTED SKEW I-BEAM BRIDGES, Studies
        of Slab and Beam Highway Bridges, Part IV, University of
        Illinois Engineering Experiment Station Bulletin No.
        439, Urbana, Illinois, 1957.

10. Clough, R. W. and Tocher, J. L.
     FINITE ELEMENT STIFFNESS MATRICES FOR THE ANALYSIS OF
     PLATE BENDING, Proc. Conference on Matrix Methods in
     Structural Mechanics, Wright Patterson Air Force Base,
     Dayton, Ohio, October 1965.

11. Dawe, D. J.
     PARALLELOGRAM ELEMENTS IN THE SOLUTION OF RHOMBIC
     CANTILEVER PLATE PROBLEMS, Journal of Strain Analysis,
     Vol. 1, No. 3, pp. 223-230, 1966.

12. DeCastro, E. S. and Kostem, C. N.
     LATERAL LOAD DISTRIBUTION IN SKEWED PRESTRESSED CONCRETE
     I-BEAM BRIDGES, Fritz Engineering Laboratory Report
     No. 400.16, July 1975.

13. DeCastro, E. S. and Kostem, C. N.
     USER'S MANUAL FOR PROGRAM PLATE, Fritz Engineering
     Laboratory Report No. 400.13, January 1975.

14. DeCastro, E. S. and Kostem, C. N.
     USER'S MANUAL FOR PROGRAM INPT, Fritz Engineering
     Laboratory Report No. 400.18, July 1975.

15. DeCastro, E. S. and Kostem, C. N.
     USER'S MANUAL FOR PROGRAM SKBRD, Fritz Engineering
     Laboratory Report No. 400.15, June 1975.

16. Douglas, W. J. and VanHorn, D. A.
     LATERAL DISTRIBUTION OF STATIC LOADS IN A PRESTRESSED
     CONCRETE BOX-BEAM BRIDGE - DREHERSVILLE BRIDGE, Fritz
     Engineering Laboratory Report No. 315.1, August 1966.

17. Felippa, C. A.
     REFINED FINITE ELEMENT ANALYSIS OF LINEAR AND NONLINEAR
     TWO-DIMENSIONAL STRUCTURES, SESM Report 66-22, Department
     of Civil Engineering, University of California, Berkeley,
     October 1966.

18. Felippa, C. A. and Clough, R. W.
     A REFINED QUADRILATERAL ELEMENT FOR ANALYSIS OF PLATE
     BENDING, Second Conference on Matrix Methods in
     Structural Mechanics, Wright Patterson Air Force Base,
     Dayton, Ohio, October 1968.

19. Gaylord, H. and Gaylord, N., Editors
     STRUCTURAL ENGINEERING HANDBOOK, McGraw Hill, New York,
     1968.

20. Green, A. E. and Zerna, W.
     THEORETICAL ELASTICITY, Clarendon Press, Oxford, 1954.

21. Guilford, A. A. and VanHorn, D. A.
         LATERAL DISTRIBUTION OF VEHICULAR LOADS IN A PRESTRESSED
         CONCRETE BOX-BEAM BRIDGE - WHITE HAVEN BRIDGE, Fritz
         Engineering Laboratory Report No. 315.7, August 1968.

22. Guilford, A. A. and VanHorn, D. A.
         LATERAL DISTRIBUTION OF VEHICULAR LOADS IN A PRESTRESSED
         CONCRETE BOX-BEAM BRIDGE - BERWICK BRIDGE, Fritz
         Engineering Laboratory Report No. 315.4, October 1967.

23. Gustafson, W. C. and Wright, R. N.
         ANALYSIS OF SKEWED COMPOSITE GIRDER BRIDGES, Journal of
         the Structural Division, Proceedings of the ASCE, Vol.
         94, ST4, pp. 919-941, April 1968.

24. Highway Research Board
         THE AASHO ROAD TEST, Report 4, Bridge Research, Special
         Report 610, National Academy of Sciences, 1962.

25. Hondros, G. and Marsh, J. G.
         LOAD DISTRIBUTION IN COMPOSITE GIRDER SLAB BRIDGES,
         Journal of the Structural Division, Proceedings of the
         ASCE, Vol. 86, ST11, pp. 79-109, November 1960.

26. Jensen, V. P.
         ANALYSIS OF SKEW SLABS, University of Illinois
         Engineering Experiment Station Bulletin, No. 332,
         Urbana, Illinois, 1941.

27. Jumppanem, P.
         BENDING OF PARALLELOGRAM PLATES, Acta Polytechnica
         Scandinavica, Civil Engineering and Building Construction
         Series No. 61, Helsinki, 1970.

28. Kennedy, J. B. and Simon, J. G.
         LINEAR AND NONLINEAR ANALYSES OF SKEWED PLATES, Journal
         of Applied Mechanics, Vol. 34, p. 2, 1967.

29. Kostem, C. N.
         ANALYTICAL MODELING OF BEAM SLAB BRIDGES, Proceedings
         of the International Symposium on Folded Plates and
         Spatial Panel Structures, Udine, Italy, September 1974.

30. Lehigh University Computing Center
         THE LEAPS USER'S GUIDE AND MANUAL, Lehigh University
         Computing Center, Bethlehem, Pennsylvania, May 1973.

31. Lin, Chen-Shung and VanHorn, D. A.
         THE EFFECT OF MIDSPAN DIAPHRAGMS ON LOAD DISTRIBUTION
         IN A PRESTRESSED CONCRETE BOX-BEAM BRIDGE - PHILADELPHIA
         BRIDGE, Fritz Engineering Laboratory Report No. 315.6,
         June 1968.

32. Macias-Rendon, M. A. and VanHorn, D. A.
        MODEL STUDY OF BEAM SLAB BRIDGE SUPERSTRUCTURES, Journal
        of the Structural Division, Proceedings of the ASCE,
        ST9, Vol. 99, pp. 1805-1821, September 1973.

33. Meek, J. L.
        MATRIX STRUCTURAL ANALYSIS, McGraw Hill, New York, 1971.

34. Melosh, R. J.
        BASIS FOR THE DERIVATION OF MATRICES FOR THE DIRECT
        STIFFNESS METHOD, AIAA Journal, Vol. 1, No. 7, July 1963.

35. Monforton, G. R. and Schmidt, L. A.
        FINITE ELEMENT ANALYSIS OF SKEW PLATES IN BENDING, AIAA
        Journal, Vol. 6, No. 6, pp. 1150-1152, 1968.

36. Morice, P. B. and Little, G.
        ANALYSIS OF RIGHT BRIDGES SUBJECTED TO NORMAL LOADING,
        Cement and Concrete Association, London, D.B.11.

37. Morley, L. S. D.
        SKEW PLATES AND STRUCTURES, Pergamon Press, McMillan
        Company, New York, 1963.

38. Motarjemi, D. and VanHorn, D. A.
        THEORETICAL ANALYSIS OF LOAD DISTRIBUTION IN PRESTRESSED
        CONCRETE BOX-BEAM BRIDGES, Fritz Engineering Laboratory
        Report No. 315.9, October 1969.

39. Newmark, N. M. and Siess, C. P.
        MOMENTS IN I-BEAM BRIDGES, University of Illinois
        Engineering Experiment Station Bulletin No. 336,
        Urbana, Illinois, 1942.

40. Newmark, N. M., Siess, C. P. and Pechham, W. M.
        TEST OF SIMPLE SPAN RIGHT I-BEAM BRIDGES, Studies of Slab
        and Beam Highway Bridges: Part I, University of Illinois
        Engineering Experiment Station Bulletin No. 363, Vol. 43,
        No. 42, Urbana, Illinois, March 1946.

41. Newmark, N. M., Siess, C. P. and Pechham, W. M.
        TEST OF SIMPLE SPAN SKEW I-BEAM BRIDGES, Studies of
        Slab and Beam Highway Bridges, Part II, University of
        Illinois Engineering Experiment Station Bulletin No.
        375, Vol. 45, No. 31, Urbana, Illinois, January 1948.

42. Pennsylvania Department of Highways
        STANDARDS FOR PRESTRESSED CONCRETE BRIDGES, ST200-ST208,
        Bureau of Design, Bridge Division, Commonwealth of
        Pennsylvania, 1960.

43. Pennsylvania Department of Transportation
    STANDARDS FOR BRIDGE DESIGN, BD-201, Bureau of Design,
    Commonwealth of Pennsylvania, June 1973.

44. Pickett, G.
    APPLICATION OF THE FOURIER METHOD TO THE SOLUTION OF
    CERTAIN BOUNDARY PROBLEMS IN THE THEORY OF ELASTICITY,
    Journal of Applied Mechanics, Vol. 11, p. 176, 1944.

45. Przemieniecki, J. S.
    THEORY OF MATRIX STRUCTURAL ANALYSIS, McGraw Hill,
    New York, 1968.

46. Rai, S. I. and Sandhu, S. R.
    FINITE ELEMENT OF AN ISOTROPIC PLATE USING Q-19
    ELEMENT, PART I, THEORETICAL DEVELOPMENT, Ohio
    University and Air Force Flight Dynamics Laboratory,
    AFFDL-TR-74-120, Wright Patterson Air Force Base,
    Ohio, October 1974.

47. Robinson, K. E.
    THE EFFECT OF SKEW ON THE BEHAVIOR OF SIMPLY SUPPORTED
    BRIDGE SLABS, Cement and Concrete Association, Technical
    Report TRB/271, July 1957.

48. Rusch, E. H. and Hergenroder, A.
    EINFLUBFELDER DER MOMENTE SCHREF-WINKLIGER PLATTEN
    (Influence Surfaces for Moments in Skew Slabs)
    Werner-Verlag, Dusseldorf, 3rd Ed., 1969, Translated by
    C. V. Amerongen.

49. Sanders, W. W., Jr. and Elleby, H. A.
    DISTRIBUTION OF WHEEL LOADS IN HIGHWAY BRIDGES,
    National Cooperative Highway Research Program,
    Report No. 83, Highway Research Board, Washington,
    D. C., 1970.

50. Sandhu, S. R.
    FINITE ELEMENT ANALYSIS OF AN ISOTROPIC PLATE USING
    Q-19 ELEMENT, PART II, INSTRUCTION FOR USERS AND
    FORTRAN LISTING, Ohio State University and Air Force
    Flight Dynamics Laboratory, Wright Patterson Air
    Force Base, Ohio, October 1974.

51. Schaffer, T. and VanHorn, D. A.
    STRUCTURAL RESPONSE OF A 45° SKEW PRESTRESSED CONCRETE
    BOX-GIRDER BRIDGE SUBJECTED TO VEHICULAR LOADING -
    BROOKVILLE BRIDGE, Fritz Engineering Laboratory
    Report No. 315.5, October 1967.

52. Schultchen, E. G. and Kostem, C. N.
    USER'S MANUAL FOR CSTPL FINITE ELEMENT PROGRAM,
    Fritz Engineering Laboratory Report No. 400.2,
    June 1971.

53. Sisodiya, R. G. and Cheung, Y. K.
    A HIGHER ORDER IN-PLANE PARALLELOGRAM ELEMENT AND
    ITS APPLICATION TO SKEWED CURVED BOX-GIRDER BRIDGES,
    Developments in Bridge Design and Constructions,
    Rockey et al, Editors, Crosby, Lockwood and Sons
    Ltd., London, 1971.

54. Timoshenko, S. P. and Goodier, V. N.
    THEORY OF ELASTICITY, 3rd Edition, McGraw Hill,
    New York, 1970.

55. Timoshenko, S. P. and Woinoswki-Krieger, S.
    THEORY OF PLATES AND SHELLS, 2nd Edition, McGraw
    Hill, New York, 1959.

56. Tottenham, H. and Brebbia, C. (Editors)
    FINITE ELEMENT TECHNIQUES IN STRUCTURAL MECHANICS, Stress
    Analysis Publishers, Southampton, England, 1970.

57. VanHorn, D. A.
    STRUCTURAL BEHAVIOR CHARACTERISTICS OF PRESTRESSED
    CONCRETE BOX-BEAM BRIDGES, Fritz Engineering Laboratory
    Report No. 315.8, December 1969.

58. Wegmuller, A. W. and Kostem, C. N.
    FINITE ELEMENT ANALYSIS OF PLATES AND ECCENTRICALLY
    STIFFENED PLATES, Fritz Engineering Laboratory Report
    No. 378A.3, February 1973.

59. William, K. J.
    FINITE ELEMENT ANALYSIS OF CELLULAR STRUCTURES, Ph.D.
    Dissertation, University of California, Berkeley, 1969.

60. William, K. J. and Scordelis, S. C.
    COMPUTER PROGRAM FOR CELLULAR STRUCTURES OF ARBITRARY
    PLAN GEOMETRY, SESM Report 70-10, Department of Civil
    Engineering, University of California, Berkeley, 1969.

61. Yen, B. T., Chen, Y. S., et al
    MODEL TESTS ON COMPOSITE BOX-BEAMS, Fritz Engineering
    Laboratory Report No. 380.6, October 1973.

62. Zellin, M. A., Kostem, C. N. and VanHorn, D. A.
    LOAD DISTRIBUTION OF LIVE LOAD IN PRESTRESSED CONCRETE
    I-BEAM BRIDGES, Fritz Engineering Laboratory Report No.
    387.2A, June 1975.

63. Zellin, M. A., Kostem, C. N. and VanHorn, D. A.
STRUCTURAL BEHAVIOR OF BEAM-SLAB HIGHWAY BRIDGES,
A Summary of Completed Research and Bibliography,
Fritz Engineering Laboratory Report No. 387.1,
May 1973.

64. Zienkiewicz, O. C. and Cheung, Y. K.
THE FINITE ELEMENT METHOD IN STRUCTURAL AND CONTINUUM
MECHANICS, McGraw Hill, New York, 1967.

65. Zienkiewicz, O. C. and Hollister, G. S.
STRESS ANALYSIS, John Wiley and Sons, New York, 1975.

10. <u>APPENDICES</u>

APPENDIX A

Q8S11 ELEMENT STIFFNESS MATRIX

The Q8D11 element approximates the in-plane behavior of the deck slab in this study. This element has 10 fundamental degrees of freedom and one generalized coordinate α describing the constant shear strain throughout the element. The derivation follows the derivation of the element Q8D9 in Ref. 59.

The relationship between the natural system of coordinate and the global right cartesian coordinate system is expressed by:

$$\left\{ \begin{array}{c} x \\ y \end{array} \right\} = \left[\begin{array}{cc} \Phi_x & 0 \\ 0 & \Phi_y \end{array} \right] \left\{ \begin{array}{c} x_i \\ y_i \end{array} \right\} \tag{A.1}$$

The assumed displacement function is a linear shape function for the corner points and a quadratic function for the internal node:

$$\left\{ \begin{array}{c} u \\ v \end{array} \right\} = \left[\begin{array}{cccc} \Phi_1 & 0 & \Phi_2 & 0 \\ 0 & \Phi_1 & 0 & \Phi_2 \end{array} \right] \left\{ \begin{array}{c} u_i \\ v_i \\ u_o \\ v_o \end{array} \right\} \tag{A.2}$$

where

$$\Phi_1 = \frac{1}{2} (1 + \zeta\zeta_i)(1 + \eta\eta_i)$$

$$\Phi_2 = (1 - \zeta^2)(1 - \eta^2)$$

-259-

The displacement gradient field can be derived from Eq. A.2 by appropriate differentiation.

$$
\{\nabla v\} =
\begin{bmatrix}
\dfrac{\partial \Phi_1}{\partial x} & 0 & \dfrac{\partial \Phi_2}{\partial x} & 0 \\[2ex]
0 & \dfrac{\partial \Phi_1}{\partial y} & 0 & \dfrac{\partial \Phi_2}{\partial y} \\[2ex]
\dfrac{\partial \Phi_1}{\partial y} & \dfrac{\partial \Phi_1}{\partial x} & \dfrac{\partial \Phi_2}{\partial y} & \dfrac{\partial \Phi_2}{\partial x}
\end{bmatrix}
\begin{Bmatrix}
u_i \\[1ex]
v_i \\[1ex]
u_o \\[1ex]
v_o
\end{Bmatrix}
\tag{A.3}
$$

Equation A.3 can be rewritten in the form

$$
\{\nabla v\} = [\nabla \Phi]
\begin{Bmatrix}
u_i \\[1ex]
v_i \\[1ex]
u_o \\[1ex]
v_o
\end{Bmatrix}
\tag{A.3a}
$$

The strain field, by assuming constant strain throughout the element, can be written as:

$$
\begin{Bmatrix}
\varepsilon x \\[1ex]
\varepsilon y \\[1ex]
\gamma_{xy}
\end{Bmatrix}
\begin{bmatrix}
\dfrac{\partial \Phi_1}{\partial x} & 0 & \dfrac{\partial \Phi_2}{\partial x} & 0 & 0 \\[2ex]
0 & \dfrac{\partial \Phi_1}{\partial y} & 0 & \dfrac{\partial \Phi_2}{\partial y} & 0 \\[2ex]
0 & 0 & 0 & 0 & 1
\end{bmatrix}
\begin{Bmatrix}
u_i \\[1ex]
v_i \\[1ex]
u_o \\[1ex]
v_o \\[1ex]
\alpha
\end{Bmatrix}
\tag{A.4}
$$

Equation A.4 can be rewritten into the form

$$\left\{ \begin{array}{c} \epsilon_x \\ \epsilon_y \\ \gamma_{xy} \end{array} \right\} = \left[\Phi_e \right] \left\{ \begin{array}{c} u_i \\ v_i \\ u_o \\ v_o \\ \alpha \end{array} \right\} \qquad (A.4a)$$

With the use of the Hu-Washizu variational principle, William has shown in Ref. 59 that the stiffness relationship is of the form

$$\left\{ \begin{array}{c} \underline{P}_v \\ \underline{0} \end{array} \right\} = \left[\begin{array}{cc} 0 & k_{ve} \\ k_{ev} & -k_{ee} \end{array} \right] \left\{ \begin{array}{c} \underline{v} \\ \underline{e} \end{array} \right\} \qquad (A.5)$$

where for this element:

$$\{\underline{P}_v\}^T = \{F_{ui} \quad F_{vi} \quad F_{uo} \quad F_{vo}\} \qquad (A.5a)$$

$$\{\underline{v}\}^T = \{u_i \quad v_i \quad u_o \quad v_o\} \qquad (A.5b)$$

$$\underline{e} = \gamma_{xy} \quad \text{strain degree of freedom} \qquad (A.5c)$$

and the individual submatrices are defined as:

$$[k_{ev}] = [k_{ve}]^T = \int [\Phi_e][D][\nabla\Phi] \, dV \qquad (A.5d)$$

$$[k_{ee}] = \int [\Phi_e][D][\Phi_e] \, dV \qquad (A.5e)$$

The submatrices are evaluated by numerical integration described in Section 2.3.3. The strain degree of freedom is eliminated by static condensation procedure as described in Section 1.3.3 resulting in the following final form of the element stiffness.

$$[k] = [k_{ev}]^T [k_{ee}]^{-1} [k_{ev}] \qquad (A.6)$$

APPENDIX B

COMPATIBLE DISPLACEMENT FUNCTIONS FOR PLATE BENDING ELEMENT Q-19

This appendix contains the displacement functions for the quadrilateral element Q-19 given by Eq. 2.29. The following is taken from Ref. 17 and reproduced here for completeness.

The displacement function for sub-element 3 in Eq. 2.29 is expressed by

$$w^{(3)} = [\hat{\Phi}^{(3)}] \{r\} \tag{B.1}$$

where

$$\{\hat{\Phi}^{(3)}\} = \Phi_{w_1}^{(3)} \; \Phi_{\theta x_1}^{(3)} \; \Phi_{\theta y_1}^{(3)} \; \Phi_{w_2}^{(3)} \; \Phi_{\theta x_2}^{(3)} \; \Phi_{\theta y_2}^{(3)} \; \Phi_{w_3}^{(3)} \; \Phi_{\theta x_3}^{(3)} \; \Phi_{\theta y_3}^{(3)} \; \Phi_{\theta_4}^{(3)} \; \Phi_{\theta_5}^{(3)} \; \Phi_{\theta_6}^{(3)} \tag{B.2}$$

and the individual functions are given by the following equations in terms of the dimensions of the complete element:

$$\Phi_{w_1}^{(3)} = \zeta_1^2 (3 - 2\zeta_1) + 6\mu_3 \zeta_1 \zeta_2 \zeta_3$$
$$+ \zeta_3^3 [3(\lambda_2 - \mu_3)\zeta_1 + (2\mu_3 - \lambda_2)\zeta_3 - 3\mu_3 \zeta_2]$$

$$\Phi_{\theta x_1}^{(3)} = \zeta_1^2 (b_2 \zeta_3 - b_3 \zeta_2) + (b_1 - b_3 \mu_3)\zeta_1 \zeta_2 \zeta_3 + \frac{1}{6}\zeta_3^2 [3(b_2 \lambda_2 + b_3 \mu_3 - 2b_1)\zeta_1 + 3(b_3 \mu_3 - b_1)\zeta_2 + (3b_1 - b_2 \lambda_2 - 2b_3 \mu_3)\zeta_3]$$

$$\Phi_{w_2}^{(3)} = \zeta_2^2 (3 - 2\zeta_2) + 6\lambda_3 \zeta_1 \zeta_2 \zeta_3 + \zeta_2^2 [3(\mu_1 - \lambda_3)\zeta_2 + (2\lambda_3 - \mu_1)\zeta_3 - 3\lambda_3 \zeta_1]$$

-263-

$$\Phi_{\theta x_2}^{(3)} = \zeta_2^2(b_3\zeta_1 - b_1\zeta_2) + (b_3\lambda_3 - b_2)\zeta_1\zeta_2\zeta_3 + \frac{1}{6}\zeta_3^2[3(2b_2$$

$$- b_3\lambda_3 - b_1\mu_1)\zeta_2 + 3(b_2 - b_3\lambda_3)\zeta_1 + (-3b_2 - b_1\mu_1 + 2b_3\lambda_3)\zeta_3]$$

$$\Phi_{w_3}^{(3)} = \zeta_3^2[3(1 + \mu_2)\zeta_1 + 3(1 + \lambda_1)\zeta_2 + (1 - \mu_2 - \lambda_1)\zeta_3]$$

$$\Phi_{\theta x_3}^{(3)} = \frac{1}{6}\zeta_3^2[3(3b_1 + b_2 + b_1\lambda_1)\zeta_2 + (b_2\mu_2 - b_1\lambda_1)\zeta_3 - 3(b_1 + 3b_2 + b_2\mu_2)\zeta_1]$$

$$\Phi_{\theta_4}^{(3)} = \frac{4A}{3L_3}[6\zeta_1\zeta_2\zeta_3 + \zeta_3^2(5\zeta_3 - 3)]$$

$$\Phi_{\theta_5}^{(3)} = \frac{4A}{3L_1}[\zeta_3^2(3\zeta_2\zeta_3)]$$

$$\Phi_{\theta_6}^{(3)} = \frac{4A}{3L_2}[\zeta_3^2(3\zeta_1 - \zeta_3)]$$

For $\Phi_{\theta yi}$, all the b's in $\Phi_{\theta xi}$ are changed to a's.

For sub-elements 1 and 2, all superscripts and subscripts permit cyclically from 1-2-3 to 2-3-1 to 3-1-2 and from 4-5-6 to 5-6-4 to 6-4-5.

APPENDIX C

WEB ELEMENT IN-PLANE STIFFNESS MATRIX

This appendix presents the derivation of the stiffness matrix for the quadrilateral element Q8SP12. This element has been developed by William in Ref. 59, and is shown here for completeness of this study. The element is used in Chapter 5 to model the in-plane behavior of the webs of box-beam structures.

The geometry of the quadrilateral is described by linear interpolation functions:

$$
\begin{Bmatrix} x \\ z \end{Bmatrix} = \begin{bmatrix} \Phi_x & 0 \\ 0 & \Phi_z \end{bmatrix} \begin{Bmatrix} u_i \\ w_i \end{Bmatrix} \tag{C.1}
$$

where

$$
\Phi_x = \Phi_z = \frac{1}{4}(1 + \zeta\zeta_i)(1 + \eta\eta_i)
$$

and η_i and ζ_i are the local coordinates corresponding to node i.

The displacement field describes the w displacement component by shape functions with cubic variation in the ζ-direction and a linear variation in the η-direction. The displacement field associated with the local derivatives at the nodes is described by cubic shape functions:

$$
\begin{Bmatrix} u \\ z \end{Bmatrix} = \begin{bmatrix} \Phi_{1i} & 0 & 0 \\ 0 & \Phi_{Ti} & \Phi_{Ri} \end{bmatrix} \begin{Bmatrix} u_i \\ w_i \\ w_{\zeta i} \end{Bmatrix} \tag{C.2}
$$

where

$$\Phi_{1i} = \frac{1}{4}(1 + \zeta\zeta_i)(1 + \eta\eta_i)$$

$$\Phi_{Ti} = \frac{1}{8}(1 + \eta\eta_i)(2 + 3\zeta\zeta_i - \zeta^3\zeta_i)$$

$$\Phi_{Ri} = \frac{1}{8}(1 + \eta\eta_i)(-\zeta_i - \zeta + \zeta^2\zeta_i + \zeta^3)$$

and

$$w_{\zeta i} = \left(\frac{\partial w}{\partial \zeta}\right)_i \quad \text{or the local derivative at node i.}$$

Using the chain rule, the local derivatives can be expressed in terms of the global derivatives at the node under consideration:

$$\frac{\partial w}{\partial \zeta} = \frac{\partial w}{\partial x} \cdot \frac{\partial x}{\partial \zeta} + \frac{\partial w}{\partial y} \cdot \frac{\partial y}{\partial \zeta} \tag{C.3}$$

However, since there are no strain components in the nodal vector, $\frac{\partial w}{\partial y}$ must be expressed from the given displacement field in terms of the given nodal degrees of freedom:

$$\frac{\partial w}{\partial y} = \frac{\partial w}{\partial \zeta} \cdot \frac{\partial \zeta}{\partial y} + \frac{\partial w}{\partial \eta} \cdot \frac{\partial y}{\partial y}$$

$$= \frac{\partial \zeta}{\partial y}\left(\frac{\partial \Phi_T}{\partial \zeta} w_i + \frac{\partial \Phi_R}{\partial \zeta} w_{\zeta i}\right) + \frac{\partial \eta}{\partial y}\left(\frac{\partial \Phi_T}{\partial \eta} w_i + \frac{\partial \Phi_R}{\partial \eta} w_{\zeta i}\right) \tag{C.4}$$

Substitution of C.4 into C.3 and evaluating at each node, $\left(\frac{\partial w}{\partial \zeta}\right)_i$ can now be expressed in terms of $\left(\frac{\partial w}{\partial x}\right)_i$ and w_i:

$$\left\{ \begin{array}{c} u \\ \\ w \end{array} \right\} = \left[\begin{array}{ccc} \Phi_{1i} & 0 & 0 \\ \\ 0 & \bar{\Phi}_{Ti} & \bar{\Phi}_{Ri} \end{array} \right] \left\{ \begin{array}{c} u_i \\ w_i \\ \theta_{xi} \end{array} \right\} \tag{C.5}$$

where $\quad \theta_{xi} = \left(\dfrac{\partial w}{\partial x}\right)_i$

$$\bar{\bar{\Phi}}_{Ti} = \Phi_{Ti} + \eta_i \left[FT1_j \, \bar{\Phi}_{Rj} + FT1_k \, \bar{\Phi}_{Rk} \right] \tag{C.6}$$

$$\bar{\Phi}_{Ri} = FT2 \; \Phi_{Ri} \tag{C.7}$$

$$FT1 = J_{12} \, J_{21}/2 \; FCT$$

$$FT2 = J_{11}(1 - J_{12} \, J_{21}/FCT) \tag{C.8}$$

$$FCT = \det \; J \; + \; J_{21} \, J_{12}$$

with $j = 1, 2, 2, 1$ and $k = 4, 3, 3, 4$ for $i = 1, 2, 3, 4$ respectively. J_{11}, J_{12}, J_{21} are the components of the associated Jacobian matrix J.

The strain field can now be defined by differentiation of the displacement field:

$$\left\{ \begin{array}{c} \epsilon_x \\ \\ \epsilon_y \\ \\ \gamma_{xy} \end{array} \right\} = \left[\begin{array}{ccc} \dfrac{\partial \Phi_1}{\partial x} & 0 & 0 \\ \\ 0 & \dfrac{\partial \bar{\bar{\Phi}}_T}{\partial y} & \dfrac{\partial \bar{\Phi}_R}{\partial y} \\ \\ \dfrac{\partial \Phi_1}{\partial y} & \dfrac{\partial \bar{\bar{\Phi}}_T}{\partial x} & \dfrac{a}{2}\dfrac{\partial \bar{\Phi}_R}{\partial x} \end{array} \right] \left\{ \begin{array}{c} u_i \\ w_i \\ \theta_{xi} \end{array} \right\} \tag{C.9}$$

or

$$\left\{ \begin{array}{c} \epsilon_x \\ \epsilon_y \\ \gamma_{xy} \end{array} \right\} = T \left\{ \begin{array}{c} u_i \\ w_i \\ \theta_{xi} \end{array} \right\} \qquad\qquad (C.9a)$$

From the definition of the stiffness matrix in Section 1.3.2,

$$[k] = \int_A [T]^T [D] [T] \, dA \qquad\qquad (C.10)$$

The stiffness coefficients are then evaluated by the Gaussian quadrature rule.

11. NOMENCLATURE

The following symbols were used in the text and appendices:

A. _Capital Latin Letters_ (matrices and scalars)

$[A]$	= Matrix of displacement functions evaluated at the nodes
A	= Area of a triangular element
A_i	= Area of sub element i in a triangular element
A_s	= Cross section area of stiffener element
$[B]$	= Matrix of differentiated displacement functions
C	= Curvature in a stiffener element
$C_{11}, C_{12}, C_{21}, C_{33}$	= Material constants
$[D]$	= Elasticity matrix relating generalized stresses to generalized displacements
$[D]_s$	= Elasticity matrix for the stiffener element
D.F.	= Distribution factor
DF_{ϕ}	= Distribution factor in a skew bridge
DF_{90}	= Distribution factor in a right bridge
E, E_1, E_2	= General and principal modulus of elasticity
E_s	= Stiffener element modulus of elasticity
$\{F_e\}$	= Statically equivalent force vector due to distributed loads

-269-

$\{F_i\}$	= Vector of element nodal forces
$\{F_E\}$	= Applied force vector associated with external nodes
$\{F_I\}$	= Applied force vector associated with internal nodes
$\{F'\}$	= Statically equivalent force vector due to concentrated load
$F_{xi}, F_{yi}, F_{zi}, M_{xi}, M_{yi}$	= Components of element nodal forces $\{F_i\}$
G, G_2	= General and second principal shear moduli
G_s	= Stiffener element shear modulus
H	= Stiffener to slab stiffness ratio, $(EI)_{stiffener}/(EI)_{slab}$
I	= Integrand expression
I_s	= Moment of inertia of stiffener element about reference plane
$J_{11}, J_{12}, J_{21}, J_{22}$	= Components of Jacobian matrix
$[K]$	= Global stiffness matrix
L	= Bridge span length, stiffener element dimension
$[M]$	= Matrix of displacement functions
M_s, N_s	= Generalized forces in stiffener element
$M_x, M_y, M_{xy}, M_1, M_2$	= Cartesian and principal plate moments
$N_x, N_y, N_{xy}, N_1, N_2$	= Cartesian and principal in-plane
M_u, M_{uv}	= Moment resultants in the direction of skew

PCTR	= Percent reduction in the distribution factor for interior I-beams
$PCTR_{(EXT)}$	= Percent reduction in the distribution factor for exterior I-beams
$PCTR_{(BOX)}$	= Percent reduction in the distribution factor for interior box-beams
$[R]$	= Global force vector
S	= Beam spacing
S_s	= First moment of the stiffener area with respect to the reference plane
$[T]$	= Transformation matrix
U, V	= In-plane strain function
$U_{(z)}, V_{(z)}$	= In-plane displacement at distance z from the reference plane
W_c	= Bridge curb to curb width
W_i, W_j	= Weight coefficients

B. <u>Small Latin Letters</u> (matrices and scalars)

a, b	= Web element dimensions
a_i, b_i	= Projected dimensions on x and y axes
d	= Stiffener element depth; distance from the centroid of a truck wheel load to the drive wheels
d_i	= $2A/\ell_i$
e	= Eccentricity of the centroid of the stiffener element cross section to the plane of reference
f_i	= In-plane displacement function

-271-

f_{si}	=	Stiffener element displacement function
h_i	=	normal distance of node i to side ℓ_i
i,j,k,ℓ	=	Node or sub element number
$[k]$	=	Element stiffness matrix
$k_{EE}, k_{EI}, k_{IE}, k_{II}$	=	Partitioned matrices of the element stiffness matrix associated with external and internal nodes
k_{ev}, k_{ve}, k_{ee}	=	Submatrices of the element stiffness matrix associated with displacement and strain formulations
$[k_I], [k_{II}]$	=	Submatrices associated with in-plane and out-of-plane behavior
$[k]_s$	=	Stiffener element stiffness matrix
$[k]_t$	=	Stiffener element stiffness matrix for torsional behavior
$[k']$	=	Transformed element stiffness matrix
ℓ_i	=	Length of side i in a triangular element
m	=	Ratio of shear modulus G_2 to elastic modulus E_2
n	=	Order of interpolation function; principal modulus of elasticity ratio, E_1/E_2
n_i	=	Normal distance of a point i to side ℓ_i in a triangular element
$P(x,y), q$	=	Distributed load intensity
$\{p_v\}$	=	Consistent force vector associated with the displacement formulation
$\{r\}$	=	Global displacement vector

-272-

$\{r_i\}$	= Element nodal displacements
$\{r^{(i)}\}$	= Sub element nodal displacements
$\{r_s\}$	= Stiffener element nodal displacements
$\{r_e\}$	= External node displacements for plate element
$\{r_o\}$	= Internal node displacements for plate element
u,v,w	= Displacement components
u_i, v_i, w_i	= Components of the element nodal displacements
$\{v_E\}$	= Nodal displacements at exterior nodes
$\{v_I\}$	= Nodal displacements at interior nodes
x,y,z	= Cartesian coordinates
x_i, y_i	= Cartesian coordinates of node i

C. <u>Capital Greek Letters</u> (matrices and scalars)

Γ	= Shear deformation parameters
$[\Phi]$	= Matrix of interpolation or shape functions
$[\hat{\Phi}]$	= Interpolation functions for a triangular element in terms of the external degrees of freedom
$[\Phi^{(i)}]$	= Sub element i interpolation function
$[\Phi_c]$	= Strain interpolation functions evaluated at the nodes

$[\Phi_c]_s$ = Strain interpolation function for the stiffener element evaluated at the nodes

$[\Phi]_t$ = Twist interpolation function for the stiffener element evaluated at the nodes

$[\Phi_e]$ = Interpolation functions associated with the external nodes

$[\Phi_o]$ = Interpolation functions associated with the internal nodes

$[\Phi_B^{(i)}]$ = Curvature interpolation functions $[\Phi^{(i)}]$ evaluated at the nodes

$\Phi_{Ti}, \overline{\Phi}_{Ti}$ = Shape functions associated with the global nodal derivatives

$\Phi_{Ri}, \overline{\Phi}_{Ri}$ = Shape functions associated with the local nodal derivatives

$[\Phi_\epsilon]$ = Strain shape functions describing the variation of strains

$[\Phi_\epsilon^{(i)}]$ = Triangular sub element strain interpolation functions describing the variation of curvature

$[\Phi_\epsilon]_t$ = Stiffener strain interpolation function describing the variation of twist

$[\Phi_x], [\Phi_y]$ = Geometric shape functions

Φ_1 = Linear shape function

Φ_2 = Quadratic shape function

$[\Phi_{1i}]$ = Linear shape functions associated with nodes i

$[^{(i)}]$ = Matrix relating curvature components to nodal degrees of freedom

D. Small Greek Letters (matrices and scalars)

$\{\alpha\}$ = Generalized coordinates

β = Angle measured from the global x-axis in the direction of which u displaces

γ_{xy} = Shear strain

$\{\epsilon\}$ = Strain field

$\{\epsilon_c\}$ = Vector of nodal strains

$\epsilon_{xx}, \epsilon_{yy}$ = Normal strains

ζ, η = Local coordinates

ζ_i, η_i = Non-dimensional nodal coordinates

θ_x, θ_y = Rotations about the global x and y axes

$\theta_{xi}, \theta_{yi}, \theta_i$ = Nodal rotations

λ_i = d_i / ℓ_i

μ_i = $1 - \lambda_i$

ν, ν_2 = Poisson's ratio

$\{\sigma\}$ = Stress field

σ_{xx}, σ_{yy} = Normal stresses

τ_{xy} = Shear stresses

ϕ = Skew angle, angle of twist

$\hat{\phi}_{wi}, \hat{\phi}_{\theta xi}, \hat{\phi}_{\theta ii}, \hat{\phi}_{\theta i}$ = Interpolation functions in terms of the nodal out-of-plane displacements

-275-

| ω | = Angle from the global x-axis about which θ_x rotates |
| $\omega_{\zeta i}$ | = Local derivative at node i |

E. Element Designation

ACM	= Adini, Clough and Melosh plate bending element
CST	= Constant strain triangle in-plane element
LCCT-12	= Linear curvature compatible triangle with 12 degrees of freedom
LCCT-11	= Linear curvature compatible triangle with 11 degrees of freedom
LSE	= Linear strain equilateral
M	= Melosh plate bending element
P	= Pappenfuss plate bending element
Q-19	= Quadrilateral plate bending element with 19 degrees of freedom
Q8D11	= Basic 8 degree of freedom in-plane element with 3 additional internal degrees of freedom
Q8SP12	= Basic 8 degree of freedom in-plane element with 4 additional nodal rotations
WK	= Wegmuller and Kostem plate bending element

12. ACKNOWLEDGMENTS